MODELING AND ANALYSIS OF CO-LOCATED AND CELL-FREE MASSIVE MIMO ENABLED UNDERLAY SPECTRUM ACCESS NETWORKS

A Thesis

Submitted in Partial Fulfilment

of the Requirements for the Degree of

Doctor of Philosophy

by

Enkonda Venkata Pothan

Roll no. 176102102

Department of Electronics and Electrical Engineering
Indian Institute of Technology Guwahati
Guwahati - 781039, Assam, India

January 2025

To

The Almighty Shiva

Acknowledgements

First and foremost, I would like to express my deepest and most sincere gratitude to my supervisor Dr. Salil Kashyap for his excellent guidance throughout my research. His kindness, dedication, hard work and attention to detail have been a source of great inspiration to me. My heartfelt thanks to him for the unlimited support and patience shown to me. I sincerely thank him for the pain he undertook in scrutinizing every work I presented to him and offering critical comments to refine my work.

I am very thankful to my doctoral committee members Prof. Rakhesh Singh Kshetrimayum, Prof. Ratnajit Bhattacharjee and Dr. Kalpana Dhaka for sparing their precious time out of their busy schedule to evaluate my progress and enrich this work with their invaluable suggestions and feedback.

I sincerely thank my parents and sister for their limitless efforts, support and blessings. I would also like to thank my friends for their kind support and cooperation. I would also like to thank the Head of the Department and other faculty members for their kind help in carrying out this work.

(Enukonda Venkata Pothan)

Abstract

The design of wireless communication networks continues to evolve in order to meet the ever-increasing requirements for higher spectral efficiency (SE) and the need to support diverse technologies, services and applications. The data rates and the number of users that can be served depend heavily on the wireless spectrum that is available. However, below 6 GHz, we do not have sufficient free spectrum available for new technologies. This has motivated spectrum regulatory bodies around the globe, for example, the Federal Communications Commission (FCC) in the USA to actively consider spectrum sharing as a potential solution to enable efficient reuse of the already allocated spectrum. In this thesis, we focus on concurrent spectrum sharing, where the cognitive user (CU) also referred to as the unlicensed user may transmit simultaneously with the incumbent primary user (PU) who owns the spectrum provided it satisfies an interference constraint. To prevent adverse impact of spectrum sharing on the primary performance, the CU must adapt its transmit power, which, in turn, limits its SE measured in bits/s/Hz.

To this end, we first investigate use of massive number of antennas at cognitive base station (BS) in reducing interference caused to PUs under incomplete and/or imperfect channel state information (CSI) without deteriorating sum SE of CUs. We derive analytical expressions for complement of interference outage probability (IOP) with incomplete and/or imperfect CSI. These novel expressions provide ballpark number for the amount of back-off required to meet interference constraint. We deduce new expressions for sum SE of CUs with MR beamforming under incomplete and/or imperfect CSI. We prove that under imperfect CSI, by deploying more antennas at cognitive BS, IOP can be reduced while keeping sum SE of CUs

fixed. And larger number of PUs can be accommodated in the network while keeping IOP at PUs and sum SE of CUs fixed. Furthermore, IOP reduces as number of channels S to which CSI is available increases, since the constraint is violated less often. And by deploying more antennas at cognitive BS, sum SE of CUs can be kept fixed even if S decreases. The impact of spatial correlation on performance is also elucidated.

Thereafter, we investigate the use of cell-free massive multiple input multiple output (mMIMO) systems in serving unmanned aerial vehicles (UAVs) and ground user equipments (GUEs) in underlay spectrum access mode by considering UAVs as CUs and GUEs as PUs. We derive a novel lower bound on complement of IOP. This result helps determine the power margin required at secondary access points (APs) to meet the IOP constraint. We deduce new analytical expressions for SE and bit error rate (BER) of UAVs and GUEs. This analysis entails finding expectation of secondary AP transmit power based on order statistics of the strongest interference channel between secondary APs and GUEs. We prove that for lower pilot power, a larger power margin is required to keep IOP fixed. We show that for a given IOP, the larger the interference threshold is, the greater (lower) the likelihood for the UAVs (GUEs) to obtain higher SE is. For a given interference threshold, probability that UAVs attain higher SE increases as IOP increases for a fixed number of secondary APs (N) or as N increases for a given IOP. The impact of interference threshold and height of UAVs on BER is also presented.

We then analyze the uplink (UL) of a cell-free mMIMO based underlay network over limited capacity fronthaul in which the CUs transmit under an IOP constraint and the impact of quantization is modeled based on Bussgang decomposition. We develop novel statistical models for the squared l_2- norm (SLN) of the true and the quantized channel estimates (QCE) based on Gamma distribution and find the corresponding shape and scale parameters. We then derive new expressions for the mean CU transmit power and correlation between SLN of true and QCE. We also

develop new expressions for IOP and UL SE of CUs and PUs as a function of the Bussgang gain and quantization noise variance, which in turn depends on the number of quantization levels. We show that to keep IOP fixed, larger back-off in SU transmit power is required when fewer bits are employed for quantization. Furthermore, the likelihood of PUs or CUs achieving a higher SE increases as number of quantization bits increases and 4 bits are sufficient to obtain same performance as an infinite capacity fronthaul.

Contents

List of Figures

List of Tables

List of Abbreviations

APs	Access Points
ASD	Angular Standard Deviation
BS	Base Station
CBRS	Citizen Broadband Radio Service
CDF	Cumulative Distribution Function
CPU	Central Processing unit
CR	Cognitive Radio
CSI	Channel State Information
CUs	Cognitive Users
DL	Downlink
EE	Energy Efficiency
GUEs	Ground User Equipments
IOP	Interference Outage Probability
LAA	License Assisted Access
LBT	Listen-Before-Talk
LoS	Line-of-sight
LTE	Long Term Evolution
MIMO	Multiple Input Multiple Output
mMIMO	Massive Multiple Input Multiple Output
MMSE	Minimum Mean Square Error
MR	Maximum Ratio

MRC	Maximum Ratio Combining
NOMA	Non-orthogonal Multiple Access
PAPs	Primary Access Points
pdf	Probability Density Function
PUs	Primary Users
QCE	Quantized Channel Estimate
rv	Random Variable
RV	Random Vector
SAPs	Secondary Access Points
SE	Spectral Efficiency
SINR	Signal to Interference plus Noise Ratio
SLN	Squared l_2-Norm
SUs	Secondary Users
UAVs	Unmanned Aerial Vehicles
UL	Uplink

List of Publications

Journal Papers

1. **E.Venkata Pothan** and Salil Kashyap, "Cell-Free Massive MIMO Based Underlay Spectrum Access Under Interference Outage Probability Constraint Over Limited Capacity Fronthaul," in *IEEE Transactions on Communications*, vol.72, no. 9, pp. 5837-5852, Sept. 2024.
2. **E.Venkata Pothan** and Salil Kashyap, "Cell-Free Massive MIMO Enabled Wireless Communication with UAVs in Underlay Spectrum Access Networks," in *IEEE Transactions on Communications,* vol. 71, no. 12, pp. 7363-7377, Dec. 2023.
3. **E.Venkata Pothan** and Salil Kashyap, "Massive MIMO Based Underlay Spectrum Access Under Incomplete And/Or Imperfect Channel State Information," in *IEEE Transactions on Cognitive Communications and Networking*, vol. 8, no. 3, pp. 1482-1496, Sept. 2022.

Publications Outside Thesis :

Conference Paper :

1. R.Gupta, S.Kashyap and **E.Venkata Pothan**, "Interference Violation Probability Constrained Underlay Cognitive Massive MIMO Network Under Imperfect Channel Knowledge," *Proc. of National Conference on Communications (NCC)*, Bangalore, India, Feb. 2019. (Finalist of the best student paper award).

1

Introduction

Contents

1.1 Motivation behind Spectrum Sharing Networks

In order to meet the ever-increasing demand for higher data rates and the necessity to support diverse wireless services and applications, the design of wireless communication networks continues to evolve. It is expected that in the next few years, billions of Internet of Things (IoT) devices, autonomous cars and unmanned aerial vehicles (UAVs) will be connected to the network [1]. However, the data rates and the number of users that can be served depend heavily on the available wireless spectrum. We note that most of the spectrum below 6 GHz is already allocated to support diverse cellular technologies such as 2G-5G and WiFi services such as IEEE 802.11 ac and IEEE 802.11 ax. This is the reason why spectrum regulatory authorities around the world are now deliberating on allowing sharing of spectrum by unlicensed cognitive users (CUs) in order to boost spectrum utilization efficiency. For example, the Federal Communications Commission (FCC) in the USA has opened up 150 MHz spectrum in the 3.5 GHz band [2] for shared use and 1.2 GHz spectrum in the 6 GHz band [3]. This 6 GHz band is currently being used by the primary users (PUs) such as satellite services or public safety services and concurrently for providing service to unlicensed CUs such as 5G new radio unlicensed (NR-U) and IEEE 802.11 ax/be [4]. Thus, these CUs must coexist with the high-priority licensed PUs who continue to use the spectrum in a cognitive radio (CR) network [5].

1.2 Challenges in Implementing Spectrum Sharing

These CR networks usually operate in three different paradigms, namely, overlay, interweave and underlay [6], [7]. While in the overlay mode of operation, the CUs are expected to have knowledge of the codebook and messages being transmitted by the PUs to enable interference cancellation at their end using sophisticated signal processing techniques, like dirty paper coding. In the interweave mode, the CUs transmit only when the PUs are silent. To achieve this, currently, a listen-before-talk (LBT) strategy is being utilized in long term evolution (LTE) based license assisted access (LAA), MulteFire, and Wi-Fi standards. In LBT, the secondary transmitter first senses the spectrum and transmits only if it finds the spectrum idle. The main challenge with such an approach is to monitor the activity of PUs and correctly detect the voids

in space, time and frequency commonly referred to as the spectrum holes to avoid interference to PUs. In other words, the PUs and the CUs in such networks can transmit simultaneously only when the spectrum hole is detected incorrectly.

In order to improve the utilization of the scarce spectrum, it makes sense to allow concurrent spectrum access in which the CUs can transmit even when the PUs are using the spectrum as long as the interference caused to the primary due to secondary transmissions is below a certain threshold. For example, in [8], the investigations related to a citizens broadband radio service (CBRS) based spectrum sharing illustrates that concurrent spectrum sharing is indeed viable and does not harm the reception by the primary naval radar systems. This implementation-friendly mode of concurrent spectrum access that we focus on in this work is commonly referred to as underlay spectrum access. To prevent the adverse effects of spectrum sharing and ensure that the interference constraint is obeyed, the CUs must adapt their transmit power based on the nature of the interference constraint and the quality of channel estimates that is available at their end. This gives rise to a limit on the maximum spectral efficiency (SE) that the CUs can achieve in underlay spectrum access networks.

1.3 Co-located Massive MIMO Based Underlay Networks

Massive multiple input multiple output (mMIMO) has already been identified as a key component of 5G cellular systems. In this, hundreds of antennas at the BS can simultaneously serve tens of users through spatial multiplexing at the same time and over the same frequency [9, 10]. Since it offers huge array gain, multiplexing gain, favorable propagation, high spatial resolution and reduced inter-user interference, the integration of mMIMO in underlay spectrum access networks may enhance the data rates of users in unlicensed cognitive network, where interference caused to the PUs, and the accuracy and the availability of the channel state information (CSI) at the cognitive BS are of prime concern and limit the power with which a cognitive BS can transmit [11].

1.4 Cell-Free mMIMO Based Underlay Networks

The co-located mMIMO architecture has low backhaul requirements. However, these systems offer lower probability of coverage and relatively poorer quality of service to cell edge users when compared to a distributed mMIMO system commonly referred to as cell-free mMIMO [12] and which we describe next. In cell-free mMIMO systems, a large number of geographically distributed access points (APs) coordinate[1] to serve users over the same time and frequency without cell boundaries. It is also a potential 6G technology [13], [14], [15]. These systems promise significant gains in SE, since these spatially distributed APs have the potential to offer uncorrelated fading to different users and can help overcome shadowing due to large obstacles. As these APs coordinate and can perform joint beamforming, these systems offer huge macro-diversity gains and unprecedented degrees-of-freedom [7]. Furthermore, the short effective transmission distance between the distributed APs and the users reduces path loss, enables transmission at lower transmit powers and simplifies interference management [16]. By exploiting the aforementioned benefits offered by these systems, a significant boost in the performance of CUs may potentially be achieved through integration of cell-free mMIMO and underlay spectrum access.

1.5 Challenges Associated with Limited Fronthaul in Cell-Free mMIMO

In cell-free mMIMO systems, the APs are connected to the CPU via fronthaul links, which are of limited capacity. These links are generally used for (i) transportation of physical layer signals that need to be transmitted on the downlink (DL), (ii) exchange of CSI, (iii) transmission of the received uplink (UL) data signals from APs to the CPUs and (iv) phase synchronization [17]. We note that there is a lot of transmission burden and signaling overhead on these links. Therefore, the data and the channel estimates need to be quantized before being forwarded to the CPU.

[1]These APs are connected to central processing units (CPUs) via fronthaul links.

1.6 Focus of Thesis and Our Contributions

In this thesis, we focus on modeling and analysis of co-located and cell-free mMIMO enabled underlay spectrum access networks. We first analyze the sum SE of a co-located mMIMO based underlay spectrum access network in which the cognitive BS is subject to a practically motivated interference outage probability (IOP) constraint under incomplete and imperfect CSI. We then investigate whether we can exploit the underlying macro-diversity, spatial multiplexing gains and simplified interference management benefits offered by cell-free mMIMO, to achieve a significant boost in the data rates offered to the CUs, for example, the unmanned aerial vehicles (UAVs) through integration of cell-free mMIMO and underlay spectrum access while minimizing the adverse impact of spectrum sharing on PUs, for example, the ground user equipments (GUEs). Thereafter, we extend our study to analyze the performance of a cell-free mMIMO enabled underlay spectrum access system over limited capacity fronthaul links under the practically relevant IOP constraint. We motivate each of these problems below and state the specific contributions that we make to the state-of-the-art.

1.6.1 mMIMO Based Underlay Network Under Incomplete And Imperfect CSI

We consider a scenario where an unlicensed N-antenna cognitive BS serves K_c CUs and accesses the spectrum concurrently with the incumbent M-antenna primary BS serving K_p PUs. The wireless channels to each of the PUs or the CUs are independent and non-identically distributed (i.n.i.d.). The main objective in this part of the work is to ascertain if we can exploit the huge array gain and high spatial resolution offered by mMIMO in underlay spectrum access networks to reduce IOP at the PUs or accommodate more number of PUs without degrading sum SE of CUs under incomplete and imperfect CSI. This is an essential first step in understanding the robustness of any wireless system in practical scenarios, in which the CSI is likely to be imperfect or incomplete. The channel knowledge may be imperfect due to errors incurred during channel estimation, the channel knowledge may as well be incomplete since the process of acquiring CSI to all the users in a timely and scalable manner is a practically challenging task. We summarize our key contributions below:

- *Modeling of Underlay Cognitive mMIMO Network Under IOP Constraint :* We consider a novel model in which the cognitive BS with massive number of antennas operates in concurrent spectrum access mode and is subject to a well-motivated and a practically relevant IOP constraint under imperfect and incomplete CSI. This constraint mandates that the power of the interference generated due to transmissions by the cognitive BS does not exceed a target threshold at any of the PUs more than a certain fraction of time [4, 18–21]. We consider this stochastic constraint since it is well-suited for primary systems that can tolerate co-channel interference, deep fades and offer voice and data services robust to delays and disruptions [4, 18].
- *IOP Analysis Under Imperfect and Incomplete CSI :* We propose simple back-off factor based power adaptation policies and derive new analytical expressions for IOP at the PUs when maximum ratio (MR) beamforming is used at the BS under three different scenarios, namely, imperfect with complete CSI, perfect with incomplete CSI and imperfect with incomplete CSI. This involves finding joint probability of the events that interference caused to each of the PUs is below a certain threshold depending on whether imperfect or incomplete CSI is available. And we use Bonferroni's inequality [2] to obtain closed-form analytical bounds that are very tight in the regime of interest. These results can be used to determine the power margin required to meet the constraint under each of the three scenarios.
- *Sum SE Analysis Under Imperfect and Incomplete CSI:* We also derive novel closed-form analytical expressions for the DL sum SE of the CUs with MR beamforming for each of the three scenarios mentioned above. This involves finding statistical mean of the cognitive BS transmit power and also the expected value of its square root. It also entails finding order statistics of strength of the estimated channels to all the PUs.
- *Performance Analysis Under Spatial Correlation:* We elucidate the impact of spatial correlation on IOP at PUs and sum SE of CUs.

[2] Bonferroni's inequality states that the probability that one or more of a given collection of random events will occur is no larger than the sum of the probabilities of the individual events [22].

- *Extensive Set of Numerical Results:* We present numerical results to confirm our mathematical analysis and also to obtain insights into the impact of different system parameters such as the back-off factor, channel estimation error, the number of PUs, the number of cognitive BS antennas, the incompleteness of CSI and the spatial correlation on IOP at PUs and the DL sum SE of CUs.

1.6.2 Cell-Free mMIMO Enabled Underlay Network Under IOP Constraint

The fundamental objective in this part of the work is to understand if we can harness the macro-diversity and the huge degrees-of-freedom offered by cell-free mMIMO networks to improve the SE of UAVs (i) while meeting the IOP constraint at the GUEs under estimated CSI, and (ii) without significantly affecting the data rate or the reliability of data detection of the GUEs. And to determine how the answer to the questions above depend on the power with which the secondary APs transmit, the interference threshold (I_p), the number of secondary and primary APs, UL pilot power and the IOP. We summarize our novel contributions below:

- *System Model:* In our model, a massive number of geographically distributed secondary access points (SAPs) communicate with UAVs and adapt their transmit power subject to the novel and practically relevant IOP constraint at the GUEs. As mentioned above, this constraint is stochastic in nature and it ensures that the power of the interference generated due to transmissions by SAPs does not exceed a pre-defined threshold at any of the GUEs more than a certain fraction of time. Furthermore, it is well-motivated since it is the most suitable underlay interference constraint to consider under imperfect CSI particularly when the voice and data services offered by primary network are robust to delays, disruptions, deep-fades and co-channel interference [4], [18], [19], [21]. For the channels from SAPs or primary access points (PAPs) to UAVs, we consider the generic Rician fading channel model, where the probability of line-of-sight (PLoS), path-loss and standard deviation of shadowing parameter depend on height of UAVs [23]. We consider the widely adopted and well-justified Rayleigh fading model for the channel from SAPs or PAPs to GUEs, since with obstacles around both the APs and the GUEs, these terrestrial users are highly likely to observe only signals coming from reflectors or

scatterers [7, 24, 25].

- *Statistical Characterization of SAP Transmit Power and Interference at GUEs:* We derive new closed-form integral free expressions for the statistical mean of SAP transmit power and also for its square root. The analysis entails finding order statistics of the strongest interference channel between the SAPs and GUEs. In order to characterize the interference caused to GUEs, we also develop an expression for the correlation between two chi-square distributed random variables (rvs) as functions of variances of the true and estimated interference channel coefficients between the SAPs and GUEs.
- *IOP Analysis:* We deduce a novel integral-free lower bound for IOP at the GUEs based on Boole-Fréchet inequality [3] and Gauss-Laguerre quadrature when normalized conjugate beamforming is used at the SAPs. It brings out the dependence of IOP on power margin, number of UAVs and GUEs, the strength of true and estimated interference channel and their underlying correlation. This result can help determine the power margin that the SAPs must maintain to satisfy the IOP constraint at the GUEs.
- *SE Analysis:* We also derive new approximate DL SE expressions for the UAVs and GUEs when the SAPs transmit subject to the IOP constraint. This rigorous mathematical analysis brings out the dependence of SE on power margin, interference threshold, the number of PAPs and SAPs, and the variances of true and estimated interference channel coefficients. We wish to emphasize that our analysis is in general valid and would apply to any model chosen for the PLoS, path-loss and the Rician factor corresponding to the channels to the UAVs [26–28].
- *Bit Error Rate (BER) Analysis:* We then develop maximum likelihood (ML) decision rules and the corresponding BER expressions to quantify the reliability of data detection at the GUEs and the UAVs. Our analysis is based on availability of statistical CSI at the GUEs or UAVs.

[3] Boole-Fréchet inequality states that the occurrence probability of a given finite-number of events is upper bounded by the maximum of sum of the probabilities of the individual events or zero [22].

- *New Design Insights:* For lower UL pilot power, a larger power margin is required to keep IOP fixed at a specific level. The IOP at the GUEs is independent of the number of SAPs. For a given IOP, the larger the interference threshold, the greater (lower) the likelihood for the UAVs (GUEs) to obtain a higher SE is. And for a given interference threshold, the probability that UAVs attain higher SE increases as IOP increases for a fixed number of SAPs (N) or as N increases for a given IOP. We also show the impact of height of UAVs and interference threshold on error performance of UAVs and GUEs.

1.6.3 Cell-Free mMIMO Based Underlay Network with Limited Fronthaul

In the last part of thesis, we focus on cell-free mMIMO based underlay CR networks with limited capacity fronthaul links, in which the primary system consists of M multi-antenna PAPs serving K PUs and the secondary system consists of N multi-antenna SAPs serving L SUs. Since the data and the channel estimates will be quantized by the APs before being forwarded to the CPUs to reduce the transmission burden on limited capacity fronthaul links, it is of fundamental interest to develop a comprehensive model to rigorously analyze the impact of quantization error thus induced on the performance of cell-free mMIMO based underlay spectrum access networks when the SUs are subject to a practically relevant IOP constraint. To this end, we make the following key contributions:

- *System Model:* We develop a comprehensive model in which the SUs transmit under an IOP constraint to a large number of spatially distributed SAPs when the fronthaul links that connect the SAPs to secondary CPUs have limited capacity. As highlighted above, the IOP constraint is a practically well-motivated constraint and controls the fraction of time the interference power due to SU transmissions is allowed to exceed a certain threshold at any of the PAPs [4, 18]. And to reduce the signaling overhead on the fronthaul, the data and the channel estimates are quantized before being sent to the respective CPUs. The impact of quantization is modeled based on Bussgang decomposition [29].
- *Statistical Modeling of Squared l_2-Norm (SLN) of Quantized Channel Estimates (QCE):* In order to derive an analytical expression for IOP at PAPs, we develop a new statistical model for the sum of the SLN of the QCE between the PAP and SUs based on Gamma

distribution and derive the corresponding shape and scale parameters.

- *Derive Average SU Transmit Power Under Quantization Error:* We deduce an integral free closed-form expression for the mean SU transmit power. The analysis is based on order statistics of the strongest interference channel between the SUs and PAPs. We also derive an expression for correlation between the SLN of true channel and QCE.
- *Deduce IOP Under Quantization Error:* We deduce novel integral-free lower bound for IOP at PAPs when the fronthaul links have limited capacity. This result helps us infer the amount of back-off that may be needed in the SU transmit power depending on the number of bits that are used to quantize the channel estimates.
- *UL SE Analysis Under Limited Capacity Fronthaul:* We derive reasonably tight approximations for the UL SE of the SUs and PUs when SUs transmit subject to an IOP constraint and the fronthaul links have limited capacity. This systematic analysis exemplifies the dependence of SE on the number of quantization levels, back-off factor, interference threshold, the number of PAPs and SAPs, number of SUs and PUs, and variances of the QCE.
- *New Design Inferences:* A larger back-off in SU transmit power is needed when fewer bits are employed to quantize channel estimates in order to maintain IOP at a fixed level. The IOP at PAPs also depends on the accuracy of interference channel estimates. We observe that the likelihood that PUs and SUs achieve a higher UL SE increases as (i) the number of quantization level increases or (ii) the number of antennas at the APs increases. Furthermore, an increase in IOP (P_o) or interference threshold ($\bar{I}_p$) improves the UL SE of SUs, while degrading the UL SE of PUs over limited capacity fronthaul links. Furthermore, we show that 4 bits suffice to achieve IOP and SE performance identical to that of an infinite capacity fronthaul network. The impact of spatial correlation on SE is also elucidated.

1.7 Organization of Thesis

The rest of the thesis is organized as follows. In Chapter 2, we present a comprehensive analysis of a co-located mMIMO based underlay spectrum access network in which the cognitive BS has imperfect and incomplete CSI of the PUs and employs MR beamformer to transmit under an IOP constraint. In Chapter 3, we investigate if we can harness the huge macro-diversity, spatial multiplexing gains, simplified interference management and uniformity of service benefits offered by cell-free mMIMO to achieve a significant boost in the data rates of secondary UAVs while serving them simultaneously with primary GUEs. In Chapter 4, we extend our study to analyze the UL SE and IOP performance of a cell-free mMIMO enabled underlay spectrum access system over limited capacity fronthaul links. This is followed by conclusions and directions for future research in Chapter 5. The proofs are given in the Appendix.

2

Massive MIMO Based Underlay Network Under Incomplete And Imperfect CSI

Contents

In this chapter, we consider a scenario where an unlicensed cognitive BS serves multiple CUs and accesses the spectrum concurrently with an incumbent primary BS, which on the other hand, serves multiple PUs. The wireless channels to each of the PUs or the CUs are assumed to be independent and non-identically distributed. The main focus in this part of thesis is to ascertain if we can exploit the huge array gain and high spatial resolution offered by mMIMO in underlay spectrum access networks to reduce IOP at the PUs and to accommodate more number of PUs without degrading sum SE of CUs under imperfect and incomplete CSI. As mentioned in chapter 1, the channel knowledge may be imperfect due to errors incurred during channel estimation, it may be incomplete as the process of acquiring CSI to all the users in a timely and scalable manner is a practically challenging task.

Given this model, we first develop new mathematical expressions for IOP and DL sum SE under imperfect and complete CSI. We then analyze performance in terms of IOP and sum SE under perfect and incomplete CSI followed by deriving new results under imperfect and incomplete CSI. Thereafter, we present extensive numerical results and discuss key design insights to illustrate the impact of different system parameters on performance. We first review some papers related to underlay cognitive mMIMO networks.

2.1 Related Literature

The authors in [30] considered an underlay cognitive mMIMO network and optimized the number of CUs that can be served on the DL under power, rate and a peak interference constraint considering availability of imperfect CSI. A multiuser mMIMO primary network and a multiple-input single-output cognitive network was considered in [31] and achievable rate was derived for a CU under a peak interference constraint. The authors in [32] considered a scenario where CUs harvest energy from PU transmissions and analyzed signal to interference plus noise ratio (SINR), energy-rate trade-off and sum rate. In [33], the authors studied UL of an underlay cognitive mMIMO network and optimized energy efficiency while ensuring fairness among CUs. A cognitive mMIMO relay network was studied in [34] and asymptotic SINR and the sum rate under different antenna configurations at the BS and the relay were analyzed.

In [35], the authors considered UL of a cognitive mMIMO network under imperfect CSI and studied joint pilot and data power allocation while ensuring max-min fairness to users. In [36], the authors investigated effects of pilot contamination on a random CR network underlaid upon a random primary network. In [37], the authors analyzed low-complexity transmission in mMIMO systems by exploiting their tolerance to incomplete CSI. The authors in [38] analyzed relay selection for a mMIMO underlay CR two-way relay network to maximize sum rate under peak interference constraint at the PU.

In [39], the performance of an underlay cognitive mMIMO network under imperfect and complete CSI. However, this analysis was done considering only one CU in the network and no analysis was done for incomplete CSI. In [40], the authors investigated the achievable rates for multiuser mMIMO relay networks operating in the underlay mode under both perfect and imperfect CSI. In [41], the authors analyzed UL of a cognitive mMIMO network under imperfect CSI where the CUs adapt their power based on statistical CSI in order to satisfy the interference constraint. In [42], the statistics of the aggregate interference at any CU due to both primary and cognitive transmissions were derived.

In [43], expressions for beamforming gain and distribution of signal and interference powers were derived in terms of gamma rvs with zero-forcing (ZF) beamforming at the BS in a non-cognitive radio setting. In [44], average interference at the PUs and complementary cumulative distribution function (CCDF) of the achievable rate of the CUs in mMIMO underlay cognitive radio networks were analyzed under imperfect CSI and with ZF beamforming. The authors in [45] proposed deep reinforcement learning algorithms for user selection and power allocation in cognitive mMIMO networks. In [46], the authors determined power allocation policy to maximize sum-rate of CUs while meeting total transmit power constraint at the BS and SINR constraints at the PUs. In [47], data rates in a wireless powered underlay cognitive mMIMO system over spatially correlated channels were analyzed. The aforementioned discussion is summarized in Table 2.1.

Table 2.1: Summary of literature focussing on sum spectral efficiency analysis of massive MIMO based underlay spectrum access networks

Interference constraint	**Perfect channel state information**	**Imperfect channel state information**	**Incomplete channel state information**
Peak interference constraint	[31] [32] [33] [34] [38] [45] [47]	[30] [35] [40] [46] [44] [41] [47]	Not applicable
SINR outage probability constraint	None	[36] [42]	None
Interference outage probability constraint	Not applicable	Analysis with single CU: [39] **Analysis with Multiple CUs: None**	**None**

2.2 Motivation

Based on the discussion above and to the best of our knowledge, no work in the existing literature has comprehensively analyzed the sum SE of a mMIMO based underlay spectrum access network in which the cognitive BS is subject to a practically motivated IOP constraint. Furthermore, most of the literature focuses on perfect or imperfect CSI and peak interference constraint only. Our new results, which deal with the practically relevant incomplete CSI scenario as well and analyze the system with multiple CUs, therefore, distinguish the first part of the thesis all the more. In other words, this is the first work that comprehensively analyzes implications of power control under the novel and practically relevant IOP constraint in mMIMO based underlay spectrum access with incomplete and imperfect CSI.

Notations: A circular symmetric complex Gaussian random vector $\boldsymbol{X}$ with zero mean vector and covariance matrix $\boldsymbol{\Lambda}$ is denoted by $\boldsymbol{X} \sim \mathcal{CN}(\mathbf{0}, \boldsymbol{\Lambda})$. We denote conjugate operator by $(\cdot)^*$, transpose by $(\cdot)^{\mathrm{T}}$ and the Euclidean norm by $\|\cdot\|$. Furthermore, $\mathbb{E}(\cdot)$ denotes the expectation operator, $\mathbf{I}_N$ denotes an $N \times N$ identity matrix, $f_X(x)$ denotes the probability density function (pdf) of an rv X, $F_X(x)$ denotes its CDF, $f_{X,Y}(x, y)$ denotes the joint pdf of two rvs X and Y and the joint probability of events $A_1, A_2 \ldots A_n$ is denoted by $\Pr(A_1, A_2 \ldots A_n)$. The cardinality of a set $\mathcal{S}$ is denoted by $|\mathcal{S}|$ and $k \in \mathcal{S}$ indicates that the element k belongs to the set $\mathcal{S}$.

The chapter is organized as follows. The system model is developed in Section 2.3. The IOP

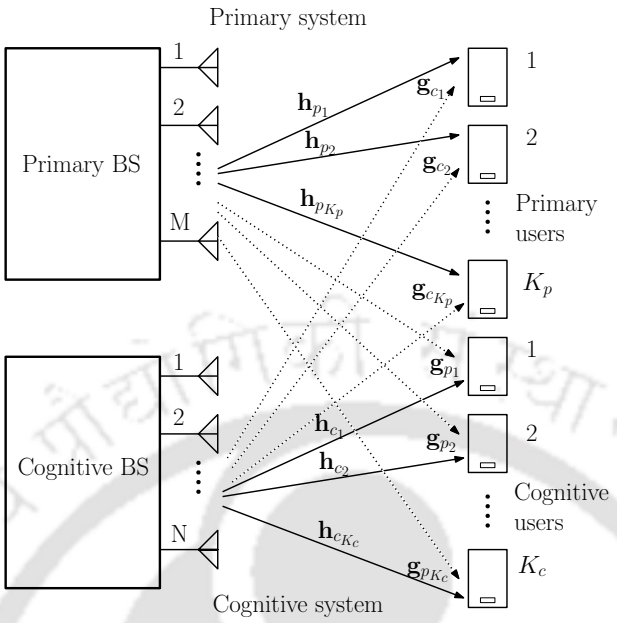

Fig. 2.1: System Model

and sum SE analysis under imperfect and complete CSI is presented in Section 2.4. The IOP and sum SE under perfect and incomplete CSI followed by imperfect and incomplete CSI are derived in Section 2.5. Our numerical results and conclusion of the chapter follow in Section 2.7 and Section 2.8, respectively. The mathematical derivations are given in Appendix A.

2.3 System Model

We consider DL of a mMIMO based underlay spectrum access system as illustrated in Figure 2.1. The model comprises of the incumbent high priority primary system who are licensed owners of the spectrum and the unlicensed cognitive system that accesses the spectrum concurrently subject to an IOP constraint set by the PUs. The primary system comprises of a primary BS with M co-located antennas providing service to K_p single-antenna PUs. The cognitive system comprises of a cognitive BS with N co-located antennas providing service to K_c single-antenna CUs. For the primary system, the channel vector from the primary BS to the k^{th} PU is denoted by $\boldsymbol{h}_{p_k} = [h_{p_{k,1}}, \ldots, h_{p_{k,M}}]^{\mathrm{T}} \in C^{M\times 1}$, where $\boldsymbol{h}_{p_k} \sim \mathcal{CN}(\mathbf{0}, \beta_k \mathbf{I}_M)$ and $h_{p_{k,i}}$ represents the small-scale fading coefficient from the i^{th} primary BS antenna to the k^{th} PU and β_k denotes the path loss from the primary BS to the k^{th} PU.

The channel vector of the interference link from the primary BS to the k^{th} CU is denoted by

$\boldsymbol{g}_{p_k}$, where $\boldsymbol{g}_{p_k} = [g_{p_{k,1}}, \ldots, g_{p_{k,M}}]^{\mathrm{T}} \in C^{M\times 1}$, $\boldsymbol{g}_{p_k} \sim C\mathcal{N}(\mathbf{0}, \phi_k \mathbf{I}_M)$ and ϕ_k denotes the large-scale fading coefficient corresponding to this link. For the cognitive system, the channel vector from the cognitive BS to the k^{th} CU is $\boldsymbol{h}_{c_k} = [h_{c_{k,1}}, \ldots, h_{c_{k,N}}]^{\mathrm{T}} \in C^{N\times 1}$ and $\boldsymbol{h}_{c_k} \sim C\mathcal{N}(\mathbf{0}, \gamma_k \mathbf{I}_N)$ where γ_k captures the path loss. The channel vector of the interference link from the cognitive BS to the k^{th} PU is denoted by $\boldsymbol{g}_{c_k} = [g_{c_{k,1}}, \ldots, g_{c_{k,N}}]^{\mathrm{T}} \in C^{N\times 1}$, where $\boldsymbol{g}_{c_k} \sim C\mathcal{N}(\mathbf{0}, \alpha_k \mathbf{I}_N)$ and $g_{c_{k,j}}$ represents the small-scale fading coefficient from the j^{th} cognitive BS antenna to the k^{th} PU and α_k denotes the path loss between cognitive BS and the k^{th} PU.

2.3.1 Data Transmission

When both the cognitive BS and the primary BS employ MR transmission,[1] then the signal received at the k^{th} CU on the DL equals

$$y_{c_k} = \sqrt{\frac{P_c}{K_c}} \sum_{k'=1}^{K_c} \frac{\boldsymbol{h}_{c_k}^{\mathrm{T}} \boldsymbol{h}_{c_{k'}}^{*} q_{k'}}{\|\boldsymbol{h}_{c_{k'}}\|} + \sqrt{\frac{P_p}{K_p}} \sum_{j=1}^{K_p} \frac{\boldsymbol{g}_{p_k}^{\mathrm{T}} \boldsymbol{h}_{p_j}^{*} s_j}{\|\boldsymbol{h}_{p_j}\|} + n_k, \tag{2.1}$$

where P_c is the cognitive BS transmit power, $q_{k'} \sim C\mathcal{N}(0,1)$ is the data symbol intended for the k'^{th} CU, P_p is the primary BS transmit power, $s_j \sim C\mathcal{N}(0,1)$ is the data symbol corresponding to the j^{th} PU and $n_k \sim C\mathcal{N}(0, \sigma^2)$ denotes additive white gaussian noise at the k^{th} CU. Furthermore, the symbols transmitted to distinct PUs or CUs are mutually uncorrelated to each other, i.e., $\mathbb{E}\left\{q_i q_j^*\right\} = 0$ and $\mathbb{E}\left\{s_i s_j^*\right\} = 0$ for $i \neq j$. Due to transmissions from the cognitive BS, the interference seen by the k^{th} PU equals

$$y_{p_k} = \sqrt{\frac{P_c}{K_c}} \boldsymbol{g}_{c_k}^{\mathrm{T}} \sum_{i=1}^{K_c} \frac{\boldsymbol{h}_{c_i}^{*}}{\|\boldsymbol{h}_{c_i}\|} q_i. \tag{2.2}$$

Based on (2.2), the instantaneous power of the interference caused to the k^{th} PU equals

$$I_{p_k} = \frac{P_c}{K_c} \sum_{i=1}^{K_c} \left| \frac{\boldsymbol{g}_{c_k}^{\mathrm{T}} \boldsymbol{h}_{c_i}^{*}}{\|\boldsymbol{h}_{c_i}\|} \right|^2, \text{ for all } 1 \leq k \leq K_p. \tag{2.3}$$

2.3.2 IOP Constraint

In this chapter, we consider a co-located mMIMO based concurrent spectrum access system in which the cognitive BS transmits subject to an *IOP constraint.* This constraint ensures that

[1] We consider MR transmission since it is computationally less intensive [31], [46], [48].

the interference power due to transmissions from the cognitive BS does not exceed a threshold $\bar{I}_p$ at any of the K_p PUs more than P_o fraction of the time. Mathematically, this can be written as

$$\Pr(I_{p_1} \leq \bar{I}_p, I_{p_2} \leq \bar{I}_p, \ldots, I_{p_{K_p}} \leq \bar{I}_p) \geq (1 - P_o)\,, \tag{2.4}$$

where P_o is referred to as the IOP. We consider this stochastic constraint since (i) it is practically relevant and its implications on a mMIMO based concurrent spectrum access system has not been thoroughly studied before; (ii) it is justified to use this constraint when the services, for example, user datagram protocol (UDP) services like voice and video offered by the primary system are robust to delays or disruptions [4, 18–20]; (iii) it need not harm primary systems that are robust to deep fades or co-channel interference [4, 19, 20]; (iv) this practically relevant constraint is widely used to design primary exclusive zones to protect the PUs in spectrum sharing networks [21] and (v) this constraint is generic and a more appropriate constraint to consider in practical scenarios where the cognitive BS has imperfect and/or incomplete CSI of its channels to the PUs. This is because under perfect and complete CSI, the peak interference caused to the PUs can be strictly kept below a threshold so that P_o is zero. However, in practical scenarios where the CSI is likely to be imperfect and/or incomplete, P_o cannot be made zero. It can however be constrained to meet a certain target level by controlling the fraction of time, the interference power exceeds the given interference threshold.

2.3.2.1 Perfect and Complete CSI

If the cognitive BS has perfect and complete knowledge of its channels to the K_p PUs and the K_c CUs and adapts its power P_c as follows:

$$P_c = \frac{\bar{I}_p}{\max\limits_{1 \leq k \leq K_p} \left\{ \frac{1}{K_c} \sum_{i=1}^{K_c} \left| \frac{\boldsymbol{g}_{c_k}^{\mathrm{T}} \boldsymbol{h}_{c_i}^{*}}{\|\boldsymbol{h}_{c_i}\|} \right|^2 \right\}}, \tag{2.5}$$

it can be shown that P_o equals zero and $\Pr(I_{p_1} \leq \bar{I}_p, I_{p_2} \leq \bar{I}_p, \ldots, I_{p_K} \leq \bar{I}_p) = 1$, i.e., the power of the interference caused by the cognitive BS is always below $\bar{I}_p$ at each of the K_p PUs.

2.3.2.2 Imperfect and Complete CSI

In practical wireless systems, CSI is estimated every coherence interval and is thus known imperfectly. With imperfect CSI, P_o will not be zero with the power adaptation policy in (2.5), where the true channel vectors are replaced by their estimates. It can, however, be constrained to satisfy a certain specified target P_o. In this part of the thesis, we consider the generic imperfect CSI model based on Gauss-Markov uncertainty [49]. Based on this model, the true interference channel vector $\boldsymbol{g}_{c_k}$ between cognitive BS and the k^{th} PU can be written as

$$\boldsymbol{g}_{c_k} = s_p\, \widehat{\boldsymbol{g}}_{c_k} + \sqrt{1 - s_p^2}\, \widetilde{\boldsymbol{g}}_{c_k}, \qquad k = 1, \ldots, K_p, \tag{2.6}$$

where $\widehat{\boldsymbol{g}}_{c_k} \sim \mathcal{CN}(\mathbf{0}, \alpha_k \mathbf{I}_N)$ is the estimate of the channel vector from the cognitive BS to the k^{th} PU, $\widetilde{\boldsymbol{g}}_{c_k} \sim \mathcal{CN}(\mathbf{0}, \alpha_k \mathbf{I}_N)$ denotes the Gaussian noise which is uncorrelated to $\widehat{\boldsymbol{g}}_{c_k}$ and s_p captures the channel estimation error. Based on this widely accepted generic imperfect CSI model, $s_p = 1$ corresponds to the case when the available CSI is perfect/error-free, $0 < s_p < 1$ corresponds to imperfect CSI case and $s_p = 0$ corresponds to no CSI scenario, in which case the available CSI is only noise that is uncorrelated and independent of the channel estimate and has the same statistics as the true channel [31, 49–52]. Similarly, the true channel vector $\boldsymbol{h}_{c_k}$ between cognitive BS and the k^{th} CU can be written as

$$\boldsymbol{h}_{c_k} = s_s\, \widehat{\boldsymbol{h}}_{c_k} + \sqrt{1 - s_s^2}\, \widetilde{\boldsymbol{h}}_{c_k}, \qquad k = 1, \ldots, K_c, \tag{2.7}$$

where $\widehat{\boldsymbol{h}}_{c_k} \sim \mathcal{CN}(\mathbf{0}, \gamma_k \mathbf{I}_N)$ is the estimate of the channel vector from the cognitive BS to the k^{th} CU, $\widetilde{\boldsymbol{h}}_{c_k} \sim \mathcal{CN}(\mathbf{0}, \gamma_k \mathbf{I}_N)$ denotes the Gaussian noise which is uncorrelated to $\widehat{\boldsymbol{h}}_{c_k}$ and as before, s_s captures the channel estimation error.

2.3.2.3 Incomplete CSI

In practice, it is possible that the cognitive BS has the CSI to only few of the PUs due to limitation of resources available for learning the wireless channel. In this chapter, we also consider the scenario where the cognitive BS knows the CSI perfectly or imperfectly only to $|\mathcal{S}|$ out of K_p PUs. Even in such scenarios, where the cognitive BS has perfect and incomplete CSI or imperfect and incomplete CSI of its links to the K_p PUs, P_o will not be exactly zero. It can,

however, be constrained to meet a certain target level.

2.4 Analysis with Imperfect and Complete CSI

In this section, we first analyze the IOP with imperfect and complete CSI. Thereafter, we analyze the DL sum SE that can be achieved by the CUs using the proposed power policy while satisfying the IOP constraint at the PUs. As mentioned above in Sec. 2.3.2.2, with imperfect and complete CSI, P_o will not be zero. However, P_o can be constrained to meet a certain target level. To this end, we propose a back-off factor based power adaptation policy in which the cognitive BS adapts its transmit power as a function of channel estimates from the cognitive BS to the K_p PUs and from the cognitive BS to the K_c CUs. Under this policy, the cognitive BS transmits with power

$$P_{ic} = \frac{\overline{I}_p}{\eta \max\limits_{1\le k\le K_p} \left\{ \frac{1}{K_c} \sum_{i=1}^{K_c} \left| \frac{\widehat{\boldsymbol{g}}_{c_k}^{\mathrm{T}} \widehat{\boldsymbol{h}}_{c_i}^{*}}{\|\widehat{\boldsymbol{h}}_{c_i}\|} \right|^2 \right\}}, \tag{2.8}$$

where the back-off factor η (>1) is chosen such that the IOP constraint under imperfect CSI is met with equality for a target P_o. In other words, given s_p, P_o, K_c, K_p and α_k for all PUs, the back-off factor η is chosen such that

$$\Pr(\widehat{I}_{p_1} \le \overline{I}_p, \widehat{I}_{p_2} \le \overline{I}_p, \ldots, \widehat{I}_{p_{K_p}} \le \overline{I}_p) = 1 - P_o \,, \tag{2.9}$$

where $\widehat{I}_{p_k} = \frac{P_{ic}}{K_c} \sum_{i=1}^{K_c} \left| \frac{\boldsymbol{g}_{c_k}^{\mathrm{T}} \widehat{\boldsymbol{h}}_{c_i}^{*}}{\|\widehat{\boldsymbol{h}}_{c_i}\|} \right|^2$, for all $1 \le k \le K_p$. We next state a lower bound on the complement of the IOP.

Theorem 2.1. *A lower bound on the complement of IOP $P_{L_{(ic)}}$ with imperfect and complete CSI is given by*

$$(1 - P_o) \ge P_{L_{(ic)}} = 1 - \sum_{i=1}^{K_p} \sum_{l=1}^{L} \frac{w_l \, {x_l}^{K_c - 1}}{\Gamma(K_c)} \prod_{j \ne i}^{K_p} \frac{\gamma\left(K_c, \frac{x_l \alpha_i}{\eta \alpha_j}\right)}{\Gamma(K_c)} \left(1 - Q_{K_c}\left(\sqrt{\frac{2\rho x_l}{(1-\rho)}}, \sqrt{\frac{2x_l}{\eta(1-\rho)}}\right)\right), \tag{2.10}$$

where $\rho = s_p^2$, $\{x_l\}$ are the integration points, $\{w_l\}$ are the corresponding weights obtained via Gauss-Laguerre integration, L is the total number of integration points, $\gamma(\cdot)$ denotes the lower incomplete Gamma function [53, (8.350.1)] and $Q_{K_c}(\cdot,\cdot)$ denotes the generalized Marcum-Q function of order K_c [54, (4.59)].

Proof. The derivation is given in Appendix A.1. □

Remarks: The integral-free expression for the lower bound $P_{L_{(ic)}}$ above brings out the dependence of P_o on the back-off factor (η), number of CUs (K_c), number of PUs (K_p), channel estimation error (s_p) and the path loss (α_j) for $1 \leq j \leq K_p$. An interesting insight that we obtain based on the analytical expression in (2.10) is that P_o is independent of s_s since it does not depend on the estimated channels to the CUs as highlighted in Appendix A.1. Furthermore, it is also independent of the number of cognitive BS antennas N because of the scaling by the norm of the channel vector in the MR precoder used at the cognitive BS. It, however, depends on the strength of the estimated channels from the cognitive BS to the PUs.

We next analyze the achievable sum SE of CUs in this scenario. The signal received at the k^{th} CU with imperfect and complete CSI at the cognitive BS is given by[2]

$$y_{c_k} = \sqrt{\frac{P_{ic}}{K_c}} \sum_{k'=1}^{K_c} \frac{\boldsymbol{h}_{c_k}^{\mathrm{T}} \widehat{\boldsymbol{h}}_{c_{k'}}^{*} q_{k'}}{\|\widehat{\boldsymbol{h}}_{c_{k'}}\|} + \sqrt{\frac{P_p}{K_p}} \sum_{j=1}^{K_p} \frac{\boldsymbol{g}_{p_k}^{\mathrm{T}} \boldsymbol{h}_{p_j}^{*} s_j}{\|\boldsymbol{h}_{p_j}\|} + n_k. \tag{2.11}$$

Using the fact that $\boldsymbol{h}_{c_k} = s_s \widehat{\boldsymbol{h}}_{c_k} + \sqrt{1 - s_s^2} \widetilde{\boldsymbol{h}}_{c_k}$ and considering availability of only statistical CSI at the CUs, (2.11) can be re-written as

$$\begin{aligned} y_{c_k} = & \underbrace{\mathbb{E}\left(\sqrt{\frac{P_{ic}}{K_c}} s_s \|\widehat{\boldsymbol{h}}_{c_k}\|\right) q_k}_{①} + \underbrace{\sqrt{\frac{P_{ic}(1-s_s^2)}{K_c}} \frac{\widetilde{\boldsymbol{h}}_{c_k}^{\mathrm{T}} \widehat{\boldsymbol{h}}_{c_k}^{*} q_k}{\|\widehat{\boldsymbol{h}}_{c_k}\|}}_{②} + \underbrace{\sqrt{\frac{P_{ic}}{K_c}} \sum_{k' \neq k}^{K_c} \frac{\boldsymbol{h}_{c_k}^{\mathrm{T}} \widehat{\boldsymbol{h}}_{c_{k'}}^{*} q_{k'}}{\|\widehat{\boldsymbol{h}}_{c_{k'}}\|}}_{③} \\ & + \underbrace{\sqrt{\frac{P_{ic}}{K_c}} s_s \|\widehat{\boldsymbol{h}}_{c_k}\| q_k - \mathbb{E}\left(\sqrt{\frac{P_{ic}}{K_c}} s_s \|\widehat{\boldsymbol{h}}_{c_k}\|\right) q_k}_{④} + \underbrace{\sqrt{\frac{P_p}{K_p}} \sum_{j=1}^{K_p} \frac{\boldsymbol{g}_{p_k}^{\mathrm{T}} \boldsymbol{h}_{p_j}^{*} s_j}{\|\boldsymbol{h}_{p_j}\|}}_{⑤} + \underbrace{n_k}_{⑥}. \end{aligned} \tag{2.12}$$

Based on the use-and-forget bound [55] and corresponding to the proposed power adaptation

[2]In the analysis that ensues, our focus is on evaluating the performance of IOP constrained CUs under imperfect and/or incomplete CSI at the cognitive BS. Therefore, we assume that primary BS know its channels perfectly to the K_p PUs [31].

policy in (2.8), the signal to interference plus noise ratio (SINR) at the k^{th} CU is written as

$$\text{SINR}_k^{ic}=\frac{\left|\mathbb{E}\left(\sqrt{\frac{P_{ic}}{K_c}}s_s\|\widehat{\boldsymbol{h}}_{c_k}\|\right)\right|^2\mathbb{E}\left(|q_k|^2\right)}{\left(\begin{array}{l}\mathbb{E}\left|\sqrt{\frac{P_{ic}(1-s_s^2)}{K_c}}\frac{\widetilde{\boldsymbol{h}}_{c_k}^{\mathrm{T}}\widehat{\boldsymbol{h}}_{c_k}^{*}q_k}{\|\widehat{\boldsymbol{h}}_{c_k}\|}\right|^2+\mathbb{E}\left|\sum\limits_{k'\neq k}^{K_c}\sqrt{\frac{P_{ic}}{K_c}}\frac{\boldsymbol{h}_{c_k}^{\mathrm{T}}\widehat{\boldsymbol{h}}_{c_{k'}}^{*}q_{k'}}{\|\widehat{\boldsymbol{h}}_{c_{k'}}\|}\right|^2+\mathbb{E}\left|\sqrt{\frac{P_{ic}}{K_c}}s_s\|\widehat{\boldsymbol{h}}_{c_k}\|q_k-\mathbb{E}\left(\sqrt{\frac{P_{ic}}{K_c}}s_s\|\widehat{\boldsymbol{h}}_{c_k}\|\right)q_k\right|^2\\ +\mathbb{E}\left|\sum\limits_{j=1}^{K_p}\sqrt{\frac{P_p}{K_p}}\frac{\boldsymbol{g}_{p_k}^{\mathrm{T}}\boldsymbol{h}_{p_j}^{*}s_j}{\|\boldsymbol{h}_{p_j}\|}\right|^2+\mathbb{E}|n_k|^2\end{array}\right)}. \tag{2.13}$$

We can clearly observe that SINR_k^{ic} is a function of I_p, s_s and the back-off factor η, which in turn depends on s_p, K_p and the target P_o. The achievable sum SE of the CUs is obtained by simplifying the SINR expression in (2.13) and is stated next as a Theorem.

Theorem 2.2. *The DL achievable sum SE of the CUs under imperfect and complete CSI while satisfying an IOP of P_o at PUs is given by*

$$SE^{ic}=\sum_{k=1}^{K_c}\log_2\left(1+SINR_k^{ic}\right), \tag{2.14}$$

where

$$SINR_k^{ic}=\frac{\frac{s_s^2\gamma_k}{K_c}\left(\zeta_{ic}\frac{\Gamma\left(N+\frac{1}{2}\right)}{\Gamma(N)}\right)^2}{\frac{(1-s_s^2)\gamma_k\psi_{ic}}{K_c}+\frac{\psi_{ic}\gamma_k(K_c-1)}{K_c}+\frac{s_s^2\gamma_k}{K_c}\left[N\psi_{ic}-\left(\zeta_{ic}\frac{\Gamma\left(N+\frac{1}{2}\right)}{\Gamma(N)}\right)^2\right]+P_p\phi_k+1}, \tag{2.15}$$

$\zeta_{ic}=\mathbb{E}\left(\sqrt{P_{ic}}\right)=\mathbb{E}\left(\sqrt{\frac{\bar{I}_p}{\eta X}}\right)\approx\sqrt{\frac{\bar{I}_p}{\eta}}\left(\frac{1}{\mathbb{E}\left(\sqrt{X}\right)}+\frac{\mathbb{V}\text{ar}\left(\sqrt{X}\right)}{\left(\mathbb{E}\left(\sqrt{X}\right)\right)^3}\right)$ *[56]*, $X=\max\limits_{1\leq k\leq K_p}\left(\widehat{Z}_k\right)$, $\mathbb{E}\left(\sqrt{X}\right)=\int_0^\infty\frac{1}{2\sqrt{x}}\left(1-F_X(x)\right)dx$, *and* $\mathbb{V}\text{ar}\left(\sqrt{X}\right)=\int_0^\infty\left(1-F_X(x)\right)dx-\left(\mathbb{E}\left(\sqrt{X}\right)\right)^2$ *[22]. Note that* $F_X(x)=\frac{1}{\left(\Gamma(K_c)\right)^{K_p}}\prod_{i=1}^{K_p}\gamma\left(K_c,\frac{K_cx}{\alpha_i}\right)$. *Furthermore,* $\psi_{ic}=\mathbb{E}\left(P_{ic}\right)=\mathbb{E}\left(\frac{\bar{I}_p}{\eta X}\right)\approx\frac{\bar{I}_p}{\eta}\left(\frac{1}{\mathbb{E}(X)}+\frac{\mathbb{V}\text{ar}(X)}{\left(\mathbb{E}(X)\right)^3}\right)$ *[56],* $\mathbb{E}\left(X\right)=\int_0^\infty\left(1-F_X(x)\right)dx$ *and* $\mathbb{V}\text{ar}\left(X\right)=\int_0^\infty 2x\left(1-F_X(x)\right)dx-\left(\mathbb{E}\left(X\right)\right)^2$ *[22].*

Proof. The derivation is given in Appendix A.2. □

Remarks: Please note that the sum SE above is a function of only the deterministic constants such as s_s, γ_k, K_c, N, ϕ_k, P_p and also depends on deterministic statistical parameters such as ζ_{ic} and ψ_{ic}. It is analytically intractable to obtain ζ_{ic} and ψ_{ic} in closed-form. Thus, we obtain the sum SE analytically using (2.15) by evaluating ζ_{ic} and ψ_{ic} through numerical integration [57], [58]. We also cross-validate this against sum SE obtained via Monte Carlo simulations in Section 2.7.

Asymptotic Analysis: We next analyze the sum SE of the CUs in the asymptotic regime, i.e., in the regime where the number of cognitive BS antennas and the number of primary BS

antennas grow to infinity. As $N \to \infty$, by weak law of large numbers, $\frac{1}{N}\widehat{\boldsymbol{h}}_{c_k}^{\mathrm{T}}\widehat{\boldsymbol{h}}_{c_i}^{*} \to \gamma_k$ for $k = i$ and $\frac{1}{N}\widehat{\boldsymbol{h}}_{c_k}^{\mathrm{T}}\widehat{\boldsymbol{h}}_{c_i}^{*} \to 0$ for $k \neq i$. Furthermore, $\frac{1}{N}\widetilde{\boldsymbol{h}}_{c_k}^{\mathrm{T}}\widehat{\boldsymbol{h}}_{c_k}^{*} \to 0$, since channel estimate is uncorrelated to estimation error and both are zero mean random vectors and $\frac{1}{N}\boldsymbol{h}_{c_k}^{\mathrm{T}}\widehat{\boldsymbol{h}}_{c_i}^{*} \to 0$ for $k \neq i$. Furthermore, $\frac{1}{M}\boldsymbol{g}_{p_k}^{\mathrm{T}}\boldsymbol{h}_{p_k}^{*} \to 0$ as $M \to \infty$, since $\boldsymbol{g}_{p_k}$ corresponds to the channel from the primary BS to the k^{th} CU and this is independent to the channel $\boldsymbol{h}_{p_k}$ from the primary BS to the k^{th} PU. Therefore, in the asymptotic regime, the sum SE of the CUs under imperfect and complete CSI simplifies to

$$\mathrm{SE}^{ic} = K_c \log_2\left(1 + \frac{\zeta_{ic}^2}{\psi_{ic} - \zeta_{ic}^2}\right). \tag{2.16}$$

We observe that in the asymptotic regime, the effects of channel estimation error, co-channel interference among CUs, noise and the interference at the CUs due to primary transmissions vanishes.

2.5 Analysis With Incomplete CSI

In a co-located mMIMO based underlay spectrum access system, the cognitive BS operating in the unlicensed frequency band must acquire knowledge of its interference channels to the K_p PUs in order to control interference caused to the PUs. When there are multiple PUs operating in the network, the process of acquiring CSI to all the PUs in a timely and scalable manner is a practically challenging task. This is because as the number of PUs in the network increases, more and more resources need to be devoted to estimate the CSI [59]. In this section, in order to obtain insights, we first analyze the perfect and incomplete CSI scenario in which the cognitive BS knows the channels to only a subset of the PUs but knows them perfectly, i.e., without any channel estimation errors. We then generalize the analysis to the imperfect and incomplete CSI scenario in which the cognitive BS knows only a noisy version of the CSI to a subset of PUs.

2.5.1 Impact of Perfect and Incomplete CSI

Let $\mathcal{S}$ denote the set of PUs to which the cognitive BS knows the channels perfectly, i.e., in this scenario, the cognitive BS knows the channels to only $S = |\mathcal{S}|$ out of the K_p PUs, where $S \leq K_p$. We propose the use of the following back-off factor based power adaptation policy in

which the cognitive BS transmits with power P_{pi} given by

$$P_{pi} = \frac{\bar{I}_p}{\eta \max\limits_{k\in\mathcal{S}} \left\{ \frac{1}{K_c} \sum_{i=1}^{K_c} \left| \frac{\boldsymbol{g}_{c_k}^{\mathrm{T}} \boldsymbol{h}_{c_i}^{*}}{\|\boldsymbol{h}_{c_i}\|} \right|^2 \right\}}. \tag{2.17}$$

Under this policy, the back-off factor η is chosen to ensure that

$$\Pr(I_{p_1} \le \bar{I}_p, I_{p_2} \le \bar{I}_p, \ldots, I_{p_{K_p}} \le \bar{I}_p) = 1 - P_o \,, \tag{2.18}$$

where the interference power I_{pk} at the k^{th} PU equals

$$I_{p_k} = \frac{P_{pi}}{K_c} \sum_{i=1}^{K_c} \left| \frac{\boldsymbol{g}_{c_k}^{\mathrm{T}} \boldsymbol{h}_{c_i}^{*}}{\|\boldsymbol{h}_{c_i}\|} \right|^2 . \tag{2.19}$$

We next state a mathematical expression to evaluate P_o in this scenario.

Theorem 2.3. *The complement of IOP under perfect and incomplete CSI is given by*

$$(1 - P_o) = \sum_{k\in\mathcal{S}} \sum_{l=1}^{L} \frac{w_l \, y_l^{K_c - 1}}{(\Gamma(K_c))^{K_p}} \prod_{k' \notin \mathcal{S}} \gamma\left(K_c, \frac{y_l \alpha_k \eta}{\alpha_{k'}}\right) \left[\prod_{\substack{i\in\mathcal{S} \\ i\neq k}} \gamma\left(K_c, \frac{y_l \alpha_k}{\alpha_i}\right) \right]. \tag{2.20}$$

Proof. The derivation is given in Appendix A.3. □

Remarks: Based on this theorem, given a target P_o and the number $S = |\mathcal{S}|$ of PUs to which the channels are known perfectly, the wireless system designer can decide on the back-off factor or power margin η which ensures that the interference power does not exceed the threshold $\bar{I}_p$ more than P_o fraction of the time at any of the K_p PUs. Note that $(1 - P_o)$ equals 1 when $S = K_p$ and when perfect CSI is available.

The signal received at the k^{th} CU with perfect and incomplete CSI at the cognitive BS is

$$y_{c_k} = \sqrt{\frac{P_{pi}}{K_c}} \sum_{k'=1}^{K_p} \frac{\boldsymbol{h}_{c_k}^{\mathrm{T}} \boldsymbol{h}_{c_{k'}}^{*} q_{k'}}{\|\boldsymbol{h}_{c_{k'}}\|} + \sqrt{\frac{P_p}{K_p}} \sum_{j=1}^{K_c} \frac{\boldsymbol{g}_{p_k}^{\mathrm{T}} \boldsymbol{h}_{p_j}^{*} s_j}{\|\boldsymbol{h}_{p_j}\|} + n_k. \tag{2.21}$$

Considering availability of statistical CSI, signal received at the k^{th} CU can be re-arranged as

$$y_{c_k} = \underbrace{\mathbb{E}\left(\sqrt{\frac{P_{pi}}{K_c}} \|\boldsymbol{h}_{c_k}\| \right) q_k}_{①} + \underbrace{\sqrt{\frac{P_{pi}}{K_c}} \|\boldsymbol{h}_{c_k}\| q_k - \mathbb{E}\left(\sqrt{\frac{P_{pi}}{K_c}} \|\boldsymbol{h}_{c_k}\| \right) q_k}_{②} + \underbrace{\sqrt{\frac{P_{pi}}{K_c}} \sum_{k'\neq k}^{K_p} \frac{\boldsymbol{h}_{c_k}^{\mathrm{T}} \boldsymbol{h}_{c_{k'}}^{*}}{\|\boldsymbol{h}_{c_{k'}}\|} q_{k'}}_{③}$$

$$+ \underbrace{\sqrt{\frac{P_p}{K_p}} \sum_{j=1}^{K_c} \frac{\boldsymbol{g}_{p_k}^{\mathrm{T}} \boldsymbol{h}_{p_j}^{*} s_j}{\|\boldsymbol{h}_{p_j}\|}}_{④} + \underbrace{n_k}_{⑤}. \quad (2.22)$$

All the terms in the equation (2.22) are mutually uncorrelated. Thus, SINR at the k^{th} CU equals (2.23).

$$SINR_k^{pi} = \frac{\left|\mathbb{E}\left(\sqrt{\frac{P_{pi}}{K_c}}\|\widehat{\boldsymbol{h}}_{c_k}\|\right)\right|^2 \mathbb{E}\left(|q_k|^2\right)}{\mathbb{E}\left|\sum\limits_{k'\neq k}^{K_c} \sqrt{\frac{P_{pi}}{K_c}} \frac{\boldsymbol{h}_{c_k}^{\mathrm{T}} \boldsymbol{h}_{c_{k'}}^{*} q_{k'}}{\|\widehat{\boldsymbol{h}}_{c_{k'}}\|}\right|^2 + \mathbb{E}\left|\sqrt{\frac{P_{pi}}{K_c}} s_s \|\boldsymbol{h}_{c_k}\| q_k - \mathbb{E}\left(\sqrt{\frac{P_{pi}}{K_c}} s_s \|\boldsymbol{h}_{c_k}\|\right) q_k\right|^2 + \mathbb{E}\left|\sum\limits_{j=1}^{K_p} \sqrt{\frac{P_p}{K_p}} \frac{\boldsymbol{g}_{p_k}^{\mathrm{T}} \boldsymbol{h}_{p_j}^{*} s_j}{\|\boldsymbol{h}_{p_j}\|}\right|^2 + \mathbb{E}|n_k|^2}. \quad (2.23)$$

Note that $SINR_k^{pi}$ is a function of η which in turn depends on the target P_o and the number of channels S that are known perfectly to the cognitive BS. We use this expression to compute the DL sum SE of the CUs in this scenario and state next as Theorem.

Theorem 2.4. *The DL achievable sum SE of CUs under perfect and incomplete CSI while satisfying an IOP of P_o at the PUs equals*

$$SE^{pi} = \sum_{k=1}^{K_c} \log_2\left(1 + SINR_k^{pi}\right), \quad (2.24)$$

where

$$SINR_k^{pi} = \frac{\frac{1}{K_c}\left(\zeta_{pi} \frac{\sqrt{\gamma_k}\,\Gamma\left(N+\frac{1}{2}\right)}{\Gamma(N)}\right)^2}{\frac{1}{K_c}\left[\psi_{pi} N\gamma_k - \left(\zeta_{pi} \frac{\sqrt{\gamma_k}\,\Gamma\left(N+\frac{1}{2}\right)}{\Gamma(N)}\right)^2\right] + \frac{\psi_{pi}}{K_c}\left(K_c - 1\right)\gamma_k + P_p\phi_k + 1}. \quad (2.25)$$

And ζ_{pi} and ψ_{pi} are computed the same way as in Theorem 2.2 with 'ic' replaced with 'pi' , K_p replaced with $S = |\mathcal{S}|$ and $X = \max\limits_{k\in\mathcal{S}}(Z_k)$.

Proof. The derivation is given in Appendix A.4. □

Remarks: The lower the value of S relative to K_p, the greater is the back-off needed in order to ensure that P_o is maintained at the same level. The reduction in the power due to back-off results in a loss in sum SE of the CUs, however this loss can be recovered by deploying more antennas at the cognitive BS.

Asymptotic Analysis: In the asymptotic regime, based on results outlined in Section 2.4,

sum SE of CUs under perfect and incomplete CSI simplifies to

$$\mathrm{SE}^{pi} = K_c \log_2\left(1 + \frac{\zeta_{pi}^2}{\psi_{pi} - \zeta_{pi}^2}\right). \tag{2.26}$$

2.5.2 Impact of Imperfect and Incomplete CSI

We now consider a scenario where the cognitive BS has an estimate of the interference channels to only a subset of the PUs. As stated before, let $\mathcal{S}$ be the set of PUs to which the cognitive BS knows the channels with estimation errors where $|\mathcal{S}| \leq K_p$. Under this scenario, the power P_{ii} with which the cognitive BS essentially transmits is given by

$$P_{ii} = \frac{\bar{I}_p}{\eta \max\limits_{k\in\mathcal{S}} \left\{ \frac{1}{K_c} \sum\limits_{i=1}^{K_c} \left| \frac{\widehat{\boldsymbol{g}}_{c_k}^{\mathrm{T}} \widehat{\boldsymbol{h}}_{c_i}^{*}}{\|\widehat{\boldsymbol{h}}_{c_i}\|} \right|^2 \right\}}, \tag{2.27}$$

where η is chosen such that the IOP constraint under incomplete and imperfect CSI is met with equality for a target P_o. In other words, given P_o, K_p and s_p, the back-off factor η is chosen such that

$$\Pr(\widehat{I}_{p_1} \leq \bar{I}_p, \widehat{I}_{p_2} \leq \bar{I}_p, \ldots, \widehat{I}_{p_{K_p}} \leq \bar{I}_p) = 1 - P_o\,, \tag{2.28}$$

where the interference power in this scenario equals

$$\widehat{I}_{p_k} = \frac{P_{ii}}{K_c} \sum_{i=1}^{K_c} \left| \frac{\boldsymbol{g}_{c_k}^{\mathrm{T}} \widehat{\boldsymbol{h}}_{c_i}^{*}}{\|\widehat{\boldsymbol{h}}_{c_i}\|} \right|^2. \tag{2.29}$$

The power with which cognitive BS transmits now depends on the channel estimates of the S available links. We state a lower bound on the complement of P_o next as a Theorem.

Theorem 2.5. *A lower bound $P_{L_{(ii)}}$ on the complement of IOP under imperfect and incomplete CSI is given by*

$$(1 - P_o) \geq P_{L_{(ii)}} = \left[1 - \sum_{k\in\mathcal{S}} \sum_{l=1}^{L} \frac{w_l x_l^{K_c-1}}{\Gamma(K_c)} \prod_{\substack{j\in\mathcal{S} \\ j\neq k}} \frac{\gamma\left(K_c, \frac{x_l\alpha_k}{\eta\alpha_j}\right)}{\Gamma(K_c)} \left(1 - Q_{K_c}\left(\sqrt{\frac{2\rho x_l}{(1-\rho)}}, \sqrt{\frac{2x_l}{\eta(1-\rho)}}\right)\right)\right] \times \left[\sum_{k\in\mathcal{S}} \sum_{l=1}^{L} \frac{w_l\, y_l^{K_c-1}}{(\Gamma(K_c))^{K_p}} \prod_{k'\notin\mathcal{S}} \gamma\left(K_c, \frac{y_l\alpha_k\eta}{\alpha_{k'}}\right) \left[\prod_{\substack{i\in\mathcal{S} \\ i\neq k}} \gamma\left(K_c, \frac{y_l\alpha_k}{\alpha_i}\right)\right]\right]. \tag{2.30}$$

Proof. The derivation is given in Appendix A.5. □

With imperfect and incomplete CSI and with the proposed power adaptation policy, the SINR at the k^{th} CU is identical to (2.13) with P_{ic} replaced by P_{ii}. And the achievable sum spectral efficiency of the CUs under this scenario is stated next as a Theorem.

Theorem 2.6. *The DL achievable sum SE of the CUs under imperfect and incomplete CSI while satisfying an IOP of P_o at the PUs is given by*

$$SE^{ii} = \sum_{k=1}^{K_c} \log_2\left(1 + SINR_k^{ii}\right), \tag{2.31}$$

where

$$SINR_k^{ii} = \frac{\frac{s_s^2\gamma_k}{K_c}\left(\zeta_{ii}\frac{\Gamma\left(N+\frac{1}{2}\right)}{\Gamma(N)}\right)^2}{\frac{\left(1-s_s^2\right)\gamma_k\psi_{ii}}{K_c} + \frac{\psi_{ii}\gamma_k(K_c-1)}{K_c} + \frac{s_s^2\gamma_k}{K_c}\left[N\psi_{ii} - \left(\zeta_{ii}\frac{\Gamma\left(N+\frac{1}{2}\right)}{\Gamma(N)}\right)^2\right] + P_p\phi_k + 1}. \tag{2.32}$$

And ζ_{ii} and ψ_{ii} are computed the same way as in Theorem 2.2 with 'ic' replaced with 'ii' and K_p replaced with $S = |\mathcal{S}|$.

Proof. This can be derived along similar lines as is done in Appendix A.2. □

Asymptotic Analysis: In the asymptotic regime, based on results outlined in Section 2.4, sum SE of CUs under imperfect and incomplete CSI simplifies to

$$\text{SE}^{ii} = K_c \log_2\left(1 + \frac{\zeta_{ii}^2}{\psi_{ii} - \zeta_{ii}^2}\right). \tag{2.33}$$

2.6 Spatially Correlated Channel Scenario

In order to analyze the effect of spatial correlation on IOP at the PUs and the sum SE at the CUs, we generate the channel covariance matrices for the channels from cognitive BS to CUs, cognitive BS to PUs, primary BS to PUs and primary BS to CUs using the Gaussian local scattering model [60]. For this model, the spatial correlation matrix for the channel from the cognitive BS to the k^{th} user is given by

$$\left[\mathbf{R}_k^{cu}\right]_{l,m} = \varpi_k^c e^{j2\pi d_H(l-m)\sin\left(\theta_k^{cu}\right)} e^{-\frac{\sigma_\theta^2}{2}\left(2\pi d_H(l-m)\cos\left(\theta_k^{cu}\right)\right)^2}, \tag{2.34}$$

where $u \in \{c, p\}$, the large-scale fading coefficient $\varpi_k^c \in \{\gamma_k, \alpha_k\}$, and the nominal angle of arrival (AoA) in the azimuthal plane $\theta_k^{cu} \in \{\theta_k^{cc}, \theta_k^{cp}\}$, depending on whether we consider the channel to any CU or to any PU. Furthermore, $l, m \in \{1, 2 \ldots, N\}$, where N denotes the number of antennas at the cognitive BS, d_H denotes the spacing among the antenna elements in the array and the parameter σ_θ referred to as the angular standard deviation captures spatial correlation. A lower value of σ_θ signifies larger spatial correlation [60]. Similarly, based on this model, the spatial correlation matrix for the channel from the primary BS to the k^{th} user is given by

$$\left[\mathbf{R}_k^{pu}\right]_{l,m} = \varpi_k^p e^{j2\pi d_H(l-m)\sin\left(\theta_k^{pu}\right)} e^{-\frac{\sigma_\theta^2}{2}\left(2\pi d_H(l-m)\cos\left(\theta_k^{pu}\right)\right)^2}, \tag{2.35}$$

where $u \in \{c, p\}$, the large-scale fading coefficient $\varpi_k^p \in \{\phi_k, \beta_k\}$, and the nominal AoA in the azimuthal plane $\theta_k^{pu} \in \{\theta_k^{pc}, \theta_k^{pp}\}$, depending on whether we consider the channel to any CU or to any PU. Furthermore, $l, m \in \{1, 2 \ldots, M\}$, where M denotes the number of antennas at the primary BS.

2.7 Numerical Results And Discussion

In this section, we present numerical results to illustrate the impact of different system parameters such as η, s_p, s_s, S, N and K_p on P_o at the PUs and on the sum SE of the CUs under different scenarios. Unless mentioned otherwise, for illustration[3], we generate the path loss values γ_k, α_j, ϕ_k and β_j independently and uniformly distributed over the interval -30 dB to -60 dB for $1 \leq k \leq K_c$ and for $1 \leq j \leq K_p$, $\sigma^2 = 1$, $M = 100$, $K_c = 10$ and $K_p = 10$ [31, 55]. Furthermore, we take $\bar{I}_p = 10$ dB, $P_p = 10$ dB, $s_s \in \{0.4, 0.6, 0.8, 1\}$, $s_p \in \{0.4, 0.6, 0.8, 1\}$ [31], $S \in \{5, 7, 10\}$ [20] and $\sigma_\theta \in \{10°, 30°\}$ [60].

Figure 2.2 plots $(1 - P_o)$ vs. η for $K_p = 10$, $K_c = 10$ and for two different values of s_p, namely, 0.6 and 0.8. We obtain exact curves through Monte Carlo simulation of (2.9). We also plot the lower bound obtained through (2.10). Please note that the lower bound is quite tight for $P_o \leq 0.2$ and we expect the target P_o at PUs to be lower than 20% in underlay spectrum access networks.[4] As the back-off factor increases, P_o decreases because the cognitive BS transmits at

[3] Please note that our mathematical analysis is in general valid for any practical simulation parameter values.

[4] The lower bound is very tight in the regime of interest where these underlay spectrum access networks are

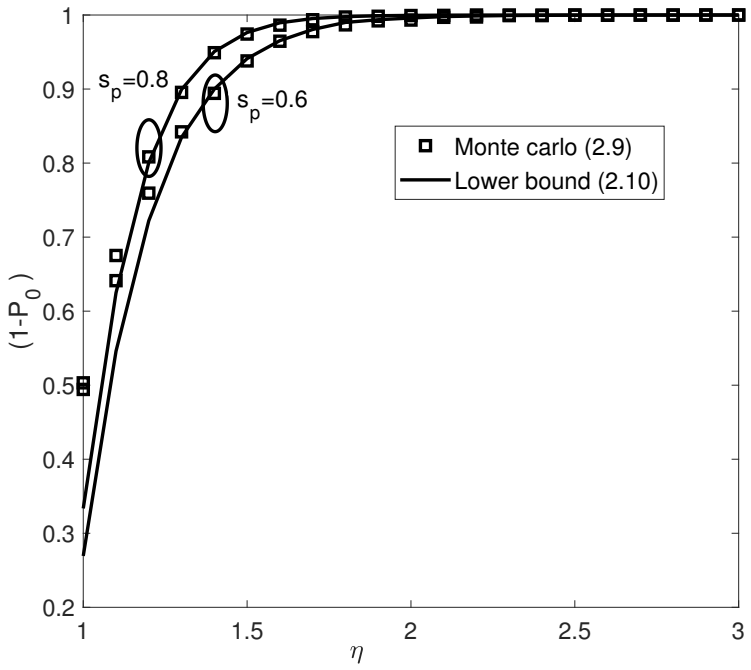

Fig. 2.2: Imperfect and Complete CSI: Impact of s_p and η on P_o ($K_p = 10$, $N = 100$ and $K_c = 10$)

a lower power. Furthermore, with the increase in s_p, the quality of channel estimates improves. Therefore, the cognitive BS violates the target P_o less often. Thus, for larger estimation errors, greater amount of back-off in power is required at cognitive BS to keep P_o at the same level. Please note that η is not affected by changes in s_s for a given P_o, since the transmit power of the cognitive BS is a function of only the channels between the cognitive BS and the K_p PUs and is independent of the channel to the CUs as also outlined in Theorem 2.1.[5]

Figure 2.3 plots $(1 - P_o)$ vs. η for $s_p = 0.4$ and 0.8, $K_c = 10$, $K_p = 10$ and for three different values of the number of cognitive BS antennas N, namely 100, 300 and 500 based on the lower bound in Theorem 1. We observe that for a given s_p, P_o is independent of N and depends only on η because of scaling by the norm of the channel vector from the cognitive BS to CUs in the MR precoder used at the cognitive BS. This result gives us an interesting design insight that the IOP at the PUs remains unaffected to changes in the number of cognitive BS antennas N. As before, a larger back-off is required to maintain P_o at the same level as s_p decreases, i.e., as the

expected to operate, i.e., in the regime ($P_o \leq 0.2$) where the interference outage probability is small enough to ensure minimal interference to PUs.

[5] P_o is independent of P_p and $\bar{I}_p$.

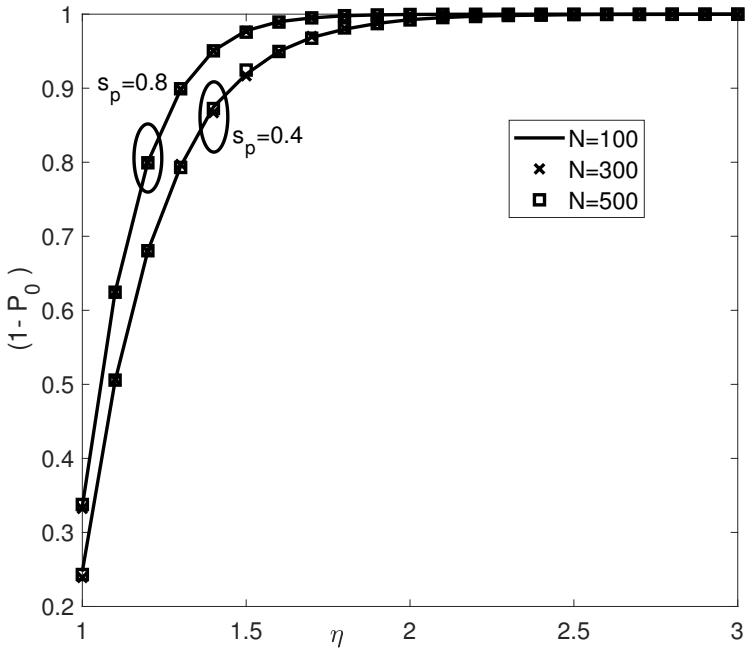

Fig. 2.3: Imperfect and Complete CSI: Impact of N and η on P_o ($K_p = 10$ and $K_c = 10$).

channel estimation error increases.

Figure 2.4 plots the sum SE (SE^{ic}) vs. N for different $(\eta, 1 - P_o)$ sampled from Figure 2.2. We show SE^{ic} using the analytical expression for SINR in (2.15) and cross-validate through Monte Carlo simulations based on SINR expression given in (2.13). The design insight that we obtain based on this result is that, for a given value of s_p and s_s, we can reduce P_o while maintaining a fixed value of SE^{ic} by deploying more antennas at the cognitive BS. For example, by increasing N from 107 to 116, we can reduce P_o from 20% to 3% while keeping the sum SE fixed at 25 (bits/s/Hz) for $s_s = 0.8$. In order to reduce P_o, the cognitive BS lowers its transmit power based on the proposed back-off power policy. The subsequent reduction in SE^{ic} due to a larger back-off at the cognitive BS is compensated by deploying more antennas at the cognitive BS. Furthermore, as s_s reduces, estimation error increases and sum SE of the CUs decreases.

Figure 2.5 plots $(1 - P_o)$ vs. η for $s_p = 0.8$ and for different values of K_p under imperfect and complete CSI. We observe that for a fixed value of η, P_o is equal to or higher with $K_p = 10$ when compared to $K_p = 20$. This is because with $K_p = 20$, the cognitive BS transmits at a reduced power as can be seen from (2.8), since the maximum value of a set consisting of 20

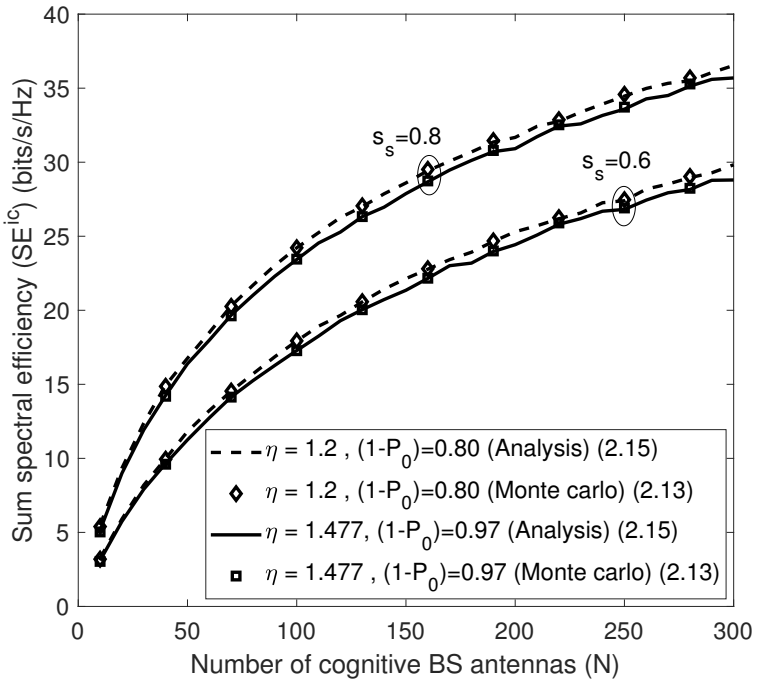

Fig. 2.4: Imperfect and Complete CSI: Impact of s_s, P_o and N on SE^{ic} ($s_p = 0.8$, $K_p = 10$, $K_c = 10$, $M = 100$, $\bar{I}_p = 10$ dB and $P_p = 10$ dB.)

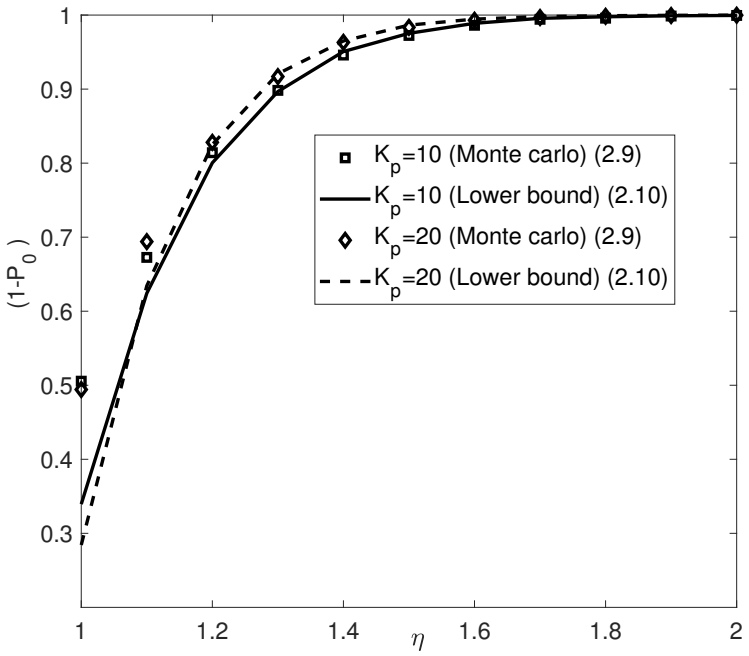

Fig. 2.5: For Imperfect and Complete CSI: Impact of K_p on P_o ($s_p = 0.8$, $N = 100$ and $K_c = 10$).

random channel coefficients is likely to be larger than the maximum value of a set with 10 random channel coefficients corresponding to $K_p = 10$.

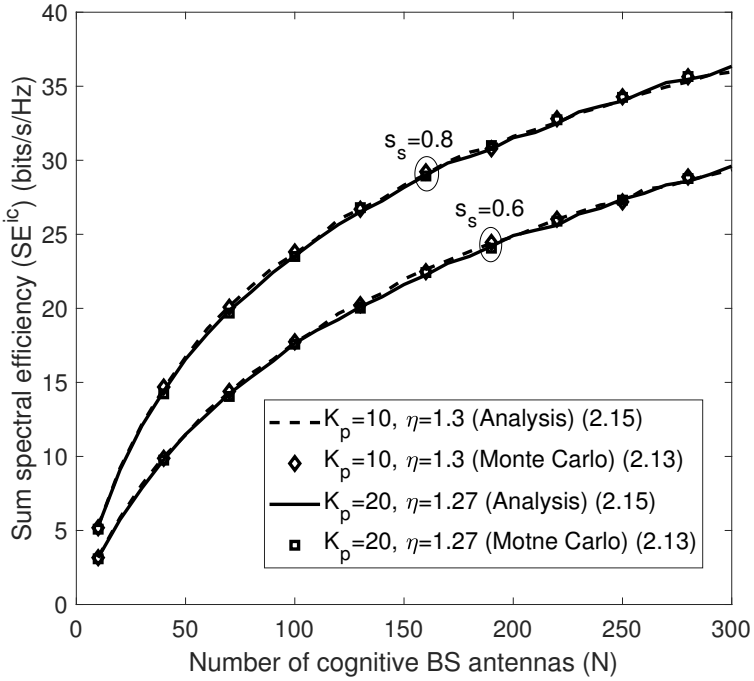

Fig. 2.6: For Imperfect and Complete CSI: Impact of K_p, N and η on SE^{ic} ($(1 - P_o) = 0.9$, $s_p = 0.8$, $K_c = 10$, $M = 100$, $\bar{I}_p = 10$ dB and $P_p = 10$ dB).

Figure 2.6 plots SE^{ic} vs. N for different $\left(K_p, \eta\right)$ sampled from Figure 2.5. We obtain SE^{ic} using the analytical expression for SINR in (2.15) and cross-validate through Monte Carlo simulations based on SINR expression given in (2.13). We observe as K_p increases, the sum SE (SE^{ic}) of CUs under imperfect and complete CSI decreases marginally since the cognitive BS transmits at a reduced power. Also, SE^{ic} decreases as s_s decreases, due to degradation in the quality of the channel estimates. Another important insight that we obtain is that even if the number of PUs increases, $(1 - P_o)$ and SE^{ic} can be kept fixed by deploying slightly more number of antennas at the BS. For example, for $s_s = 0.8$ and $P_o = 0.1$, we can accommodate ten more PUs in the network while keeping the DL sum SE of the CUs fixed at 20 (bits/s/Hz) by increasing N from 69 to 72.

Figure 2.7 plots $(1 - P_o)$ vs. η for $K_p = 10$ and for different S considering that the cognitive BS has perfect CSI to S out of the K_p PUs. We obtain the curves corresponding to the analytical

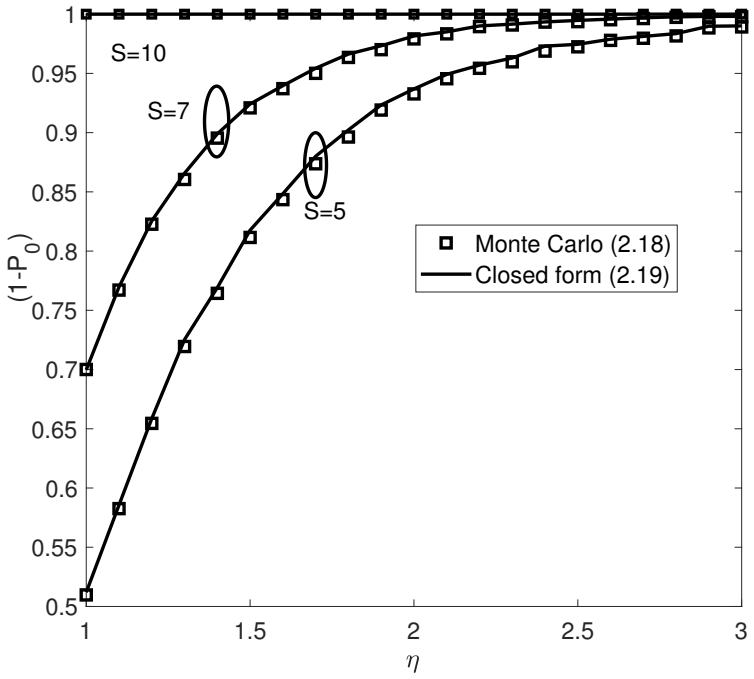

Fig. 2.7: Perfect and incomplete CSI: Impact of S on $(1-P_o)$ ($s_p = 0.8$, $K_p = 10$, $K_c = 10$ and $N = 100$).

expression in (2.20) and cross-validate it via Monte Carlo simulation based on (2.18). We observe that as the number of channels in set $\mathcal{S}$ (known perfectly to the cognitive BS) increases, P_o reduces. This is primarily because as S increases, the cognitive BS violates the IOP constraint less often. In other words, the lesser the number of channels that are known perfectly to the cognitive BS, the larger is the back-off required to maintain P_o at the same level.

Figure 2.8 plots $(1 - P_o)$ vs. η for $S = 5$, $K_p = 10$, $N = 100$ and for two different values of s_p, namely, 0.4 and 0.8. We obtain exact curves through Monte Carlo simulation of (2.28) with imperfect and incomplete CSI. We also plot the lower bound obtained through the analytical expression in (2.30). We observe that even under incomplete CSI, as s_p increases, the quality of channel estimates improves and IOP constraint is violated less often.

Figure 2.9 plots the sum SE (SE^{pi}) of CUs under perfect and incomplete CSI (simulations based on SINR in (2.23) and analysis based on SINR in (2.25)) with respect to N for $s_s = 1$, for two different values of S, namely, 5 and 7 and $(\eta, 1 - P_o)$ sampled from Figure 2.7. We also plot the sum SE (SE^{ii}) of CUs under imperfect and incomplete CSI (simulations based on SINR in (2.13) with P_{ic} replaced by P_{ii} and the analysis based on SINR in (2.32)), where, $(\eta, 1 - P_o)$ is

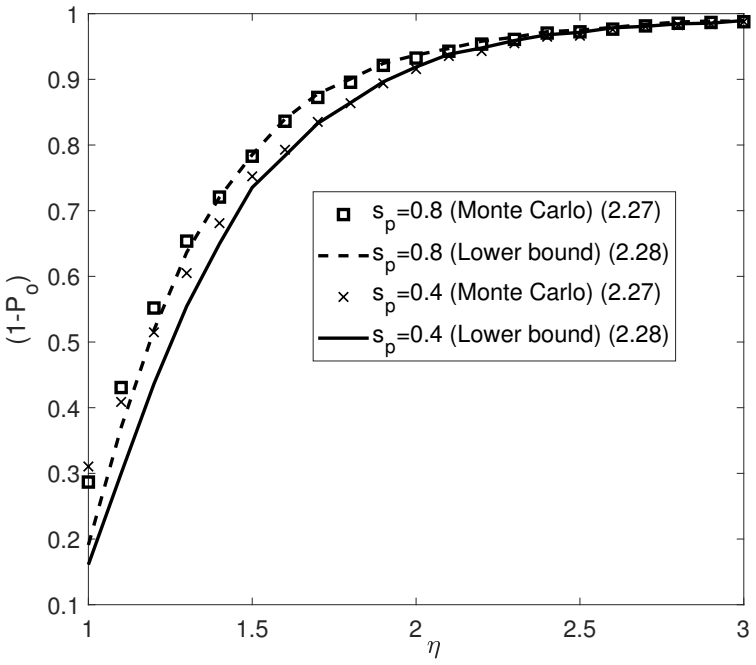

Fig. 2.8: Imperfect and incomplete CSI: Impact of s_p and η on $1 - P_o$ ($S = 5$, $K_p = 10$, $K_c = 10$ and $N = 100$).

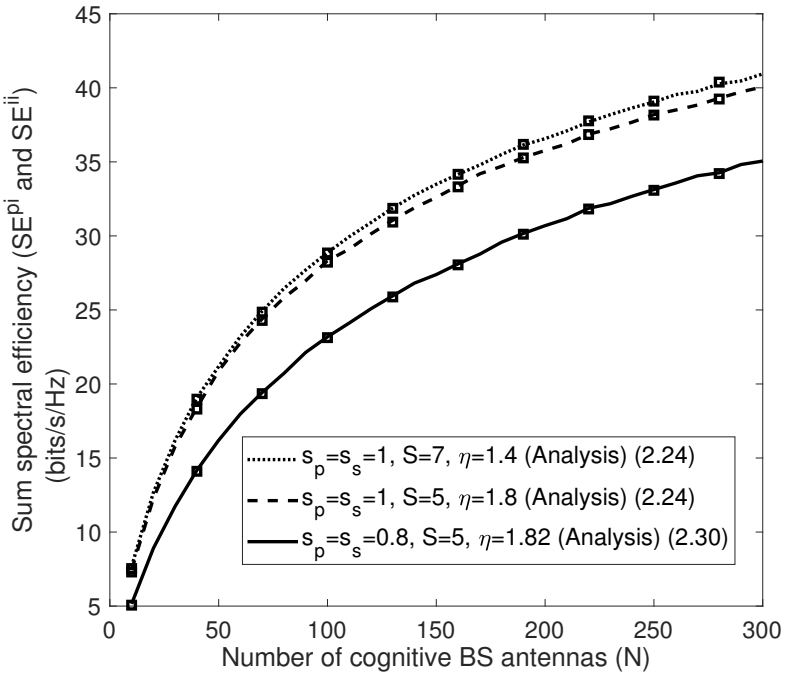

Fig. 2.9: Perfect/Imperfect and incomplete CSI: Impact of S, s_s, s_p and N on SE^{pi} and SE^{ii} $(1 - P_o) = 0.9$, $K_p = 10$, $K_c = 10$, $M = 100$, $\bar{I}_p = 10$ dB and $P_p = 10$ dB). Corresponding Monte Carlo simulations are shown using the marker □.

sampled from Figure 2.8 for $s_s = 0.8$ and $S = 5$. We observe that simulations and the analysis are in close agreement with each other. An interesting design insight that we obtain based on this result is that the sum SE of CUs and P_o can be maintained at the same level even under incomplete CSI as s_s decreases by deploying a higher N at the cognitive BS. Furthermore, the sum SE improves as S increases.

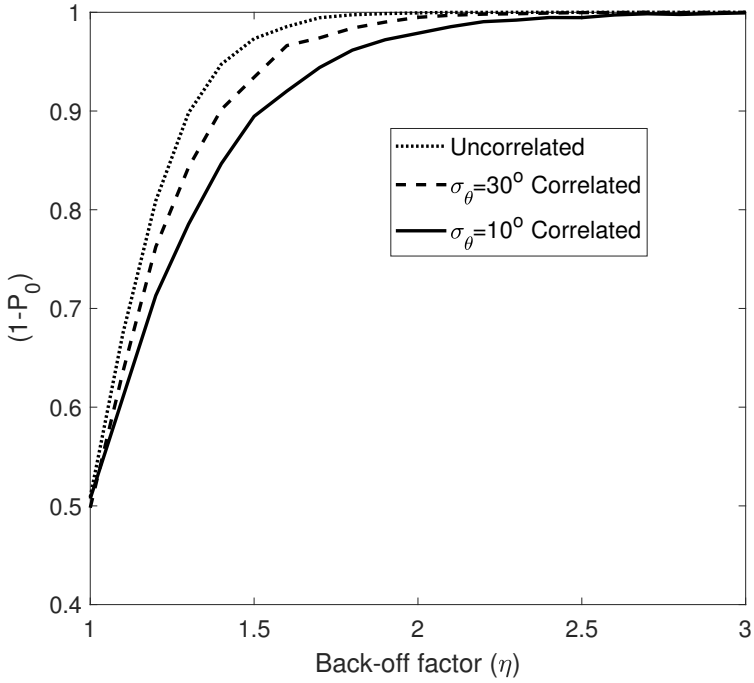

Fig. 2.10: Impact of spatial correlation on IOP ($s_p = 0.8$, $S = K_p = 10$, $K_c = 10$ and $\theta_k^{cu} = \theta_k^{pu} = 30°$ for all k).

Figure 2.10 plots $(1 - P_o)$ as a function of η for two different values of σ_θ, namely 10° and 30°. As a benchmark, we plot $(1 - P_o)$ for the uncorrelated case as well. As the angular standard deviation σ_θ decreases from 30° to 10°, the spatial correlation increases. This results into an increase in the power of the interference caused to the PUs due to transmission by the cognitive BS. This is the reason why a larger back-off is required as spatial correlation increases in order to maintain IOP at the PUs at the same target level.

Figure 2.11 plots the sum SE of the CUs as a function of N for two different values of σ_θ, namely 10° and 30°. The corresponding back-off factors obtained from the result in Figure 2.10 for $P_o = 0.03$ have also been marked in the legend. We observe that the sum SE degrades as

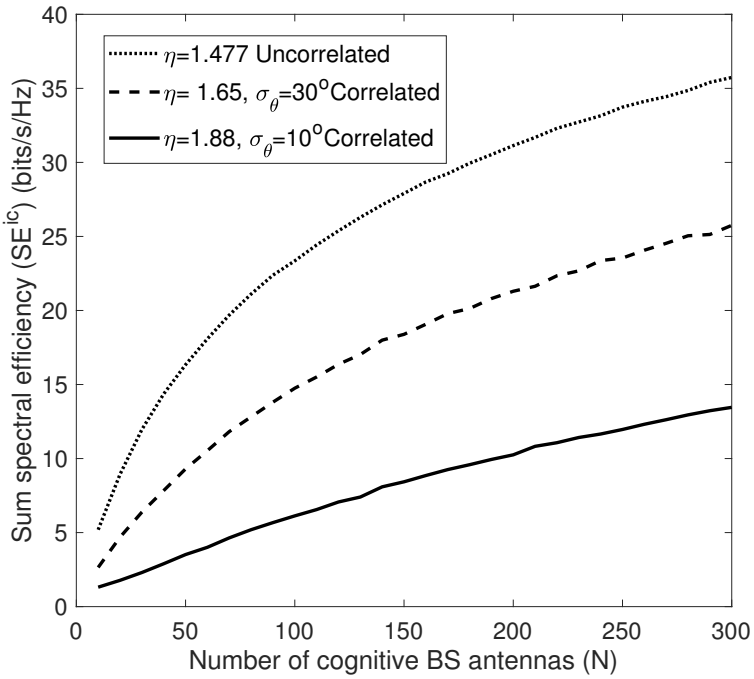

Fig. 2.11: Impact of spatial correlation on sum SE ($(1-P_o)=0.97$, $s_s=s_p=0.8$, $K_p=10$, $K_c=10$, $M=100$, $\bar{I}_p=10$ dB, $P_p=10$ dB and $\theta_k^{cu}=\theta_k^{pu}=30^\circ$ for all k).

spatial correlation increases due to decrease in the angular standard deviation σ_θ from 30° to 10°. This is because as the spatial correlation increases, the cognitive BS transmits at a lower power in order to maintain P_o at the same level. In other words, by deploying more antennas at the cognitive BS, a higher spatial correlation may be tolerated for a given P_o at the PUs while maintaining the sum SE of the CUs at a fixed level. For example, in order to maintain the sum SE of CUs at $\text{SE}^{ic}=10$ (bits/s/Hz), for $P_o=0.03$ at the PUs, the uncorrelated scenario requires $N=23$, the mildly correlated scenario with $\sigma_\theta=30^\circ$ requires $N=56$ and the severely correlated wireless channel scenario with $\sigma_\theta=10^\circ$ requires $N=193$ antennas at cognitive BS.

2.8 Summary

We considered a co-located mMIMO based underlay spectrum access network in which the cognitive BS transmits under an IOP constraint and has an imperfect and/or incomplete estimate of its channels to the PUs. We proposed new back off factor based power adaptation policies for the cognitive BS such that the interference power does not exceed an interference threshold more than P_o fraction of the time at any of the K_p PUs under either incomplete and/or imperfect

CSI. The novel mathematical expressions for $(1 - P_o)$ offer the wireless system designer a ball-park number for η that must be chosen to meet the constraint under imperfect and/or incomplete CSI. New expressions for sum SE of CUs under each of the scenarios were derived.

We observed that interference outage probability (P_o) is independent of channel estimates from cognitive BS to CUs. We also observed that it is independent of number of cognitive BS antennas and depends only on the strength of the channel estimates from cognitive BS to PUs. We proved that for larger estimation errors along the link from cognitive BS to the PUs, a larger power margin is required at the cognitive BS to maintain P_o at the same level. We showed that under imperfect CSI, by deploying more antennas at the cognitive BS, (1) sum SE of CUs can be maintained at a constant level while reducing P_o, and (2) larger number of PUs can be accommodated in the network while keeping P_o and sum SE of CUs fixed. Furthermore, we showed that P_o reduces as the number of channels to which CSI is known perfectly or imperfectly increases. And by deploying more antennas at the cognitive BS, sum SE of CUs can be kept fixed even if S decreases. And as spatial correlation increases, a larger power margin is required at cognitive BS to keep P_o fixed.

While this chapter focused on comprehensive modeling and performance analysis of co-located mMIMO assisted underlay spectrum sharing networks under imperfect and incomplete CSI. However, in literature, these co-located massive MIMO systems are shown to obtain relatively lower probability of coverage and poorer quality of service to cell edge users when compared to a cell-free mMIMO configuration [12]. Therefore, in the next chapter, we delve deeper into addressing challenges associated with modeling and analyzing cell-free enabled underlay networks.

3

Cell-Free mMIMO Enabled Wireless Communication with UAVs in Underlay Network

Contents

In this chapter, we investigate if the UAVs that are expected to be deployed in several service sectors such as logistics, assessment of critical infrastructure, surveillance, search-and-rescue operations, agriculture and wildlife conservation [13], [61], [62] can be served as unlicensed or CUs in underlay spectrum access mode concurrently with the licensed users such as the GUEs to achieve high spectrum utilization efficiency. To be specific, the UAVs can be allowed to opportunistically share the spectrum with the incumbent GUEs subject to a constraint on the interference that the secondary transmissions can potentially cause to the GUEs [6], [63]. To ensure this, the SAPs must control and adapt their transmit power depending on the quality of the channel estimate that is available at their end. This, therefore, puts a constraint on the maximum data rate that these UAVs can achieve.

To this end, we want to understand if we can harness the spatial multiplexing gains and simplified interference management benefits offered by cell-free massive MIMO to improve the SE of UAVs by integrating cell-free massive MIMO and underlay spectrum access. We first develop the system model, discuss UL pilot transmission and channel estimation. Thereafter, we analyze IOP at the GUEs followed by SE analysis of both UAVs and GUEs considering estimated CSI. Below, we review some of the related works.

3.1 Related Literature

In [41], the data rates of SUs and PUs were derived for different pilot sharing strategies under peak interference constraint in a co-located massive MIMO network. In [31], the statistical characterization of the DL SINR was developed for co-located mMIMO secondary network under peak interference constraint. In [40], UL data rates were derived for SUs for different pilot sequence designs when the SUs and the secondary relays are subject to an average interference constraint at the primary mMIMO BS with co-located antennas. In [64], the authors studied an underlay two-way mMIMO relay network under relay selection and peak interference constraint. In [45], the authors investigated user selection and power allocation using deep reinforcement learning. The authors in [42] derived the aggregate interference at any CU caused by both primary and cognitive transmissions. In [47], the authors investigated the performance

of a wireless powered underlay mMIMO system over spatially correlated channels.

Table 3.1: Summary of the literature related to co-located and cell-free massive MIMO based underlay spectrum sharing

Interference constraint	**Co-located massive MIMO**	**Cell-free massive MIMO**
Peak/Average interference constraint	[31], [30], [32], [35], [33], [40], [34], [46], [38], [44], [45], [41], [47].	[65], [7], [24], [25].
SINR outage probability constraint	[36], [42].	None
Interference violation probability constraint	**[39], [66].**	**None**

In [67], DL sum rate of SUs were derived in a mMIMO based non-orthogonal multiple access (NOMA) underlay spectrum sharing network under average interference constraint. The authors in [44] optimized the number of SUs that can be served under power, rate and peak interference constraint in a cognitive mMIMO network with co-located antennas. In [66], the authors derived the sum DL data rate of SUs in cognitive mMIMO networks with incomplete and/or imperfect CSI under IOP constraint and data rate was derived for single SU under imperfect CSI in [39]. In [65], data rate of SUs in a secondary cell-free mMIMO NOMA network was derived when this network operates concurrently with a primary mMIMO network with co-located antennas. In [7, 24], the authors deduced the achievable DL rates of PUs and SUs in a cognitive cell-free mMIMO network with geographically distributed APs under peak interference constraint. In [25], the authors studied the energy efficiency of an underlay cell-free mMIMO network that operates concurrently with a primary mMIMO network. The aforementioned discussion is summarized in Table 3.1.

3.2 Motivation

Based on the discussion above, we wish to emphasize that there is no work in the existing literature that investigates co-existence of primary cell-free mMIMO APs that serve GUEs and secondary cell-free mMIMO APs that serve UAVs and quantify the gain in performance that

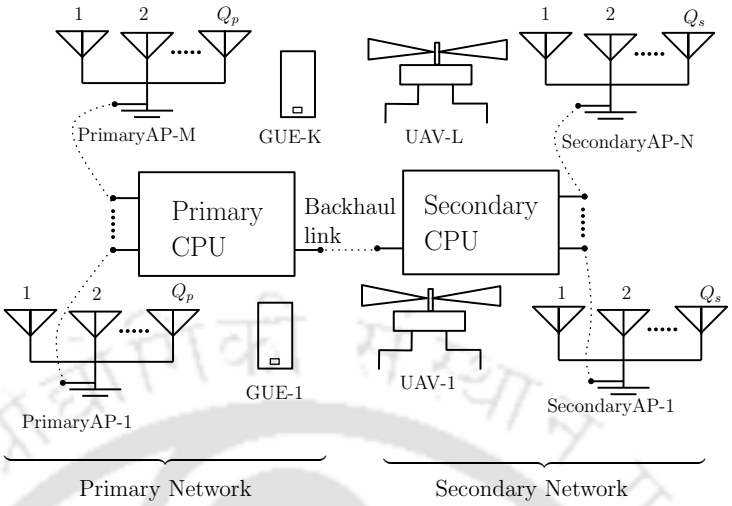

Fig. 3.1: System model

can be obtained by integrating cell-free mMIMO in underlay networks under an IOP constraint. This stochastic constraint changes the mathematical analysis when compared to the state-of-the-art.

Notations: The notation $\boldsymbol{X} \sim \mathcal{CN}(\boldsymbol{\mu}, \boldsymbol{\Sigma})$ denotes that $\boldsymbol{X}$ is a complex-valued Gaussian distributed random vector with mean $\boldsymbol{\mu}$ and covariance $\boldsymbol{\Sigma}$ and $Y \sim \mathcal{U}[0, 2\pi]$ denotes that Y is uniformly distributed between 0 and 2π. The notation $(\cdot)^{\mathrm{H}}$ denote the conjugate-transpose. The variance operator is denoted by $\mathbb{V}\mathrm{ar}(\cdot)$.

Organization: The rest of the manuscript is organized as follows. In Section 3.3, we present our system model. In Section 3.4, we present analysis of IOP at GUEs, SE and BER of GUEs and UAVs. Numerical results and conclusions follow in Sections 3.5 and 3.6, respectively. The proofs are given in Appendix B.

3.3 System Model

We consider the DL of a cell-free mMIMO enabled opportunistic spectrum access network as illustrated in Figure 3.1. It consists of a primary network that owns the spectrum and a secondary network that is allowed to access the spectrum concurrently subject to an interference constraint. The primary network comprises of M APs, each having Q_p antennas and offering service to K GUEs. The secondary network comprises of N APs, each having Q_s antennas and offering service to L UAVs. The channel vector between the m^{th} PAP and the k^{th} GUE is denoted

by $\boldsymbol{h}_{mk}^{p} = \left[\left[h_{mk}^{p}\right]_1, \ldots, \left[h_{mk}^{p}\right]_{Q_p}\right]^{\mathrm{T}}$, where $m \in \{1, 2, \ldots, M\}$ and $k \in \{1, 2, \ldots, K\}$. The interference channel between the n^{th} SAP and the k^{th} GUE is denoted by $\boldsymbol{g}_{nk}^{s} = \left[\left[g_{nk}^{s}\right]_1, \ldots, \left[g_{nk}^{s}\right]_{Q_s}\right]^{\mathrm{T}}$, where $n \in \{1, 2, \ldots, N\}$. We consider Rayleigh fading for these two links. Thus, $\boldsymbol{h}_{mk}^{p} \sim \mathcal{CN}\left(0, \beta_{mk}^{p}\mathbf{I}_{Q_p}\right)$ and $\boldsymbol{g}_{nk}^{s} \sim \mathcal{CN}\left(0, \beta_{nk}^{s}\mathbf{I}_{Q_s}\right)$, where β_{mk}^{p} and β_{nk}^{s} denote the corresponding large-scale fading coefficients.

Furthermore, we denote the channel vector from the n^{th} SAP to l^{th} UAV by $\boldsymbol{h}_{nl}^{s} = \left[\left[h_{nl}^{s}\right]_1, \ldots, \left[h_{nl}^{s}\right]_{Q_s}\right]^{\mathrm{T}}$, where $l \in \{1, 2, \ldots, L\}$. Note that $\boldsymbol{h}_{nl}^{s} \in \mathbb{C}^{Q_s \times 1}$ and the q_s^{th} element of this vector is given by

$$[h_{nl}^{s}]_{q_s} = \sqrt{\frac{\beta_{nl}^{s}}{K_{nl}^{s}+1}}\left[\sqrt{K_{nl}^{s}}e^{j[\theta_{nl}^{s}]_{q_s}}e^{j[\phi_{nl}^{s}]_{q_s}} + [z_{nl}]_{q_s}\right], \tag{3.1}$$

for $1 \le q_s \le Q_s$, where β_{nl}^{s} captures large-scale fading, K_{nl}^{s} denotes the Rician factor and $[z_{nl}]_{q_s} \sim \mathcal{CN}(0, 1)$ models small-scale fading over this link that varies independently across n, l and q_s. Also, $\left[\theta_{nl}^{s}\right]_{q_s} \sim \mathcal{U}[0, 2\pi]$ denotes the phase offset and $\left[\phi_{nl}^{s}\right]_{q_s}$ models the angle of arrival (departure) at (from) antenna q_s of the secondary AP and is given by [62]

$$[\phi_{nl}^{s}]_{q_s} = -\frac{2\pi}{\lambda}\left(\|\boldsymbol{r}_{n1} - \boldsymbol{r}_{l}\| - \left\|\boldsymbol{r}_{nq_s} - \boldsymbol{r}_{l}\right\|\right), \tag{3.2}$$

where $\boldsymbol{r}_{nq_s}$ and $\boldsymbol{r}_{l}$ are the 3D vectors representing the positions of antenna q_s of the n^{th} SAP and l^{th} UAV, respectively. Here $\left[h_{nl}^{s}\right]_{q_s} \sim \mathcal{CN}\left(\left[\bar{h}_{nl}^{s}\right]_{q_s}, \frac{\beta_{nl}^{s}}{K_{nl}^{s}+1}\right)$, where $\left[\bar{h}_{nl}^{s}\right]_{q_s} = \sqrt{\frac{\beta_{nl}^{s}K_{nl}^{s}}{K_{nl}^{s}+1}}e^{j[\theta_{nl}^{s}]_{q_s}}e^{j[\phi_{nl}^{s}]_{q_s}}$. The LoS (line-of-sight) component of the channel vector $\boldsymbol{h}_{nl}^{s}$ is represented by $\bar{\boldsymbol{h}}_{nl}^{s} = \left[\left[\bar{h}_{nl}^{s}\right]_1, \ldots, \left[\bar{h}_{nl}^{s}\right]_{Q_s}\right]^{T}$.

And the channel vector between the m^{th} PAP and the l^{th} UAV is denoted by $\boldsymbol{g}_{ml}^{p} = \left[\left[g_{ml}^{p}\right]_1, \ldots, \left[g_{ml}^{p}\right]_{Q_p}\right]^{\mathrm{T}}$. Note that $\boldsymbol{g}_{ml}^{p} \in \mathbb{C}^{Q_p \times 1}$ and the q_p^{th} element of this vector is given by

$$\left[g_{ml}^{p}\right]_{q_p} = \sqrt{\frac{\beta_{ml}^{p}}{K_{ml}^{p}+1}}\left[\sqrt{K_{ml}^{p}}e^{j[\theta_{ml}^{p}]_{q_p}}e^{j[\phi_{ml}^{p}]_{q_p}} + [z_{ml}]_{q_p}\right], \tag{3.3}$$

for $1 \le q_p \le Q_p$, where β_{ml}^{p} captures large-scale fading, K_{ml}^{p} denotes the Rician factor and $[z_{ml}]_{q_p} \sim \mathcal{CN}(0, 1)$ models small-scale fading over this link. Furthermore, $[z_{ml}]_{q_p}$ varies independently across m, l and q_p. Also, $\left[\theta_{ml}^{p}\right]_{q_p} \sim \mathcal{U}[0, 2\pi]$ denotes the phase offset and $\left[\phi_{ml}^{p}\right]_{q_p}$

models the angle of arrival (departure) at (from) antenna q_p of the PAP and is given by [62]

$$\left[\phi_{ml}^{p}\right]_{q_p} = -\frac{2\pi}{\lambda}\left(\|\boldsymbol{r}_{m1} - \boldsymbol{r}_l\| - \left\|\boldsymbol{r}_{mq_p} - \boldsymbol{r}_l\right\|\right), \tag{3.4}$$

where $\boldsymbol{r}_{mq_p}$ denotes the 3D vector representing the position of antenna q_p of the m^{th} PAP. Here $\left[g_{ml}^{p}\right]_{q_p} \sim \mathcal{CN}\left(\left[\bar{g}_{ml}^{p}\right]_{q_p}, \frac{\beta_{ml}^{p}}{K_{ml}^{p}+1}\right)$, where $\left[\bar{g}_{ml}^{p}\right]_{q_p} = \sqrt{\frac{\beta_{ml}^{p} K_{ml}^{p}}{K_{ml}^{p}+1}} e^{j[\theta_{ml}^{p}]_{q_p}} e^{j[\phi_{ml}^{p}]_{q_p}}$. The LoS component for this link is represented by $\bar{\boldsymbol{g}}_{ml}^{p} = \left[\left[\bar{g}_{ml}^{p}\right]_1, \ldots, \left[\bar{g}_{ml}^{p}\right]_{Q_p}\right]^T$.

3.3.1 UL Pilot Transmission and Channel Estimation

Let $\boldsymbol{\Phi}_p \in \mathbb{C}^{\tau_p \times K}$ denote the pilot matrix transmitted by the GUEs and $\boldsymbol{\Phi}_s \in \mathbb{C}^{\tau_p \times L}$ denote the pilot matrix transmitted by the UAVs, where $\tau_p \leq \tau_c$ denotes the length of the pilot sequences, and τ_c denotes the length of the coherence interval. We focus on orthogonal pilot transmission. Therefore, τ_p has to be at least equal to $K + L$.

Estimate Channels Between PAPs and GUEs: The signal received at antenna q_p of the m^{th} PAP during UL training of GUEs and UAVs is given by

$$[\boldsymbol{y}_m]_{q_p} = \sum_{k'=1}^{K} \sqrt{p_t^p \tau_p}[h_{mk'}^{p}]_{q_p} \boldsymbol{\phi}_p^{k'} + \sum_{l=1}^{L} \sqrt{p_t^s \tau_p}[g_{ml}^{p}]_{q_p} \boldsymbol{\phi}_s^{l} + [\boldsymbol{w}_m]_{q_p}, \tag{3.5}$$

where $[\boldsymbol{y}_m]_{q_p} \in \mathbb{C}^{\tau_p \times 1}$, $\boldsymbol{\phi}_p^{k'} \in \mathbb{C}^{\tau_p \times 1}$ denotes the k'^{th} column of $\boldsymbol{\Phi}_p$, $\boldsymbol{\phi}_s^{l} \in \mathbb{C}^{\tau_p \times 1}$ denotes the l^{th} column of $\boldsymbol{\Phi}_s$, $[\boldsymbol{w}_m]_{q_p} \in \mathbb{C}^{\tau_p \times 1}$ and $[\boldsymbol{w}_m]_{q_p} \sim \mathcal{CN}(\boldsymbol{0}, \sigma_w^2 \boldsymbol{I}_{\tau_p})$, p_t^p and p_t^s represent the pilot powers of GUEs and UAVs, respectively. To obtain the channel estimate of the k^{th} GUE, $[\boldsymbol{y}_m]_{q_p}$ is projected on $\boldsymbol{\phi}_p^{k\,\text{H}}$ to obtain

$$[y_{mk}]_{q_p} = \boldsymbol{\phi}_p^{k\,\text{H}} [\boldsymbol{y}_m]_{q_p} = \sqrt{p_t^p \tau_p}\left[h_{mk}^{p}\right]_{q_p} + \boldsymbol{\phi}_p^{k\,\text{H}} [\boldsymbol{w}_m]_{q_p}, \tag{3.6}$$

where we use the fact that $\boldsymbol{\phi}_p^{k\,\text{H}} \boldsymbol{\phi}_p^{k'} = \delta_{kk'}$ which equals 1 if $k = k'$ and 0 for $k \neq k'$ and $\boldsymbol{\phi}_p^{k\,\text{H}} \boldsymbol{\phi}_s^{l} = 0$. Based on $[y_{mk}]_{q_p}$, the MMSE estimate of $\left[h_{mk}^{p}\right]_{q_p}$ equals [68]

$$\begin{aligned}\left[\widehat{h}_{mk}^{p}\right]_{q_p} &= \left[h_{mk}^{p}\right]_{q_p} - \left(\frac{\sigma_w^2\left[h_{mk}^{p}\right]_{q_p} - \sqrt{p_t^p \tau_p}\beta_{mk}^{p} \boldsymbol{\phi}_p^{k\,\text{H}} [\boldsymbol{w}_m]_{q_p}}{\tau_p p_t^p \beta_{mk}^{p} + \sigma_w^2}\right), \\ &= \left[h_{mk}^{p}\right]_{q_p} - \left[\widetilde{h}_{mk}^{p}\right]_{q_p},\end{aligned} \tag{3.7}$$

where it can be shown that $\left[\widehat{h}^{p}_{mk}\right]_{q_p} \sim \mathcal{CN}\left(0, \zeta^{p}_{mk}\right)$, $\zeta^{p}_{mk} = \frac{p^{p}_{t}\tau_p\left(\beta^{p}_{mk}\right)^2}{\tau_p p^{p}_{t}\beta^{p}_{mk}+\sigma^2_w}$ and the channel estimation error $\left[\widetilde{h}^{p}_{mk}\right]_{q_p} \sim \mathcal{CN}\left(0, \beta^{p}_{mk} - \zeta^{p}_{mk}\right)$ and is independent of $\left[\widehat{h}^{p}_{mk}\right]_{q_p}$.

Estimate Channels Between SAPs and UAVs: The signal received at antenna q_s of the n^{th} secondary AP during UL training is given by

$$[\boldsymbol{y}_n]_{q_s} = \sum_{l'=1}^{L} \sqrt{p^{s}_{t}\tau_p}[h^{s}_{nl'}]_{q_s}\boldsymbol{\phi}^{l'}_{s} + \sum_{k'=1}^{K} \sqrt{p^{p}_{t}\tau_p}\,[g^{s}_{nk'}]_{q_s}\boldsymbol{\phi}^{k'}_{p} + [\boldsymbol{w}_n]_{q_s}, \tag{3.8}$$

where $[\boldsymbol{w}_n]_{q_s} \in \mathbb{C}^{\tau_p \times 1}$, $[\boldsymbol{y}_n]_{q_s} \in \mathbb{C}^{\tau_p \times 1}$, $\boldsymbol{\phi}^{l'}_{s} \in \mathbb{C}^{\tau_p \times 1}$, $\boldsymbol{\phi}^{k'}_{p} \in \mathbb{C}^{\tau_p \times 1}$ and $[\boldsymbol{w}_n]_{q_s} \sim \mathcal{CN}(\boldsymbol{0}, \sigma^2_w \boldsymbol{I}_{\tau_p})$.

To obtain an estimate of the channel to the l^{th} UAV, $[\boldsymbol{y}_n]_{q_s}$ is projected on $\boldsymbol{\phi}^{l\,\text{H}}_{s}$ to yield

$$[y_{nl}]_{q_s} = \boldsymbol{\phi}^{l\,\text{H}}_{s}[\boldsymbol{y}_n]_{q_s} = \sqrt{p^{s}_{t}\tau_p}\,[h^{s}_{nl}]_{q_s} + \boldsymbol{\phi}^{l\,\text{H}}_{s}[\boldsymbol{w}_n]_{q_s}. \tag{3.9}$$

Based on $[y_{nl}]_{q_s}$, the MMSE estimate of $\left[h^{s}_{nl}\right]_{q_s}$ is [68]

$$\begin{aligned}\left[\widehat{h}^{s}_{nl}\right]_{q_s} &= [h^{s}_{nl}]_{q_s} - \left(\frac{\sigma^2_w\left(\left[h^{s}_{nl}\right]_{q_s} - \left[\bar{h}^{s}_{nl}\right]_{q_s}\right) - \frac{\sqrt{p^{s}_{t}\tau_p}\beta^{s}_{nl}\boldsymbol{\phi}^{l\,\text{H}}_{s}[\boldsymbol{w}_n]_{q_s}}{K^{s}_{nl}+1}}{\left(\frac{\tau_p p^{s}_{t}\beta^{s}_{nl}}{K^{s}_{nl}+1}\right)+\sigma^2_w}\right), \\ &= [h^{s}_{nl}]_{q_s} - \left[\widetilde{h}^{s}_{nl}\right]_{q_s},\end{aligned} \tag{3.10}$$

where it can be shown that $\left[\widehat{h}^{s}_{nl}\right]_{q_s} \sim \mathcal{CN}\left([\bar{h}^{s}_{nl}]_{q_s}, \zeta^{s}_{nl}\right)$, $\zeta^{s}_{nl} = \frac{p^{s}_{t}\tau_p\left(\frac{\beta^{s}_{nl}}{K^{s}_{nl}+1}\right)^2}{\tau_p p^{s}_{t}\left(\frac{\beta^{s}_{nl}}{K^{s}_{nl}+1}\right)+\sigma^2_w}$ and the channel estimation error $\left[\widetilde{h}^{s}_{nl}\right]_{q_s} \sim \mathcal{CN}\left(0, \frac{\beta^{s}_{nl}}{K^{s}_{nl}+1} - \zeta^{s}_{nl}\right)$ and is independent of $\left[\widehat{h}^{s}_{nl}\right]_{q_s}$.

Estimate Channels Between SAPs and GUEs: We consider that the pilots of GUEs are shared periodically with SAPs through a backhaul link that connects the primary CPU to the secondary CPU [46], [69], [70], [71]. Therefore, to estimate the channel between the n^{th} SAP and the k^{th} GUE, $[\boldsymbol{y}_n]_{q_s}$ can be projected on $\boldsymbol{\phi}^{k}_{p}$ to obtain

$$[y_{nk}]_{q_s} = \boldsymbol{\phi}^{k\,\text{H}}_{p}[\boldsymbol{y}_n]_{q_s} = \sqrt{p^{p}_{t}\tau_p}\,[g^{s}_{nk}]_{q_s} + \boldsymbol{\phi}^{k\,\text{H}}_{p}[\boldsymbol{w}_n]_{q_s}. \tag{3.11}$$

Thus, based on $[y_{nk}]_{q_s}$, the MMSE estimate of $\left[g^{s}_{nk}\right]_{q_s}$ is given by [68]

$$[\widehat{g}^{s}_{nk}]_{q_s} = [g^{s}_{nk}]_{q_s} - \left(\frac{\sigma^2_w\left[g^{s}_{nk}\right]_{q_s} - \sqrt{p^{p}_{t}\tau_p}\beta^{p}_{mk}\boldsymbol{\phi}^{k\,\text{H}}_{p}[\boldsymbol{w}_n]_{q_s}}{\tau_p p^{p}_{t}\beta^{p}_{mk} + \sigma^2_w}\right),$$

$$= [g^s_{nk}]_{q_s} - [\widetilde{g}^s_{nk}]_{q_s}, \tag{3.12}$$

where again it can be shown that $\left[\widehat{g}^s_{nk}\right]_{q_s} \sim \mathcal{CN}\left(0, \zeta^s_{nk}\right)$, $\zeta^s_{nk} = \frac{p^p_t \tau_p \left(\beta^s_{nk}\right)^2}{\tau_p p^p_t \beta^s_{nk} + \sigma^2_w}$ and the channel estimation error $\left[\widetilde{g}^s_{nk}\right]_{q_s} \sim \mathcal{CN}\left(0, \beta^s_{nk} - \zeta^s_{nk}\right)$ and is independent of $\left[\widehat{g}^s_{nk}\right]_{q_s}$.

3.3.2 DL Data Transmission

The PAPs employ conjugate beamformer designed based on channel estimates acquired on the UL to transmit data to GUEs on the DL. And the signal transmitted by the m^{th} PAP is given by

$$\boldsymbol{x}_m = \sum_{k=1}^{K} \sqrt{\eta_{mk}}\, \widehat{\boldsymbol{h}}^{p*}_{mk}\, q_k, \tag{3.13}$$

where $q_k \sim \mathcal{CN}(0,1)$ denotes the information symbol corresponding to the k^{th} GUE, $\mathbb{E}\left(q_{k'} q_k\right) = 0$ for $k \neq k'$ and η_{mk} is the power control coefficient given by

$$\eta_{mk} = \frac{P^p_d}{\sum\limits_{j=1}^{K} \mathbb{E}\|\widehat{\boldsymbol{h}}^p_{mj}\|^2} = \frac{P^p_d}{\sum\limits_{j=1}^{K} Q_p \zeta^p_{mj}}, \text{ for } k = 1, \ldots, K. \tag{3.14}$$

This choice ensures that $\mathbb{E}\|\boldsymbol{x}_m\|^2 \leq P^p_d$, where P^p_d is the DL transmission power of PAPs. Based on the channel estimates acquired by SAPs during UL training, the SAPs perform normalized conjugate beamforming. And the signal transmitted by n^{th} SAP is given by

$$\boldsymbol{x}_n = \sum_{l=1}^{L} \sqrt{\frac{P^s_d}{L}} \frac{\widehat{\boldsymbol{h}}^{s*}_{nl}}{\|\widehat{\boldsymbol{h}}^s_{nl}\|} s_l, \tag{3.15}$$

where $s_l \sim \mathcal{CN}(0,1)$ is the signal intended for the l^{th} UAV and is chosen such that $\mathbb{E}\left(s_l s_{l'}\right) = 0$ for $l \neq l'$. The signal $\boldsymbol{x}_n$ satisfies the transmit power constraint $\mathbb{E}\|\boldsymbol{x}_n\|^2 \leq P^s_d$, where P^s_d is the DL transmission power of SAPs.

3.4 Analysis of IOP, SE and BER

In this section, we first develop a lower bound on the IOP at the GUEs due to transmissions by the SAPs. We then derive the DL SE expressions for both the GUEs and the UAVs under estimated CSI and when the SAPs transmit subject to an IOP constraint. This is followed by BER analysis.

3.4.1 IOP Analysis

The signal received at the k^{th} GUE when both PAPs and SAPs transmit simultaneously equals

$$y_k = \underbrace{\sum_{k'=1}^{K}\sum_{m=1}^{M}\sqrt{\eta_{mk'}}\boldsymbol{h}_{mk}^{p\mathrm{T}}\widehat{\boldsymbol{h}}_{mk'}^{p*}q_{k'}}_{①} + \underbrace{\sum_{l=1}^{L}\sum_{n=1}^{N}\sqrt{\frac{P_d^s}{L}}\frac{\boldsymbol{g}_{nk}^{s\mathrm{T}}\widehat{\boldsymbol{h}}_{nl}^{s*}s_l}{\|\widehat{\boldsymbol{h}}_{nl}^{s}\|}}_{②} + \underbrace{n_k}_{③}. \tag{3.16}$$

Note that in the equation above, term ① represents the signal received at the k^{th} GUE from M PAPs, term ② captures the interference generated at the k^{th} GUE due to simultaneous transmission by N SAPs and term ③ represents noise at the k^{th} GUE. The power I_k^p of interference generated at the k^{th} GUE due to concurrent spectrum access by the SAPs is given by

$$I_k^p = \mathbb{E}\left(\left|\sum_{l=1}^{L}\sum_{n=1}^{N}\sqrt{\frac{P_d^s}{L}}\frac{\boldsymbol{g}_{nk}^{s\mathrm{T}}\widehat{\boldsymbol{h}}_{nl}^{s*}}{\|\widehat{\boldsymbol{h}}_{nl}^{s}\|}s_l\right|^2\right) = \sum_{l=1}^{L}\frac{P_d^s}{L}\left|\sum_{n=1}^{N}\frac{\boldsymbol{g}_{nk}^{s\mathrm{T}}\widehat{\boldsymbol{h}}_{nl}^{s*}}{\|\widehat{\boldsymbol{h}}_{nl}^{s}\|}\right|^2. \tag{3.17}$$

In this chapter, we focus on an underlay cell-free mMIMO network architecture in which the SAPs adapt their transmit power based on an IOP constraint. This constraint requires that the interference power arising due to concurrent spectrum access by the SAPs must not be larger than a threshold $\bar{I}_p$ at any of the K GUEs more than P_o times. Mathematically, this can be expressed as

$$\Pr(I_1^p \le \bar{I}_p, I_2^p \le \bar{I}_p, \ldots, I_K^p \le \bar{I}_p) \ge (1 - P_o), \tag{3.18}$$

where P_o is referred to as the IOP.

We next develop a simple power adaptation rule that helps us determine the power margin that must be adopted to satisfy the constraint in (3.18). Based on this rule, the SAPs transmit with power

$$P_d^s = \frac{\bar{I}_p}{\eta \max\limits_{1\le k\le K}\left\{\frac{1}{L}\sum\limits_{l=1}^{L}\left|\sum\limits_{n=1}^{N}\frac{\widehat{\boldsymbol{g}}_{nk}^{s\mathrm{T}}\widehat{\boldsymbol{h}}_{nl}^{s*}}{\|\widehat{\boldsymbol{h}}_{nl}^{s}\|}\right|^2\right\}}, \tag{3.19}$$

where the power margin η (> 1) is set such that the IOP constraint in (3.18) is satisfied with equality for a given P_o under estimated CSI.

Proposition 3.1. *The power $P_d^s = \frac{\bar{I}_p}{\eta}X$ with which any SAP transmits is a function of the RV*

$X = \frac{1}{\max\limits_{1\le k\le K}\left\{\frac{1}{L}\sum\limits_{l=1}^{L}\left|\sum\limits_{n=1}^{N}\frac{\widehat{g}_{nk}^{s\,T}\widehat{h}_{nl}^{s\,*}}{\|\widehat{h}_{nl}^{s}\|}\right|^2\right\}}$ *whose pdf is given by*

$$f_X(x) = \frac{1}{(\Gamma(L))^K}\sum_{j=1}^{K}\left[\left(\frac{L}{\mu_j}\right)^L \frac{e^{-\left(\frac{L}{\mu_j x}\right)}}{x^{L+1}}\prod_{\substack{i=1\\ i\neq j}}^{K}\gamma\left(L,\frac{L}{\mu_i x}\right)\right]; x \geq 0, \tag{3.20}$$

where $\mu_i = \sum\limits_{n=1}^{N}\zeta_{ni}^{s}$ *and* $\gamma(\cdot)$ *denotes the lower incomplete Gamma function [53, (8.350.1)]. Furthermore, the statistical mean of* P_d^s *equals*

$$\xi = \mathbb{E}\left(P_d^s\right) = \frac{\bar{I}_p}{\eta(\Gamma(L))^K}\sum_{j=1}^{K}\sum_{l=1}^{T}\frac{L w_l x_l^{L-2}}{\mu_j}\prod_{\substack{i=1\\ i\neq j}}^{K}\gamma\left(L,\frac{\mu_j x_l}{\mu_i}\right), \tag{3.21}$$

where $\{x_l\}$ *denote the Gauss-Laguerre integration points,* $\{w_l\}$ *are the corresponding weights and* T *denotes the number of integration points [72, (25.4.45)].*

Proof. The proof is given in Appendix B.1. □

Corollary 3.1. *The square root of the power* $\sqrt{P_d^s} = \sqrt{\frac{\bar{I}_p}{\eta}}W$ *with which any SAP transmits is a function of the RV* $W = \frac{1}{\sqrt{\max\limits_{1\le k\le K}\left\{\frac{1}{L}\sum\limits_{l=1}^{L}\left|\sum\limits_{n=1}^{N}\frac{\widehat{g}_{nk}^{s\,T}\widehat{h}_{nl}^{s\,*}}{\|\widehat{h}_{nl}^{s}\|}\right|^2\right\}}}$ *whose pdf can be expressed in closed form as*

$$f_W(w) = \frac{1}{(\Gamma(L))^K}\sum_{j=1}^{K}\left[\left(\frac{L}{\mu_j}\right)^L \frac{2e^{-\left(\frac{L}{\mu_j w^2}\right)}}{w^{2L+1}}\prod_{\substack{i=1\\ i\neq j}}^{K}\gamma\left(L,\frac{L}{\mu_i w^2}\right)\right]; w \geq 0. \tag{3.22}$$

Furthermore, the statistical mean of $\sqrt{P_d^s}$ *is given by*

$$\lambda = \mathbb{E}\left(\sqrt{P_d^s}\right) = \sqrt{\frac{\bar{I}_p}{\eta}}\frac{1}{(\Gamma(L))^K}\sum_{j=1}^{K}\sum_{l=1}^{T}\left(\frac{L}{\mu_j}\right)^{\frac{1}{2}} w_l x_l^{L-\frac{3}{2}}\prod_{\substack{i=1\\ i\neq j}}^{K}\gamma\left(L,\frac{\mu_j x_l}{\mu_i}\right). \tag{3.23}$$

Proof: This can be proved using the ideas in Appendix B.1 and through transformation of rvs.

We will use these new results developed in Proposition 3.1 and Corollary 3.1 in the SE analysis in Sections 3.4.2 and 3.4.3. Based on the power control rule in (3.19), the power margin η is set so that

$$(1 - P_o) = \Pr(I_1^p \leq \bar{I}_p, I_2^p \leq \bar{I}_p, \ldots, I_K^p \leq \bar{I}_p), \tag{3.24}$$

where

$$I_k^p = \frac{\frac{\bar{I}_p}{L}\sum_{l=1}^{L}\left|\sum_{n=1}^{N}\frac{\mathbf{g}_{nk}^{s\,\mathrm{T}}\widehat{\mathbf{h}}_{nl}^{s\,*}}{\|\widehat{\mathbf{h}}_{nl}^{s}\|}\right|^2}{\eta\max\limits_{1\le k\le K}\left\{\frac{1}{L}\sum_{l=1}^{L}\left|\sum_{n=1}^{N}\frac{\widehat{\mathbf{g}}_{nk}^{s\,\mathrm{T}}\widehat{\mathbf{h}}_{nl}^{s\,*}}{\|\widehat{\mathbf{h}}_{nl}^{s}\|}\right|^2\right\}}. \tag{3.25}$$

Let $Z_k = \frac{1}{L}\sum_{l=1}^{L}\left|\sum_{n=1}^{N}\frac{\mathbf{g}_{nk}^{s\,\mathrm{T}}\widehat{\mathbf{h}}_{nl}^{s\,*}}{\|\widehat{\mathbf{h}}_{nl}^{s}\|}\right|^2$ and $\widehat{Z}_k = \frac{1}{L}\sum_{l=1}^{L}\left|\sum_{n=1}^{N}\frac{\widehat{\mathbf{g}}_{nk}^{s\,\mathrm{T}}\widehat{\mathbf{h}}_{nl}^{s\,*}}{\|\widehat{\mathbf{h}}_{nl}^{s}\|}\right|^2$. In order to characterize the interference caused to the k^{th} GUE, we need to determine the correlation between Z_k and $\widehat{Z}_k$.

Proposition 3.2. *The correlation between Z_k and $\widehat{Z}_k$ is given by $\rho_k = \frac{\mu_k}{\alpha_k}$ where $\alpha_k = \sum_{n=1}^{N}\beta_{nk}^{s}$ and $\mu_k = \sum_{n=1}^{N}\zeta_{nk}^{s}$ as mentioned in Proposition 3.1.*

Proof. The proof is given in Appendix B.2. □

Given the power adaptation rule in (3.19) and using ρ_k as stated in Proposition 3.2, we next state a simplified lower bound on the IOP at the GUEs as a Theorem.

Theorem 3.1. *With estimated CSI, the probability that the interference constraint is not violated at any of the GUEs due to transmissions by SAPs is lower bounded by*

$$(1-P_o) \ge P_L = \max\Bigg(0, 1 - \sum_{i=1}^{K}\sum_{l=1}^{T}\frac{w_l x_l^{L-1}}{\Gamma(L)}\prod_{\substack{j=1\\ i\ne j}}^{K}\frac{\gamma\left(L, \frac{x_l\alpha_i}{\eta\mu_j}\right)}{\Gamma(L)} \times\left(1 - Q_L\left(\sqrt{\frac{2\rho_i x_l}{(1-\rho_i)}}, \sqrt{\frac{2x_l\alpha_i}{\eta\mu_i(1-\rho_i)}}\right)\right)\Bigg), \tag{3.26}$$

where $\rho_i = \frac{\mu_i}{\alpha_i}$, $\alpha_i = \sum_{n=1}^{N}\beta_{ni}^{s}$, $\mu_j = \sum_{n=1}^{N}\zeta_{nj}^{s}$, and as before $\{x_l\}$ denote the Gauss-Laguerre integration points, $\{w_l\}$ denote the corresponding weights, T denotes the number of integration points and $Q_L(\cdot,\cdot)$ denotes the generalized Marcum-Q function of order L [54, (4.59)].

Proof. The proof is given in Appendix B.3. □

Remarks: The integral free expression in (3.26) brings out the dependence of IOP on the power margin (η), the number of UAVs (L), the number of GUEs (K), the strength of true and estimated interference channel coefficients and also on the correlation coefficient (ρ_i). Interestingly, we note that P_o does not depend on the number of SAPs (N). This is because we employ

normalized MR precoder at the SAPs. Furthermore, this result can help a wireless system designer in determining the power margin that the SAPs must maintain in order to satisfy the IOP constraint at the GUEs.

3.4.2 SE Analysis

We now derive SE of the k^{th} GUE. Based on (3.7), we express the true channel vector as $\boldsymbol{h}_{mk}^{p} = \widehat{\boldsymbol{h}}_{mk}^{p} + \widetilde{\boldsymbol{h}}_{mk}^{p}$ and re-write the signal received at the k^{th} GUE in (3.16) as

$$y_k = \underbrace{\sum_{m=1}^{M} \sqrt{\eta_{mk}} \mathbb{E}\|\widehat{\boldsymbol{h}}_{mk}^{p}\|^2 q_k}_{①} + \underbrace{\sum_{m=1}^{M} \sqrt{\eta_{mk}} \left(\|\widehat{\boldsymbol{h}}_{mk}^{p}\|^2 - \mathbb{E}\|\widehat{\boldsymbol{h}}_{mk}^{p}\|^2\right) q_k}_{②} + \underbrace{\sum_{m=1}^{M} \sqrt{\eta_{mk}} \widetilde{\boldsymbol{h}}_{mk}^{p\mathrm{T}} \widehat{\boldsymbol{h}}_{mk}^{p*} q_k}_{③}$$
$$+ \underbrace{\sum_{\substack{k'=1 \\ k' \neq k}}^{K} \sum_{m=1}^{M} \sqrt{\eta_{mk'}} \boldsymbol{h}_{mk}^{p\mathrm{T}} \widehat{\boldsymbol{h}}_{mk'}^{p*} q_{k'}}_{④} + \underbrace{\sum_{l=1}^{L} \sum_{n=1}^{N} \sqrt{\frac{P_d^s}{L}} \frac{\boldsymbol{g}_{nk}^{s\mathrm{T}} \widehat{\boldsymbol{h}}_{nl}^{s*}}{\|\widehat{\boldsymbol{h}}_{nl}^{s}\|} s_l}_{⑤} + \underbrace{n_k}_{⑥}. \quad (3.27)$$

It can be shown that all the terms in (3.27) above are uncorrelated to each other. Based on (3.27), the SINR at the k^{th} GUE is given by (3.28).

$$\text{SINR}_k = \frac{\left|\sum_{m=1}^{M} \sqrt{\eta_{mk}} \mathbb{E}\|\widehat{\boldsymbol{h}}_{mk}^{p}\|^2\right|^2}{\left(\begin{array}{l} \mathbb{E}\left|\sum_{m=1}^{M} \sqrt{\eta_{mk}} \left(\|\widehat{\boldsymbol{h}}_{mk}^{p}\|^2 - \mathbb{E}\|\widehat{\boldsymbol{h}}_{mk}^{p}\|^2\right)\right|^2 + \mathbb{E}\left|\sum_{m=1}^{M} \sqrt{\eta_{mk}} \widetilde{\boldsymbol{h}}_{mk}^{p\mathrm{T}} \widehat{\boldsymbol{h}}_{mk}^{p*}\right|^2 \\ + \sum_{\substack{k'=1 \\ k' \neq k}}^{K} \mathbb{E}\left|\sum_{m=1}^{M} \sqrt{\eta_{mk}} \boldsymbol{h}_{mk}^{p\mathrm{T}} \widehat{\boldsymbol{h}}_{mk'}^{p*}\right|^2 + \sum_{l=1}^{L} \mathbb{E}\left|\sum_{n=1}^{N} \sqrt{\frac{P_d^s}{L}} \frac{\boldsymbol{g}_{nk}^{s\mathrm{T}} \widehat{\boldsymbol{h}}_{nl}^{s*}}{\|\widehat{\boldsymbol{h}}_{nl}^{s}\|}\right|^2 + \mathbb{E}|n_k|^2 \end{array}\right)}. \quad (3.28)$$

The SE of the k^{th} GUE is obtained by simplifying (3.28) and is stated next as a Theorem.

Theorem 3.2. *The SE of the k^{th} GUE $\left(SE_k^g\right)$ in a concurrent spectrum access network where the SAP controls its transmit power based on an IOP constraint is given by*

$$SE_k^g \approx \left(1 - \frac{\tau_p}{\tau_c}\right) \log_2 \left(1 + \frac{\left(\sum_{m=1}^{M} \sqrt{\eta_{mk}} Q_p \zeta_{mk}^{p}\right)^2}{\sum_{k'=1}^{K} \sum_{m=1}^{M} \eta_{mk'} Q_p \zeta_{mk'}^{p} \beta_{mk}^{p} + \sum_{n=1}^{N} \xi \beta_{nk}^{s} + \sigma_w^2}\right), \quad (3.29)$$

where $\xi = \frac{\bar{I}_p}{\eta(\Gamma(L))^K} \sum_{j=1}^{K} \sum_{l=1}^{T} \frac{L w_l x_l^{L-2}}{\mu_j} \prod_{\substack{i=1 \\ i \neq j}}^{K} \gamma\left(L, \frac{\mu_j x_l}{\mu_i}\right)$ as stated in Proposition 3.1.

Proof. The proof is given in Appendix B.4. □

Remarks: This result brings out the dependence of the SE of GUEs on interference threshold ($\bar{I}_p$), number of PAPs and SAPs (M and N), number of antennas at PAP (Q_p), number of PUs (K), number of SUs (L) and also on the variance of the interference channel estimate.

We next analyze the SE of the l^{th} UAV on the DL. The signal received at the l^{th} UAV equals

$$y_l = \underbrace{\sum_{l'=1}^{L}\sum_{n=1}^{N}\frac{\sqrt{P_d^s}\boldsymbol{h}_{nl}^{s\mathrm{T}}\widehat{\boldsymbol{h}}_{nl'}^{s*}s_{l'}}{\sqrt{L}\|\widehat{\boldsymbol{h}}_{nl'}^{s}\|}}_{①} + \underbrace{\sum_{k=1}^{K}\sum_{m=1}^{M}\sqrt{\eta_{mk}}\boldsymbol{g}_{ml}^{p\mathrm{T}}\widehat{\boldsymbol{h}}_{mk}^{p*}q_k}_{②} + \underbrace{n_l}_{③}. \tag{3.30}$$

Based on (3.10), we state the true channel vector as $\boldsymbol{h}_{nl}^s = \widehat{\boldsymbol{h}}_{nl}^s + \widetilde{\boldsymbol{h}}_{nl}^s$, to re-write the signal received at the l^{th} UAV in (3.30) as

$$\begin{aligned} y_l = {} & \underbrace{\sum_{n=1}^{N}\frac{\mathbb{E}\left(\sqrt{P_d^s}\|\widehat{\boldsymbol{h}}_{nl}^s\|\right)s_l}{\sqrt{L}}}_{①} + \underbrace{\sum_{n=1}^{N}\left(\frac{\sqrt{P_d^s}\|\widehat{\boldsymbol{h}}_{nl}^s\|}{\sqrt{L}} - \frac{\mathbb{E}(\sqrt{P_d^s}\|\widehat{\boldsymbol{h}}_{nl}^s\|)}{\sqrt{L}}\right)s_l}_{②} + \underbrace{\sum_{n=1}^{N}\sqrt{\frac{P_d^s}{L}}\frac{\widetilde{\boldsymbol{h}}_{nl}^{s\mathrm{T}}\widehat{\boldsymbol{h}}_{nl}^{s*}}{\|\widehat{\boldsymbol{h}}_{nl}^s\|}s_l}_{③} \\ & + \underbrace{\sum_{\substack{l'=1\\l'\neq l}}^{L}\sum_{n=1}^{N}\frac{\sqrt{P_d^s}\boldsymbol{h}_{nl}^{s\mathrm{T}}\widehat{\boldsymbol{h}}_{nl'}^{s*}}{\sqrt{L}\|\widehat{\boldsymbol{h}}_{nl'}^s\|}s_{l'}}_{④} + \underbrace{\sum_{k=1}^{K}\sum_{m=1}^{M}\sqrt{\eta_{mk}}\boldsymbol{g}_{ml}^{p\mathrm{T}}\widehat{\boldsymbol{h}}_{mk}^{p*}q_k}_{⑤} + \underbrace{n_l}_{⑥}. \end{aligned} \tag{3.31}$$

Again, it can be shown that all the terms in (3.31) above are uncorrelated to each other. And based on (3.31), the SINR at the l^{th} UAV is given by (3.32).

$$\mathrm{SINR}_l = \frac{\left|\sum_{n=1}^{N}\frac{\mathbb{E}\left(\sqrt{P_d^s}\|\widehat{\boldsymbol{h}}_{nl}^s\|\right)}{\sqrt{L}}\right|^2}{\left(\begin{aligned} & \mathbb{E}\left|\sum_{n=1}^{N}\left(\frac{\sqrt{P_d^s}\|\widehat{\boldsymbol{h}}_{nl}^s\|}{\sqrt{L}} - \frac{\mathbb{E}\left(\sqrt{P_d^s}\|\widehat{\boldsymbol{h}}_{nl}^s\|\right)}{\sqrt{L}}\right)\right|^2 + \mathbb{E}\left|\sum_{n=1}^{N}\frac{\sqrt{P_d^s}\widetilde{\boldsymbol{h}}_{nl}^{s\mathrm{T}}\widehat{\boldsymbol{h}}_{nl}^{s*}}{\sqrt{L}\|\widehat{\boldsymbol{h}}_{nl}^s\|}\right|^2 + \sum_{\substack{l'=1\\l'\neq l}}^{L}\mathbb{E}\left|\sum_{n=1}^{N}\frac{\sqrt{P_d^s}\boldsymbol{h}_{nl}^{s\mathrm{T}}\widehat{\boldsymbol{h}}_{nl'}^{s*}}{\sqrt{L}\|\widehat{\boldsymbol{h}}_{nl'}^s\|}\right|^2 \\ & + \sum_{k=1}^{K}\mathbb{E}\left|\sum_{m=1}^{M}\sqrt{\eta_{mk}}\boldsymbol{g}_{ml}^{p\mathrm{T}}\widehat{\boldsymbol{h}}_{mk}^{p*}\right|^2 + \mathbb{E}|n_l|^2 \end{aligned}\right)}. \tag{3.32}$$

We simplify this SINR expression further and state the SE of l^{th} UAV as a Theorem.

Theorem 3.3. *The SE of the l^{th} UAV (SE_l^u) when the SAP transmits under an IOP constraint is given by*

$$SE_l^u \approx \left(1 - \frac{\tau_p}{\tau_c}\right)\log_2\left(1 + \frac{DS_l}{BU_l + CEE_l + ISAP_l + IPAP_l + \sigma_w^2}\right), \tag{3.33}$$

where DS_l denotes the power of the desired signal at l^{th} UAV and is given by

$$DS_l \triangleq \begin{cases} \left| \sum_{n=1}^{N} \frac{\lambda \delta_{nl}^s}{\sqrt{L}} \right|^2, & if\ PLoS \neq 1, \\ \left| \sum_{n=1}^{N} \frac{\lambda \sqrt{Q_s \beta_{nl}^s}}{\sqrt{L}} \right|^2, & if\ PLoS = 1, \end{cases} \tag{3.34}$$

where $\lambda = \sqrt{\frac{\bar{I}_p}{\eta}} \frac{1}{(\Gamma(L))^K} \sum_{j=1}^{K} \sum_{l=1}^{T} \left(\frac{L}{\mu_j}\right)^{1/2} w_l y_l^{L-\frac{3}{2}} \prod_{\substack{i=1 \\ i \neq j}}^{K} \gamma\left(L, \frac{\mu_j y_l}{\mu_i}\right)$ *and is also stated in Corollary 3.1,* $\delta_{nl}^s = \int_0^\infty \frac{2u^{Q_s+1}}{\zeta_{nl}^s \|\bar{\boldsymbol{h}}_{nl}^s\|^{Q_s-1}} \exp\left(-\frac{\|\bar{\boldsymbol{h}}_{nl}^s\|^2+u^2}{\zeta_{nl}^s}\right) I_{Q_s-1}\left(\frac{\|\bar{\boldsymbol{h}}_{nl}^s\| u}{\zeta_{nl}^s}\right) du$, $I_{Q_s-1}(.)$ *represents the modified Bessel function of the first kind and order* $(Q_s - 1)$ *[72, (9.6.19)],* BU_l *represents the power of the beamforming uncertainty at* l^{th} *UAV and equals*

$$BU_l \triangleq \sum_{n=1}^{N} \left(\frac{\xi Q_s \left(\zeta_{nl}^s + \frac{\beta_{nl}^s K_{nl}^s}{K_{nl}^s+1}\right)}{L} - \frac{\left(\lambda \delta_{nl}^s\right)^2}{L} \right), \tag{3.35}$$

CEE_l represents the variance of the term arising due to error incurred in estimating the channel to the l^{th} UAV and is given by

$$CEE_l \triangleq \sum_{n=1}^{N} \frac{\xi}{L} \left(\frac{\beta_{nl}^s}{K_{nl}^s + 1} - \zeta_{nl}^s \right), \tag{3.36}$$

$ISAP_l$ represents the power of interference caused to the l^{th} UAV due to signals intended for other UAVs and is given by

$$ISAP_l \triangleq \sum_{\substack{l'=1 \\ l' \neq l}}^{L} \frac{\xi}{L} \left[\sum_{n=1}^{N} \left(\frac{\beta_{nl}^s}{K_{nl}^s + 1} + \frac{\bar{\boldsymbol{h}}_{nl}^{s\,H} (\zeta_{nl'}^s \mathbf{I}_{Q_s} + \bar{\boldsymbol{h}}_{nl'}^s \bar{\boldsymbol{h}}_{nl'}^{s\,H}) \bar{\boldsymbol{h}}_{nl}^s}{Q_s \left(\zeta_{nl'}^s + \frac{\beta_{nl'}^s K_{nl'}^s}{K_{nl'}^s+1}\right)} \right) \right.$$
$$\left. + \sum_{n=1}^{N} \sum_{\substack{m=1 \\ m \neq n}}^{N} \left(\frac{\left(\bar{\boldsymbol{h}}_{nl'}^{sT} \bar{\boldsymbol{h}}_{nl}^{s*}\right)\left(\bar{\boldsymbol{h}}_{ml}^{sT} \bar{\boldsymbol{h}}_{ml'}^{s*}\right)}{\sqrt{Q_s^2 \left(\zeta_{nl'}^s + \frac{\beta_{nl'}^s K_{nl'}^s}{K_{nl'}^s+1}\right)\left(\zeta_{ml'}^s + \frac{\beta_{ml'}^s K_{ml'}^s}{K_{ml'}^s+1}\right)}} \right) \right], \tag{3.37}$$

and $IPAP_l$ denotes the power of the interference caused to the l^{th} UAV due to signals transmitted by PAPs and equals

$$IPAP_l \triangleq \sum_{k=1}^{K} \sum_{m=1}^{M} \eta_{mk} Q_p \zeta_{mk}^p \beta_{ml}^p. \tag{3.38}$$

Proof. The proof is given in Appendix B.5. □

Remarks: The SE of UAVs depends on deterministic constants such as number of PAPs (M), number of SAPs (N), number of antennas at PAP (Q_p), number of antennas at SAP (Q_s), number

of GUEs (K), number of UAVs (L) and on the variance of the true and estimated interference channel coefficients. We obtain δ^s_{nl} numerically, since it is analytically intractable [57], [58]. SE now depends on height of the UAVs. This result is valid in general for any model chosen for the PLoS, path loss and Rician factor corresponding to the channels of UAVs.

3.4.3 BER Analysis

Based on (3.16) in this chapter and the fact that the true channel $\boldsymbol{h}^p_{mk}$ between m^{th} PAP and the k^{th} GUE is given by $\boldsymbol{h}^p_{mk} = \widehat{\boldsymbol{h}}^p_{mk} + \widetilde{\boldsymbol{h}}^p_{mk}$, where $\widehat{\boldsymbol{h}}^p_{mk}$ denotes the MMSE estimate of $\boldsymbol{h}^p_{mk}$ and $\widetilde{\boldsymbol{h}}^p_{mk}$ denotes channel estimation error, the data signal received at the k^{th} GUE equals

$$y_k = \sum_{m=1}^{M} \sqrt{\eta_{mk}} \|\widehat{\boldsymbol{h}}^p_{mk}\|^2 q_k + \sum_{m=1}^{M} \sqrt{\eta_{mk}} \widetilde{\boldsymbol{h}}^{p\mathrm{T}}_{mk} \widehat{\boldsymbol{h}}^{p*}_{mk} q_k + \sum_{\substack{k'=1 \\ k' \neq k}}^{K} \sum_{m=1}^{M} \sqrt{\eta_{mk'}} \boldsymbol{h}^{p\mathrm{T}}_{mk} \widehat{\boldsymbol{h}}^{p*}_{mk'} q_{k'} + \sum_{l=1}^{L} \sum_{n=1}^{N} \sqrt{\frac{P^s_d}{L}} \frac{\boldsymbol{g}^{s\mathrm{T}}_{nk} \widehat{\boldsymbol{h}}^{s*}_{nl}}{\|\widehat{\boldsymbol{h}}^s_{nl}\|} s_l + n_k. \quad (3.39)$$

Based on (3.39), the objective is to detect the data symbol q_k intended for the k^{th} GUE based on the observable y_k. Note that the data symbol corresponding to the k^{th} GUE is chosen such that $|q_k|^2 = 1$. In this chapter, we focus on non-coherent detection and consider that the GUEs do not have access to instantaneous CSI, since there are no pilots transmitted on the DL. The GUEs, however, rely on the knowledge of statistical CSI [17, 73]. Thus, the ML decision rule to detect q_k based on y_k is given by

$$\arg \max_{q_k \in \mathcal{S}} \{f(y_k|q_k)\}, \quad (3.40)$$

where $f(y_k|q_k)$ denotes the conditional pdf of y_k given q_k and $\mathcal{S}$ represents the set of constellation points. Furthermore, we use the Gaussian approximation for the interference plus noise terms in (3.39), since it is a widely adopted model in the mMIMO literature, for example, in [74–76]. Therefore, given q_k, y_k is complex Gaussian rv with conditional mean

$$\mathbb{E}[y_k|q_k] = \mathbb{E}\left[\sum_{m=1}^{M} \sqrt{\eta_{mk}} \|\widehat{\boldsymbol{h}}^p_{mk}\|^2 q_k\right] = \chi_k q_k, \quad (3.41)$$

where $\chi_k = \sum_{m=1}^{M} \sqrt{\eta_{mk}} Q_p \zeta_{mk}^p$. We note that given q_k, the conditional mean of all other terms except the first term in y_k equals zero. Furthermore, it can be shown that the conditional variance $\varpi_k^2 = \mathbb{V}\text{ar}\left[y_k | q_k\right]$ equals

$$\varpi_k^2 = \mathbb{E}\left[|y_k - \chi_k\, q_k|^2 \,|q_k\right] = \left(\sum_{k'=1}^{K}\sum_{m=1}^{M} \eta_{mk'} Q_p \zeta_{mk'}^p \beta_{mk}^p + \sum_{n=1}^{N} \xi \beta_{nk}^s + \sigma_w^2\right). \tag{3.42}$$

Upon further simplification, the ML rule in (3.40) simplifies to

$$\arg\min_{q_k \in \mathcal{S}} \{|y_k - \chi_k q_k|^2\}. \tag{3.43}$$

We let $S = |\mathcal{S}|$ denote the cardinality of set $\mathcal{S}$. Given this ML decision rule and availability of statistical CSI, the BER of GUEs for M-PSK $\left(\psi = \frac{\pi}{S}\right)$ is given by [77, 78]

$$\text{BER}_k^{\text{GUE}} \approx \frac{1}{\pi \log_2 S} \int_0^{\pi - \frac{\pi}{S}} \exp\left(-\frac{\chi_k^2 \sin^2(\pi/S)}{\varpi_k^2 \sin^2 \alpha}\right) d\alpha. \tag{3.44}$$

where χ_k and ϖ_k^2 are given in (3.41) and (3.42), respectively.

Following similar ideas, it can be shown that the ML decision rule for UAV is given by

$$\arg\min_{s_l \in \mathcal{S}} \{|y_l - \chi_l s_l|^2\}. \tag{3.45}$$

And BER of UAVs equals

$$\text{BER}_l^{\text{UAV}} \approx \frac{1}{\pi \log_2 S} \int_0^{\pi - \frac{\pi}{S}} \exp\left(-\frac{\chi_l^2 \sin^2(\pi/S)}{\varpi_l^2 \sin^2 \alpha}\right) d\alpha, \tag{3.46}$$

where $\chi_l = \mathbb{E}\left[y_l | s_l\right]$ equals

$$\chi_l = \begin{cases} \sum\limits_{n=1}^{N} \frac{\lambda \delta_{nl}^s}{\sqrt{L}}, & \text{if PLoS} \neq 1, \\ \sum\limits_{n=1}^{N} \frac{\lambda \sqrt{Q_s \beta_{nl}^s}}{\sqrt{L}}, & \text{if PLoS} = 1, \end{cases} \tag{3.47}$$

and it can be shown that the conditional variance $\varpi_l^2 = \text{Var}\left[y_l | s_l\right]$ is given by

$$\begin{aligned} \varpi_l^2 &= \mathbb{E}\left[|y_l - \chi_l\, s_l|^2 \,|s_l\right] = \mathbb{E}\left[|y_l|^2 \,|s_l\right] - {\chi_l}^2, \\ &= \left(\text{BU}_l + \text{CEE}_l + \text{ISAP}_l + \text{IPAP}_l + \sigma_w^2\right). \end{aligned} \tag{3.48}$$

3.5 Numerical Results

We next present numerical results to validate our analysis and to elucidate the impact of estimation error, power margin, number of SAPs and interference threshold on IOP at GUEs and SE of UAVs and GUEs. We consider a square area of dimension 500 m × 500 m. Unless mentioned otherwise, we take $N = 100$, $M = 100$, $K = 10$, $Q_p = Q_s = 4$, $p_t^p = p_t^s = -30$ dB, $P_d^p = -30$ dB, $L = 10$ and $\tau_p = 20$. We take $f_c = 1.9$ GHz, bandwidth = 20 MHz and noise power spectral density of −174 dBm/Hz. The inter-antenna spacing at both PAPs and SAPs is $\lambda_c/2$ where λ_c represents the carrier wavelength. To avoid boundary effects, we consider that the square area is wrapped around at the edges. The vertical height of both PAPs and SAPs is considered to be 15 m, the height of the GUE is taken as 1.65 m and the height of the UAVs is considered to be uniformly distributed between 22.5 m and 300 m.

The large scale fading coefficient β_{ab}^x between the a^{th} AP and the b^{th} GUE is modeled as [14] $\beta_{ab}^x = 10^{\frac{PL_{ab}^x}{10}} 10^{\frac{\sigma_{ab}^x z_{ab}^x}{10}}$, where PLoS represents probability of line-of-sight, $1 \leq b \leq K$, $x \in \{p, s\}$ and $1 \leq a \leq M$ or $1 \leq a \leq N$ depending on whether the large scale fading coefficient corresponds to the PAP or the SAP. Furthermore, PL_{ab}^x represents the path loss corresponding to this link and for which we consider the three slope model as in [14], and $10^{\frac{\sigma_{ab}^x z_{ab}^x}{10}}$ represents shadow fading with standard deviation $(\sigma_{ab}^x) = 8$ dB, and $z_{ab}^x \sim \mathcal{N}(0, 1)$. The Rician factor between the a^{th} AP and the c^{th} UAV is modeled as $K_{ac}^x = \frac{\text{PLoS}_{ac}^x}{1-\text{PLoS}_{ac}^x}$, where $1 \leq c \leq L$, $x \in \{p, s\}$ and $1 \leq a \leq M$ or $1 \leq a \leq N$ depending on whether the Rician factor corresponds to the PAP or the SAP. And the LoS probability is evaluated based on Table B-1 for the urban micro (UMi) scenario [23]. The large scale fading between a^{th} AP and c^{th} UAV is modeled as $\beta_{ac}^x = 10^{\frac{-PL_{ac}^x}{10}} 10^{\frac{\sigma_{ac}^x z_{ac}^x}{10}}$ where PL_{ac}^x is the path loss evaluated based on Table B-2 corresponding to the UMi scenario in [23], σ_{ac}^x represents the standard deviation of the shadow fading parameter and is evaluated based on Table B-3 in [23] and $z_{ac}^x \sim \mathcal{N}(0, 1)$ models the shadow fading coefficient.

Figure 3.2 plots $(1 - P_o)$ as a function of the power margin for $K = 10$, $L = 10$ and for two different values of p_t^p, namely −30 dB and −40 dB. Exact curves are obtained through Monte Carlo simulation of (3.24). Lower bound obtained through (3.26) is also plotted. We

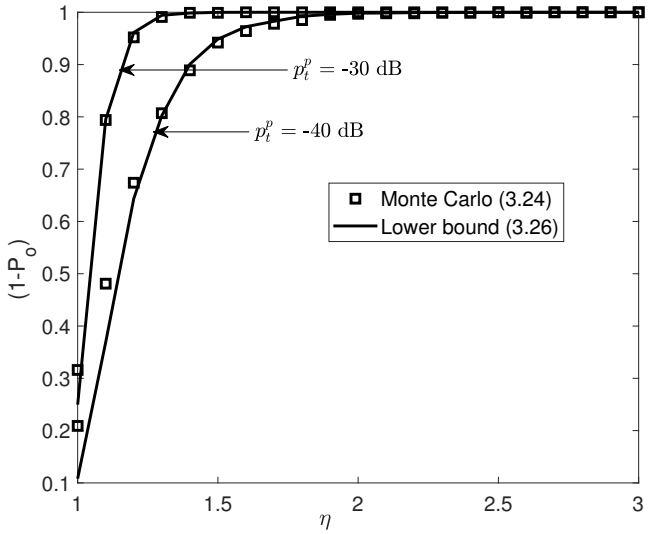

Fig. 3.2: Impact of p_t^p on IOP ($K = L = 10, M = N = 100, Q_p = Q_s = 4, \tau_p = 20$).

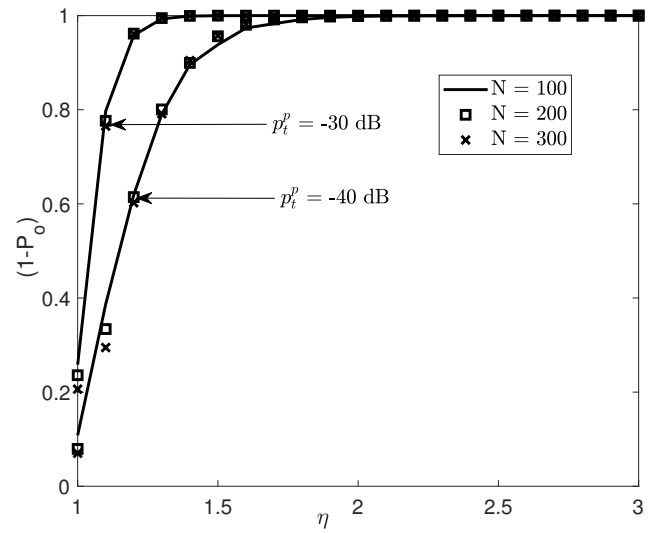

Fig. 3.3: Impact of N on IOP ($K = L = 10, M = 100, Q_p = Q_s = 4, \tau_p = 20$).

observe that the lower bound is fairly close to the simulation result for $P_o \leq 0.2$. And this (target $P_o \leq 0.2$) is precisely the operational regime where the SAPs would communicate with the UAVs in concurrent spectrum access networks to ensure low interference to GUEs. As the power margin (η) increases, the SAPs transmit at lower power. Moreover, as the pilot power p_t^p increases, the estimation error decreases. Therefore, the SAPs violate the target P_o less often. In other words, for poorer channel estimates, a larger power margin is needed at SAPs to keep P_o fixed at the same level.

Figure 3.3 plots $(1-P_o)$ vs. power margin for $p_t^p = -30$ dB and -40 dB, $K = L = 10$ and for $N = 100, N = 200, N = 300$ using the lower bound in (3.26). We infer that for a given p_t^p, IOP does not depend on N and varies only with η because of the use of normalized MR precoder at the SAPs for DL transmission, where the normalization factor depends on the channels from SAPs to UAVs. Thus, we obtain a key design insight that P_o at the GUEs remains the same irrespective of the changes in the number of SAPs. Similar to our observation in Figure 3.2, a larger power margin is needed to keep P_o fixed at the same level as p_t^p decreases, i.e., as the variance of the estimation error increases.

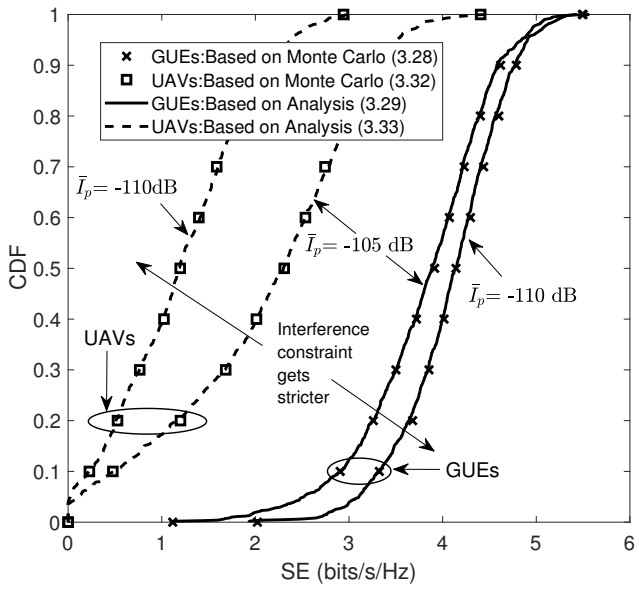

Fig. 3.4: Impact of $\bar{I}_p$ on CDF of SE ($K = L = 10$, $M = N = 100$, $P_o = 0.01$, $\eta = 1.3$, $Q_p = Q_s = 4$, $\tau_p = 20$, $H_{\max} = 300$ m and $p_t^p = -30$ dB).

Figure 3.4 plots the CDF of the DL SE of GUEs and UAVs, for two different values of the interference threshold $(\bar{I}_p)$ namely -105 dB and -110 dB. We observe that analysis matches Monte Carlo simulations, thus validating our analysis. As $\bar{I}_p$ decreases, the interference constraint gets stricter. And based on Figure 3.4, we can observe that the larger the interference threshold $\bar{I}_p$ is, the greater the likelihood for UAVs to obtain a higher SE is and the lower the probability of achieving a higher SE for GUEs is. This is because a higher $\bar{I}_p$ gives the SAPs, the flexibility to transmit at a higher power while causing more interference to GUEs and lowering their SINR. This is also the reason why the probability that SE of GUEs exceeds a certain

target value reduces as $\bar{I}_p$ increases.

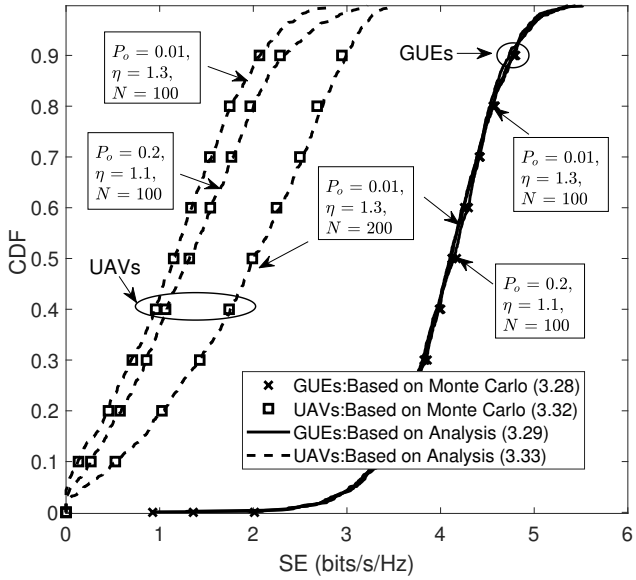

Fig. 3.5: Effect of η and N on CDF of SE ($K = L = 10$, $M = 100$, $Q_p = Q_s = 4$, $\tau_p = 20$, $\bar{I}_p = -105$ dB, $H_{\max} = 300$ m and $p_t^p = -30$ dB).

Figure 3.5 plots the CDF of the DL SE of UAVs and GUEs at $\bar{I}_p = -105$ dB for different values of $(1-P_o, \eta)$ sampled from Figure 3.2. We observe that for a stricter constraint (lower P_o) the probability of UAVs attaining higher SE decreases due to increased power margin. We also obtain a key design insight that the reduction in the SE of UAVs due to increased power margin or lower P_o can be countered by increasing number of SAPs N. For example, if SE^u represents the SE of UAVs then from Figure 3.5, we can observe that $\Pr(\text{SE}^u \geq 2.5 \text{ bits/s/Hz}) = 0.69$ for $N = 100$ at $P_o = 0.2$, $\Pr(\text{SE}^u \geq 2.5 \text{ bits/s/Hz}) = 0.55$ for $N = 100$ at $P_o = 0.01$, whereas $\Pr(\text{SE}^u \geq 2.5 \text{ bits/s/Hz}) = 0.92$ for $N = 200$ at $P_o = 0.01$. Thus, the likelihood that the UAVs attain higher SE increases either due to increase in P_o (reduced power margin) for a given N or increase in N for a given P_o. We see only a marginal degradation in the CDF of SE of GUEs due to increase in P_o and reduced η resulting into marginally higher interference due to SAP transmissions.

From Figure 3.6, we observe that as we increase $\bar{I}_p$, the interference caused to the ground users increases and the effect of the back-off factor on performance of GUEs is clearer. To be specific, as the back-off factor increases, while the performance of UAVs degrades due to

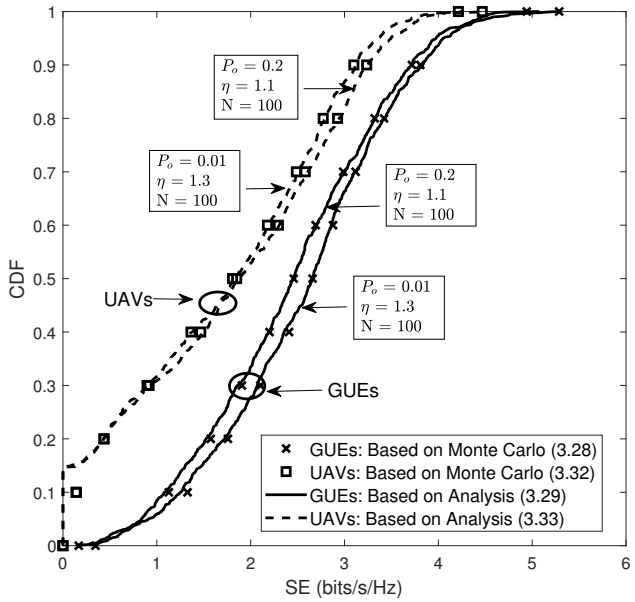

Fig. 3.6: Effect of η and N on CDF of SE ($K = L = 10$, $M = 100$, $Q_p = Q_s = 4$, $\tau_p = 20$, $\bar{I}_p = -95$ dB, $H_{\max} = 300$ m and $p_t^p = -30$ dB).

limitations imposed on the SAP transmit power, the performance of GUEs improves due to reduced interference.

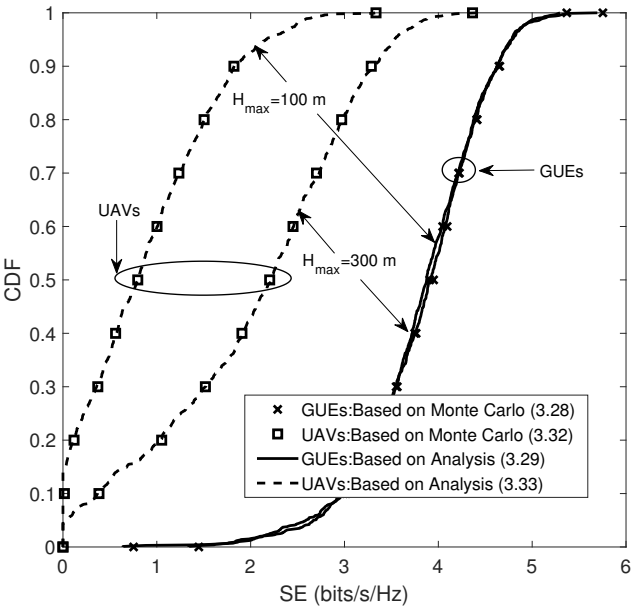

Fig. 3.7: Effect of height of UAVs on CDF of SE ($K = L = 10$, $M = N = 100$, $P_o = 0.01$, $\eta = 1.3$, $Q_p = Q_s = 4$, $\tau_p = 20$, $\bar{I}_p = -105$ dB and $p_t^p = -30$ dB).

Figure 3.7 shows that the likelihood (probability) of UAVs attaining a higher spectral ef-

ficiency increases as $H_{\max}$ increases due to an increase in the strength of the LoS component. Another interesting insight that we obtain based on this result is that SE of GUEs remains unaffected due to changes in $H_{\max}$ of UAVs. We consider that the height of any UAV is uniformly distributed between 22.5 metres and $H_{\max}$.

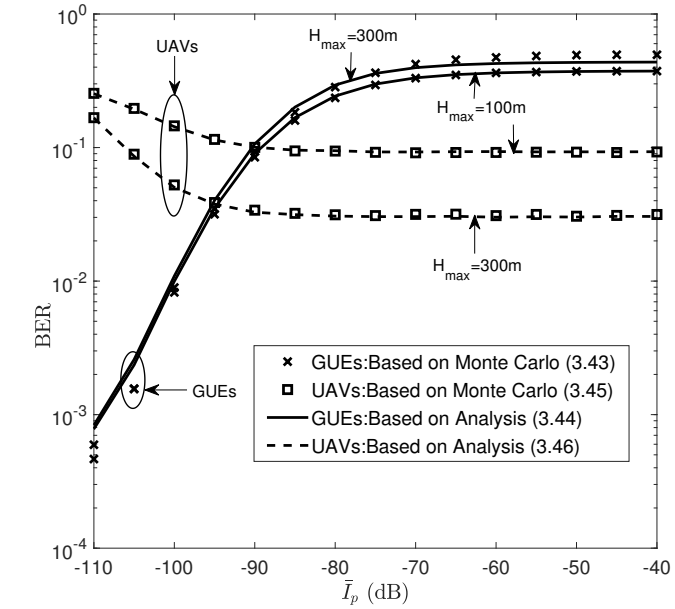

Fig. 3.8: Effect of height of UAVs on BER ($K = L = 10$, $M = N = 100$, $P_o = 0.01$, $\eta = 1.3$, $Q_p = Q_s = 4, \tau_p = 20$, $S = 4$ and $p_t^p = -30$ dB).

Figure 3.8 plots the BER vs. the interference threshold ($\bar{I}_p$) for GUEs and UAVs for two different values of $H_{\max}$. We observe that for a given $H_{\max}$, the BER of UAVs initially decreases as the interference threshold increases and it eventually saturates because the SINR at the UAVs captured by the ratio of the square of the statistical mean to the variance of the effective noise becomes independent of the interference threshold in this regime. Furthermore, it is observed that as we increase $H_{\max}$, the BER of UAVs improves and we see a reduction in the error floor since the strength of the LoS component increases as $H_{\max}$ increases. Also, as expected, the BER of GUEs increases as the interference threshold increases due to increased interference from secondary transmissions.

Figure 3.9 shows that the BER of both the UAVs and the GUEs improves as we increase Q_p and Q_s from 4 to 8. We observe that the BER of GUEs degrades as the interference threshold

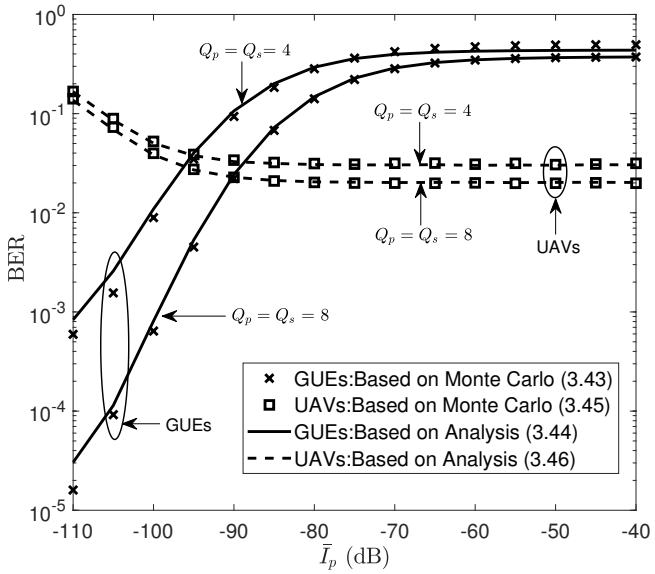

Fig. 3.9: Effect of Qp and Q_s on BER ($K = L = 10$, $M = N = 100$, $P_o = 0.01$, $\eta = 1.3$, $\tau_p = 20$, $S = 4$, $\bar{I}_p = -105$ dB, $H_{\max} = 300$ m and $p_t^p = -30$ dB).

increases due to increased interference from secondary transmissions. We also observe that both the UAVs and GUEs obtain identical BER at $\bar{I}_p = -95$ dB (strict interference threshold) with $Q_p = Q_s = 4$. However, with $Q_p = Q_s = 8$, identical BER can be obtained even at $\bar{I}_p = -90$ dB (relaxed interference threshold). This gives us an interesting design insight that as the number of antennas at the PAPs or the SAPs increase, a greater amount of interference can be tolerated at the GUEs while keeping the BER of both the UAVs and the GUEs identical.

3.6 Summary

We considered a cell-free mMIMO assisted underlay spectrum sharing system in which the SAPs communicate with UAVs subject to an IOP constraint. New integral free lower bound on IOP is derived. Based on this, the system designer can get an idea about the power margin that the SAPs must maintain to meet the IOP constraint at the GUEs. We also derived new approximate DL SE expressions for the UAVs and GUEs. The BER of UAVs and GUEs was also analyzed considering availability of statistical CSI at the user end.

We proved both analytically and through numerical simulations that the SE of UAVs can be improved in a cell-free mMIMO enabled underlay system while keeping the IOP at GUEs fixed at a specific level. Furthermore, we observed that for a given IOP, the larger the interference

threshold is, the larger is the probability of attaining a higher SE for UAVs and the lower is the probability of obtaining higher SE for GUEs. It is also observed that for a given interference threshold, the likelihood that the UAVs attain higher SE increases as IOP increases or as the number of SAPs increases. The impact of height and interference threshold on BER was also elucidated.

While in this chapter, the focus was on modeling and detailed performance analysis of cell-free mMIMO enabled underlay system where the SAPs communicate with UAVs subject to an IOP constraint. The link connecting the APs to the CPU was considered to be of infinite capacity. However, in practice, these fronthaul links that connect the APs to the CPU are of limited capacity. Therefore, the data and the channel estimates have to be quantized at the APs before they are forwarded to the CPUs. In the next chapter, to reduce the signaling burden on these limited fronthaul links, we extend our study to understand the impact of quantizing data and channel estimates on performance of CUs and PUs.

4

Cell-Free Massive MIMO Based Underlay Network with Limited Fronthaul

Contents

In this chapter, we consider a practically realistic scenario where the fronthaul links connecting the APs and CPU in a cell-free configuration have limited capacity. Since, the data and the channel estimates need to be quantized by the APs before being forwarded to the CPUs to reduce the transmission burden and the signaling overhead on the limited capacity fronthaul links, it is of fundamental interest to develop a comprehensive model to rigorously analyze the impact of quantization error thus induced on the performance of cell-free mMIMO based underlay spectrum access networks when the SUs are subject to a practically relevant IOP constraint.

We first develop the system model, discuss the quantization model and UL data transmission. Thereafter, we analyze IOP at PUs and SE of PUs and CUs under estimated quantized CSI. We first review some of the related works.

4.1 Related Literature

Below we categorize papers on cell-free mMIMO depending on whether these networks operate in (i) underlay mode under an interference constraint over infinite capacity fronthaul links or, (ii) non-underlay mode under no interference constraint but consider limited capacity fronthaul in their study. The discussion below is also summarized in Table 4.1.

4.1.1 Cell-free mMIMO based underlay papers that consider interference constraint but do not consider limited capacity fronthaul

In [7], DL rates of PUs and DL rates of SUs when they transmit subject to an average interference constraint were derived. In [65], the authors derived DL rate of SUs when they perform non-orthogonal multiple access (NOMA) based transmission and operate simultaneously with a co-located primary mMIMO network. In [25], the energy efficiency (EE) of a secondary cell-free mMIMO system that operates along with a co-located primary mMIMO network was analyzed. In [16], the authors analyzed the DL SE performance of GUEs and UAVs that transmit subject to an IOP constraint. However, they did not consider quantized estimates to reduce the signalling burden on the limited capacity fronthaul in their study. The aforementioned discussion is summarized in Table 4.1.

Table 4.1: Summary of the literature related to cell-free massive MIMO with and without interference constraint under infinite or limited capacity fronthaul

Interference constraint	Fronthaul link capacity	Cell-free massive MIMO
Peak/Average interference constraint	Infinite capacity	[65], [7], [24], [25].
Unconstrained (Non-cognitive)	Finite capacity.	[29, 79], [80, 81] [82, 83] [84, 85]
Interference violation probability constraint	Infinite capacity	[16]
	Finite capacity	**None**

4.1.2 Cell-free mMIMO based papers that consider limited capacity fronthaul and non-underlay mode without any interference constraint

In [29], the authors analyzed max-min optimal UL and DL data rates considering limited capacity fronthaul links. In [79], weighted sum EE was optimized for the UL of cell-free mMIMO network using deep determinant policy gradient. In [84], performance analysis and decentralized optimization was done for full-duplex cell-free mMIMO systems. In [83], the achievable rate of a limited fronthaul cell-free mMIMO using local MMSE detection was studied. In [80] and [81], the authors investigated EE and developed deep-learning based power adaptation rule for limited capacity fronthaul links, respectively. In [85], the performance of limited fronthaul cell-free mMIMO was compared to that of an unlimited fronthaul network. In [82], the authors studied UL SE of cell-free mMIMO over limited capacity fronthaul link between APs and CPU under hardware impairments.

4.2 Motivation

Based on the discussion above, we observe that most of the existing papers in the literature have investigated cell-free mMIMO based underlay spectrum sharing networks under an interference constraint over infinite capacity fronthaul [7, 16, 25, 65]. However, papers on cell-free mMIMO networks that included limited capacity fronthaul in their analysis, did not consider any interference constraint and underlay mode of operation of the cognitive radio [29, 79–85]. To be specific, no paper in the existing literature has comprehensively analyzed the SE of PUs

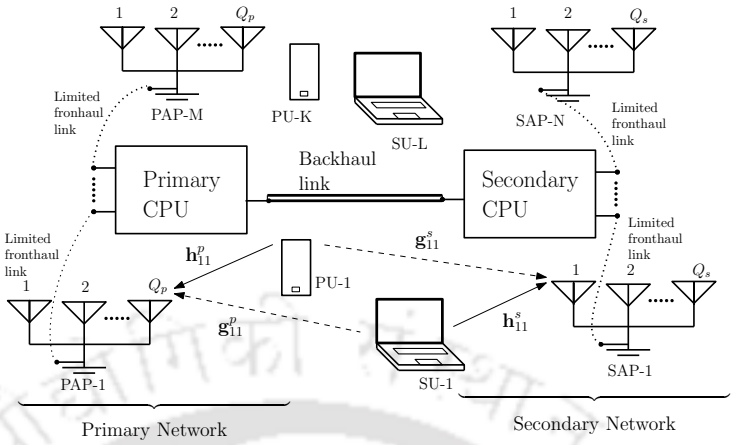

Fig. 4.1: System model

and SUs in cell-free mMIMO based underlay spectrum sharing networks (i) when the data and the channel estimates are quantized by the APs before being forwarded to the CPUs to reduce the transmission burden on limited capacity fronthaul links, and (ii) the transmissions by the SUs are subject to an IOP constraint. This probabilistic constraint and the quantization error thus induced substantially changes the mathematical analysis and this is what we focus on in this chapter.

Notations: We use $z \sim \mathcal{CN}(\mathbf{0}, \mathbf{\Sigma})$ to represent a circular symmetric complex Gaussian RV with zero mean and covariance matrix $\mathbf{\Sigma}$. The notation $x \sim \mathcal{U}[a, b]$ denotes that the rv x is uniformly distributed between a and b. The notation $y \sim \Gamma(c, d)$ refers to a Gamma distributed rv y with shape parameter c and scale parameter d. The probability of an event A is denoted by $\Pr(A)$. The absolute value of a scalar and l_2-norm of a vector are represented by $|\cdot|$ and $\|\cdot\|$, respectively.

Organization: The remainder of the chapter is organized as follows. Section 4.3 describes the system model, reviews the optimal uniform quantization model and discusses UL data transmission. Section 4.4 presents the IOP analysis. Section 4.5 presents UL SE analysis of PUs and SUs. Numerical results and conclusions are given in Sections 4.7 and 4.8, respectively. The proofs are given in Appendix C.

4.3 System Model

We consider UL of a cell-free mMIMO aided underlay CR system. As shown in Figure 4.1, it consists of M multi-antenna PAPs that serve K PUs and N multi-antenna SAPs that serve L SUs. Every PAP is equipped with Q_p antennas and every SAP has Q_s antennas. The PAPs are connected to the primary CPU and the SAPs are connected to the secondary CPU through their respective fronthaul links.

For the primary network, the channel between the m^{th} PAP and the k^{th} PU is represented by $\boldsymbol{h}_{mk}^{p} = \left[\left[h_{mk}^{p}\right]_1, \ldots, \left[h_{mk}^{p}\right]_{Q_p}\right]^T$, where $m \in \{1, 2, \ldots, M\}$ and $k \in \{1, 2, \ldots, K\}$. We consider Rayleigh fading. Thus, $\boldsymbol{h}_{mk}^{p} \sim \mathcal{CN}\left(\boldsymbol{0}, \beta_{mk}^{p}\mathbf{I}_{Q_p}\right)$, where β_{mk}^{p} represents large scale fading between any antenna at the m^{th} PAP and the k^{th} PU. The interference channel between the m^{th} PAP and l^{th} SU is denoted by $\boldsymbol{g}_{ml}^{p} = \left[\left[g_{ml}^{p}\right]_1, \ldots, \left[g_{ml}^{p}\right]_{Q_p}\right]^T$ for $l \in \{1, \ldots, L\}$ and $\boldsymbol{g}_{ml}^{p} \sim \mathcal{CN}\left(\boldsymbol{0}, \beta_{ml}^{p}\mathbf{I}_{Q_p}\right)$, where β_{ml}^{p} represents large scale fading between any antenna at the m^{th} PAP and the l^{th} SU. For the secondary network, the channel between the n^{th} SAP and l^{th} SU is denoted by $\boldsymbol{h}_{nl}^{s} = \left[\left[h_{nl}^{s}\right]_1, \ldots, \left[h_{nl}^{s}\right]_{Q_s}\right]^T$ where $n \in \{1, 2, \ldots, N\}$ and $\boldsymbol{h}_{nl}^{s} \sim \mathcal{CN}\left(\boldsymbol{0}, \beta_{nl}^{s}\mathbf{I}_{Q_s}\right)$. Note that β_{nl}^{s} denotes the large scale fading over this link. The interference channel between the n^{th} SAP and the k^{th} PU is denoted by $\boldsymbol{g}_{nk}^{s} = \left[\left[g_{nk}^{s}\right]_1, \ldots, \left[g_{nk}^{s}\right]_{Q_s}\right]^T$ and we consider that $\boldsymbol{g}_{nk}^{s} \sim \mathcal{CN}\left(\boldsymbol{0}, \beta_{nk}^{s}\mathbf{I}_{Q_s}\right)$, where β_{nk}^{s} is the corresponding large scale fading over this link.

In this chapter, we consider Gauss-Markov uncertainty based imperfect CSI model [49]. According to this generic model, the true channel between the k^{th} PU and m^{th} PAP equals

$$\boldsymbol{h}_{mk}^{p} = s_r\, \widehat{\boldsymbol{h}}_{mk}^{p} + \sqrt{1 - s_r^2}\, \widetilde{\boldsymbol{h}}_{mk}^{p}, \tag{4.1}$$

where $0 \leq s_r \leq 1$ captures the channel estimation accuracy, $\widehat{\boldsymbol{h}}_{mk}^{p} \sim \mathcal{CN}\left(\boldsymbol{0}, \beta_{mk}^{p}\mathbf{I}_{Q_p}\right)$ represents channel estimate and $\widetilde{\boldsymbol{h}}_{mk}^{p} \sim \mathcal{CN}\left(\boldsymbol{0}, \beta_{mk}^{p}\mathbf{I}_{Q_p}\right)$ denotes channel estimation error. Note that $\widetilde{\boldsymbol{h}}_{mk}^{p}$ is uncorrelated to $\widehat{\boldsymbol{h}}_{mk}^{p}$. For the secondary network, the true channel between the n^{th} SAP and l^{th} SU equals

$$\boldsymbol{h}_{nl}^{s} = s_s\, \widehat{\boldsymbol{h}}_{nl}^{s} + \sqrt{1 - s_s^2}\, \widetilde{\boldsymbol{h}}_{nl}^{s}, \tag{4.2}$$

where $\widehat{\boldsymbol{h}}_{nl}^{s} \sim \mathcal{CN}\left(\boldsymbol{0}, \beta_{nl}^{s}\mathbf{I}_{Q_s}\right)$ and $\widetilde{\boldsymbol{h}}_{nl}^{s} \sim \mathcal{CN}\left(\boldsymbol{0}, \beta_{nl}^{s}\mathbf{I}_{Q_s}\right)$. As before, $\widetilde{\boldsymbol{h}}_{nl}^{s}$ is uncorrelated to $\widehat{\boldsymbol{h}}_{nl}^{s}$ and

$0 \leq s_s \leq 1$. The interference channel between the m^{th} PAP and l^{th} SU equals

$$\boldsymbol{g}_{ml}^{p} = s_p \, \widehat{\boldsymbol{g}}_{ml}^{p} + \sqrt{1 - s_p^2} \, \widetilde{\boldsymbol{g}}_{ml}^{p}, \tag{4.3}$$

where $\widehat{\boldsymbol{g}}_{ml}^{p} \sim \mathcal{CN}\left(\mathbf{0}, \beta_{ml}^{p} \mathbf{I}_{Q_p}\right)$ and $\widetilde{\boldsymbol{g}}_{ml}^{p} \sim \mathcal{CN}\left(\mathbf{0}, \beta_{ml}^{p} \mathbf{I}_{Q_p}\right)$. We wish to highlight that $\widetilde{\boldsymbol{g}}_{ml}^{p}$ is uncorrelated to $\widehat{\boldsymbol{g}}_{ml}^{p}$ and $0 \leq s_p \leq 1$ models the estimation accuracy.

4.3.1 Optimal Uniform Quantization Model

From the APs, the channel estimates and received signals are sent to the CPUs over respective fronthaul links. We consider that these fronthaul links are of limited capacity. And therefore, only the quantized versions of the estimated CSI and the received signals can be transferred by the APs to the CPUs. Based on Bussgang's theorem, the quantized version $Q(\widehat{\boldsymbol{g}}_{ml}^{p})$ of the channel estimate of the link between the m^{th} PAP and l^{th} SU is given by [29], [86]

$$Q(\widehat{\boldsymbol{g}}_{ml}^{p}) = \dot{a} \widehat{\boldsymbol{g}}_{ml}^{p} + \boldsymbol{e}_{ml}^{\widehat{g}^p}, \tag{4.4}$$

where $\dot{a}$ represents the normalized Bussgang gain and $\boldsymbol{e}_{ml}^{\widehat{g}^p}$ denotes the noise induced due to quantization error. We consider that $\boldsymbol{e}_{ml}^{\widehat{g}^p}$ has zero mean and variance $\sigma_{\dot{e}}^2 \, \beta_{ml}^{p}$ where $\sigma_{\dot{e}}^2 = \dot{b} - \dot{a}^2$ and $\dot{b}$ represents the normalized variance of the quantizer output. The parameters $\dot{a}$ and $\dot{b}$ are obtained from an optimal normalized step size $\dot{\Delta}_{\text{opt}}$ of a mid-rise uniform quantizer and are given by

$$\dot{a} = \sum_{l=1}^{\left(\frac{L_q}{2}-1\right)} \frac{2\dot{\Delta}_{\text{opt}}}{\sqrt{2\pi}} \exp\left(\frac{-(l\dot{\Delta}_{\text{opt}})^2}{2}\right) + \frac{\dot{\Delta}_{\text{opt}}}{\sqrt{2\pi}}, \tag{4.5}$$

$$\dot{b} = \dot{\Delta}_{\text{opt}}^{2} \left(\frac{1}{4} + \sum_{l=1}^{\left(\frac{L_q}{2}-1\right)} 4lQ\left(l\dot{\Delta}_{\text{opt}}\right)\right), \tag{4.6}$$

where $L_q = 2^{\alpha}$ denotes the number of quantization levels and α denotes the number of quantization bits. The values of $\dot{\Delta}_{\text{opt}}$ corresponding to different α is given in Table I of [29]. The QCE of all other links can be expressed in a similar way as in (4.4).

4.3.2 UL Data Transmission

Let $x_k = \sqrt{P_u^p} q_k$ denote the signal transmitted by the k^{th} PU, where P_u^p represents UL transmission power of PUs and q_k represents the information symbol of the k^{th} PU. Furthermore, $q_k \sim \mathcal{CN}(0,1)$ and $\mathbb{E}\{q_i q_j^*\} = 0$ for $i \neq j$. Similarly, let $x_l = \sqrt{\widehat{P}_{uq}^s} s_l$ be the signal sent by the l^{th} SU, where $\widehat{P}_{uq}^s$ represents UL transmission power of SUs and s_l represents the information symbol of the l^{th} SU chosen such that $s_l \sim \mathcal{CN}(0,1)$ and $\mathbb{E}\{s_i s_j^*\} = 0$ for $i \neq j$.

When both the PUs and SUs transmit their respective information symbols, then the signal received at the m^{th} PAP equals

$$\begin{aligned} \boldsymbol{y}_m &= \sum_{k=1}^{K} \boldsymbol{h}_{mk}^p x_k + \sum_{l=1}^{L} \boldsymbol{g}_{ml}^p x_l + \boldsymbol{n}_m, \\ &= \sum_{k=1}^{K} \sqrt{P_u^p} \boldsymbol{h}_{mk}^p q_k + \sum_{l=1}^{L} \sqrt{\widehat{P}_{uq}^s} \boldsymbol{g}_{ml}^p s_l + \boldsymbol{n}_m, \end{aligned} \tag{4.7}$$

where $\boldsymbol{n}_m \sim \mathcal{CN}\left(\boldsymbol{0}, \sigma_w^2 \mathbf{I}_{Q_p}\right)$ represents noise at the m^{th} PAP. The signal received at the n^{th} SAP due to simultaneous UL transmissions by PUs and SUs is given by

$$\begin{aligned} \boldsymbol{y}_n &= \sum_{l'=1}^{L} \boldsymbol{h}_{nl'}^s x_{l'} + \sum_{k=1}^{K} \boldsymbol{g}_{nk}^s x_k + \boldsymbol{n}_n, \\ &= \sum_{l'=1}^{L} \sqrt{\widehat{P}_{uq}^s} \boldsymbol{h}_{nl'}^s s_{l'} + \sum_{k=1}^{K} \sqrt{P_u^p} \boldsymbol{g}_{nk}^s q_k + \boldsymbol{n}_n, \end{aligned} \tag{4.8}$$

where $\boldsymbol{n}_n \sim \mathcal{CN}\left(\boldsymbol{0}, \sigma_w^2 \mathbf{I}_{Q_s}\right)$ denotes noise at the n^{th} SAP.

4.4 IOP Analysis

From (4.7), the interference power at the m^{th} PAP due to simultaneous transmission by the SUs is given by

$$I_m^p = \mathbb{E}\left(\left| \sum_{l=1}^{L} \sqrt{\widehat{P}_{uq}^s} \boldsymbol{g}_{ml}^p s_l \right|^2 \right) = \sum_{l=1}^{L} \|\boldsymbol{g}_{ml}^p\|^2 \widehat{P}_{uq}^s = \widehat{P}_{uq}^s Z_m, \tag{4.9}$$

where $Z_m \triangleq \sum_{l=1}^{L} \|\boldsymbol{g}_{ml}^p\|^2$ for all $1 \leq m \leq M$ and the expectation is taken over the distribution of s_l. Note that Z_m is the sum of SLN of L independent complex Gaussian RVs each having zero mean and a different covariance matrix. It is analytically intractable to derive the exact pdf

of Z_m, since $\boldsymbol{g}_{ml}^p$ is not identically distributed across $1 \leq l \leq L$. Therefore, we propose a new statistical model for Z_m based on Gamma distribution. This result as stated below in Lemma 4.1 will be used in the IOP analysis later in this section.

Lemma 4.1. *$Z_m \sim \Gamma(\alpha_m, \beta_m)$ with pdf given by*

$$f_{Z_m}(z_m) = \frac{1}{\beta_m \Gamma(\alpha_m)} \left(\frac{z_m}{\beta_m}\right)^{\alpha_m - 1} e^{-\frac{z_m}{\beta_m}}, \quad z_m \geq 0, \tag{4.10}$$

where the shape parameter $\alpha_m = \frac{\left(\sum_{l=1}^{L} Q_p \beta_{ml}^p\right)^2}{\sum_{l=1}^{L} Q_p (\beta_{ml}^p)^2}$ and the scale parameter $\beta_m = \frac{\sum_{l=1}^{L} Q_p (\beta_{ml}^p)^2}{\sum_{l=1}^{L} Q_p \beta_{ml}^p}$.

Proof. The proof is given in Appendix C.1 □

Remarks: Based on Lemma 4.1, we observe that the shape parameter (α_m) and the scale parameter (β_m) of Z_m depend on system parameters such as the number of antennas (Q_p) at the PAPs, the number of SUs (L) and on the strength of the interference channels between the SUs and the PAPs.

In this chapter, as before, we consider a simultaneous spectrum access system where the SUs transmit in underlay mode and are subject to an IOP constraint. This probabilistic constraint requires that the interference power due to transmission by SUs does not exceed threshold $\bar{I}_p$ at any of the M PAPs more than P_o fraction of the time [16], [66]. Mathematically, this can be stated as

$$\Pr(I_1^p \leq \bar{I}_p, I_2^p \leq \bar{I}_p, \ldots, I_M^p \leq \bar{I}_p) \geq (1 - P_o)\,, \tag{4.11}$$

where P_o denotes the IOP.

We next discuss the back-off factor based power adaptation policy for the SUs. According to this policy, the SU transmit power is given by

$$\widehat{P}_{uq}^s = \frac{\bar{I}_p}{\eta \max\limits_{1 \leq m \leq M} \left\{ \sum\limits_{l=1}^{L} \|Q(\widehat{\boldsymbol{g}}_{ml}^p)\|^2 \right\}} = \frac{\bar{I}_p}{\eta \max\limits_{1 \leq m \leq M} \left\{ \widehat{Z}_m^q \right\}}, \tag{4.12}$$

where $\bar{I}_p$ denotes the interference threshold, $Q(\widehat{\boldsymbol{g}}_{ml}^p)$ represents the quantized channel estimate (QCE) of the link between the m^{th} PAP and l^{th} SU, the back-off factor $\eta(>1)$ is chosen such that the IOP constraint under QCE is met with equality[1] for a given P_o and $\widehat{Z}_m^q = \sum_{l=1}^{L} \|Q(\widehat{\boldsymbol{g}}_{ml}^p)\|^2 =$

[1] In practice, the PAPs will estimate the interference channels to the SUs based on the observables received

$\sum_{l=1}^{L} \|\dot{a}\widehat{\boldsymbol{g}}_{ml}^{p} + \boldsymbol{e}_{ml}^{\widehat{g}^p}\|^2$. Note that $\widehat{Z}_m^q$ denotes the sum of SLN of L independent zero mean RVs that model QCE each having different statistics. We consider that $\text{Re}\{[\boldsymbol{e}_{ml}^{\widehat{g}^p}]_i\}$ and $\text{Img}\{[\boldsymbol{e}_{ml}^{\widehat{g}^p}]_i\} \sim \sigma_{\dot{e}}\sqrt{\frac{\beta_{ml}^p}{2}}\,\mathcal{U}[-\sqrt{3},\sqrt{3}]$ for $1 \le i \le Q_p$ so that the variance of $[\boldsymbol{e}_{ml}^{\widehat{g}^p}]_i$ equals $\sigma_{\dot{e}}^2\beta_{ml}^p$ [88]. Since each RV in the sum has a different statistics, it is analytically intractable to derive the exact pdf of $\widehat{Z}_m^q$. We therefore, develop a new statistical model for $\widehat{Z}_m^q$ that we will use in our IOP and SE analysis.

Lemma 4.2. *$\widehat{Z}_m^q \sim \Gamma(\widehat{\alpha}_m^q, \widehat{\beta}_m^q)$ with pdf given by*

$$f_{\widehat{Z}_m^q}(\widehat{z}_m^q) = \frac{1}{\widehat{\beta}_m^q \Gamma(\widehat{\alpha}_m^q)} \left(\frac{\widehat{z}_m^q}{\widehat{\beta}_m^q}\right)^{\widehat{\alpha}_m^q - 1} e^{-\frac{\widehat{z}_m^q}{\widehat{\beta}_m^q}}, \quad \widehat{z}_m^q \ge 0, \tag{4.13}$$

where the shape parameter

$$\widehat{\alpha}_m^q = \frac{\left(\sum_{l=1}^{L} Q_p \dot{b}\beta_{ml}^p\right)^2}{\left(\frac{3\dot{a}^4}{2} + \frac{9\sigma_{\dot{e}}^4}{10} + \frac{6\dot{a}^2\sigma_{\dot{e}}^2}{2} - \frac{\dot{b}^2}{2}\right)\sum_{l=1}^{L} Q_p(\beta_{ml}^p)^2}, \tag{4.14}$$

and the scale parameter

$$\widehat{\beta}_m^q = \frac{\left(\frac{3\dot{a}^4}{2} + \frac{9\sigma_{\dot{e}}^4}{10} + \frac{6\dot{a}^2\sigma_{\dot{e}}^2}{2} - \frac{\dot{b}^2}{2}\right)\sum_{l=1}^{L} Q_p(\beta_{ml}^p)^2}{\sum_{l=1}^{L} Q_p \dot{b}\beta_{ml}^p}. \tag{4.15}$$

Proof. The proof is given in Appendix C.2. □

Remarks: Based on Lemma 4.2, we observe that the shape parameter $(\widehat{\alpha}_m^q)$ and the scale parameter $(\widehat{\beta}_m^q)$ of $\widehat{Z}_m^q$ under quantization and channel estimation errors depend on several system parameters such as the Bussgang gain $(\dot{a})$, variance of quantization error $(\sigma_{\dot{e}}^2)$, normalized variance of the quantizer output $(\dot{b})$ which in turn depends on the optimal normalized step size and the number of quantization bits. Furthermore, $(\widehat{\alpha}_m^q)$ and $(\widehat{\beta}_m^q)$ also depend on the number of antennas (Q_p) at the PAPs, the number of SUs (L) and on the strength of the interference channels between the SUs and the PAPs.

during the training phase and the pilot information of SUs shared among the CPUs over the backhaul link [46], [69], [70], [71], [87]. These interference channel estimates will be quantized at the PAPs before being forwarded to the primary CPU over the limited capacity fronthaul. At the primary CPU, the back-off factor and the power with which the SUs must transmit will be computed for a given $\bar{I}_p$ and P_o and forwarded to the secondary CPU over the backhaul which will then broadcast the power value to each of the SUs.

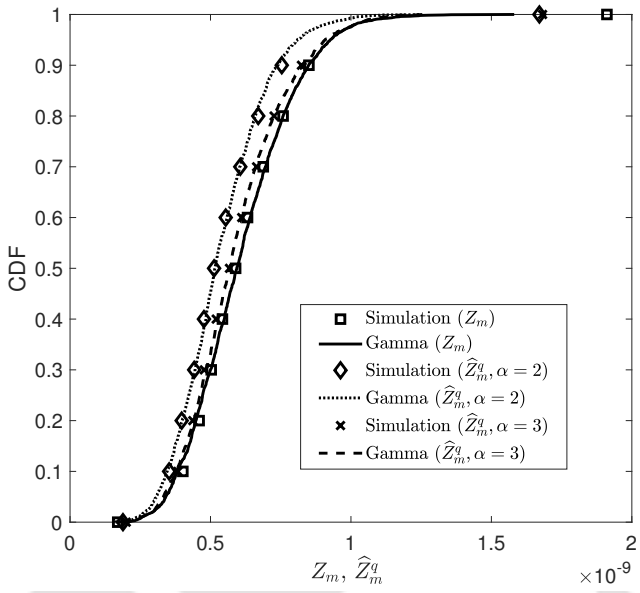

Fig. 4.2: CDF of Z_m and $\widehat{Z}_m^q$.

Model Validation: Figure 4.2 plots the CDF of Z_m and $\widehat{Z}_m^q$ for $\alpha = 2$ and 3 bits, respectively obtained empirically from 2000 samples through Monte Carlo simulations. We also plot the CDF of Gamma rvs with the corresponding shape and scale parameters as stated in Lemmas 4.1 and 4.2. We observe that the simulations and the Gamma CDF match reasonably well for Z_m and $\widehat{Z}_m^q$ for $\alpha = 2$ and 3. This confirms that the Gamma modeling of both Z_m and $\widehat{Z}_m^q$ is reasonably accurate. We use the statistical model developed for $\widehat{Z}_m^q$ in Lemma 4.2 to derive an analytical expression for the expectation of SU transmit power $\widehat{P}_{uq}^s$ in (4.12) and also for its square root.

Proposition 4.1. *The SU transmit power* $\widehat{P}_{uq}^s = \frac{\bar{I}_p}{\eta} X$ *is a scaled version of rv* $X = \frac{1}{\max\limits_{1\le m\le M}\left\{\sum\limits_{l=1}^{L} \|\widehat{a}\widehat{\boldsymbol{g}}_{ml}^p + \widehat{\boldsymbol{e}}_{ml}^{gp}\|^2\right\}}$ *whose pdf is given by*

$$f_X(x) = \sum_{j=1}^{M}\left[\left(\frac{1}{\widehat{\beta}_j^q}\right)^{\widehat{\alpha}_j^q}\left(\frac{1}{\Gamma(\widehat{\alpha}_j^q)}\right)\left(\frac{1}{x}\right)^{\widehat{\alpha}_j^q+1} e^{-\frac{1}{x\widehat{\beta}_j^q}}\prod_{i\neq j}^{M}\left(\frac{\gamma\left(\widehat{\alpha}_i^q, \frac{1}{\widehat{\beta}_i^q x}\right)}{\Gamma(\widehat{\alpha}_i^q)}\right)\right]. \tag{4.16}$$

Furthermore, the expected value of $\widehat{P}_{uq}^s$ *equals*

$$\xi = \mathbb{E}\left(\widehat{P}_{uq}^s\right) = \frac{\bar{I}_p}{\eta}\sum_{j=1}^{M}\sum_{l=1}^{T}\left[\frac{w_l(x_l)^{\widehat{\alpha}_j^q-2}}{\widehat{\beta}_j^q\Gamma(\widehat{\alpha}_j^q)}\prod_{i\neq j}^{M}\left(\frac{\gamma\left(\widehat{\alpha}_i^q, \frac{\widehat{\beta}_j^q x_l}{\widehat{\beta}_i^q}\right)}{\Gamma(\widehat{\alpha}_i^q)}\right)\right], \tag{4.17}$$

where $\{x_l\}$ are referred to as the Gauss-Laguerre integration points, the corresponding weights are denoted by $\{w_l\}$ and T is the number of integration points [72, (25.4.29)].

Proof. The proof is given in Appendix C.3. □

Remarks: The analytical expression in (4.17) highlights that the mean SU transmit power is dependent on the shape $\left(\widehat{\alpha}_j^q\right)$ and scale $\left(\widehat{\beta}_j^q\right)$ parameters of $\widehat{Z}_j^q$, which in turn depends on the Bussgang gain ($\dot{a}$), variance of quantization error ($\sigma_{\dot{e}}^2$), number of quantization levels (L_q), number of PAPs (M), interference threshold ($\bar{I}_p$) and the back-off factor (η).

Corollary 4.1. *The square root of the SU transmit power $\sqrt{\widehat{P}_{uq}^s} = \sqrt{\frac{\bar{I}_p}{\eta}}W$ is obtained through a simple transformation of rv $W = \frac{1}{\sqrt{\max\limits_{1\le m\le M}\{\widehat{Z}_m^q\}}}$ whose pdf is given by*

$$f_W(w) = \sum_{j=1}^{M}\left[\left(\frac{1}{\widehat{\beta}_j^q}\right)^{\widehat{\alpha}_j^q}\frac{2e^{-\frac{1}{\widehat{\beta}_j^q w^2}}}{\Gamma(\widehat{\alpha}_j^q)(w)^{2\widehat{\alpha}_j^q+1}}\prod_{i\neq j}^{M}\left(\frac{\gamma\left(\widehat{\alpha}_i^q, \frac{1}{\widehat{\beta}_i^q w^2}\right)}{\Gamma(\widehat{\alpha}_i^q)}\right)\right]. \tag{4.18}$$

Furthermore,

$$\lambda = \mathbb{E}\left(\sqrt{\widehat{P}_{uq}^s}\right) = \sqrt{\frac{\bar{I}_p}{\eta}}\sum_{j=1}^{M}\sum_{l=1}^{T}\left[\frac{w_l(x_l)^{\widehat{\alpha}_j^q-\frac{3}{2}}}{\left(\widehat{\beta}_j^q\right)^{\frac{1}{2}}\Gamma(\widehat{\alpha}_j^q)}\prod_{i\neq j}^{M}\left(\frac{\gamma\left(\widehat{\alpha}_i^q, \frac{\widehat{\beta}_j^q x_l}{\widehat{\beta}_i^q}\right)}{\Gamma(\widehat{\alpha}_i^q)}\right)\right]. \tag{4.19}$$

This can be proved using (4.16) *and based on transformation of rvs.*

The results stated in Proposition 4.1 and Corollary 4.1 will be used in analyzing UL SE in Section IV. Now, according to the power control in (4.12), η is set so that

$$\Pr(I_1^p \le \bar{I}_p, I_2^p \le \bar{I}_p, \ldots, I_M^p \le \bar{I}_p) = (1 - P_o). \tag{4.20}$$

Substituting for I_m^p, $1 \le m \le M$ from (4.9), we can re-write (4.20) as

$$\Pr\left(Z_1 \le \eta \max_{1\le m\le M}\{\widehat{Z}_m^q\}, \ldots, Z_M \le \eta \max_{1\le m\le M}\{\widehat{Z}_M^q\}\right) = (1 - P_o). \tag{4.21}$$

In order to find the analytical expression for $(1 - P_o)$ as stated above, we need to first analyze the correlation between Z_m and $\widehat{Z}_m^q$.

Proposition 4.2. *The correlation coefficient between Z_m and $\widehat{Z}_m^q$ is given by*

$$\rho_m = \frac{s_p^2 \dot{a}^2}{\sqrt{\left(\frac{3\dot{a}^4}{2} + \frac{9\sigma_{\dot{e}}^4}{10} + \frac{6\dot{a}^2\sigma_{\dot{e}}^2}{2} - \frac{\dot{b}^2}{2}\right)}}. \tag{4.22}$$

Proof. The proof is given in Appendix C.4.

Remarks: We observe that the correlation coefficient ρ_m is independent of the PAP index m. We also note that ρ_m is a function of the Bussgang gain and the variance of quantization noise, which in turn depends on α.

From the power policy in (4.12) and using ρ_m in (4.22), we next state a lower bound on $(1 - P_o)$.

Theorem 4.1. *Under estimated and quantized CSI in a cell-free mMIMO based underlay network over limited capacity fronthaul, $(1 - P_o)$ is lower bounded by*

$$P_L = \max\left(0, 1 - \sum_{i=1}^{M}\sum_{l=1}^{T} \frac{w_l x_l^{\alpha_i - 1}}{\Gamma(\alpha_i)} \prod_{\substack{j=1 \\ i \neq j}}^{M} \frac{\gamma\left(\widehat{\alpha}_j^q, \frac{x_l \beta_i}{\eta \widehat{\beta}_j^q}\right)}{\Gamma(\widehat{\alpha}_j)} \times \left(1 - Q_{\alpha_i}\left(\sqrt{\frac{2\rho_i x_l}{(1-\rho_i)}}, \sqrt{\frac{2x_l\beta_i}{\eta\widehat{\beta}_i^q(1-\rho_i)}}\right)\right)\right), \tag{4.23}$$

where $Q_{\alpha_i}(\cdot,\cdot)$ denotes the generalized Marcum-Q function of order α_i [54, (4.59)].

Proof. The proof is given in Appendix C.5. □

Remarks: The closed-form expression in (4.23) highlights the dependence of IOP on the back-off factor (η), the number of PAPs (M), the number of SUs (L), the number of quantization bits (α), s_p that captures quality of channel estimates, the correlation coefficient (ρ_i) and the strength of the interference channel between the SUs and the PAPs.

4.5 UL SE Analysis

All the PAPs and the SAPs send quantized versions of the channel estimates and the signal received during the data phase to their respective CPUs through the limited capacity fronthaul links. Then, both primary and secondary CPUs align the quantized received signals along their respective QCE. Finally, the primary and secondary CPUs combine all the projected signals to form a sufficient statistic to detect the desired signal.

4.5.1 UL SE Analysis of PUs

We derive the UL SE of the k^{th} PU based on the quantized estimates of the channel between k^{th} PU and m^{th} PAP. Note that $Q(\widehat{\boldsymbol{h}}^{p}_{mk}) = \dot{a}\widehat{\boldsymbol{h}}^{p}_{mk} + \boldsymbol{e}^{\widehat{h}^{p}}_{mk}$, where $\widehat{\boldsymbol{h}}^{p}_{mk} \sim \mathcal{CN}\left(\boldsymbol{0}, \beta^{p}_{mk}\mathbf{I}_{Q_p}\right)$, $\boldsymbol{e}^{\widehat{h}^{p}}_{mk} \in C^{Q_p \times 1}$ denotes noise due to quantization error with covariance $\sigma^2_{\dot{e}}\,\beta^{p}_{mk}\mathbf{I}_{Q_p}$. The quantized received signal vector at the m^{th} PAP is given by

$$Q(\boldsymbol{y}_m) = \dot{a}\boldsymbol{y}_m + \boldsymbol{e}^{y}_{m}, \tag{4.24}$$

where it can be shown that $\boldsymbol{y}_m \sim \mathcal{CN}\left(\boldsymbol{0}, \left(\sum_{k'=1}^{K} P^{p}_{u}\beta^{p}_{mk'} + \sum_{l=1}^{L}\xi\beta^{p}_{ml} + \sigma^2_{w}\right)\mathbf{I}_{Q_p}\right)$ and $\boldsymbol{e}^{y}_{m}$ denotes the quantization noise vector with covariance $\sigma^2_{\dot{e}}\left(\sum_{k'=1}^{K} P^{p}_{u}\beta^{p}_{mk'} + \sum_{l=1}^{L}\xi\beta^{p}_{ml} + \sigma^2_{w}\right)\mathbf{I}_{Q_p}$. After maximum ratio combining (MRC), the processed signal corresponding to the k^{th} PU at the primary CPU is given by

$$\begin{aligned} z^{q}_{k} &= \sum_{m=1}^{M} Q\left(\widehat{\boldsymbol{h}}^{p\mathrm{H}}_{mk}\right) Q\left(\boldsymbol{y}_m\right), \\ &= \sum_{m=1}^{M}\left(\dot{a}^2\,\widehat{\boldsymbol{h}}^{p\mathrm{H}}_{mk}\boldsymbol{y}_m + \dot{a}\boldsymbol{e}^{\widehat{h}^{p}\,\mathrm{H}}_{mk}\boldsymbol{y}_m + \dot{a}\widehat{\boldsymbol{h}}^{p\mathrm{H}}_{mk}\boldsymbol{e}^{y}_{m} + \boldsymbol{e}^{\widehat{h}^{p}\,\mathrm{H}}_{mk}\boldsymbol{e}^{y}_{m}\right). \end{aligned} \tag{4.25}$$

Using (4.1) and (4.7), z^{q}_{k} can be re-written as

$$\begin{aligned} z^{q}_{k} = \sum_{m=1}^{M}\Bigg(&\dot{a}^2 s_r\sqrt{P^{p}_{u}}\|\widehat{\boldsymbol{h}}^{p}_{mk}\|^2 q_k + \dot{a}^2\sqrt{(1-s_r{}^2)P^{p}_{u}}\,\widehat{\boldsymbol{h}}^{p\mathrm{H}}_{mk}\widetilde{\boldsymbol{h}}^{p}_{mk}q_k + \sum_{k'\neq k}^{K}\dot{a}^2\sqrt{P^{p}_{u}}\,\widehat{\boldsymbol{h}}^{p\mathrm{H}}_{mk}\boldsymbol{h}^{p}_{mk'}q_{k'} \\ &+ \sum_{l=1}^{L}\dot{a}^2\sqrt{\widehat{P}^{s}_{uq}}\,\widehat{\boldsymbol{h}}^{p\mathrm{H}}_{mk}\boldsymbol{g}^{p}_{ml}s_l + \dot{a}^2\,\widehat{\boldsymbol{h}}^{p\mathrm{H}}_{mk}\boldsymbol{n}_m + \dot{a}\boldsymbol{e}^{\widehat{h}^{p}\,\mathrm{H}}_{mk}\boldsymbol{y}_m + \dot{a}\widehat{\boldsymbol{h}}^{p\mathrm{H}}_{mk}\boldsymbol{e}^{y}_{m} + \boldsymbol{e}^{\widehat{h}^{p}\,\mathrm{H}}_{mk}\boldsymbol{e}^{y}_{m}\Bigg). \end{aligned} \tag{4.26}$$

By using use and then forget bound, we can write z^{q}_{k} as [14], [89].

$$\begin{aligned} z^{q}_{k} = &\sum_{m=1}^{M}\dot{a}^2 s_r\sqrt{P^{p}_{u}}\mathbb{E}\|\widehat{\boldsymbol{h}}^{p}_{mk}\|^2 q_k + \sum_{m=1}^{M}\dot{a}^2\sqrt{(1-s_r{}^2)P^{p}_{u}}\widehat{\boldsymbol{h}}^{p\mathrm{H}}_{mk}\widetilde{\boldsymbol{h}}^{p}_{mk}q_k + \sum_{m=1}^{M}\dot{a}^2 s_r\sqrt{P^{p}_{u}}\left(\|\widehat{\boldsymbol{h}}^{p}_{mk}\|^2 - \mathbb{E}\|\widehat{\boldsymbol{h}}^{p}_{mk}\|^2\right)q_k \\ &+ \sum_{m=1}^{M}\dot{a}^2\widehat{\boldsymbol{h}}^{p\mathrm{H}}_{mk}\boldsymbol{n}_m + \sum_{m=1}^{M}\sum_{l=1}^{L}\dot{a}^2\sqrt{\widehat{P}^{s}_{uq}}\widehat{\boldsymbol{h}}^{p\mathrm{H}}_{mk}\boldsymbol{g}^{p}_{ml}s_l + \sum_{m=1}^{M}\sum_{k'\neq k}^{K}\dot{a}^2\sqrt{P^{p}_{u}}\widehat{\boldsymbol{h}}^{p\mathrm{H}}_{mk}\boldsymbol{h}^{p}_{mk'}q_{k'} \\ &+ \sum_{m=1}^{M}\left(\dot{a}\boldsymbol{e}^{\widehat{h}^{p}\,\mathrm{H}}_{mk}\boldsymbol{y}_m + \dot{a}\widehat{\boldsymbol{h}}^{p\mathrm{H}}_{mk}\boldsymbol{e}^{y}_{m} + \boldsymbol{e}^{\widehat{h}^{p}\,\mathrm{H}}_{mk}\boldsymbol{e}^{y}_{m}\right). \end{aligned} \tag{4.27}$$

All the terms in (4.27) can be shown to be uncorrelated to each other. Using (4.27), the SINR corresponding to the k^{th} PU is given by

$$\text{SINR}_k^q = \frac{\left|\sum_{m=1}^{M} \dot{a}^2 s_r \sqrt{P_u^p}\mathbb{E}\{\|\widehat{\boldsymbol{h}}_{mk}^p\|^2\}\right|^2}{\left(\begin{array}{l}\mathbb{E}\left|\sum_{m=1}^{M}\dot{a}^2 s_r \sqrt{P_u^p}\left(\|\widehat{\boldsymbol{h}}_{mk}^p\|^2 - \mathbb{E}\{\|\widehat{\boldsymbol{h}}_{mk}^p\|^2\}\right)\right|^2 + \mathbb{E}\left|\sum_{m=1}^{M}\dot{a}^2\sqrt{(1-s_r{}^2)P_u^p}\,\widehat{\boldsymbol{h}}_{mk}^{p\text{H}}\widetilde{\boldsymbol{h}}_{mk}^p\right|^2 \\ +\mathbb{E}\left|\sum_{m=1}^{M}\dot{a}^2\widehat{\boldsymbol{h}}_{mk}^{p\text{H}}\boldsymbol{n}_m\right|^2 + \sum_{k'\neq k}^{K}\dot{a}^4 P_u^p\mathbb{E}\left|\sum_{m=1}^{M}\widehat{\boldsymbol{h}}_{mk}^{p\text{H}}\boldsymbol{h}_{mk'}^p\right|^2 + \sum_{l=1}^{L}\mathbb{E}\left|\sum_{m=1}^{M}\dot{a}^2\sqrt{\widehat{P}_{uq}^s}\widehat{\boldsymbol{h}}_{mk}^{p\text{H}}\boldsymbol{g}_{ml}^p\right|^2 \\ +\mathbb{E}\left|\sum_{m=1}^{M}\left(\dot{a}\boldsymbol{e}_{mk}^{\widehat{h}^p\,\text{H}}\boldsymbol{y}_m + \dot{a}\widehat{\boldsymbol{h}}_{mk}^{p\text{H}}\boldsymbol{e}_m^y + \boldsymbol{e}_{mk}^{\widehat{h}^p\,\text{H}}\boldsymbol{e}_m^y\right)\right|^2\end{array}\right)}. \tag{4.28}$$

Simplifying (4.28) further, we obtain UL SE of k^{th} PU in closed-form that we state next as a Theorem.

Theorem 4.2. *Under estimated and quantized CSI, the UL SE of k^{th} PU in a cell-free mMIMO based underlay network where the SUs are subject to an IOP constraint is given by* [2]

$$SE_k^q \approx \left(1 - \frac{\tau_p}{\tau_c}\right)\log_2\left(1 + SINR_k^q\right), \tag{4.29}$$

where

$$SINR_k^q = \frac{\frac{1}{\left(\dot{a}^2+\sigma_e^2\right)^2}\left(\sum_{m=1}^{M}\dot{a}^2 s_r\sqrt{P_u^p}Q_p\,\beta_{mk}^p\right)^2}{\left(\sum_{k'=1}^{K}\sum_{m=1}^{M}P_u^p Q_p\,\beta_{mk'}^p\beta_{mk}^p + \sum_{m=1}^{M}Q_p\,\beta_{mk}^p\sigma_w^2 + \sum_{l=1}^{L}\sum_{m=1}^{M}\xi Q_p\,\beta_{ml}^p\,\beta_{mk}^p\right)}. \tag{4.30}$$

Proof. The proof is given in Appendix C.6. □

Remarks: This result highlights the dependence of the UL SE of PUs on the number of quantization bits (α) through the Bussgang gain, interference threshold ($\bar{I}_p$), number of antennas at each PAP (Q_p), the number of PUs (K), the number of SUs (L), s_r that captures channel estimation accuracy and on the strength of the interference channel between PAPs and SUs.

Corollary 4.2. *With infinite capacity fronthaul links, i.e., if we consider unquantized channel*

[2]Note that τ_p denotes the length of the pilot sequence assigned to every user and τ_c denotes the length of the coherence interval.

estimates and received signals for which $\dot{a} = 1$ *and* $\sigma_{\dot{e}}^2 = 0$, $SINR_k^q$ *in* (4.30) *simplifies to*

$$SINR_k^q = \frac{\left(\sum_{m=1}^{M} s_r \sqrt{P_u^p} Q_p \beta_{mk}^p\right)^2}{\left(\sum_{k'=1}^{K}\sum_{m=1}^{M} P_u^p Q_p \beta_{mk'}^p \beta_{mk}^p + \sum_{m=1}^{M} Q_p \beta_{mk}^p \sigma_w^2 + \sum_{l=1}^{L}\sum_{m=1}^{M} \xi Q_p \beta_{ml}^p \beta_{mk}^p\right)}. \tag{4.31}$$

Note that (4.31) can help determine the SE of PUs in UL cell-free mMIMO networks in underlay mode when it operates under an IOP constraint without quantization errors.

4.5.2 UL SE Analysis of SUs

Now we derive the UL SE of the l^{th} SU based on the quantized estimates of the channel between l^{th} SU and n^{th} SAP. We note that $Q(\widehat{\boldsymbol{h}}_{nl}^s) = \dot{a}\widehat{\boldsymbol{h}}_{nl}^s + \boldsymbol{e}_{nl}^{\widehat{h}^s}$, where $\widehat{\boldsymbol{h}}_{nl}^s \sim \mathcal{CN}\left(\boldsymbol{0}, \beta_{nl}^s \mathbf{I}_{Q_s}\right)$, $\boldsymbol{e}_{nl}^{\widehat{h}^s} \in C^{Q_s \times 1}$ denotes noise due to quantization error with covariance $\sigma_{\dot{e}}^2 \beta_{nl}^s \mathbf{I}_{Q_s}$. The quantized received signals at the n^{th} SAP is given by

$$Q(\boldsymbol{y}_n) = \dot{a}\boldsymbol{y}_n + \boldsymbol{e}_n^y, \tag{4.32}$$

where it can be shown that $\boldsymbol{y}_n \sim \mathcal{CN}\left(\boldsymbol{0}, \left(\sum_{l'=1}^{L} \xi\beta_{nl}^s + \sum_{k=1}^{K} P_u^p \beta_{nk}^s + \sigma_w^2\right)\mathbf{I}_{Q_s}\right)$ and $\boldsymbol{e}_n^y$ denotes the quantization noise vector with covariance $\sigma_{\dot{e}}^2\left(\sum_{l'=1}^{L} \xi\beta_{nl}^s + \sum_{k=1}^{K} P_u^p \beta_{nk}^s + \sigma_w^2\right)\mathbf{I}_{Q_s}$. The MRC processed signal corresponding to the l^{th} SU at the secondary CPU is given by

$$z_l^q = \sum_{n=1}^{N} Q\left(\widehat{\boldsymbol{h}}_{nl}^{s\text{H}}\right) Q\left(\boldsymbol{y}_n\right) = \sum_{n=1}^{N}\left(\dot{a}^2 \widehat{\boldsymbol{h}}_{nl}^{s\text{H}} \boldsymbol{y}_n + \dot{a}\boldsymbol{e}_{nl}^{\widehat{h}^s\text{H}} \boldsymbol{y}_n + \dot{a}\widehat{\boldsymbol{h}}_{nl}^{s\text{H}} \boldsymbol{e}_n^y + \boldsymbol{e}_{nl}^{\widehat{h}^s\text{H}} \boldsymbol{e}_n^y\right). \tag{4.33}$$

Using (4.2) and (4.8), z_l^q can be re-written as

$$z_l^q = \sum_{n=1}^{N}\Bigg(s_s \dot{a}^2 \sqrt{\widehat{P}_{uq}^s}\|\widehat{\boldsymbol{h}}_{nl}^s\|^2 s_l + \dot{a}^2\sqrt{(1-s_s{}^2)\widehat{P}_{uq}^s}\widehat{\boldsymbol{h}}_{nl}^{s\text{H}}\widetilde{\boldsymbol{h}}_{nl}^s s_l + \sum_{l'\neq l}^{L} \dot{a}^2\sqrt{\widehat{P}_{uq}^s}\widehat{\boldsymbol{h}}_{nl}^{s\text{H}}\boldsymbol{h}_{nl'}^s s_{l'}$$
$$+ \sum_{k=1}^{K} \dot{a}^2\sqrt{P_u^p}\widehat{\boldsymbol{h}}_{nl}^{s\text{H}}\boldsymbol{g}_{nk}^s q_k + \dot{a}^2\widehat{\boldsymbol{h}}_{nl}^{s\text{H}}\boldsymbol{n}_n + \dot{a}\boldsymbol{e}_{nl}^{\widehat{h}^s\text{H}}\boldsymbol{y}_n + \dot{a}\widehat{\boldsymbol{h}}_{nl}^{s\text{H}}\boldsymbol{e}_n^y + \boldsymbol{e}_{nl}^{\widehat{h}^s\text{H}}\boldsymbol{e}_n^y\Bigg). \tag{4.34}$$

By invoking use and then forget bound, z_l^q can be expressed as [14], [89].

$$z_l^q = \sum_{n=1}^{N} s_s \dot{a}^2 \mathbb{E}\left(\sqrt{\widehat{P}_{uq}^s}\|\widehat{\boldsymbol{h}}_{nl}^s\|^2\right) s_l + \sum_{n=1}^{N}\sqrt{(1-s_s{}^2)\widehat{P}_{uq}^s}\dot{a}^2\widehat{\boldsymbol{h}}_{nl}^{s\text{H}}\widetilde{\boldsymbol{h}}_{nl}^s s_l + \sum_{n=1}^{N}\dot{a}^2\widehat{\boldsymbol{h}}_{nl}^{s\text{H}}\boldsymbol{n}_n$$

$$+\sum_{n=1}^{N} s_s \dot{a}^2 \left(\sqrt{\widehat{P}^s_{uq}} \|\widehat{\boldsymbol{h}}^s_{nl}\|^2 - \mathbb{E}\left(\sqrt{\widehat{P}^s_{uq}} \|\widehat{\boldsymbol{h}}^s_{nl}\|^2 \right) \right) s_l + \sum_{n=1}^{N} \sum_{l' \neq l}^{L} \dot{a}^2 \sqrt{\widehat{P}^s_{uq}} \widehat{\boldsymbol{h}}^{s\mathrm{H}}_{nl} \boldsymbol{h}^s_{nl'} s_{l'}$$
$$+\sum_{n=1}^{N} \sum_{k=1}^{K} \dot{a}^2 \sqrt{P^p_u} \widehat{\boldsymbol{h}}^{s\mathrm{H}}_{nl} \boldsymbol{g}^s_{nk} q_k + \sum_{n=1}^{N} \left(\dot{a} \boldsymbol{e}^{\widehat{h}^s\mathrm{H}}_{nl} \boldsymbol{y}_n + \dot{a} \widehat{\boldsymbol{h}}^{s\mathrm{H}}_{nl} \boldsymbol{e}^y_n + \boldsymbol{e}^{\widehat{h}^s\mathrm{H}}_{nl} \boldsymbol{e}^y_n \right). \quad (4.35)$$

All the terms in (4.35) are uncorrelated to each other. Using (4.35), the SINR for the l^{th} SU is given by

$$\mathrm{SINR}^q_l = \frac{\left| \sum_{n=1}^{N} \dot{a}^2 s_s \mathbb{E}\left(\sqrt{\widehat{P}^s_{uq}} \|\widehat{\boldsymbol{h}}^s_{nl}\|^2 \right) \right|^2}{\left(\begin{array}{l} \mathbb{E}\left| \sum_{n=1}^{N} \dot{a}^2 s_s \left(\sqrt{\widehat{P}^s_{uq}} \|\widehat{\boldsymbol{h}}^s_{nl}\|^2 - \mathbb{E}\left(\sqrt{\widehat{P}^s_{uq}} \|\widehat{\boldsymbol{h}}^s_{nl}\|^2 \right) \right) \right|^2 + \mathbb{E}\left| \sum_{n=1}^{N} \dot{a}^2 \sqrt{(1 - s_s{}^2) \widehat{P}^s_{uq}} \widehat{\boldsymbol{h}}^{s\mathrm{H}}_{nl} \widetilde{\boldsymbol{h}}^s_{nl} \right|^2 \\ + \sum_{l' \neq l}^{L} \mathbb{E}\left| \sum_{n=1}^{N} \dot{a}^2 \sqrt{\widehat{P}^s_{uq}} \widehat{\boldsymbol{h}}^{s\mathrm{H}}_{nl} \boldsymbol{h}^s_{nl'} \right|^2 + \sum_{k=1}^{K} \mathbb{E}\left| \sum_{n=1}^{N} \dot{a}^2 \sqrt{P^p_u} \widehat{\boldsymbol{h}}^{s\mathrm{H}}_{nl} \boldsymbol{g}^s_{nk} \right|^2 + \mathbb{E}\left| \sum_{n=1}^{N} \dot{a}^2 \widehat{\boldsymbol{h}}^{s\mathrm{H}}_{nl} \boldsymbol{n}_n \right|^2 \\ + \mathbb{E}\left| \sum_{n=1}^{N} \left(\dot{a} \boldsymbol{e}^{\widehat{h}^s\mathrm{H}}_{nl} \boldsymbol{y}_n + \dot{a} \widehat{\boldsymbol{h}}^{s\mathrm{H}}_{nl} \boldsymbol{e}^y_n + \boldsymbol{e}^{\widehat{h}^s\mathrm{H}}_{nl} \boldsymbol{e}^y_n \right) \right|^2 \end{array} \right)}. \quad (4.36)$$

Simplifying (4.36) further, we obtain the UL SE of l^{th} SU that we state next as Theorem.

Theorem 4.3. *Under estimated and quantized CSI, the UL SE of l^{th} SU in a cell-free mMIMO based underlay network that operates under an IOP constraint is given by*

$$SE^q_l \approx \left(1 - \frac{\tau_p}{\tau_c}\right) \log_2\left(1 + SINR^q_l\right), \quad (4.37)$$

where $SINR^q_l$ is given as

$$SINR^q_l = \frac{\left(\sum_{n=1}^{N} s_s \lambda Q_s \beta^s_{nl} \right)^2}{\left(\begin{array}{l} \sum_{n=1}^{N} s_s{}^2 \left(\xi - \lambda^2\right) \left(\beta^s_{nl}\right)^2 Q_s^2 + \left(\dot{a}^2 + \sigma^2_{\dot{e}}\right)^2 \left(\sum_{l'=1}^{L} \sum_{n=1}^{N} \xi Q_s \beta^s_{nl'} \beta^s_{nl} + \sum_{k=1}^{K} \sum_{n=1}^{N} P^p_u Q_s \beta^s_{nl} \beta^s_{nk} \right. \\ \left. + \sum_{n=1}^{N} Q_s \beta^s_{nl} \sigma^2_w \right) \end{array} \right)}. \quad (4.38)$$

Proof. The proof is given in Appendix C.7. □

Remarks: Based on this theorem, we observe that the UL SE of l^{th} SU depends on interference threshold ($\bar{I}_p$), number of antennas (Q_s) at each SAP, number of PUs (K), number of SUs (L), channel estimation error coefficient (s_s) and also on the strength of the interference channel

between SAPs and PUs. It also depends on the Bussgang gain ($\dot{a}$).

Corollary 4.3. *For infinite capacity fronthaul links, i.e., in case we consider unquantized channel estimates and received signals for which* $\dot{a} = 1$ *and* $\sigma_{\dot{e}}^2 = 0$, $SINR_l^q$ *in* (4.38) *simplifies to*

$$SINR_l^q = \frac{\left(\sum_{n=1}^{N} s_s \lambda Q_s \beta_{nl}^s\right)^2}{\left(\sum_{n=1}^{N} {s_s}^2 \left(\xi - \lambda^2\right)\left(\beta_{nl}^s\right)^2 Q_s^2 + \left(\sum_{l'=1}^{L}\sum_{n=1}^{N} \xi Q_s \beta_{nl'}^s \beta_{nl}^s + \sum_{k=1}^{K}\sum_{n=1}^{N} P_u^p Q_s \beta_{nl}^s \beta_{nk}^s + \sum_{n=1}^{N} Q_s \beta_{nl}^s \sigma_w^2\right)\right)}. \tag{4.39}$$

Note that (4.39) *can help calculate the SE of SUs in underlay mode in UL cell-free mMIMO when they are subject to IOP constraint under no quantization errors.*

4.6 Spatially Correlated Transmission Channel

In order to analyze the impact of spatially correlated channels on IOP at the PAPs and the SE of PUs and SUs, we generate the covariance matrices for the channels from PAPs to PUs, PAPs to SUs, SAPs to SUs and SAPs to PUs using the Gaussian local scattering model [60], [90], [91]. For this model, the spatial correlation matrix for the channel from the m^{th} PAP to the k^{th} PU is given by [60]

$$\left[\mathbf{R}_{mk}^p\right]_{x,y} = \beta_{mk}^p \int_{-\infty}^{\infty} e^{j2\pi d_H (x-y)\sin(\phi_{mk}^p + \delta_{mk}^p)} \frac{e^{-\frac{\delta_{mk}^{p2}}{2\sigma_\phi^2}}}{\sqrt{2\pi}\sigma_\phi} d\delta_{mk}^p, \tag{4.40}$$

where β_{mk}^p denotes the large-scale fading coefficient over this link, d_H denotes the inter-antenna spacing, $1 \le x, y \le Q_p$, ϕ_{mk}^p denotes the nominal azimuthal angle and it is drawn from $\mathcal{U}[-\pi, \pi]$ distribution, $\delta_{mk}^p \sim \mathcal{N}(0, \sigma_\phi^2)$ represents the Gaussian distributed deviation from ϕ_{mk}^p and σ_ϕ denotes the angular standard deviation (ASD).

The spatial correlation matrix for the channel from the m^{th} PAP to the l^{th} SU is given by [60]

$$\left[\mathbf{R}_{ml}^p\right]_{x,y} = \beta_{ml}^p \int_{-\infty}^{\infty} e^{j2\pi d_H (x-y)\sin(\phi_{ml}^p + \delta_{ml}^p)} \frac{e^{-\frac{\delta_{ml}^{p2}}{2\sigma_\phi^2}}}{\sqrt{2\pi}\sigma_\phi} d\delta_{ml}^p, \tag{4.41}$$

where β_{ml}^p is the corresponding large-scale fading coefficient, $1 \le x, y \le Q_p$ as before, $\phi_{ml}^p \in \mathcal{U}[-\pi, \pi]$ denotes the nominal azimuthal angle, $\delta_{ml}^p \sim \mathcal{N}(0, \sigma_\phi^2)$ is a Gaussian distributed deviation from nominal azimuthal angle ϕ_{ml}^p with ASD σ_ϕ.

Similarly, based on this Gaussian local scattering model, the spatial correlation matrix for the channel from the n^{th} SAP to the l^{th} SU is given by [60]

$$[\mathbf{R}^s_{nl}]_{x,y} = \beta^s_{nl} \int_{-\infty}^{\infty} e^{j2\pi d_H(x-y)\sin(\phi^s_{nl}+\delta^s_{nl})} \frac{e^{-\frac{\delta^{s2}_{nl}}{2\sigma^2_\phi}}}{\sqrt{2\pi}\sigma_\phi} d\delta^s_{nl}, \tag{4.42}$$

where β^s_{nl} is the large-scale fading coefficient corresponding to this link, $1 \leq x, y \leq Q_s$ in this case, ϕ^s_{nl} as before refers to the nominal azimuthal angle drawn from $\mathcal{U}[-\pi, \pi]$ distribution, $\delta^s_{nl} \sim \mathcal{N}(0, \sigma^2_\phi)$ is a Gaussian distributed deviation from ϕ^s_{nl} with ASD σ_ϕ.

Lastly, the correlation matrix for the channel from the n^{th} SAP to the k^{th} PU is given by [60]

$$[\mathbf{R}^s_{nk}]_{x,y} = \beta^s_{nk} \int_{-\infty}^{\infty} e^{j2\pi d_H(x-y)\sin(\phi^s_{nk}+\delta^s_{nk})} \frac{e^{-\frac{\delta^{s\,2}_{nk}}{2\sigma^2_\phi}}}{\sqrt{2\pi}\sigma_\phi} d\delta^s_{nk}, \tag{4.43}$$

where β^s_{nk} captures large-scale fading over this link, $1 \leq x, y \leq Q_s$ for this case, ϕ^s_{nk} as above denotes the nominal azimuthal angle and it is drawn from $\mathcal{U}[-\pi, \pi]$ distribution, $\delta^s_{nk} \sim \mathcal{N}(0, \sigma^2_\phi)$ denotes the deviation from ϕ^s_{nk} and it has an ASD of σ_ϕ.

4.7 Numerical Results

We now present numerical results to show the impact of number of quantization bits on the IOP at PAPs and also on the UL SE of PUs and SUs. We consider 500 m × 500 m square area that is wrapped around at the edges to avoid boundary effects. We consider $\tau_p = 20$, $\tau_c = 200$, $P^p_u = 0$ dBm, $f_c = 1.9$ GHz, $W = 20$ MHz and noise power spectral density of -174 dBm/Hz. The large scale fading β^x_{ab} between a^{th} AP and b^{th} user is modeled as [14],

$$\beta^x_{ab} = 10^{\frac{PL^x_{ab}}{10}} 10^{\frac{\sigma_{sh}\zeta^x_{ab}}{10}}, \tag{4.44}$$

where $x \in \{p, s\}$ depending on whether x corresponds to PAP or SAP, $1 \leq a \leq M$ or $1 \leq a \leq N$ based on whether large scale fading corresponds to PAP or SAP, $1 \leq b \leq K$ or $1 \leq b \leq L$ depending on whether it corresponds to PUs or SUs. In addition, the path loss PL^x_{ab} corresponding to the link between the a^{th} AP and b^{th} user is characterized based on the three slope model [14], and $10^{\frac{\sigma_{sh}\zeta^x_{ab}}{10}}$ represents shadow fading with standard deviation $(\sigma_{sh}) = 8$ dB

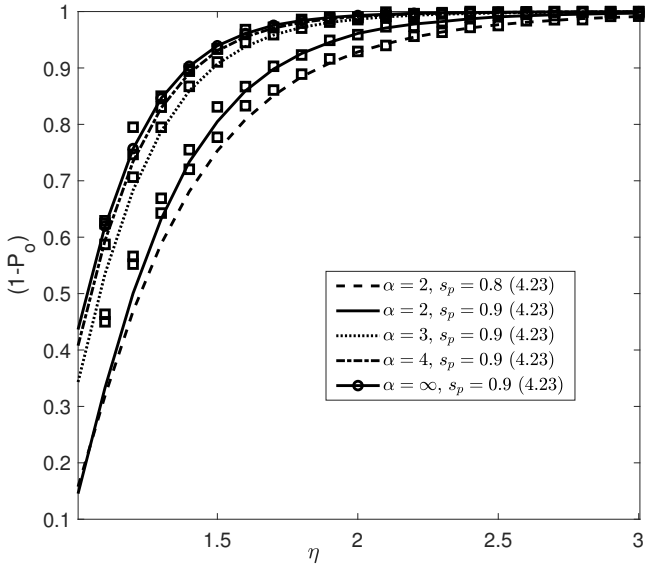

Fig. 4.3: Effect of quantization and imperfect CSI on $(1 - P_o)$ ($K = L = 10$, $N = M = 100$, $s_s = s_r = 0.9$ and $Q_p = Q_s = 4$). Corresponding Monte Carlo simulations are shown using the marker □.

and $\zeta_{ab}^{x} \sim \mathcal{N}(0, 1)$.

Effect of quantization and imperfect CSI on IOP: Figure 4.3 plots $(1 - P_o)$ vs. η for $K = L = 10$ for four different values of α, namely, 2, 3, 4 and infinity (infinite capacity fronthaul). We observe that for a given s_p which is a parameter that captures the channel estimation accuracy and is a function of the pilot power [49, 52], larger back-off in power is needed as the number of quantization bits α decreases. In other words, the smaller the value of α, the larger is the quantization error and larger is the power back-off needed to maintain IOP at a fixed level. We observe that as α reduces from infinity to 2, η increases from 1.95 to 2.5 in order to keep P_o fixed at 0.01 for $s_p = 0.9$. Furthermore, the IOP performance with $\alpha = 4$ is close to that obtained with $\alpha = \infty$. It is also observed that the Monte Carlo simulations match well with the lower bound in the regime $(1 - P_o) \geq 0.90$. We wish to again point out that this is the regime where the SUs are expected to operate in practice. The curves corresponding to $s_p = 0.8$ and $s_p = 0.9$ for $\alpha = 2$ quantization bits suggest that for larger s_p, where the estimation error is relatively lower, a lower power back-off is needed to achieve the desired IOP. Therefore, this result helps us understand the joint impact of errors induced due to quantization and channel estimation on IOP.

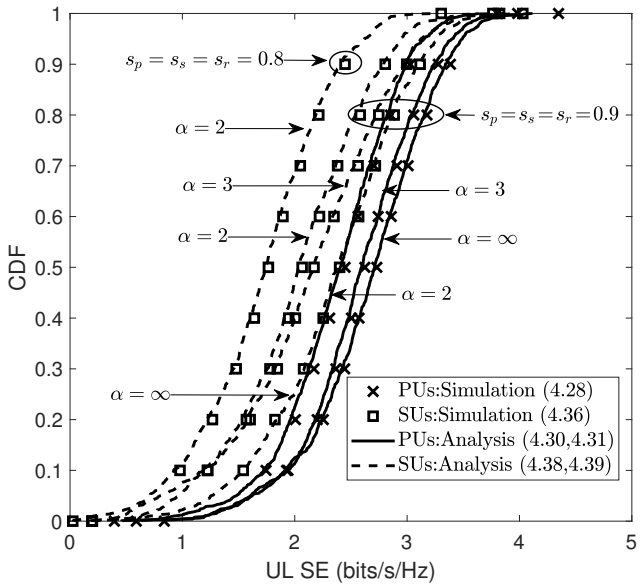

Fig. 4.4: Effect of quantization and imperfect CSI on CDF of UL SE ($K = L = 10$, $N = M = 100$, $P_o = 0.01$, $\bar{I}_p = -100$ dB and $Q_p = Q_s = 4$).

Effect of quantization and imperfect CSI on SE: Figure 4.4 plots the CDF of the UL SE of PUs and SUs for different values of α. It is observed that for a given channel estimation accuracy, the UL SE of PUs and SUs improve with increase in α, because larger α results in smaller quantization error, thereby, leading to an improvement in the SINR of PUs and SUs. For example, if SE_s^q represents the SE of SUs, then from Figure 4.4 for $s_p = s_s = s_r = 0.9$, we observe that $\Pr(\text{SE}_s^q \geq 2.5 \text{ bits/s/Hz}) = 0.22$ for $\alpha = 2$, it increases to 0.31 and 0.42 for $\alpha = 3$ and $\alpha = \infty$, respectively. Thus, the likelihood of SUs achieving UL SE greater than a certain threshold increases as α increases. We observe similar trends in the SE of PUs and the probability of PUs getting higher UL SE also increases with increase in α. We observe that the UL SE degrades for smaller values of s_p, s_s and s_r, i.e., for the case when the channel estimation accuracy decreases. For example, we observe that at $\alpha = 2$ and for $s_p = s_s = s_r = 0.9$, $\Pr(\text{SE}_s^q \geq 2.5 \text{ bits/s/Hz}) = 0.22$, while it reduces to 0.08 for $s_p = s_s = s_r = 0.8$. We also observe that Monte Carlo simulations match well with analysis. This result illustrates the combined effects of quantization and imperfect CSI on the UL SE of PUs and SUs.

Effect of P_o on SE: Figure 4.5 plots the CDF of UL SE of PUs and SUs that can be achieved over limited capacity fronthaul links for two different values of P_o, namely, 0.01 and 0.2 for

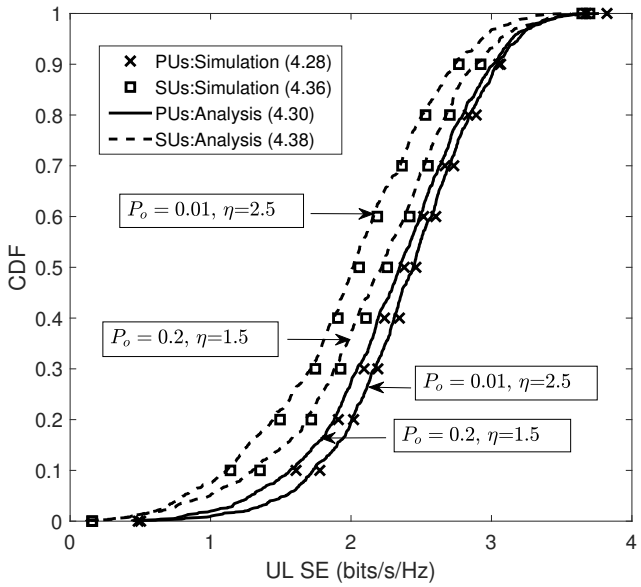

Fig. 4.5: Impact of P_o on CDF of UL SE under quantization error for $\bar{I}_p = -100$ dB ($K = L = 10$, $N = M = 100$, $s_p = s_s = s_r = 0.9$, $\alpha = 2$ and $Q_p = Q_s = 4$).

$\alpha = 2$. We observe that the probability that PUs obtain a higher SE increases as P_o decreases from 0.2 to 0.01 since the decrement of P_o makes the IOP constraint stricter thereby reducing the fraction of time the interference threshold is violated at the PUs. As P_o decreases, the likelihood that the SUs obtain a higher SE, on the other hand, reduces since the SUs need to back-off their transmit power by a larger factor.

Effect of $\bar{I}_p$ on SE: Figure 4.6 plots the CDF of the UL SE of PUs and SUs for two different values of $\bar{I}_p$, namely, -100 dB and -105 dB at $P_o = 0.01$ under quantization error with $\alpha = 2$ quantization bits. We observe that as the interference threshold $\bar{I}_p$ increases, the power with which the SUs can transmit increases. As a result, the likelihood that SUs obtain higher UL SE increases. On the other hand, as $\bar{I}_p$ increases, the likelihood for the PUs to obtain higher UL SE decreases, since higher $\bar{I}_p$ results in more interference at PUs. For example, if SE_s^q represents the SE of SUs, then from Figure 6, we observe that $\Pr(\text{SE}_s^q \geq 2.5 \text{ bits/s/Hz}) = 0.04$ for $\bar{I}_p = -105$ dB and it increases to 0.22 for $\bar{I}_p = -100$ dB. Furthermore, if we let SE_p^q represent the SE of PUs then $\Pr(\text{SE}_p^q \geq 2.5 \text{ bits/s/Hz}) = 0.50$ for $\bar{I}_p = -105$ dB and it decreases to 0.43 for $\bar{I}_p = -100$ dB due to increased interference.

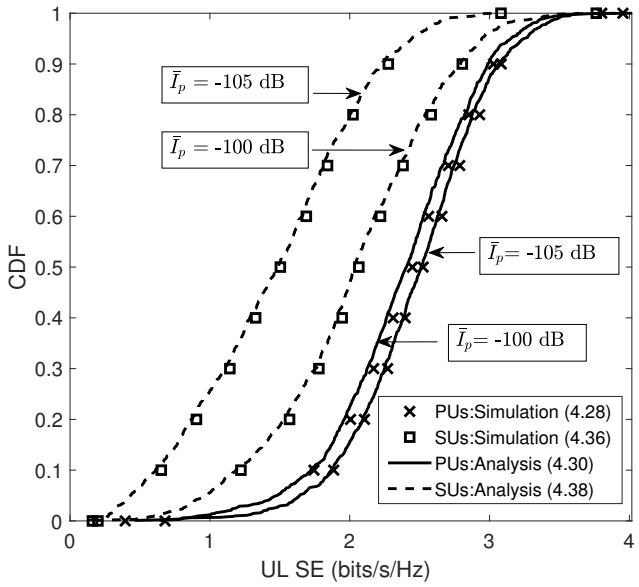

Fig. 4.6: Impact of $\bar{I}_p$ on CDF of UL SE under quantization error for $P_o = 0.01$ and $\eta = 2.5$ ($K = L = 10$, $N = M = 100$, $s_p = s_s = s_r = 0.9$, $\alpha = 2$ and $Q_p = Q_s = 4$).

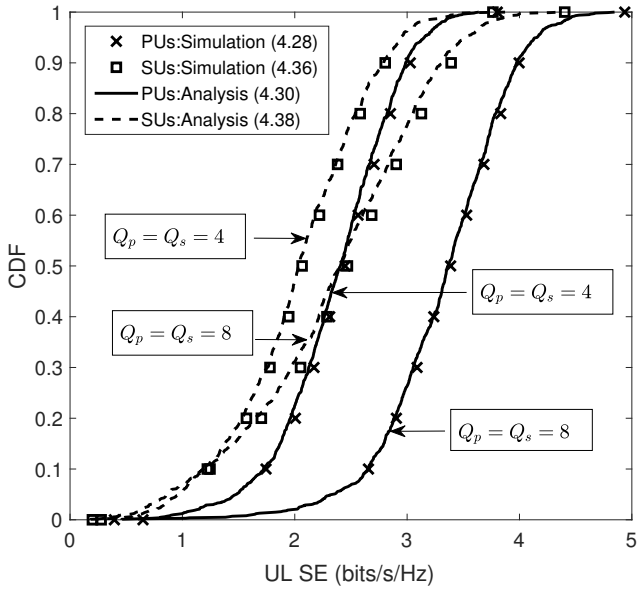

Fig. 4.7: Impact of Q_p and Q_s on CDF of UL SE under quantization error for $P_o = 0.01$ and $\eta = 2.5$ ($K = L = 10$, $N = M = 100$, $s_p = s_s = s_r = 0.9$, $\alpha = 2$ and $\bar{I}_p = -100$ dB).

Effect of Q_p and Q_s on SE: Figure 4.7 plots CDF of UL SE of PUs and SUs for two different values of Q_p and Q_s, namely, 4 and 8 under quantization error for $\alpha = 2$ quantization bits. With higher values of Q_p and Q_s, the likelihood that the SUs or PUs attain a higher SE over limited capacity fronthaul increases due to increased beamforming gain. We observe that $\Pr(\text{SE}_s^q \geq 2.5 \text{ bits/s/Hz}) = 0.22$ for $Q_p = Q_s = 4$ and it increases to 0.45 for $Q_p = Q_s = 8$. Furthermore, $\Pr(\text{SE}_p^q \geq 2.5 \text{ bits/s/Hz}) = 0.42$ for $Q_p = Q_s = 4$ and it increases to 0.93 for $Q_p = Q_s = 8$.

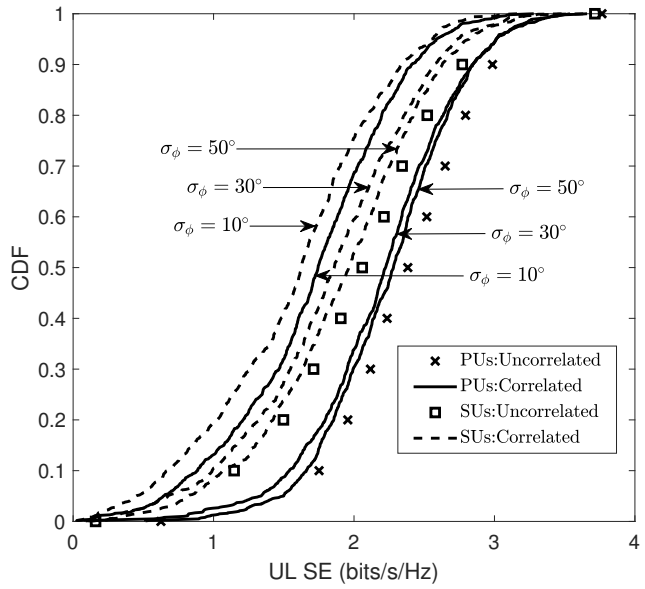

Fig. 4.8: Impact of spatial correlation on CDF of UL SE ($K = L = 10, N = M = 100, P_o = 0.01, \eta = 2.5, s_p = s_s = s_r = 0.9, Q_p = Q_s = 4, \bar{I}_p = -100$ dB).

Effect of spatial correlation on the UL SE of PUs and SUs: Figure 4.8 plots the CDF of UL SE of SUs and PUs for three different values of angular standard deviation, namely, $\sigma_\phi = 10°$, $\sigma_\phi = 30°$ and $\sigma_\phi = 50°$. We also plot results for the uncorrelated scenario. We observe that the likelihood that the PUs and SUs obtain higher UL SE increases as σ_ϕ increases from 10° to 50° and performance approaches that obtained with uncorrelated channels. This is primarily because spatial correlation decreases as σ_ϕ increases from 10° to 50° and this results in an increase in the power of the desired signal term [60]. For example, if SE_p^q represents the SE of PUs then from Figure 4.8, we observe that $\Pr(\text{SE}_p^q > 2.5\text{bits/s/Hz}) = 0.09$ for $\sigma_\phi = 10°$, it increases to 0.36, 0.46 and 0.54 for $\sigma_\phi = 30°$, $\sigma_\phi = 50°$ and the uncorrelated scenario.

4.8 Summary

We considered the UL of a cell-free mMIMO based underlay network over limited capacity fronthaul links, in which the SUs adapt their transmit power subject to an IOP constraint. Based on Bussgang's decomposition, we applied optimal uniform quantization on the received signal and the channel estimates. We developed novel statistical models for the SLN of the true channel and QCE based on Gamma distribution and derived the corresponding shape and scale parameters. New mathematical expressions for the mean SU transmit power and also for the correlation coefficient between the true channel and the QCE were derived. We also developed new analytical expressions for IOP and UL SE of SUs and PUs, and expressed their dependence on Bussgang gain and the variance of the quantization noise, which in turn are functions of the number of bits employed for quantization.

We showed that the SU must back-off its transmit power by a greater extent when fewer bits are used for quantization. We also illustrate that the probability of PUs or SUs achieving a higher SE increases as the number of quantization bits increases. In fact, we observed that it is sufficient to use 4 bits for quantization to obtain performance identical to that of an infinite capacity fronthaul. We also observed that an increase in P_o or $\bar{I}_p$ deteriorates the the UL SE of PUs while improving the UL SE of SUs. The impact of correlation on SE of PUs and SUs was also investigated.

5

Conclusions and Future Work

Contents

5.1 Conclusions

Driven by the necessity to support diverse wireless services and applications, the design of wireless communication networks continues to evolve. It is predicted that in the next few years, billions of IoT devices, autonomous cars and UAVs will be connected to the network [1]. However, the data rates and the number of users that can be served depend heavily on the bandwidth that is available for communication. As mentioned in Chapter 1, most of the spectrum below 6 GHz is already allocated to support diverse cellular technologies. This is why spectrum regulatory authorities around the world are now emphasizing on allowing sharing of spectrum by unlicensed CUs in order to boost spectrum utilization efficiency. To circumvent the adverse impact of underlay spectrum sharing, the cognitive network must adopt power control so that the interference constraint at the primary is obeyed. To this end, in this thesis, we focus on modeling and analysis of co-located and cell-free mMIMO enabled underlay spectrum access networks and explore implications of power control to obey IOP constraint in such networks.

We first considered a co-located mMIMO based underlay spectrum access network in which the cognitive BS has an imperfect and incomplete estimate of its channels to the K_p PUs and employs MR beamfomer to transmit under an IOP constraint. We developed novel back-off factor based power control policies for the cognitive BS such that the interference power exceeds an interference threshold no more than P_o fraction of the time at any of the K_p PUs under either incomplete and imperfect CSI. The new analytical expressions for $(1 - P_o)$ offer the wireless system designer a ballpark number for η that must be chosen to satisfy the constraint under imperfect or incomplete CSI. We then derived new expressions for sum SE of CUs under each of the scenarios. We observed and quantified that by exploiting the huge array gain and the high spatial resolution offered by a mMIMO cognitive BS, P_o can be reduced without incurring a degradation in the sum SE of the CUs under imperfect CSI. To be specific, P_o reduces since the cognitive BS transmits at a reduced power, and due to this the CUs may suffer loss in the sum SE. However, this loss can be recovered by deploying more cognitive BS antennas. Also, more number of PUs can be served while keeping P_o at the PUs and the sum SE of the CUs fixed

at a constant level by deploying a larger number of antennas at the cognitive BS. Furthermore, we observed that P_o increases as S reduces and in order to keep the sum SE of CUs fixed as S reduces, more antennas need to be deployed at the cognitive BS. The impact of spatial correlation on P_o at PUs and sum SE of CUs was also elucidated.

We then considered a cell-free mMIMO enabled underlay spectrum access network in which the SAPs communicate with UAVs under IOP constraint at GUEs. We derived an integral-free lower bound on the IOP at the GUEs, based on which the system designer can get an idea about the power margin that the SAPs must obey to satisfy the IOP constraint at the GUEs. We derived new approximate achievable DL SE expressions for the UAVs and GUEs. We also analyzed BER of UAVs and GUEs based on availability of statistical CSI at the user end. We proved both analytically and through numerical simulations that the huge degrees-of-freedom provided by cell-free mMIMO can be utilized to improve the SE of UAVs while keeping the IOP at GUEs fixed at a specific level. Furthermore, we observed that for a given IOP, the larger the $\bar{I}_p$ is, the larger the probability of attaining a higher SE for UAVs is and the lower the probability of obtaining higher SE for GUEs is. It is also observed that for a given $\bar{I}_p$, the likelihood that the UAVs attain higher SE increases as IOP increases or as the number of SAPs increases. Effect of height and $\bar{I}_p$ on BER was also illustrated.

In the last part of our thesis, we analyzed the UL of a cell-free mMIMO based underlay spectrum access system over limited capacity fronthaul links, in which the SUs communicate with SAPs under an IOP constraint. Using Bussgang decomposition, we applied optimal uniform quantization on the received signal and the channel estimates. We developed new statistical models for the SLN of the true and QCE based on Gamma distribution and determined the corresponding shape and scale parameters. We then developed a new expression for the mean SU transmit power and also for the correlation coefficient between the true and the QCE. We also derived new analytical expressions for IOP and UL SE of SUs and PUs, and expressed them as a function of the Bussgang gain and the variance of the quantization noise, which in turn has a dependence on the number of bits employed for quantization. We observed that larger back-off in SU transmit power is required when fewer bits are used for quantization. It is also

observed that the probability of PUs or SUs achieving a higher SE increases as the number of quantization bits increases and it suffices to employ 4 bits for quantization in order to obtain performance similar to that of infinite capacity fronthaul. We also observed that an increase in P_o or $\bar{I}_p$ improves the UL SE of SUs while deteriorating the UL SE of PUs.

5.2 Directions for Future Research

The fundamental ideas and the mathematical analysis presented in this thesis can be extended in several ways. Some probable directions for future research are as follows:

(i) *Intelligent Reflecting Surface (IRS) Enabled Underlay Spectrum Access Under IOP Constraint:* IRS is promising 6G technology. It is essentially a planar array consisting of a large number of passive elements, where each element is capable of inducing an amplitude and a phase change to the signal that is incident on it [92], [93]. By appropriately programming these elements, the received signal power at the SU may be boosted while suppressing the interference caused to the PUs. One possible extension to the work carried out in this thesis could be to develop a comprehensive model and analysis for an IRS enabled underlay spectrum sharing system that operates under an IOP constraint. The challenge would be to develop algorithms for phase configuration at the IRS to maximize the SE of SUs under an IOP constraint. The IOP at PUs and BER of SUs and PUs may also be analyzed under both perfect and estimated CSI.

(ii) *IRS Assisted MIMO Based Underlay Spectrum Access Under IOP Constraint:* Considering multiple antennas at the source, another possible direction for future work is to develop algorithms for joint beamforming at secondary transmitter and phase programming at the IRS to maximize the sum SE of SUs when the transmission from secondary is subject to an IOP constraint. The goal would also be analyze performance in terms of BER, SE and IOP at PUs. The study may further be extended to a distributed antennas set-up.

(iii) *Cell-free mMIMO based underlay spectrum access under statistical or incomplete CSI:* If the SAPs in a cell-free network have access only to the statistical CSI of the channel

to the PUs or have incomplete CSI, it would be of interest to study the right interference constraint that should be considered for use in such a scenario. The corresponding impact on performance in terms of interference caused to PUs, BER and SE of PUs and SUs may also be studied both under finite and infinite capacity fronthaul links. Another objective would be to understand how pilot contamination arising due to sharing of pilots impacts performance of cell-free massive MIMO based underlay spectrum sharing networks. Performance under non-linear quantization is another interesting avenue for future research.

(iv) *Cell-Free Enabled UAV Communication Under Impairments:* Another possible direction could be to analyze the performance of UAVs in a cell-free enabled underlay network considering polarization losses arising due to misalignment of the antennas at the SAPs and at the UAVs. One can also optimize the trajectory of these UAVs such that the sum SE of UAVs is maximized while meeting the interference constraint at the primary network.

A

Appendix

A.1 Proof of Theorem 2.1

Let $u_{k,i} = \frac{1}{\sqrt{K_c}} \frac{\boldsymbol{g}_{c_k}^{\mathrm{T}} \widehat{\boldsymbol{h}}_{c_i}^{*}}{\|\widehat{\boldsymbol{h}}_{c_i}\|}$ and $\widehat{u}_{k,i} = \frac{1}{\sqrt{K_c}} \frac{\widehat{\boldsymbol{g}}_{c_k}^{\mathrm{T}} \widehat{\boldsymbol{h}}_{c_i}^{*}}{\|\widehat{\boldsymbol{h}}_{c_i}\|}$ for $1 \leq k \leq K_p$. It can be shown that conditioned on $\widehat{\boldsymbol{h}}_{c_i}$, both $u_{k,i}$ and $\widehat{u}_{k,i}$ are $\mathcal{CN}\left(0, \frac{\alpha_k}{K_c}\right)$ random variables and are independent of $\widehat{\boldsymbol{h}}_{c_i}$. We need to find the distribution of $Z_k = \sum_{i=1}^{K_c} |u_{k,i}|^2$ and $\widehat{Z}_k = \sum_{i=1}^{K_c} |\widehat{u}_{k,i}|^2$. To do so, we note that both $\chi_k = \frac{2K_c}{\alpha_k} Z_k$ and $\widehat{\chi}_k = \frac{2K_c}{\alpha_k} \widehat{Z}_k$ are chi-square distributed rvs with $2K_c$ degrees of freedom, since each of them is the sum of absolute squares of $2K_c$ i.i.d. $\mathcal{N}(0,1)$ rvs. Based on this and by transformation of rvs, the pdf of Z_k equals

$$f_{Z_k}(z_k) = \frac{K_c}{\alpha_k} \frac{1}{\Gamma(K_c)} \left(\frac{K_c}{\alpha_k} z_k\right)^{K_c - 1} \mathrm{e}^{-\frac{K_c}{\alpha_k} z_k} \tag{A.1}$$

and the pdf of $\widehat{Z}_k$ is given by

$$f_{\widehat{Z}_k}(\widehat{z}_k) = \frac{K_c}{\alpha_k} \frac{1}{\Gamma(K_c)} \left(\frac{K_c}{\alpha_k} \widehat{z}_k\right)^{K_c - 1} \mathrm{e}^{-\frac{K_c}{\alpha_k} \widehat{z}_k}. \tag{A.2}$$

Note that Z_k and $\widehat{Z}_k$ are correlated chi-square distributed rvs and the joint pdf is given by [94]

$$f_{Z_k, \widehat{Z}_k}(z_k, \widehat{z}_k) = \frac{\left(\frac{2K_c}{\alpha_k}\right)^{K_c+1} (z_k \widehat{z}_k)^{\frac{K_c-1}{2}} I_{K_c-1}\left(\frac{2K_c \sqrt{\rho z_k \widehat{z}_k}}{\alpha_k(1-\rho)}\right)}{\Gamma(K_c) 2^{K_c+1} (1-\rho) \rho^{\frac{K_c-1}{2}}} \exp\left(\frac{-1}{1-\rho}\left(\frac{K_c z_k}{\alpha_k} + \frac{K_c \widehat{z}_k}{\alpha_k}\right)\right), \tag{A.3}$$

where $\rho = s_p^2$ is the correlation coefficient between Z_k and $\widehat{Z}_k$ and $I_{K_c-1}(\cdot)$ is the modified Bessel function of the first kind and order $K_c - 1$ [54]. Thus, (2.9) can be written as

$$(1 - P_o) = \Pr\left(Z_1 \leq \eta \max_{1\leq k\leq K_p}\{\widehat{Z}_k\}, \ldots, Z_{K_p} \leq \eta \max_{1\leq k\leq K_p}\{\widehat{Z}_k\}\right). \tag{A.4}$$

Using Bonferroni's inequality [22], a lower bound on (A.4) is given by

$$\begin{aligned}(1 - P_o) &\geq \sum_{i=1}^{K_p} \Pr\left(Z_i \leq \eta \max_{1\leq k\leq K_p}\{\widehat{Z}_k\}\right) - K_p + 1,\\ &= 1 - \sum_{i=1}^{K_p} \Pr\left(Z_i \geq \eta \max_{1\leq k\leq K_p}\{\widehat{Z}_k\}\right),\\ &= 1 - \sum_{i=1}^{K_p} \Pr\left(\widehat{Z}_1 \leq \frac{Z_i}{\eta}, \widehat{Z}_2 \leq \frac{Z_i}{\eta} \ldots \widehat{Z}_{K_p} \leq \frac{Z_i}{\eta}\right).\end{aligned} \tag{A.5}$$

This can be rewritten as

$$(1 - P_o) \geq 1 - \sum_{i=1}^{K_p} \int_{z_i=0}^{\infty} \int_{\widehat{z}_i=0}^{z_i/\eta} \prod_{j\neq i}^{K_p} \Pr\left(\widehat{Z}_j \leq \frac{z_i}{\eta}\right) f_{Z_i,\widehat{Z}_i}(z_i, \widehat{z}_i)\, d\widehat{z}_i dz_i. \tag{A.6}$$

Using the pdf given in (A.2), it can be shown that

$$\Pr\left(\widehat{Z}_j \leq \frac{z_i}{\eta}\right) = \frac{1}{\Gamma(K_c)}\gamma\left(K_c, \frac{K_c z_i}{\eta\alpha_j}\right), \tag{A.7}$$

where $\gamma(\cdot)$ is the lower incomplete Gamma function [53]. Substituting (A.7) in (A.6), we get

$$(1 - P_o) \geq 1 - \sum_{i=1}^{K_p} \int_{z_i=0}^{\infty} \int_{\widehat{z}_i=0}^{z_i/\eta} \prod_{j\neq i}^{K_p} \frac{\gamma\left(K_c, \frac{K_c z_i}{\eta\alpha_j}\right) f_{Z_i,\widehat{Z}_i}(z_i, \widehat{z}_i)\, d\widehat{z}_i dz_i}{\Gamma(K_c)}. \tag{A.8}$$

Upon re-arrangement, (A.8) can be written as

$$(1 - P_o) \geq 1 - \sum_{i=1}^{K_p} \int_{z_i=0}^{\infty} \prod_{j\neq i}^{K_p} \frac{\gamma\left(K_c, \frac{K_c z_i}{\eta\alpha_j}\right)}{\Gamma(K_c)} \left(f_{Z_i}(z_i) - \int_{\widehat{z}_i=z_i/\eta}^{\infty} f_{Z_i,\widehat{Z}_i}(z_i, \widehat{z}_i)\, d\widehat{z}_i\right) dz_i. \tag{A.9}$$

Substituting the joint pdf from (A.3) and simplifying using the identity [54, (4.59)], the lower bound in (A.9) simplifies to

$$(1 - P_o) \geq P_{L_{(ic)}} = 1 - \sum_{i=1}^{K_p} \int_{z_i=0}^{\infty} \prod_{j\neq i}^{K_p} \frac{\gamma\left(K_c, \frac{K_c z_i}{\eta\alpha_j}\right)}{\Gamma(K_c)} f_{Z_i}(z_i) \left(1 - Q_{K_c}\left(\sqrt{\frac{2K_c\rho z_i}{\alpha_i(1-\rho)}}, \sqrt{\frac{2K_c z_i}{\eta\alpha_i(1-\rho)}}\right)\right) dz_i. \tag{A.10}$$

This is further simplified using Gauss Laguerre integration [72, (25.4.29)] to obtain (2.10).

A.2 Proof of Theorem 2.2

We are interested in simplifying the SINR expression in (2.13) obtained from (2.12). To this end, we compute the variance of each of the terms in (2.12). The variance of term ① is given by

$$\begin{aligned}\mathbb{V}\mathrm{ar}\,(\text{term}①) &= \left|\mathbb{E}\left(\sqrt{\frac{P_{ic}}{K_c}}\left(s_s\|\widehat{\boldsymbol{h}}_{c_k}\|\right)\right)\right|^2 \mathbb{E}\left(|q_k|^2\right),\\ &= \frac{s_s^2}{K_c}\left(\mathbb{E}\left(\sqrt{P_{ic}}\right)\right)^2\left(\mathbb{E}\left(\|\widehat{\boldsymbol{h}}_{c_k}\|\right)\right)^2,\\ &= \frac{s_s^2}{K_c}\left(\zeta_{ic}\sqrt{\gamma_k}\frac{\Gamma\left(N+\frac{1}{2}\right)}{\Gamma(N)}\right)^2. \end{aligned} \tag{A.11}$$

The second equality above follows from the fact that $\mathbb{E}\left(|q_k|^2\right) = 1$ and the fact that P_{ic} depends only on $\widehat{\boldsymbol{g}}_{c_k}$ and is independent and uncorrelated to $\widehat{\boldsymbol{h}}_{c_k}$. Note that

$$\zeta_{ic} = \mathbb{E}\left(\sqrt{P_{ic}}\right) = \mathbb{E}\left(\sqrt{\frac{\bar{I}_p}{\eta X}}\right) \approx \sqrt{\frac{\bar{I}_p}{\eta}}\left(\frac{1}{\mathbb{E}\left(\sqrt{X}\right)} + \frac{\mathbb{V}\mathrm{ar}\left(\sqrt{X}\right)}{\left(\mathbb{E}\left(\sqrt{X}\right)\right)^3}\right) \tag{A.12}$$

[56], where $X = \max\limits_{1\le k\le K_p}\left(\widehat{Z}_k\right)$, and its CDF

$$F_X(x) = \frac{1}{(\Gamma(K_c))^{K_p}}\prod_{i=1}^{K_p}\gamma\left(K_c, \frac{K_c x}{\alpha_i}\right). \tag{A.13}$$

Furthermore, $\mathbb{E}\left(\sqrt{X}\right) = \int_0^\infty \frac{1}{2\sqrt{x}}\left(1 - F_X(x)\right)dx$ and $\mathbb{V}\mathrm{ar}(\sqrt{X}) = \int_0^\infty \left(1 - F_X(x)\right)dx - \left(\mathbb{E}\left(\sqrt{X}\right)\right)^2$ [22]. Also, let $U = \|\widehat{\boldsymbol{h}}_{c_k}\|^2$. Since, $\widehat{h}_{c_{k_i}} \sim \mathcal{CN}(0, \gamma_k)$, it can be shown that

$$f_U(u) = \frac{1}{(\gamma_k)^N}\frac{1}{\Gamma(N)}(u)^{N-1}\,\mathrm{e}^{-\frac{u}{\gamma_k}}, \tag{A.14}$$

$\mathbb{E}(U) = N\gamma_k$ and $\mathbb{E}\left(\sqrt{U}\right) = \sqrt{\gamma_k}\frac{\Gamma\left(N+\frac{1}{2}\right)}{\Gamma(N)}$ [22].

The variance of the second term is given by

$$\mathbb{V}\mathrm{ar}\,(\text{term}②) = \frac{\left(1 - s_s^2\right)\mathbb{E}\left(P_{ic}\right)}{K_c}\mathbb{E}\left|\widetilde{\boldsymbol{h}}_{c_k}^{\mathrm{T}}\frac{\widehat{\boldsymbol{h}}_{c_k}^*}{\|\widehat{\boldsymbol{h}}_{c_k}^*\|}\right|^2\mathbb{E}|q_k|^2,$$

$$
\begin{aligned}
&= \frac{\left(1-s_s^2\right)\mathbb{E}\left(P_{ic}\right)}{K_c}\mathbb{E}\left[\frac{\widehat{\boldsymbol{h}}_{c_k}^{\mathrm{T}}\widetilde{\boldsymbol{h}}_{c_k}^{*}\widetilde{\boldsymbol{h}}_{c_k}^{\mathrm{T}}\widehat{\boldsymbol{h}}_{c_k}^{*}}{\|\widehat{\boldsymbol{h}}_{c_k}^{*}\|^2}\right], \\
&= \frac{\left(1-s_s^2\right)}{K_c}\mathbb{E}\left(\widehat{P}_{ic}\right)\mathbb{E}\left[\frac{\widehat{\boldsymbol{h}}_{c_k}^{T}}{\|\widehat{\boldsymbol{h}}_{c_k}^{*}\|}\mathbb{E}\left(\widetilde{\boldsymbol{h}}_{c_k}^{*}\widetilde{\boldsymbol{h}}_{c_k}^{T}\right)\frac{\widehat{\boldsymbol{h}}_{c_k}^{*}}{\|\widehat{\boldsymbol{h}}_{c_k}^{*}\|}\right] \qquad \text{From [95]} \\
&= \frac{\left(1-s_s^2\right)}{K_c}\psi_{ic}\gamma_k. \qquad (A.15)
\end{aligned}
$$

The first equality above is due to the fact that $\widehat{P}_{ic}$ is independent and uncorrelated to both $\widetilde{\boldsymbol{h}}_{c_k}$ and $\widehat{\boldsymbol{h}}_{c_k}$. And the last equality follows since $\widetilde{\boldsymbol{h}}_{c_k}$ is uncorrelated and independent of $\widehat{\boldsymbol{h}}_{c_k}$ and the fact that $\mathbb{E}\left(\widetilde{\boldsymbol{h}}_{c_k}^{*}\widetilde{\boldsymbol{h}}_{c_k}^{\mathrm{T}}\right) = \gamma_k\mathbf{I}_N$. Note that $\psi_{ic} = \mathbb{E}\left(P_{ic}\right) = \mathbb{E}\left(\frac{\bar{I}_p}{\eta X}\right) \approx \frac{\bar{I}_p}{\eta}\left(\frac{1}{\mathbb{E}(X)} + \frac{\mathbb{V}\mathrm{ar}(X)}{(\mathbb{E}(X))^3}\right)$ [56], $\mathbb{E}\left(X\right) = \int_0^\infty \left(1-F_X(x)\right)dx$ and $\mathbb{V}\mathrm{ar}\left(X\right) = \int_0^\infty 2x\left(1-F_X(x)\right)dx - \left(\mathbb{E}\left(X\right)\right)^2$ [22].

To compute the variance of the third term, we use the facts that P_{ic}, $\boldsymbol{h}_{c_k}$ and $\widehat{\boldsymbol{h}}_{c_{k'}}$ are mutually independent for any k or k' and that $\mathbb{E}\left\{q_i q_j^*\right\} = 0$ for $i \neq j$ to simplify as follows:

$$
\begin{aligned}
\mathbb{V}\mathrm{ar}\left(\text{term}③\right) &= \mathbb{E}\left|\sqrt{\frac{P_{ic}}{K_c}}\sum_{k'\neq k}^{K_c}\frac{\boldsymbol{h}_{c_k}^{\mathrm{T}}\widehat{\boldsymbol{h}}_{c_{k'}}^{*}q_{k'}}{\|\widehat{\boldsymbol{h}}_{c_{k'}}\|}\right|^2, \\
&= \frac{\mathbb{E}\left(P_{ic}\right)}{K_c}\sum_{k'\neq k}^{K_c}\mathbb{E}\left|\frac{\boldsymbol{h}_{c_k}^{\mathrm{T}}\widehat{\boldsymbol{h}}_{c_{k'}}^{*}}{\|\widehat{\boldsymbol{h}}_{c_{k'}}\|}\right|^2\mathbb{E}|q_{k'}|^2, \\
&= \frac{\mathbb{E}(P_{pi})}{K_c}\sum_{k'\neq k}^{K_c}\mathbb{E}\left[\frac{\widehat{\boldsymbol{h}}_{c_{k'}}^{T}}{\|\widehat{\boldsymbol{h}}_{c_{k'}}^{*}\|}\boldsymbol{h}_{c_k}^{*}\boldsymbol{h}_{c_k}^{T}\frac{\widehat{\boldsymbol{h}}_{c_{k'}}^{*}}{\|\widehat{\boldsymbol{h}}_{c_{k'}}^{*}\|}\right], \\
&= \frac{\mathbb{E}\left(P_{ic}\right)}{K_c}\sum_{k'\neq k}^{K_c}\mathbb{E}\left[\frac{\widehat{\boldsymbol{h}}_{c_{k'}}^{\mathrm{T}}\mathbb{E}\left(\boldsymbol{h}_{c_k}^{*}\boldsymbol{h}_{c_k}^{\mathrm{T}}\right)\widehat{\boldsymbol{h}}_{c_{k'}}^{*}}{\|\widehat{\boldsymbol{h}}_{c_{k'}}\|^2}\right], \\
&= \frac{\psi_{ic}}{K_c}\left(K_c-1\right)\gamma_k. \qquad (A.16)
\end{aligned}
$$

The variance of the fourth term arising due to beamforming uncertainty is given by

$$
\begin{aligned}
\mathbb{V}\mathrm{ar}\left(\text{term}④\right) &= \frac{s_s^2}{K_c}\mathbb{E}\left|\sqrt{P_{ic}}\|\widehat{\boldsymbol{h}}_{c_k}\| - \mathbb{E}\left(\sqrt{P_{ic}}\right)\mathbb{E}(\|\widehat{\boldsymbol{h}}_{c_k}\|)\right|^2\mathbb{E}|q_k|^2, \\
&= \frac{s_s^2}{K_c}\left[\mathbb{E}\left(P_{ic}\right)N\gamma_k - \left(\mathbb{E}\left(\sqrt{P_{ic}}\right)\sqrt{\gamma_k}\frac{\Gamma\left(N+\frac{1}{2}\right)}{\Gamma\left(N\right)}\right)^2\right] \\
&= \frac{s_s^2}{K_c}\left[\psi_{ic}N\gamma_k - \left(\zeta_{ic}\sqrt{\gamma_k}\frac{\Gamma\left(N+\frac{1}{2}\right)}{\Gamma\left(N\right)}\right)^2\right]. \qquad (A.17)
\end{aligned}
$$

To compute the variance of term ⑤, we exploit the facts that $\mathbb{E}\left\{s_i s_j^*\right\} = 0$ for $i \neq j$ and that the channel from the primary BS to any PU is uncorrelated to the channel from the primary BS to any CU. Thus, the variance of the fifth term arising due to interference from PUs is given by

$$\mathbb{V}\text{ar}\,(\text{term}⑤) = \mathbb{E}\left|\sqrt{\frac{P_p}{K_p}}\sum_{j=1}^{K_p}\frac{\boldsymbol{g}_{p_k}^{\mathrm{T}}\boldsymbol{h}_{p_j}^{*}s_j}{\|\boldsymbol{h}_{p_j}\|}\right|^2 = \frac{P_p}{K_p}\sum_{j=1}^{K_p}\mathbb{E}\left|\frac{\boldsymbol{g}_{p_k}^{\mathrm{T}}\boldsymbol{h}_{p_j}^{*}}{\|\boldsymbol{h}_{p_j}\|}\right|^2\mathbb{E}\left|s_j\right|^2 = \frac{P_p}{K_p}\sum_{j=1}^{K_p}\phi_k = P_p\phi_k. \quad \text{(A.18)}$$

And the variance of noise equals $\mathbb{E}\left(|n_k|^2\right) = 1$.

A.3 Proof of Theorem 2.3

We can re-write (2.18) as

$$(1 - P_o) = \Pr\left(Z_1 \leq \eta \max_{k\in\mathcal{S}}\{Z_k\} \ldots Z_{K_p} \leq \eta \max_{k\in\mathcal{S}}\{Z_k\}\right), \quad \text{(A.19)}$$

where, $Z_k = \sum_{i=1}^{K_c}\left|\sqrt{\frac{1}{K_c}}\frac{\boldsymbol{g}_{c_k}^{\mathrm{T}}\boldsymbol{h}_{c_i}^{*}}{\|\boldsymbol{h}_{c_i}\|}\right|^2$. Since we know the channel to $|\mathcal{S}|$ out of the K_p PUs, we can modify (A.19) as follows:

$$\begin{aligned}(1 - P_o) =& \Pr\left(\left(\max_{k\in\mathcal{S}}(Z_k) \leq \eta \max_{k\in\mathcal{S}}(Z_k)\right) \cap \left(\max_{k'\notin\mathcal{S}}(Z_k) \leq \eta \max_{k\in\mathcal{S}}(Z_k)\right)\right),\\ =& \Pr\left(\max_{k\in\mathcal{S}}(Z_k) \leq \eta \max_{k\in\mathcal{S}}(Z_k)\right)\Pr\left(\max_{k'\notin\mathcal{S}}(Z_k) \leq \eta \max_{k\in\mathcal{S}}(Z_k)\right). \quad \text{(A.20)}\end{aligned}$$

Note that the event $\{\max_{k\in\mathcal{S}}(Z_k) \leq \eta \max_{k\in\mathcal{S}}(Z_k)\}$ will always be true, i.e., it is sure event.

Therefore, $\Pr\left(\max_{k\in\mathcal{S}}(Z_k) \leq \eta \max_{k\in\mathcal{S}}(Z_k)\right) = 1$. And, $(1 - P_o)$ above can be written down in a further simplified form as

$$(1 - P_o) = \Pr\left(\max_{k'\notin\mathcal{S}}(Z_k) \leq \eta \max_{k\in\mathcal{S}}(Z_k)\right). \quad \text{(A.21)}$$

Now in order to evaluate this probability, let $Y_1 = \max_{k'\notin\mathcal{S}}(Z_{k'})$ and $Y_2 = \eta \max_{k\in\mathcal{S}}(Z_k)$. Therefore, we are interested in evaluating

$$(1 - P_o) = \Pr(Y_1 \leq Y_2). \quad \text{(A.22)}$$

Since, Y_1 is independent of Y_2, therefore,

$$(1 - P_o) = \Pr(Y_1 \leq Y_2) = \int_0^\infty F_{Y_1}(y_2) f_{Y_2}(y_2) dy_2. \quad \text{(A.23)}$$

To simplify this further, we need to find the CDF of Y_1 and the pdf of Y_2. Based on the analysis in Appendix A.1, it can be shown that the CDF of Y_1 equals

$$F_{Y_1}(y_2) = \Pr(Y_1 \leq y_2) = \frac{\prod\limits_{k' \notin \mathcal{S}} \gamma\left(K_c, \frac{K_c y_2}{\alpha_{k'}}\right)}{(\Gamma(K_c))^{K_p - S}}, \tag{A.24}$$

and the CDF of Y_2 equals

$$F_{Y_2}(y_2) = \Pr(Y_2 \leq y_2) = \frac{1}{(\Gamma(K_c))^S} \prod_{k \in \mathcal{S}} \gamma\left(K_c, \frac{K_c y_2}{\alpha_k \eta}\right). \tag{A.25}$$

The pdf of Y_2 can be found by taking the derivative of $F_{Y_2}(y_2)$ w.r.t. y_2 and simplified further to obtain [96]

$$f_{Y_2}(y_2) = \frac{(K_c)^{K_c} y_2^{K_c - 1}}{(\Gamma(K_c))^S \eta^{K_c}} \sum_{k \in \mathcal{S}} \frac{e^{-\frac{K_c y_2}{\alpha_k \eta}}}{\alpha_k^{K_c}} \prod_{\substack{i \in \mathcal{S} \\ i \neq k}} \gamma\left(K_c, \frac{K_c y_2}{\alpha_i \eta}\right). \tag{A.26}$$

By substituting (A.24) and (A.26) in (A.23), we get

$$(1 - P_o) = \int_0^\infty \frac{K_c^{K_c} y^{K_c - 1}}{(\Gamma(K_c))^{K_p} \eta^{K_c}} \prod_{k' \notin \mathcal{S}} \gamma\left(K_c, \frac{K_c y}{\alpha_{k'}}\right) \left(\sum_{k \in \mathcal{S}} \frac{e^{-\frac{K_c y}{\alpha_k \eta}}}{\alpha_k^{K_c}} \left[\prod_{\substack{i \in \mathcal{S} \\ i \neq k}} \gamma\left(K_c, \frac{K_c y}{\alpha_i \eta}\right) \right] \right) dy. \tag{A.27}$$

Using Gauss Laguerre integration [72, (25.4.29)], this can be further simplified to obtain (2.20).

A.4 Proof of Theorem 2.4

We are interested in simplifying the SINR expression in (2.23) obtained from (2.22). To this end, we compute the variance of each of the terms in (2.22). The variance of term① equals

$$\begin{aligned} \mathbb{V}\text{ar}(\text{term①}) &= \frac{1}{K_c} \left(\mathbb{E}\left(\sqrt{P_{pi}} \right) \right)^2 \left(\mathbb{E}\left(\|\boldsymbol{h}_{c_k}\| \right) \right)^2, \\ &= \frac{1}{K_c} \left(\mathbb{E}\left(\sqrt{P_{pi}} \right) \sqrt{\gamma_k} \frac{\Gamma\left(N + \frac{1}{2}\right)}{\Gamma(N)} \right)^2, \\ &= \frac{1}{K_c} \left(\zeta_{pi} \frac{\sqrt{\gamma_k} \Gamma\left(N + \frac{1}{2}\right)}{\Gamma(N)} \right)^2. \end{aligned} \tag{A.28}$$

The first equality above follows from the fact that $\mathbb{E}\left(|q_k|^2\right) = 1$ and the fact that P_{pi} being a function of $\boldsymbol{g}_{c_k}$ is independent and uncorrelated to $\boldsymbol{h}_{c_k}$. Note that

$$\zeta_{pi} = \mathbb{E}\left(\sqrt{P_{pi}}\right) = \mathbb{E}\left(\sqrt{\frac{\bar{I}_p}{\eta X}}\right) \approx \sqrt{\frac{\bar{I}_p}{\eta}}\left(\frac{1}{\mathbb{E}\left(\sqrt{X}\right)} + \frac{\mathbb{V}\mathrm{ar}\left(\sqrt{X}\right)}{\left(\mathbb{E}\left(\sqrt{X}\right)\right)^3}\right), \tag{A.29}$$

where $X = \max_{k\in\mathcal{S}}(Z_k)$, and its CDF

$$F_X(x) = \frac{1}{(\Gamma(K_c))^S}\prod_{i\in\mathcal{S}}\gamma\left(K_c, \frac{K_c x}{\alpha_i}\right). \tag{A.30}$$

Furthermore, $\mathbb{E}\left(\sqrt{X}\right) = \int_0^\infty \frac{1}{2\sqrt{x}}(1-F_X(x))dx$, and $\mathbb{V}\mathrm{ar}(\sqrt{X}) = \int_0^\infty (1-F_X(x))dx - \left(\mathbb{E}\left(\sqrt{X}\right)\right)^2$ [22]. Also, let $U = \|\boldsymbol{h}_{c_k}\|^2$, where $h_{c_{k_i}} \sim \mathcal{CN}(0, \gamma_k)$, it can be shown that

$$f_U(u) = \frac{1}{(\gamma_k)^N}\frac{1}{\Gamma(N)}(u)^{N-1}\,\mathrm{e}^{-\frac{u}{\gamma_k}}, \tag{A.31}$$

$\mathbb{E}(U) = N\gamma_k$ and $\mathbb{E}\left(\sqrt{U}\right) = \sqrt{\gamma_k}\frac{\Gamma\left(N+\frac{1}{2}\right)}{\Gamma(N)}$ [22].

The variance of the second term is given by

$$\begin{aligned}\mathbb{V}\mathrm{ar}\,(\text{term}②) &= \frac{1}{K_c}\mathbb{E}\left|\sqrt{P_{pi}}\|\boldsymbol{h}_{c_k}\| - \mathbb{E}\left(\sqrt{P_{pi}}\right)\mathbb{E}(\|\boldsymbol{h}_{c_k}\|)\right|^2\mathbb{E}|q_k|^2,\\ &= \frac{1}{K_c}\left[\psi_{pi}N\gamma_k - \left(\zeta_{pi}\frac{\sqrt{\gamma_k}\Gamma\left(N+\frac{1}{2}\right)}{\Gamma(N)}\right)^2\right].\end{aligned} \tag{A.32}$$

The first equality above is due to the fact that P_{pi} is independent and uncorrelated to $\boldsymbol{h}_{c_k}$. Note that $\psi_{pi} = \mathbb{E}\left(P_{pi}\right) = \mathbb{E}\left(\frac{\bar{I}_p}{\eta X}\right) \approx \frac{\bar{I}_p}{\eta}\left(\frac{1}{\mathbb{E}(X)} + \frac{\mathbb{V}\mathrm{ar}(X)}{(\mathbb{E}(X))^3}\right)$, $\mathbb{E}(X) = \int_0^\infty (1-F_X(x))dx$ and $\mathbb{V}\mathrm{ar}(X) = \int_0^\infty 2x(1-F_X(x))dx - (\mathbb{E}(X))^2$ [22].

To compute the variance of the third term, we use the facts that P_{pi}, $\boldsymbol{h}_{c_k}$ and $\boldsymbol{h}_{c_{k'}}$ are mutually independent for any k or k' and that the symbols transmitted by different users are uncorrelated to each other to simplify as follows:

$$\begin{aligned}\mathbb{V}\mathrm{ar}\,(\text{term}③) &= \mathbb{E}\left|\sqrt{\frac{P_{pi}}{K_c}}\sum_{k'\neq k}^{K_c}\frac{\boldsymbol{h}_{c_k}^{\mathrm{T}}\boldsymbol{h}_{c_{k'}}^{*}q_{k'}}{\|\boldsymbol{h}_{c_{k'}}\|}\right|^2,\\ &= \frac{\mathbb{E}\left(P_{pi}\right)}{K_c}\sum_{k'\neq k}^{K_c}\mathbb{E}\left|\frac{\boldsymbol{h}_{c_k}^{\mathrm{T}}\boldsymbol{h}_{c_{k'}}^{*}}{\|\boldsymbol{h}_{c_{k'}}\|}\right|^2\mathbb{E}|q_{k'}|^2,\end{aligned}$$

$$= \frac{\mathbb{E}(P_{pi})}{K_c} \sum_{i \neq k}^{K_c} \mathbb{E}\left[\frac{\widehat{\boldsymbol{h}}_{c_i}^{T}}{\|\widehat{\boldsymbol{h}}_{c_i}^{*}\|} \boldsymbol{h}_{c_k}^{*} \boldsymbol{h}_{c_k}^{T} \frac{\widehat{\boldsymbol{h}}_{c_i}^{*}}{\|\widehat{\boldsymbol{h}}_{c_i}^{*}\|} \right]$$
$$= \frac{\psi_{pi}}{K_c} (K_c - 1) \gamma_k. \tag{A.33}$$

The variance of term④ in (2.22) is already derived in Appendix A.2. And the variance of noise equals $\mathbb{E}\left(|n_k|^2\right) = 1$.

A.5 Proof of Theorem 2.5

We can rewrite (2.28) as

$$(1 - P_o) = \Pr\left(Z_1 \leq \eta \max_{k \in S}\{\widehat{Z}_k\} \ldots Z_{K_p} \leq \eta \max_{k \in S}\{\widehat{Z}_k\}\right), \tag{A.34}$$

where, $Z_k = \sum_{i=1}^{K_c} \left| \sqrt{\frac{1}{K_c}} \frac{\boldsymbol{g}_{c_k}^{\mathrm{T}} \widehat{\boldsymbol{h}}_{c_i}^{*}}{\|\widehat{\boldsymbol{h}}_{c_i}\|} \right|^2$ and $\widehat{Z}_k = \sum_{i=1}^{K_c} \left| \sqrt{\frac{1}{K_c}} \frac{\widehat{\boldsymbol{g}}_{c_k}^{\mathrm{T}} \widehat{\boldsymbol{h}}_{c_i}^{*}}{\|\widehat{\boldsymbol{h}}_{c_i}\|} \right|^2$. Since we know the channel estimates to $|\mathcal{S}|$ out of the K_p PUs, we can modify (A.34) as follows:

$$(1 - P_o) = \Pr\left(\left(\max_{k \in S}(Z_k) \leq \eta \max_{k \in S}\left(\widehat{Z}_k\right)\right) \cap \left(\max_{k' \notin S}(Z_k) \leq \eta \max_{k \in S}\left(\widehat{Z}_k\right)\right)\right),$$
$$= \Pr\left(\max_{k \in S}(Z_k) \leq \eta \max_{k \in S}\left(\widehat{Z}_k\right)\right) \Pr\left(\max_{k' \notin S}(Z_k) \leq \eta \max_{k \in S}\left(\widehat{Z}_k\right)\right). \tag{A.35}$$

Using Bonferroni's inequality [22], a lower bound on $\Pr\left(\max_{k \in S}(Z_k) \leq \eta \max_{k \in S}\left(\widehat{Z}_k\right)\right)$ is

$$\Pr\left(\max_{k \in S}(Z_k) \leq \eta \max_{k \in S}\left(\widehat{Z}_k\right)\right) \geq \sum_{i \in \mathcal{S}} \Pr\left(Z_i \leq \eta \max_{k \in S}\left(\widehat{Z}_k\right)\right) - S + 1 = 1 - \sum_{i \in \mathcal{S}} \Pr\left(Z_i \geq \eta \max_{k \in \mathcal{S}}\{\widehat{Z}_k\}\right). \tag{A.36}$$

We can use the joint pdf of Z_i and $\widehat{Z}_i$ to simplify and write down the above equation as

$$\Pr\left(\max_{k \in S}(Z_k) \leq \eta \max_{k \in S}\left(\widehat{Z}_k\right)\right) \geq 1 - \sum_{i \in \mathcal{S}} \int_{z_i=0}^{\infty} \frac{f_{Z_i}(z_i)}{\Gamma(K_c)^{S-1}} \prod_{\substack{j \in \mathcal{S} \\ j \neq i}} \gamma\left(K_c, \frac{K_c z_i}{\eta \alpha_j}\right)$$
$$\times \left(1 - Q_{K_c}\left(\sqrt{\frac{2K_c \rho z_i}{\alpha_i(1-\rho)}}, \sqrt{\frac{2K_c z_i}{\eta \alpha_i (1-\rho)}}\right)\right) dz_i. \tag{A.37}$$

Now in order to evaluate the probability $\Pr\left(\max_{k' \notin S}(Z_k) \leq \eta \max_{k \in S}\left(\widehat{Z}_k\right)\right)$, let $W_1 = \max_{k' \notin S}(Z_{k'})$ and $W_2 = \eta \max_{k \in S}\left(\widehat{Z}_k\right)$. Since, W_1 is independent of W_2, therefore,

$$\Pr(W_1 \leq W_2) = \int_0^\infty F_{W_1}(w_2) f_{W_2}(w_2) dw_2. \tag{A.38}$$

To simplify this further, we need to find CDF of W_1 and pdf of W_2. The CDF of W_1 equals

$$F_{W_1}(w_2) = \Pr(W_1 \leq W_2) = \frac{\prod_{k' \notin S} \gamma\left(K_c, \frac{K_c w_2}{\alpha_{k'}}\right)}{(\Gamma(K_c))^{K_p - S}}, \tag{A.39}$$

and the CDF of W_2 equals

$$F_{W_2}(w_2) = \Pr(W_2 \leq w_2) = \frac{\prod_{k \in S} \gamma\left(K_c, \frac{K_c w_2}{\alpha_k \eta}\right)}{(\Gamma(K_c))^{S}}. \tag{A.40}$$

The pdf of W_2 is found by taking derivative of $F_{W_2}(w_2)$ w.r.t. w_2 and simplified further to obtain [96]

$$f_{W_2}(w_2) = \frac{(K_c)^{K_c} w_2^{K_c - 1}}{(\Gamma(K_c))^S \eta^{K_c}} \sum_{k \in S} \frac{e^{-\frac{K_c w_2}{\alpha_k \eta}}}{\alpha_k^{K_c}} \prod_{\substack{i \in S \\ i \neq k}} \gamma\left(K_c, \frac{K_c w_2}{\alpha_i \eta}\right). \tag{A.41}$$

By substituting (A.39) and (A.41) in (A.38), and also using (A.37), we get

$$\begin{aligned}(1 - P_o) \geq P_{L_{(ii)}} = \Bigg[1 - \sum_{k \in S} \int_{z_k=0}^\infty \frac{f_{Z_k}(z_k)}{(\Gamma(K_c))^{S-1}} \prod_{\substack{j \in S \\ j \neq k}} \gamma\left(K_c, \frac{K_c z_k}{\eta \alpha_j}\right) \\ \times \left(1 - Q_{K_c}\left(\sqrt{\frac{2K_c \rho z_k}{\alpha_k(1-\rho)}}, \sqrt{\frac{2K_c z_k}{\eta \alpha_k (1-\rho)}}\right)\right) dz_k\Bigg] \Bigg[\int_0^\infty \frac{K_c^{K_c} y^{K_c - 1}}{(\Gamma(K_c))^{K_p} \eta^{K_c}} \prod_{k' \notin S} \gamma\left(K_c, \frac{K_c y}{\alpha_{k'}}\right) \\ \times \left(\sum_{k \in S} \frac{e^{-\frac{K_c y}{\alpha_k \eta}}}{\alpha_k^{K_c}} \left[\prod_{\substack{i \in S \\ i \neq k}} \gamma\left(K_c, \frac{K_c y}{\alpha_i \eta}\right)\right]\right) dy\Bigg].\end{aligned} \tag{A.42}$$

Using Gauss Laguerre integration, this can be further simplified to obtain (2.30).

B

Appendix

B.1 Proof of Proposition 3.1

From (3.19), we know that $P_d^s = \dfrac{\bar{I}_p}{\eta \max\limits_{1\le k\le K}\left\{\frac{1}{L}\sum\limits_{l=1}^{L}\left|\sum\limits_{n=1}^{N}\frac{\widehat{\boldsymbol{g}}_{nk}^{s\mathrm{T}}\widehat{\boldsymbol{h}}_{nl}^{s*}}{\|\widehat{\boldsymbol{h}}_{nl}^{s}\|}\right|^2\right\}}$. Let

$$\widehat{V}_{lk} = \frac{1}{\sqrt{L}}\sum_{n=1}^{N}\frac{\widehat{\boldsymbol{g}}_{nk}^{s\mathrm{T}}\,\widehat{\boldsymbol{h}}_{nl}^{s*}}{\|\widehat{\boldsymbol{h}}_{nl}^{s}\|},\ \text{for } 1\le k\le K. \tag{B.1}$$

It can be shown that conditioned on $\widehat{\boldsymbol{h}}_{nl}^s$, $\widehat{V}_{lk} \sim \mathcal{CN}\left(0, \frac{\mu_k}{L}\right)$ where $\mu_k = \sum\limits_{n=1}^{N}\zeta_{nk}^s$. Also, $\widehat{V}_{lk}$ is independent of $\widehat{\boldsymbol{h}}_{nl}^s$. Let $\widehat{Z}_k = \sum\limits_{l=1}^{L}|\widehat{V}_{lk}|^2$ then, $\widehat{X}_k = \frac{2L}{\mu_k}\widehat{Z}_k$ turns out to be a chi-square distributed rv with $2L$ degrees of freedom, since it essentially is the sum of squares of $2L$ i.i.d. $\mathcal{N}(0,1)$ rvs. Using transformation of rvs and given the pdf of $\widehat{X}_k$, the pdf of $\widehat{Z}_k$ can be obtained as [97]

$$f_{\widehat{Z}_k}(\widehat{z}_k) = \frac{L}{\mu_k}\frac{1}{\Gamma(L)}\left(\frac{L}{\mu_k}\widehat{z}_k\right)^{L-1}\mathrm{e}^{-\frac{L}{\mu_k}\widehat{z}_k}. \tag{B.2}$$

In order to evaluate the average value of P_d^s, we express P_d^s in terms of $\widehat{Z}_k$ as follows

$$P_d^s = \frac{\bar{I}_p}{\eta\max\limits_{1\le k\le K}\left\{\widehat{Z}_k\right\}} = \frac{\bar{I}_p}{\eta}\min_{1\le k\le K}\left\{\frac{1}{\widehat{Z}_k}\right\}. \tag{B.3}$$

Let us now take $\widehat{Y}_k = \frac{1}{\widehat{Z}_k}$. Then, using the pdf of $\widehat{Z}_k$, one can express the pdf of $\widehat{Y}_k$ as

$$f_{\widehat{Y}_k}(\widehat{y}_k) = \frac{1}{\Gamma(L)}\left(\frac{L}{\mu_k}\right)^L \left(\frac{1}{\widehat{y}_k}\right)^{L+1} \mathrm{e}^{-\frac{L}{\mu_k \widehat{y}_k}}. \tag{B.4}$$

We now define a new rv $X = \min\limits_{1\le k\le K}\{\widehat{Y}_k\}$. Then, its CDF can be computed as

$$\begin{aligned} F_X(x) &= 1 - \Pr\left(\min_{1\le k\le K}\{\widehat{Y}_k\} \ge x\right), \\ &\overset{(a)}{=} 1 - \prod_{j=1}^{K} \Pr(\widehat{Y}_j \ge x) \overset{(b)}{=} 1 - \prod_{j=1}^{K} \frac{\gamma\left(L, \frac{L}{\mu_j x}\right)}{\Gamma(L)}. \end{aligned} \tag{B.5}$$

where (a) holds since $\widehat{Y}_j$s are independent across j and (b) holds since

$$\Pr(\widehat{Y}_j \ge x) = \int_x^{\infty} \frac{1}{\Gamma(L)}\left(\frac{L}{\mu_j}\right)^L \left(\frac{1}{\widehat{y}_j}\right)^{L+1} \mathrm{e}^{-\frac{L}{\mu_j \widehat{y}_j}} d\widehat{y}_j. \tag{B.6}$$

To evaluate this integral, we substitute $\frac{L}{\mu_j \widehat{y}_j} = t$. Then,

$$\Pr(\widehat{Y}_j \ge x) = \int_0^{\frac{L}{\mu_j x}} \frac{1}{\Gamma(L)} (t)^{L-1} \mathrm{e}^{-t} dt = \frac{\gamma\left(L, \frac{L}{\mu_j x}\right)}{\Gamma(L)}. \tag{B.7}$$

To evaluate $\mathbb{E}(P_d^s)$, we obtain the pdf of X by taking derivative of its CDF in (B.5) as follows

$$\begin{aligned} f_X(x) &= -\frac{d}{dx}\left(\prod_{j=1}^{K} \frac{\gamma\left(L, \frac{L}{\mu_j x}\right)}{\Gamma(L)}\right), \\ &\overset{(c)}{=} \frac{1}{(\Gamma(L))^K} \sum_{j=1}^{K} \left[\left(\frac{L}{\mu_j}\right)^L \left(\frac{1}{x}\right)^{L+1} e^{-\left(\frac{L}{\mu_j x}\right)} \prod_{i\ne j}^{K} \gamma\left(L, \frac{L}{\mu_i x}\right)\right]. \end{aligned} \tag{B.8}$$

Note that we invoke the Leibniz integral rule in (c) to obtain (B.8). The SAP transmit power is a function of the rv X. And its statistical mean is given by

$$\begin{aligned} \mathbb{E}(P_d^s) &= \frac{\bar{I}_p}{\eta}\mathbb{E}(X), \\ &= \int_0^{\infty} \frac{\bar{I}_p x}{\eta(\Gamma(L))^K} \sum_{j=1}^{K} \left[\left(\frac{L}{\mu_j}\right)^L \left(\frac{1}{x}\right)^{L+1} e^{-\left(\frac{L}{\mu_j x}\right)} \prod_{i\ne j}^{K} \gamma\left(L, \frac{L}{\mu_i x}\right)\right] dx. \end{aligned} \tag{B.9}$$

Using Gauss-Laguerre integration [72, (25.4.29)], we further simplify (B.9) to obtain (3.21).

B.2 Proof of Proposition 3.2

We write $Z_k = \sum_{l=1}^{L} |V_{lk}|^2$, where $V_{lk} = \frac{1}{\sqrt{L}} \sum_{n=1}^{N} \frac{\mathbf{g}_{nk}^{s\,\mathrm{T}} \widehat{\boldsymbol{h}}_{nl}^{s\,*}}{\|\widehat{\boldsymbol{h}}_{nl}^{s}\|}$. We note that $V_{lk} \sim \mathcal{CN}\left(0, \frac{\alpha_k}{L}\right)$ and $\alpha_k = \sum_{n=1}^{N} \beta_{nk}^{s}$. Using the fact $\mathbf{g}_{nk}^{s} = \widehat{\mathbf{g}}_{nk}^{s} + \widetilde{\mathbf{g}}_{nk}^{s}$ from (3.12), Z_k can be expressed as

$$\begin{aligned} Z_k &= \sum_{l=1}^{L} |V_{lk}|^2 = \sum_{l=1}^{L} \left| \widehat{V}_{lk} + \widetilde{V}_{lk} \right|^2, \\ &= \sum_{l=1}^{L} \left(\left| \widehat{V}_{lk} \right|^2 + \left| \widetilde{V}_{lk} \right|^2 + \widehat{V}_{lk} \widetilde{V}_{lk}^{*} + \widehat{V}_{lk}^{*} \widetilde{V}_{lk} \right), \end{aligned} \tag{B.10}$$

where $\widetilde{V}_{lk} = \frac{1}{\sqrt{L}} \sum_{n=1}^{N} \frac{\widetilde{\mathbf{g}}_{nk}^{s\,\mathrm{T}} \widehat{\boldsymbol{h}}_{nl}^{s\,*}}{\|\widehat{\boldsymbol{h}}_{nl}^{s}\|}$. It can be shown that $\widetilde{V}_{lk} \sim \mathcal{CN}\left(0, \frac{\psi_k}{L}\right)$ and $\psi_k = \alpha_k - \mu_k$. In terms of $\widehat{Z}_k$ and $\widetilde{Z}_k$, (B.10) can be re-written as

$$Z_k = \widehat{Z}_k + \widetilde{Z}_k + \sum_{l=1}^{L} \widehat{V}_{lk} \widetilde{V}_{lk}^{*} + \sum_{l=1}^{L} \widehat{V}_{lk}^{*} \widetilde{V}_{lk}. \tag{B.11}$$

Furthermore, $\widehat{V}_{lk}$ and $\widetilde{V}_{lk}$ are zero mean uncorrelated RVs, since the MMSE channel estimate $\widehat{\mathbf{g}}_{nk}^{s}$ and the channel estimation error $\widetilde{\mathbf{g}}_{nk}^{s}$ are independent and uncorrelated to each other. Therefore, $\widehat{Z}_k$ and $\widetilde{Z}_k$ are independent of each other. Multiplying $\widehat{Z}_k$ on both sides of (B.11) and by taking expectation we obtain

$$\mathbb{E}(Z_k \widehat{Z}_k) = \mathbb{E}\left(\widehat{Z}_k^2\right) + \mathbb{E}\left(\widetilde{Z}_k\right) \mathbb{E}\left(\widehat{Z}_k\right), \tag{B.12}$$

and this is because $\mathbb{E}\left(\widehat{V}_{lk} \widetilde{V}_{lk}^{*} \widehat{Z}_k\right) = \mathbb{E}\left(\widehat{V}_{lk}^{*} \widetilde{V}_{lk} \widehat{Z}_k\right) = 0$.

The correlation coefficient of Z_k and $\widehat{Z}_k$ is given by

$$\rho_k = \frac{\mathbb{E}\left(Z_k \widehat{Z}_k\right) - \mathbb{E}\left(\widehat{Z}_k\right) \mathbb{E}\left(Z_k\right)}{\sqrt{\mathbb{V}\mathrm{ar}\left(Z_k\right) \mathbb{V}\mathrm{ar}\left(\widehat{Z}_k\right)}}, \tag{B.13}$$

where it can be shown that $\mathbb{E}\left(\widehat{Z}_k\right) = \mu_k$, $\mathbb{E}\left(\widehat{Z}_k^2\right) = \mu_k^2 \left(1 + \frac{1}{L}\right)$, $\mathbb{V}\mathrm{ar}\left(\widehat{Z}_k\right) = \frac{\mu_k^2}{L}$, $\mathbb{E}\left(\widehat{Z}_k\right) = \alpha_k$, $\mathbb{V}\mathrm{ar}\left(Z_k\right) = \frac{\alpha_k^2}{L}$ and $\mathbb{E}\left(\widetilde{Z}_k\right) = \psi_k$. Substituting (B.12) in ρ_k and using the statistical parameters, we get $\rho_k = \frac{\mu_k}{\alpha_k}$.

B.3 Proof of Theorem 3.1

In terms of Z_k and $\widehat{Z}_k$, (3.24) can be re-written as

$$(1-P_o) = \Pr\left(Z_1 \leq \eta \max_{1\leq k\leq K}\{\widehat{Z}_k\}, \ldots, Z_K \leq \eta \max_{1\leq k\leq K}\{\widehat{Z}_k\}\right), \tag{B.14}$$

where $Z_k \triangleq \sum_{l=1}^{L}|V_{lk}|^2$, $\widehat{Z}_k = \sum_{l=1}^{L}|\widehat{V}_{lk}|^2$, $V_{lk} \sim \mathcal{CN}\left(0, \frac{\alpha_k}{L}\right)$ and $\widehat{V}_{lk} \sim \mathcal{CN}\left(0, \frac{\mu_k}{L}\right)$.

Furthermore, both Z_k and $\widehat{Z}_k$ are correlated chi-square distributed RVs and their joint pdf is given by [98, (3.14)]

$$f_{Z_k,\widehat{Z}_k}(z_k,\widehat{z}_k) = \frac{(L)^{L+1}(z_k\widehat{z}_k)^{\frac{L-1}{2}} I_{L-1}\left(\frac{2L\sqrt{\rho_k z_k \widehat{z}_k}}{\sqrt{\alpha_k\mu_k}(1-\rho_k)}\right)}{\Gamma(L)(\alpha_k\mu_k)^{\frac{L+1}{2}}(1-\rho_k)\rho_k^{\frac{L-1}{2}}} \exp\left(\frac{-1}{1-\rho_k}\left(\frac{Lz_k}{\alpha_k}+\frac{L\widehat{z}_k}{\mu_k}\right)\right), \tag{B.15}$$

where $\rho_k = \frac{\mu_k}{\alpha_k}$ as shown in Appendix B.2 and $I_{L-1}(\cdot)$ is modified Bessel function of first kind and order $(L-1)$ [72, (9.6.19)].

Using Boole-Fréchet inequality [99, (17)], a lower bound on $(1-P_o)$ is given by

$$\begin{aligned}(1-P_o) &\geq \max\left(0, \sum_{i=1}^{K}\Pr\left(Z_i \leq \eta \max_{1\leq k\leq K}\{\widehat{Z}_k\}\right) - K + 1\right), \\ &= \max\left(0, 1 - \sum_{i=1}^{K}\Pr\left(\widehat{Z}_1 \leq \frac{Z_i}{\eta}, \ldots, \widehat{Z}_K \leq \frac{Z_i}{\eta}\right)\right).\end{aligned} \tag{B.16}$$

Let us define $P_i \triangleq \Pr\left(\widehat{Z}_1 \leq \frac{Z_i}{\eta}, \ldots, \widehat{Z}_K \leq \frac{Z_i}{\eta}\right)$, then P_i can be expressed as

$$\begin{aligned}P_i &= \prod_{j=1}^{K}\Pr\left(\widehat{Z}_j \leq \frac{z_i}{\eta}\right), \\ &= \int_{z_i=0}^{\infty}\int_{\widehat{z}_i=0}^{z_i/\eta}\prod_{j\neq i}^{K}\Pr\left(\widehat{Z}_j \leq \frac{z_i}{\eta}\right) f_{Z_i,\widehat{Z}_i}(z_i,\widehat{z}_i)\, d\widehat{z}_i dz_i.\end{aligned} \tag{B.17}$$

Using (B.2),

$$\Pr\left(\widehat{Z}_j \leq \frac{z_i}{\eta}\right) = \int_0^{\frac{z_i}{\eta}} \frac{L}{\mu_j}\frac{1}{\Gamma(L)}\left(\frac{L}{\mu_j}\widehat{z}_j\right)^{L-1} e^{-\frac{L\widehat{z}_j}{\mu_j}} d\widehat{z}_j = \frac{\gamma\left(L, \frac{Lz_i}{\eta\mu_j}\right)}{\Gamma(L)}. \tag{B.18}$$

Substituting (B.18) in (B.17), we obtain

$$P_i = \int_{z_i=0}^{\infty}\int_{\widehat{z}_i=0}^{z_i/\eta}\prod_{j\neq i}^{K}\frac{\gamma\left(L, \frac{Lz_i}{\eta\mu_j}\right)}{\Gamma(L)} f_{Z_i,\widehat{Z}_i}(z_i,\widehat{z}_i)\, d\widehat{z}_i dz_i. \tag{B.19}$$

Based on (B.19), we note that

$$(1-P_o) \geq \max\left(0, 1-\sum_{i=1}^{K}\int_{z_i=0}^{\infty}\prod_{j\neq i}^{K}\frac{\gamma\left(L,\frac{Lz_i}{\eta\mu_j}\right)}{\Gamma(L)}\left(f_{Z_i}(z_i)-\int_{\widehat{z}_i=z_i/\eta}^{\infty} f_{Z_i,\widehat{Z}_i}(z_i,\widehat{z}_i)\,d\widehat{z}_i\right)\right)dz_i. \tag{B.20}$$

Substituting the joint pdf of Z_k and $\widehat{Z}_k$ from (B.15) and simplifying using the identity [54, (4.59)] related to generalized Marcum-Q function, (B.20) can be re-written as

$$(1-P_o) \geq \max\left(0, 1-\sum_{i=1}^{K}\int_{z_i=0}^{\infty}\prod_{j\neq i}^{K}\frac{\gamma\left(L,\frac{Lz_i}{\eta\mu_j}\right)f_{Z_i}(z_i)}{\Gamma(L)} \times\left(1-Q_L\left(\sqrt{\frac{2L\rho_i z_i}{\alpha_i(1-\rho_i)}},\sqrt{\frac{2Lz_i}{\eta\mu_i(1-\rho_i)}}\right)\right)dz_i\right). \tag{B.21}$$

Simplifying (B.21) further using Gauss-Laguerre integration [72, (25.4.45)], we get (3.26).

B.4 Proof of Theorem 3.2

To simplify the SINR expression in (3.28), we compute variance of each of the terms in (3.27). The variance of term ① equals

$$\mathbb{V}\text{ar}\,(\text{term}①) = \left|\sum_{m=1}^{M}\sqrt{\eta_{mk}}\mathbb{E}\|\widehat{\boldsymbol{h}}_{mk}^{p}\|^2\right|^2\mathbb{E}|q_k|^2 = \left(\sum_{m=1}^{M}\sqrt{\eta_{mk}}Q_p\zeta_{mk}^{p}\right)^2. \tag{B.22}$$

The variance of the second term is given by

$$\begin{aligned}\mathbb{V}\text{ar}\,(\text{term}②) &= \mathbb{E}\left|\sum_{m=1}^{M}\sqrt{\eta_{mk}}\|\widehat{\boldsymbol{h}}_{mk}^{p}\|^2\right|^2 - \left|\sum_{m=1}^{M}\sqrt{\eta_{mk}}\mathbb{E}\|\widehat{\boldsymbol{h}}_{mk}^{p}\|^2\right|^2,\\ &= \sum_{m=1}^{M}\eta_{mk}\mathbb{E}\|\widehat{\boldsymbol{h}}_{mk}^{p}\|^4 + \sum_{m=1}^{M}\sum_{n\neq m}^{M}\sqrt{\eta_{mk}\eta_{nk}}{Q_p}^2\zeta_{mk}^{p}\zeta_{nk}^{p} - \left|\sum_{m=1}^{M}\sqrt{\eta_{mk}}Q_p\zeta_{mk}^{p}\right|^2,\\ &= \sum_{m=1}^{M}\eta_{mk}Q_p\left(\zeta_{mk}^{p}\right)^2,\end{aligned} \tag{B.23}$$

where we have applied the result that $\mathbb{E}\|\widehat{\boldsymbol{h}}_{mk}^{p}\|^4 = \left(Q_p+Q_p^2\right)\left(\zeta_{mk}^{p}\right)^2$.

To evaluate the variance of the third term, we note that $\widetilde{\boldsymbol{h}}_{mk}^{p}$ and $\widehat{\boldsymbol{h}}_{mk}^{p}$ are uncorrelated random

vectors and use this fact to simplify further as follows :

$$\begin{aligned}\mathbb{V}\text{ar}\,(\text{term}③) &= \mathbb{E}\left|\sum_{m=1}^{M}\sqrt{\eta_{mk}}\widetilde{\boldsymbol{h}}_{mk}^{p\mathrm{T}}\widehat{\boldsymbol{h}}_{mk}^{p*}\right|^2 = \sum_{m=1}^{M}\eta_{mk}\mathbb{E}\left|\widetilde{\boldsymbol{h}}_{mk}^{p\mathrm{T}}\widehat{\boldsymbol{h}}_{mk}^{p*}\right|^2 \\ &\quad+\sum_{m=1}^{M}\sum_{n\neq m}^{M}\sqrt{\eta_{mk}\eta_{nk}}\mathbb{E}\left(\left(\widetilde{\boldsymbol{h}}_{mk}^{p\mathrm{T}}\widehat{\boldsymbol{h}}_{mk}^{p*}\right)^{\mathrm{H}}\left(\widetilde{\boldsymbol{h}}_{nk}^{p\mathrm{T}}\widehat{\boldsymbol{h}}_{nk}^{p*}\right)\right), \\ &=\sum_{m=1}^{M}\eta_{mk}\mathbb{E}\left(\widehat{\boldsymbol{h}}_{mk}^{p\mathrm{T}}\mathbb{E}\left(\widetilde{\boldsymbol{h}}_{mk}^{p*}\widetilde{\boldsymbol{h}}_{mk}^{p\mathrm{T}}\right)\widehat{\boldsymbol{h}}_{mk}^{p*}\right), \\ &=\sum_{m=1}^{M}\eta_{mk}\mathbb{E}\left(\widehat{\boldsymbol{h}}_{mk}^{p\mathrm{T}}\left(\beta_{mk}^{p}-\zeta_{mk}^{p}\right)\widehat{\boldsymbol{h}}_{mk}^{p*}\right), \\ &=\sum_{m=1}^{M}\eta_{mk}Q_p\left(\zeta_{mk}^{p}\beta_{mk}^{p}-\left(\zeta_{mk}^{p}\right)^2\right). \end{aligned} \tag{B.24}$$

The fourth term denotes the co-channel interference caused by PAPs and to evaluate its variance, we exploit the fact that $\boldsymbol{h}_{mk}^{p}$ and $\widehat{\boldsymbol{h}}_{mk'}^{p}$ are independent of each other and the fact that $\mathbb{E}\,(q_k q_{k'}) = 0$, for $k \neq k^{'}$. Thus,

$$\begin{aligned}\mathbb{V}\text{ar}\,(\text{term}④) &= \sum_{k'\neq k}^{K}\mathbb{E}\left|\sum_{m=1}^{M}\sqrt{\eta_{mk'}}\boldsymbol{h}_{mk}^{p\mathrm{T}}\widehat{\boldsymbol{h}}_{mk'}^{p*}\right|^2, \\ &=\sum_{k'\neq k}^{K}\left(\sum_{m=1}^{M}\eta_{mk'}\mathbb{E}\left|\boldsymbol{h}_{mk}^{p\mathrm{T}}\widehat{\boldsymbol{h}}_{mk'}^{p*}\right|^2\right. \\ &\quad\left.+\sum_{m=1}^{M}\sum_{n\neq m}^{M}\sqrt{\eta_{mk'}\eta_{nk'}}\mathbb{E}\left(\left(\boldsymbol{h}_{mk}^{p\mathrm{T}}\widehat{\boldsymbol{h}}_{mk'}^{p*}\right)^{\mathrm{H}}\left(\boldsymbol{h}_{nk}^{p\mathrm{T}}\widehat{\boldsymbol{h}}_{nk'}^{p*}\right)\right)\right), \\ &=\sum_{k'\neq k}^{K}\sum_{m=1}^{M}\eta_{mk'}\mathbb{E}\left(\widehat{\boldsymbol{h}}_{mk'}^{p\mathrm{T}}\mathbb{E}\left(\boldsymbol{h}_{mk}^{p*}\boldsymbol{h}_{mk}^{p\mathrm{T}}\right)\widehat{\boldsymbol{h}}_{mk'}^{p*}\right), \\ &=\sum_{k'\neq k}^{K}\sum_{m=1}^{M}\eta_{mk'}Q_p\zeta_{mk'}^{p}\beta_{mk}^{p}. \end{aligned} \tag{B.25}$$

The variance of the fifth term captures the power of the interference generated by the SAPs. To compute this, we use the fact that $\mathbb{E}\,(s_l s_{l'}) = 0$ for $l \neq l^{'}$ and approximate $\|\widehat{\boldsymbol{h}}_{nl}^{s}\|^2$ with $\mathbb{E}\|\widehat{\boldsymbol{h}}_{nl}^{s}\|^2$. This is justified because the channel from SAP to any UAV is Rician in nature and has a strong LoS component [17], [100], [60]. Therefore,

$$\mathbb{V}\text{ar}\,(\text{term}⑤) = \sum_{l=1}^{L}\mathbb{E}\left|\sum_{n=1}^{N}\sqrt{\frac{P_d^s}{L}}\frac{\boldsymbol{g}_{nk}^{s\mathrm{T}}\widehat{\boldsymbol{h}}_{nl}^{s*}}{\|\widehat{\boldsymbol{h}}_{nl}^{s}\|}\right|^2,$$

$$
\begin{aligned}
&\approx \sum_{l=1}^{L}\sum_{n=1}^{N} \frac{\mathbb{E}\left(P_d^s\right)}{L} \frac{\mathbb{E}\left|\boldsymbol{g}_{nk}^{s\mathrm{T}}\,\widehat{\boldsymbol{h}}_{nl}^{s*}\right|^2}{\mathbb{E}\|\widehat{\boldsymbol{h}}_{nl}^{s}\|^2}, \\
&\approx \sum_{l=1}^{L}\sum_{n=1}^{N} \frac{\mathbb{E}\left(P_d^s\right)}{L} \frac{\mathbb{E}\left(\widehat{\boldsymbol{h}}_{nl}^{s\mathrm{T}}\mathbb{E}\left(\boldsymbol{g}_{nk}^{s*}\boldsymbol{g}_{nk}^{s\mathrm{T}}\right)\widehat{\boldsymbol{h}}_{nl}^{s*}\right)}{\mathbb{E}\|\widehat{\boldsymbol{h}}_{nl}^{s}\|^2}, \\
&\approx \sum_{l=1}^{L}\sum_{n=1}^{N} \frac{\mathbb{E}\left(P_d^s\right)}{L} \frac{\mathbb{E}\left(\widehat{\boldsymbol{h}}_{nl}^{s\mathrm{T}}\beta_{nk}^{s}\widehat{\boldsymbol{h}}_{nl}^{s*}\right)}{\mathbb{E}\|\widehat{\boldsymbol{h}}_{nl}^{s}\|^2}, \\
&= \sum_{l=1}^{L}\sum_{n=1}^{N} \frac{\mathbb{E}\left(P_d^s\right)}{L}\beta_{nk}^{s} = \sum_{n=1}^{N} \xi\beta_{nk}^{s},
\end{aligned} \tag{B.26}
$$

where ξ is given in Proposition 3.1 in (3.21).

And the variance of noise equals $\mathbb{E}\,|n_k|^2 = \sigma_w^2$.

B.5 Proof of Theorem 3.3

In order to simplify the SINR expression in (3.32), we evaluate the variance of every term in (3.31). The variance of the first term is given by

$$
\begin{aligned}
\mathrm{DS}_l \triangleq \mathbb{V}\mathrm{ar}\,(\mathrm{term}①) &= \left|\sum_{n=1}^{N} \frac{\mathbb{E}\left(\sqrt{P_d^s}\|\widehat{\boldsymbol{h}}_{nl}^{s}\|\right)}{\sqrt{L}}\right|^2 \mathbb{E}|s_l|^2, \\
&= \left|\sum_{n=1}^{N} \frac{\mathbb{E}\left(\sqrt{P_d^s}\right)\mathbb{E}\|\widehat{\boldsymbol{h}}_{nl}^{s}\|}{\sqrt{L}}\right|^2 = \left|\sum_{n=1}^{N} \frac{\lambda\delta_{nl}^{s}}{\sqrt{L}}\right|^2,
\end{aligned} \tag{B.27}
$$

where $\lambda = \mathbb{E}\left(\sqrt{P_d^s}\right)$ is given in Corollary 3.1 and $\delta_{nl}^{s} = \mathbb{E}\|\widehat{\boldsymbol{h}}_{nl}^{s}\|$ for PLoS$\neq$ 1 and $\delta_{nl}^{s} = \sqrt{Q_s\beta_{nl}^{s}}$ for PLoS=1. It can be shown that the rv $U = \|\widehat{\boldsymbol{h}}_{nl}^{s}\|$ is non-central chi distributed rv and its pdf is obtained as [97]

$$
f_U(u) = \frac{2u^{Q_s}}{\zeta_{nl}^{s}\|\bar{\boldsymbol{h}}_{nl}^{s}\|^{Q_s-1}} \exp\left(-\frac{\|\bar{\boldsymbol{h}}_{nl}^{s}\|^2 + u^2}{\zeta_{nl}^{s}}\right) \mathrm{I}_{Q_s-1}\left(\frac{2\|\bar{\boldsymbol{h}}_{nl}^{s}\|u}{\zeta_{nl}^{s}}\right). \tag{B.28}
$$

Using (B.28), the statistical mean of U denoted by δ_{nl}^{s} can be expressed as

$$
\delta_{nl}^{s} = \int_0^{\infty} \frac{2u^{Q_s+1}}{\zeta_{nl}^{s}\|\bar{\boldsymbol{h}}_{nl}^{s}\|^{Q_s-1}} \exp\left(-\frac{\|\bar{\boldsymbol{h}}_{nl}^{s}\|^2 + u^2}{\zeta_{nl}^{s}}\right) \mathrm{I}_{Q_s-1}\left(\frac{2\|\bar{\boldsymbol{h}}_{nl}^{s}\|u}{\zeta_{nl}^{s}}\right) du. \tag{B.29}
$$

The variance of the second term arising due to beamforming uncertainity equals

$$\begin{aligned}
\mathrm{BU}_l &\triangleq \mathbb{V}\mathrm{ar}\left(\text{term}\textcircled{2}\right), \\
&= \mathbb{E}\left|\sum_{n=1}^{N}\left(\frac{\sqrt{P_d^s}\|\widehat{\boldsymbol{h}}_{nl}^s\|}{\sqrt{L}} - \frac{\mathbb{E}\left(\sqrt{P_d^s}\|\widehat{\boldsymbol{h}}_{nl}^s\|\right)}{\sqrt{L}}\right)\right|^2, \\
&= \sum_{n=1}^{N}\mathbb{E}\left|\left(\frac{\sqrt{P_d^s}\|\widehat{\boldsymbol{h}}_{nl}^s\|}{\sqrt{L}} - \frac{\mathbb{E}\left(\sqrt{P_d^s}\|\widehat{\boldsymbol{h}}_{nl}^s\|\right)}{\sqrt{L}}\right)\right|^2, \\
&\approx \sum_{n=1}^{N}\left(\frac{\mathbb{E}\left(P_d^s\right)\mathbb{E}\|\widehat{\boldsymbol{h}}_{nl}^s\|^2}{L} - \frac{\left(\mathbb{E}\left(\sqrt{P_d^s}\right)\mathbb{E}\|\widehat{\boldsymbol{h}}_{nl}^s\|\right)^2}{L}\right), \\
&= \sum_{n=1}^{N}\left(\frac{\xi Q_s\left(\zeta_{nl}^s + \frac{\beta_{nl}^s K_{nl}^s}{K_{nl}^s+1}\right)}{L} - \frac{\left(\lambda\delta_{nl}^s\right)^2}{L}\right).
\end{aligned} \tag{B.30}$$

In order to compute the variance of the third term arising due to channel estimation error, we approximate $\|\widehat{\boldsymbol{h}}_{nl}^s\|^2$ with $\mathbb{E}\|\widehat{\boldsymbol{h}}_{nl}^s\|^2$, since the channel from SAP to UAV is Rician in nature and has a strong LoS component [17], [60], [100]. Thus,

$$\begin{aligned}
\mathrm{CEE}_l &\triangleq \mathbb{V}\mathrm{ar}\left(\text{term}\textcircled{3}\right), \\
&= \mathbb{E}\left|\sum_{n=1}^{N}\frac{\sqrt{P_d^s}\,\widetilde{\boldsymbol{h}}_{nl}^{s\mathrm{T}}\widehat{\boldsymbol{h}}_{nl}^{s*}}{\sqrt{L}\|\widehat{\boldsymbol{h}}_{nl}^s\|}\right|^2, \\
&\approx \sum_{n=1}^{N}\frac{\mathbb{E}\left(P_d^s\right)}{L}\mathbb{E}\left|\frac{\widetilde{\boldsymbol{h}}_{nl}^{s\mathrm{T}}\widehat{\boldsymbol{h}}_{nl}^{s*}}{\sqrt{\mathbb{E}\|\widehat{\boldsymbol{h}}_{nl}^s\|^2}}\right|^2, \\
&= \sum_{n=1}^{N}\frac{\mathbb{E}\left(P_d^s\right)}{L}\frac{\mathbb{E}\left(\widehat{\boldsymbol{h}}_{nl}^{s\mathrm{T}}\,\mathbb{E}\left(\widetilde{\boldsymbol{h}}_{nl}^{s*}\widetilde{\boldsymbol{h}}_{nl}^{s\mathrm{T}}\right)\widehat{\boldsymbol{h}}_{nl}^{s*}\right)}{\mathbb{E}\|\widehat{\boldsymbol{h}}_{nl}^s\|^2}, \\
&= \sum_{n=1}^{N}\frac{\mathbb{E}\left(P_d^s\right)}{L}\left(\frac{\beta_{nl}^s}{K_{nl}^s+1} - \zeta_{nl}^s\right).
\end{aligned} \tag{B.31}$$

The variance of the fourth term (ISAP_l) captures the power in the co-channel interference caused by SAPs. Again to simplify this, we note that $\boldsymbol{h}_{nl}^s$ and $\widehat{\boldsymbol{h}}_{nl'}^s$ are mutually independent of

each other, $\mathbb{E}\left(s_l s_{l'}\right) = 0$ for $l \neq l^{'}$ and approximate $\|\widehat{\boldsymbol{h}}^{s}_{nl'}\|^2$ with $\mathbb{E}\|\widehat{\boldsymbol{h}}^{s}_{nl'}\|^2$. Then,

$$\begin{aligned}\mathbb{V}\text{ar}\left(\text{term}④\right) &= \sum_{l' \neq l}^{L} \mathbb{E}\left|\sum_{n=1}^{N} \frac{\sqrt{P^s_d}\boldsymbol{h}^{s\mathrm{T}}_{nl}\widehat{\boldsymbol{h}}^{s*}_{nl'}}{\sqrt{L}\|\widehat{\boldsymbol{h}}^{s}_{nl'}\|}\right|^2, \\ &\approx \sum_{l' \neq l}^{L} \frac{\mathbb{E}\left(P^s_d\right)}{L}\left[\sum_{n=1}^{N}\mathbb{E}\left|\frac{\boldsymbol{h}^{s\mathrm{T}}_{nl}\widehat{\boldsymbol{h}}^{s*}_{nl'}}{\sqrt{\mathbb{E}\|\widehat{\boldsymbol{h}}^{s}_{nl'}\|^2}}\right|^2 + \sum_{n=1}^{N}\sum_{m\neq n}^{N}\mathbb{E}\left(\frac{\left(\boldsymbol{h}^{s\mathrm{T}}_{nl}\widehat{\boldsymbol{h}}^{s*}_{nl'}\right)^{\mathrm{H}}\left(\boldsymbol{h}^{s\mathrm{T}}_{ml}\widehat{\boldsymbol{h}}^{s*}_{ml'}\right)}{\sqrt{\mathbb{E}\|\widehat{\boldsymbol{h}}^{s}_{nl'}\|^2\,\mathbb{E}\|\widehat{\boldsymbol{h}}^{s}_{ml'}\|^2}}\right)\right]. \end{aligned} \tag{B.32}$$

The variance of the fifth term denotes the power of the interference from the PAPs. We again exploit the facts that $\boldsymbol{g}^{p}_{ml}$ and $\widehat{\boldsymbol{h}}^{p}_{mk}$ are independent of each other and $\mathbb{E}\left(q_k q_{k'}\right) = 0$, for $k \neq k^{'}$. Thus,

$$\begin{aligned}\text{IPAP}_l \triangleq \mathbb{V}\text{ar}\left(\text{term}⑤\right) &= \sum_{k=1}^{K}\sum_{m=1}^{M}\eta_{mk}\mathbb{E}\left(\widehat{\boldsymbol{h}}^{p\mathrm{T}}_{mk}\beta^{p}_{ml}\mathbf{I}_{Q_p}\widehat{\boldsymbol{h}}^{p*}_{mk}\right), \\ &= \sum_{k=1}^{K}\sum_{m=1}^{M}\eta_{mk}\; Q_p\; \zeta^{p}_{mk}\,\beta^{p}_{ml}. \end{aligned} \tag{B.33}$$

C Appendix

C.1 Proof of Lemma 4.1

As $Z_m \triangleq \sum_{l=1}^{L} \|\boldsymbol{g}_{ml}^{p}\|^2$, its mean

$$\mu_m = \mathbb{E}(Z_m) = \sum_{l=1}^{L} Q_p \beta_{ml}^{p}, \tag{C.1}$$

and variance $\sigma_m^2 = \mathrm{Var}(Z_m) = \sum_{l=1}^{L} Q_p \left(\beta_{ml}^{p}\right)^2$. The shape and scale parameters of Z_m are then given by $\alpha_m = \left(\frac{\mu_m}{\sigma_m}\right)^2$ and $\beta_m = \frac{\sigma_m^2}{\mu_m}$.

C.2 Proof of Lemma 4.2

The quantized version of the interference channel estimate between m^{th} PAP and l^{th} SU is

$$Q(\widehat{\boldsymbol{g}}_{ml}^{p}) = \dot{a}\widehat{\boldsymbol{g}}_{ml}^{p} + \boldsymbol{e}_{ml}^{\widehat{g}^p}, \tag{C.2}$$

then $Q([\widehat{\boldsymbol{g}}_{ml}^{p}]_i) = \dot{a}[\widehat{\boldsymbol{g}}_{ml}^{p}]_i + [\boldsymbol{e}_{ml}^{\widehat{g}^p}]_i$ for $1 \le i \le Q_p$. Furthermore,

$$\|Q(\widehat{\boldsymbol{g}}_{ml}^{p})\|^2 = |Q([\widehat{\boldsymbol{g}}_{ml}^{p}]_1)|^2 + |Q([\widehat{\boldsymbol{g}}_{ml}^{p}]_2)|^2 + \cdots + |Q([\widehat{\boldsymbol{g}}_{ml}^{p}]_{Q_p})|^2, \tag{C.3}$$

where

$$|Q([\widehat{\boldsymbol{g}}_{ml}^{p}]_i)|^2 = \left(\dot{a}\,\mathrm{Re}\{[\widehat{\boldsymbol{g}}_{ml}^{p}]_i\} + \mathrm{Re}\{[\boldsymbol{e}^{\widehat{g^p}}_{ml}]_i\}\right)^2 + \left(\dot{a}\,\mathrm{Img}\{[\widehat{\boldsymbol{g}}_{ml}^{p}]_i\} + \mathrm{Img}\{[\boldsymbol{e}^{\widehat{g^p}}_{ml}]_i\}\right)^2. \tag{C.4}$$

Let us assume that $X = \mathrm{Re}\{[\widehat{\boldsymbol{g}}_{ml}^{p}]_i\}$, then it can be shown that $\mathbb{E}(X) = 0$, $\mathbb{E}(X^2) = \frac{\beta_{ml}^{p}}{2}$, $\mathbb{E}(X^3) = 0$ and $\mathbb{E}(X^4) = \frac{3(\beta_{ml}^{p})^2}{4}$. Similarly, let us assume that $Y = \mathrm{Re}\{[\boldsymbol{e}^{\widehat{g^p}}_{ml}]_i\}$, then $\mathbb{E}(Y) = 0$, $\mathbb{E}(Y^2) = \frac{\sigma_e^2\beta_{ml}^{p}}{2}$, $\mathbb{E}(Y^3) = 0$ and $\mathbb{E}(Y^4) = \frac{9\sigma_e^4(\beta_{ml}^{p})^2}{20}$. The mean of $\widehat{Z}_m^q$ is then given by

$$\begin{aligned}\mathbb{E}\left(\widehat{Z}_m^q\right) &= \mathbb{E}\left(\sum_{l=1}^{L}\|Q\left(\widehat{\boldsymbol{g}}_{ml}^{p}\right)\|^2\right) = \mathbb{E}\left(\sum_{l=1}^{L}\left(\sum_{i=1}^{Q_p}\left|Q\left([\widehat{\boldsymbol{g}}_{ml}^{p}]_i\right)\right|^2\right)\right),\\ &= \sum_{l=1}^{L}\left(\dot{a}^2 Q_p\beta_{ml}^{p} + \sigma_{\dot{e}}^2\beta_{ml}^{p}\right) = \sum_{l=1}^{L} Q_p\dot{b}\beta_{ml}^{p}.\end{aligned} \tag{C.5}$$

The variance of $\widehat{Z}_m^q$ is calculated as

$$\begin{aligned}\mathrm{Var}\left(\widehat{Z}_m^q\right) &= \mathbb{E}\left(\left(\widehat{Z}_m^q\right)^2\right) - \left(\mathbb{E}\left(\widehat{Z}_m^q\right)\right)^2,\\ &= \mathbb{E}\left(\left(\sum_{l=1}^{L}\left(\sum_{i=1}^{Q_p}\left|Q([\widehat{\boldsymbol{g}}_{ml}^{p}]_i)\right|^2\right)\right)^2\right) - \left(\sum_{l=1}^{L} Q_p\dot{b}\beta_{ml}^{p}\right)^2,\\ &= \sum_{l=1}^{L}\left(\sum_{i=1}^{Q_p}\mathbb{E}\left|Q([\widehat{\boldsymbol{g}}_{ml}^{p}]_i)\right|^4 + \sum_{i=1}^{Q_p}\sum_{j\neq i}^{Q_p}\mathbb{E}\left|Q([\widehat{\boldsymbol{g}}_{ml}^{p}]_i)\right|^2\,\mathbb{E}\left|Q([\widehat{\boldsymbol{g}}_{ml}^{p}]_j)\right|^2\right)\\ &\quad + \sum_{l=1}^{L}\sum_{l'\neq l}^{L}\left(\sum_{i=1}^{Q_p}\mathbb{E}\left|Q([\widehat{\boldsymbol{g}}_{ml}^{p}]_i)\right|^2\right)\left(\sum_{i=1}^{Q_p}\mathbb{E}\left|Q([\widehat{\boldsymbol{g}}_{ml'}^{p}]_i)\right|^2\right) - \left(\sum_{l=1}^{L} Q_p\dot{b}\beta_{ml}^{p}\right)^2,\\ &= \sum_{l=1}^{L}\left(\sum_{i=1}^{Q_p}\left(\frac{3\dot{a}^4}{2} + \frac{9\sigma_{\dot{e}}^4}{10} + \frac{6\dot{a}^2\sigma_{\dot{e}}^2}{2} + \frac{\dot{b}^2}{2}\right)(\beta_{ml}^{p})^2 + Q_p(Q_p-1)\dot{b}^2(\beta_{ml}^{p})^2\right)\\ &\quad + \sum_{l=1}^{L}\sum_{l'\neq l}^{L} Q_p^2\dot{b}^2\beta_{ml}^{p}\beta_{ml'}^{p} - \left(\sum_{l=1}^{L} Q_p\dot{b}\beta_{ml}^{p}\right)^2.\end{aligned} \tag{C.6}$$

The mean and the variance thus calculated can be used to compute shape and scale parameters as given in (4.14) and (4.15).

C.3 Proof of Proposition 4.1

From (4.12), we know that $\widehat{P}_{uq}^{s} = \frac{\bar{I}_p}{\eta\,\max\limits_{1\leq m\leq M}\{\widehat{Z}_m^q\}}$ where $\widehat{Z}_m^q = \sum_{l=1}^{L}\|\dot{a}\widehat{\boldsymbol{g}}_{ml}^{p} + \boldsymbol{e}^{\widehat{g^p}}_{ml}\|^2$.

We can re-write $\widehat{P}^s_{uq}$ as

$$\widehat{P}^s_{uq} = \frac{\bar{I}_p}{\eta} \min_{1\le m\le M} \left\{ \frac{1}{\widehat{Z}^q_m} \right\}. \tag{C.7}$$

Let $\widehat{Y}^q_m \triangleq \frac{1}{\widehat{Z}^q_m}$. Then, based on transformation of rvs and using the pdf of $\widehat{Z}^q_m$ from (4.13) in Lemma 4.2, we can express the pdf of $\widehat{Y}^q_m$ as

$$f_{\widehat{Y}^q_m}(\widehat{y}^q_m) = \left(\frac{1}{\widehat{\beta}^q_m}\right)^{\widehat{\alpha}^q_m} \frac{1}{\Gamma(\widehat{\alpha}^q_m)} \left(\frac{1}{\widehat{y}^q_m}\right)^{\widehat{\alpha}^q_m+1} e^{-\frac{1}{\widehat{y}^q_m \widehat{\beta}^q_m}}, \widehat{y}^q_m \ge 0. \tag{C.8}$$

We now define another rv $X = \min\limits_{1\le m\le M} \{\widehat{Y}^q_m\}$. Then its CDF can be computed as

$$\begin{aligned} F_X(x) &= \Pr(X \le x) = 1 - \Pr(X \ge x), \\ &= 1 - \Pr\left(\min_{1\le m\le M} \left\{ \widehat{Y}^q_m \right\} \ge x \right), \\ &= 1 - \Pr\left(\widehat{Y}^q_1 \ge x, \widehat{Y}^q_2 \ge x, \ldots, \widehat{Y}^q_M \ge x \right), \\ &\overset{(a)}{=} 1 - \prod_{m=1}^{M} \Pr\left(\widehat{Y}^q_m \ge x \right), \end{aligned} \tag{C.9}$$

where (a) holds since $\widehat{Y}^{q\,'}_m$s are independent across m. Using the pdf of $\widehat{Y}^q_m$ in (C.8),

$$P\left(\widehat{Y}^q_m \ge x\right) = \int_x^\infty \left(\frac{1}{\widehat{\beta}^q_m}\right)^{\widehat{\alpha}^q_m} \frac{1}{\Gamma(\widehat{\alpha}^q_m)} \left(\frac{1}{\widehat{y}^q_m}\right)^{\widehat{\alpha}^q_m+1} e^{-\frac{1}{\widehat{y}^q_m \widehat{\beta}^q_m}} d\widehat{y}^q_m. \tag{C.10}$$

To simplify (C.10), we substitute $\frac{1}{\widehat{y}^q_m \widehat{\beta}^q_m} = t$. Then, we obtain

$$P\left(\widehat{Y}^q_m \ge x\right) = \frac{\gamma\left(\widehat{\alpha}^q_m, \frac{1}{\widehat{\beta}^q_m x}\right)}{\Gamma(\widehat{\alpha}^q_m)}. \tag{C.11}$$

Thus, $F_X(x)$ in (C.9) can be re-written as

$$F_X(x) = 1 - \prod_{m=1}^{M} \frac{\gamma\left(\widehat{\alpha}^q_m, \frac{1}{\widehat{\beta}^q_m x}\right)}{\Gamma(\widehat{\alpha}^q_m)}. \tag{C.12}$$

To obtain the pdf of X, we take the derivative of $F_X(x)$ to obtain

$$f_X(x) = -\frac{d}{dx}\left(\prod_{m=1}^{M} \frac{\gamma\left(\widehat{\alpha}^q_m, \frac{1}{\widehat{\beta}^q_m x}\right)}{\Gamma(\widehat{\alpha}^q_m)} \right),$$

$$= \sum_{j=1}^{M} \left[\left(\frac{1}{\widehat{\beta}_j^q} \right)^{\widehat{\alpha}_j^q} \frac{e^{-\frac{1}{x\,\widehat{\beta}_j^q}}}{\Gamma(\widehat{\alpha}_j^q)} \left(\frac{1}{x} \right)^{\widehat{\alpha}_j^q+1} \prod_{i\neq j}^{M} \left(\frac{\gamma\left(\widehat{\alpha}_i^q, \frac{1}{\widehat{\beta}_i^q x}\right)}{\Gamma(\widehat{\alpha}_i^q)} \right) \right]. \tag{C.13}$$

We use Leibniz rule of integration [53] to obtain (C.13). Thus,

$$\begin{aligned} \mathbb{E}\left(\widehat{P}_{uq}^{s}\right) &= \frac{\bar{I}_p}{\eta}\mathbb{E}(X), \\ &= \int_0^{\infty} \frac{\bar{I}_p x}{\eta} \sum_{j=1}^{M} \left(\frac{1}{\widehat{\beta}_j^q} \right)^{\widehat{\alpha}_j^q} \frac{e^{-\frac{1}{x\,\widehat{\beta}_j^q}}}{\Gamma(\widehat{\alpha}_j^q)} \left(\frac{1}{x} \right)^{\widehat{\alpha}_j^q+1} \prod_{i\neq j}^{M} \left(\frac{\gamma\left(\widehat{\alpha}_i^q, \frac{1}{\widehat{\beta}_i^q x}\right)}{\Gamma(\widehat{\alpha}_i^q)} \right) dx. \end{aligned} \tag{C.14}$$

Based on Gauss-Laguerre integration [72, (25.4.29)], we further simplify (C.14) to obtain (4.17).

C.4 Proof of Proposition 4.2

We know that $Z_m = \sum_{l=1}^{L} \|\boldsymbol{g}_{ml}^p\|^2$ and using (4.3), Z_m can be expanded as

$$\begin{aligned} Z_m &= \sum_{l=1}^{L} \|s_p\, \widehat{\boldsymbol{g}}_{ml}^p + \sqrt{1-s_p^2}\, \widetilde{\boldsymbol{g}}_{ml}^p\|^2, \\ &= \sum_{l=1}^{L} \left(s_p \widehat{\boldsymbol{g}}_{ml}^p + \sqrt{1-s_p^2}\, \widetilde{\boldsymbol{g}}_{ml}^p \right)^{\mathrm{H}} \left(s_p \widehat{\boldsymbol{g}}_{ml}^p + \sqrt{1-s_p^2}\, \widetilde{\boldsymbol{g}}_{ml}^p \right), \\ &= s_p^2 \sum_{l=1}^{L} \|\widehat{\boldsymbol{g}}_{ml}^p\|^2 + s_p \sqrt{1-s_p^2} \left(\sum_{l=1}^{L} \widetilde{\boldsymbol{g}}_{ml}^{p\mathrm{H}}\, \widehat{\boldsymbol{g}}_{ml}^p + \sum_{l=1}^{L} \widehat{\boldsymbol{g}}_{ml}^{p\ \mathrm{H}} \widetilde{\boldsymbol{g}}_{ml}^p \right) \\ &\qquad + (1-s_p^2) \sum_{l=1}^{L} \|\widetilde{\boldsymbol{g}}_{ml}^p\|^2. \end{aligned} \tag{C.15}$$

Similarly, we use (4.4) to write $\widehat{Z}_m^q = \sum_{l=1}^{L} \|Q(\widehat{\boldsymbol{g}}_{ml}^p)\|^2$ in expanded form as

$$\begin{aligned} \widehat{Z}_m^q &= \sum_{l=1}^{L} \|\dot{a}\widehat{\boldsymbol{g}}_{ml}^p + \boldsymbol{e}_{ml}^{\widehat{g}^p}\|^2 = \sum_{l=1}^{L} \left(\dot{a}\widehat{\boldsymbol{g}}_{ml}^p + \boldsymbol{e}_{ml}^{\widehat{g}^p} \right)^{\mathrm{H}} \left(\dot{a}\widehat{\boldsymbol{g}}_{ml}^p + \boldsymbol{e}_{ml}^{\widehat{g}^p} \right), \\ &= \dot{a}^2 \sum_{l=1}^{L} \|\widehat{\boldsymbol{g}}_{ml}^p\|^2 + \dot{a} \sum_{l=1}^{L} \widehat{\boldsymbol{g}}_{ml}^{p\ \mathrm{H}} \boldsymbol{e}_{ml}^{\widehat{g}^p} + \dot{a} \sum_{l=1}^{L} \boldsymbol{e}_{ml}^{\widehat{g}^p\ \mathrm{H}} \widehat{\boldsymbol{g}}_{ml}^p + \sum_{l=1}^{L} \|\boldsymbol{e}_{ml}^{\widehat{g}^p}\|^2. \end{aligned} \tag{C.16}$$

The correlation coefficient of Z_m and $\widehat{Z}_m^q$ is given by

$$\rho_m = \frac{\mathbb{E}\left(Z_m \widehat{Z}_m^q\right) - \mathbb{E}\left(Z_m\right)\mathbb{E}(\widehat{Z}_m^q)}{\sqrt{\mathrm{Var}\left(Z_m\right)\mathrm{Var}\left(\widehat{Z}_m^q\right)}}. \tag{C.17}$$

In order to compute ρ_m in (C.17), we need to find $\mathbb{E}\left(Z_m \widehat{Z}_m^q\right)$.

We note that

$$\begin{aligned}
\mathbb{E}\left(Z_m \widehat{Z}_m^q\right) =& s_p^2 \dot{a}^2 \mathbb{E}\left(\sum_{l=1}^{L} \|\widehat{\boldsymbol{g}}_{ml}^p\|^2\right)^2 + s_p^2 \mathbb{E}\left(\sum_{l=1}^{L} \|\widehat{\boldsymbol{g}}_{ml}^p\|^2\right) \mathbb{E}\left(\sum_{l=1}^{L} \|\widehat{\boldsymbol{e}}_{ml}^{\widehat{g}^p}\|^2\right) \\
&+ \left(1 - s_p^2\right) \dot{a}^2 \mathbb{E}\left(\sum_{l=1}^{L} \|\widetilde{\boldsymbol{g}}_{ml}^p\|^2\right) \mathbb{E}\left(\sum_{l=1}^{L} \|\widehat{\boldsymbol{g}}_{ml}^p\|^2\right) \\
&+ \left(1 - s_p^2\right) \mathbb{E}\left(\sum_{l=1}^{L} \|\widetilde{\boldsymbol{g}}_{ml}^p\|^2\right) \mathbb{E}\left(\sum_{l=1}^{L} \|\widehat{\boldsymbol{e}}_{ml}^{\widehat{g}^p}\|^2\right), \\
=& s_p^2 \dot{a}^2 \left(\sum_{l=1}^{L} Q_p (Q_p + 1) (\beta_{ml}^p)^2 + \sum_{l=1}^{L} \sum_{l'=1}^{L} Q_p^2 \beta_{ml}^p \beta_{ml'}^p\right) \\
&+ s_p^2 \left(\sum_{l=1}^{L} Q_p \beta_{ml}^p\right) \left(\sum_{l=1}^{L} Q_p {\sigma_{\dot{e}}}^2 \beta_{ml}^p\right) + \left(1 - s_p^2\right) \dot{a}^2 \left(\sum_{l=1}^{L} Q_p \beta_{ml}^p\right)^2 \\
&+ \left(1 - s_p^2\right) \left(\sum_{l=1}^{L} Q_p \beta_{ml}^p\right) \left(\sum_{l=1}^{L} Q_p {\sigma_{\dot{e}}}^2 \beta_{ml}^p\right), \\
=& s_p^2 \dot{a}^2 \sum_{l=1}^{L} Q_p \left(\beta_{ml}^p\right)^2 + \dot{a}^2 \left(\sum_{l=1}^{L} Q_p \beta_{ml}^p\right) + {\sigma_{\dot{e}}}^2 \left(\sum_{l=1}^{L} Q_p \beta_{ml}^p\right)^2. \qquad \text{(C.18)}
\end{aligned}$$

We substitute $\mathbb{E}(Z_m)$ and $\mathrm{Var}(Z_m)$ from Lemma 4.1, $\mathbb{E}(\widehat{Z}_m^q)$ and $\mathrm{Var}(\widehat{Z}_m^q)$ from Lemma 4.2 and $\mathbb{E}\left(Z_m \widehat{Z}_m^q\right)$ from (C.18) in (C.17) to obtain ρ_m in (4.22).

C.5 Proof of Theorem 4.1

In terms of Z_m and $\widehat{Z}_m^q$, (4.20) can be re-written as

$$(1 - P_o) = \Pr\left(Z_1 \le \eta \max_{1 \le m \le M} \{\widehat{Z}_m^q\}, \cdots, Z_M \le \eta \max_{1 \le m \le M} \{\widehat{Z}_M^q\}\right), \qquad \text{(C.19)}$$

where $Z_m \triangleq \sum_{l=1}^{L} \|\boldsymbol{g}_{ml}^p\|^2$ and $\widehat{Z}_m^q \triangleq \sum_{l=1}^{L} \|Q(\widehat{\boldsymbol{g}}_{ml}^p)\|^2$.

Furthermore, the joint pdf of correlated Gamma rvs with same shape and distinct scale parameters is given by [94]

$$f_{XY}(x, y) = \frac{(xy)^{\frac{\mu-1}{2}} I_{\mu-1}\left(\frac{2\sqrt{\rho xy}}{\sqrt{\beta_x \beta_y}(1-\rho)}\right)}{\Gamma(\mu)(\beta_x \beta_y)^{\frac{\mu+1}{2}}(1-\rho)\rho^{\frac{\mu-1}{2}}} \exp\left(\frac{-1}{1-\rho}\left(\frac{x}{\beta_x} + \frac{y}{\beta_y}\right)\right), \qquad \text{(C.20)}$$

where X and Y are Gamma rvs with scale parameters β_x and β_y, and shape parameter μ.

In our case, Z_m and $\widehat{Z}_m^q$ are correlated Gamma rvs, with distinct shape and scale parameters. We approximate $\widehat{\alpha}_m^q \approx \alpha_m$ and assume that both the Gamma rvs have the same shape parameter α_m.[1] Thus, the joint pdf of Z_m and $\widehat{Z}_m^q$ can be approximated by

$$f_{Z_m,\widehat{Z}_m^q}(z_m,\widehat{z}_m^q) \approx \frac{(z_m\widehat{z}_m^q)^{\frac{\alpha_m-1}{2}} I_{\alpha_m-1}\left(\frac{2\sqrt{\rho_m z_m \widehat{z}_m^q}}{\sqrt{\beta_m\widehat{\beta}_m^q(1-\rho_m)}}\right)}{\Gamma(\alpha_m)(\beta_m\widehat{\beta}_m^q)^{\frac{\alpha_m+1}{2}}(1-\rho_m)\rho_m^{\frac{\alpha_m-1}{2}}} \exp\left(\frac{-1}{1-\rho_m}\left(\frac{z_m}{\beta_m}+\frac{\widehat{z}_m^q}{\widehat{\beta}_m^q}\right)\right), \tag{C.21}$$

where ρ_m is given in Proposition 4.2 and $I_{\alpha_m-1}(\cdot)$ is modified Bessel function of first kind and order (α_m-1) [72, (9.6.19)].

Using Boole-Fréchet inequality [99, (17)], a lower bound on $(1-P_o)$ is given by

$$\begin{aligned}(1-P_o) &\geq \max\left(0, \sum_{i=1}^{M}\Pr\left(Z_i \leq \eta \max_{1\leq m\leq M}\{\widehat{Z}_m^q\}\right) - M + 1\right),\\ &= \max\left(0, 1-\sum_{i=1}^{M}\Pr\left(Z_i \geq \eta \max_{1\leq m\leq M}\{\widehat{Z}_m^q\}\right)\right),\\ &= \max\left(0, 1-\sum_{i=1}^{M}\Pr\left(\widehat{Z}_1 \leq \frac{Z_i}{\eta},\ldots,\widehat{Z}_M \leq \frac{Z_i}{\eta}\right)\right).\end{aligned} \tag{C.22}$$

Let us define $P_i \triangleq \Pr\left(\widehat{Z}_1 \leq \frac{Z_i}{\eta},\ldots,\widehat{Z}_M \leq \frac{Z_i}{\eta}\right)$, then P_i can be expressed as

$$P_i = \prod_{j=1}^{M}\Pr\left(\widehat{Z}_j \leq \frac{z_i}{\eta}\right) = \int_{z_i=0}^{\infty}\int_{\widehat{z}_i=0}^{z_i/\eta}\prod_{j\neq i}^{M}\Pr\left(\widehat{Z}_j \leq \frac{z_i}{\eta}\right) f_{Z_i,\widehat{Z}_i}(z_i,\widehat{z}_i)\, d\widehat{z}_i\, dz_i. \tag{C.23}$$

Using (4.13),

$$\Pr\left(\widehat{Z}_j \leq \frac{z_i}{\eta}\right) = \int_0^{\frac{z_i}{\eta}} \frac{1}{\beta_j^q\Gamma(\widehat{\alpha}_j^q)}\left(\frac{\widehat{z}_j^q}{\beta_j^q}\right)^{\widehat{\alpha}_j^q-1} e^{-\frac{\widehat{z}_j^q}{\beta_j^q}} d\widehat{z}_j = \frac{\gamma\left(\widehat{\alpha}_j, \frac{z_i}{\eta\widehat{\beta}_j}\right)}{\Gamma(\widehat{\alpha}_j)}. \tag{C.24}$$

Substituting (C.24) in (C.23), we obtain

$$P_i = \int_{z_i=0}^{\infty}\int_{\widehat{z}_i=0}^{z_i/\eta}\prod_{j\neq i}^{M}\frac{\gamma\left(\widehat{\alpha}_j, \frac{z_i}{\eta\widehat{\beta}_j}\right)}{\Gamma(\widehat{\alpha}_j)} f_{Z_i,\widehat{Z}_i}(z_i,\widehat{z}_i)\, d\widehat{z}_i dz_i. \tag{C.25}$$

[1] This ensures analytical tractability. Our numerical simulations, further confirm that $\frac{\alpha_m}{\widehat{\alpha}_m^q} \approx 1$ and that this approximation is fairly tight.

Using (C.25), we note that

$$(1-P_o) \geq \max\left(0, 1-\sum_{i=1}^{M}\int_{z_i=0}^{\infty}\prod_{j\neq i}^{M}\frac{\gamma\left(\widehat{\alpha}_j, \frac{z_i}{\eta\widehat{\beta}_j}\right)}{\Gamma(\widehat{\alpha}_j)} \times\left(f_{Z_i}(z_i) - \int_{\widehat{z}_i=z_i/\eta}^{\infty} f_{Z_i,\widehat{Z}_i}(z_i,\widehat{z}_i)\, d\widehat{z}_i\right)\right) dz_i. \quad \text{(C.26)}$$

Using the joint pdf of Z_m and $\widehat{Z}_m^q$ from (C.21) and simplifying using [54, (4.59)], (C.26) can be re-written as

$$(1-P_o) \geq \max\left(0, 1-\sum_{i=1}^{M}\int_{z_i=0}^{\infty}\prod_{j\neq i}^{M}\frac{\gamma\left(\widehat{\alpha}_j, \frac{z_i}{\eta\widehat{\beta}_j}\right)}{\Gamma(\widehat{\alpha}_j)}\, f_{Z_i}(z_i)\left(1-Q_{\alpha_i}\left(\sqrt{\frac{2\rho_i z_i}{\beta_i(1-\rho_i)}}, \sqrt{\frac{2z_i}{\eta\widehat{\beta}_i(1-\rho_i)}}\right)\right) dz_i\right), \quad \text{(C.27)}$$

where $f_{Z_i}(z_i) = \frac{1}{\beta_i\Gamma(\alpha_i)}\left(\frac{z_i}{\beta_i}\right)^{\alpha_i-1} e^{-\frac{z_i}{\beta_i}}$.

Simplifying (C.27) further using Gauss-Laguerre integration [72, (25.4.45)], we get (4.23).

C.6 Proof of Theorem 4.2

To simplify (4.28), we compute the variance of every term in (4.27). Now

$$\begin{aligned}\mathbb{V}\text{ar}\,(\text{term}①) &= \left|\sum_{m=1}^{M}\dot{a}^2 s_r\sqrt{P_u^p}\mathbb{E}\|\widehat{\boldsymbol{h}}_{mk}^p\|^2\right|^2 \mathbb{E}|q_k|^2,\\ &= \left(\sum_{m=1}^{M}\dot{a}^2 s_r\sqrt{P_u^p}Q_p\beta_{mk}^p\right)^2. \end{aligned} \quad \text{(C.28)}$$

To compute variance of term②, we note that $\widetilde{\boldsymbol{h}}_{mk}^p$ and $\widehat{\boldsymbol{h}}_{mk}^p$ are uncorrelated RVs and use this to simplify further as:

$$\begin{aligned}\mathbb{V}\text{ar}\,(\text{term}②) &= \mathbb{E}\left|\sum_{m=1}^{M}\dot{a}^2\sqrt{1-{s_r}^2}\sqrt{P_u^p}\widehat{\boldsymbol{h}}_{mk}^{p\,\mathrm{H}}\widetilde{\boldsymbol{h}}_{mk}^p\right|^2,\\ &= (1-{s_r}^2)\dot{a}^4 P_u^p\mathbb{E}\left|\sum_{m=1}^{M}\widehat{\boldsymbol{h}}_{mk}^{p\,\mathrm{H}}\widetilde{\boldsymbol{h}}_{mk}^p\right|^2,\\ &= \left(1-{s_r}^2\right)\dot{a}^4\left[\sum_{m=1}^{M}P_u^p\mathbb{E}\left(\widetilde{\boldsymbol{h}}_{mk}^{p\mathrm{H}}\mathbb{E}\left(\widehat{\boldsymbol{h}}_{mk}^p\,\widehat{\boldsymbol{h}}_{mk}^{p\mathrm{H}}\right)\widetilde{\boldsymbol{h}}_{mk}^p\right)\right.\\ &\qquad \left.+\sum_{m=1}^{M}\sum_{n\neq m}^{M}P_u^p\mathbb{E}\left(\left(\widetilde{\boldsymbol{h}}_{mk}^{p\mathrm{H}}\,\widetilde{\boldsymbol{h}}_{mk}^p\right)^{\mathrm{H}}\left(\widetilde{\boldsymbol{h}}_{nk}^{p\mathrm{H}}\widetilde{\boldsymbol{h}}_{nk}^p\right)\right)\right],\\ &= \sum_{m=1}^{M}\left(1-{s_r}^2\right)\dot{a}^4 P_u^p\mathbb{E}\left(\widetilde{\boldsymbol{h}}_{mk}^{p\mathrm{H}}\mathbb{E}\left(\widehat{\boldsymbol{h}}_{mk}^p\widehat{\boldsymbol{h}}_{mk}^{p\mathrm{H}}\right)\widetilde{\boldsymbol{h}}_{mk}^p\right),\end{aligned}$$

$$= \sum_{m=1}^{M} \left(1 - {s_r}^2\right) \dot{a}^4 P_u^p Q_p \left(\beta_{mk}^p\right)^2. \tag{C.29}$$

Next

$$\begin{aligned}
\mathbb{V}\text{ar}\,(\text{term}③) &= \mathbb{E}\left|\sum_{m=1}^{M} \dot{a}^2 s_r \sqrt{P_u^p} \|\widehat{\boldsymbol{h}}_{mk}^p\|^2\right|^2 - \left|\sum_{m=1}^{M} \dot{a}^2 s_r \sqrt{P_u^p} \mathbb{E}\|\widehat{\boldsymbol{h}}_{mk}^p\|^2\right|^2, \\
&= \sum_{m=1}^{M} \dot{a}^4 s_r^2 P_u^p \mathbb{E}\|\widehat{\boldsymbol{h}}_{mk}^p\|^4 + \sum_{m=1}^{M}\sum_{n\neq m}^{M} \dot{a}^4 s_r^2 P_u^p {Q_p}^2 \beta_{mk}^p \beta_{nk}^p \\
&\qquad - \left|\sum_{m=1}^{M} \dot{a}^2 s_r \sqrt{P_u^p} Q_p \beta_{mk}^p\right|^2, \\
&= \sum_{m=1}^{M} \dot{a}^4 s_r^2 P_u^p Q_p \left(\beta_{mk}^p\right)^2,
\end{aligned} \tag{C.30}$$

where we use the result that $\mathbb{E}\|\widehat{\boldsymbol{h}}_{mk}^p\|^4 = \left(Q_p + Q_p^2\right)\left(\beta_{mk}^p\right)^2$.

The variance of term④ equals

$$\mathbb{V}\text{ar}\,(\text{term}④) = \sum_{m=1}^{M} \mathbb{E}\left|\dot{a}^2 \widehat{\boldsymbol{h}}_{mk}^{p\,\mathrm{H}} \boldsymbol{n}_m\right|^2 = \sum_{m=1}^{M} \dot{a}^4 Q_p \beta_{mk}^p \sigma_w^2. \tag{C.31}$$

And $\mathbb{E}\|\boldsymbol{n}_m\|^2 = Q_p \sigma_w^2$.

Variance of term⑤ represents interference power due to SUs and is given by

$$\begin{aligned}
\mathbb{V}\text{ar}\,(\text{term}⑤) &= \sum_{l=1}^{L} \mathbb{E}\left|\sum_{m=1}^{M} \dot{a}^2 \sqrt{\widehat{P}_{uq}^s}\, \widehat{\boldsymbol{h}}_{mk}^{p\mathrm{H}} \boldsymbol{g}_{ml}^p\right|^2, \\
&\approx \sum_{l=1}^{L} \mathbb{E}\left(\widehat{P}_{uq}^s\right) \dot{a}^4 \left(\sum_{m=1}^{M} \mathbb{E}\left|\widehat{\boldsymbol{h}}_{mk}^{p\mathrm{H}} \boldsymbol{g}_{ml}^p\right|^2 \right. \\
&\qquad \left. + \sum_{m=1}^{M}\sum_{n\neq m}^{M} \mathbb{E}\left(\left(\widehat{\boldsymbol{h}}_{mk}^{p\mathrm{H}} \boldsymbol{g}_{ml}^p\right)^{\mathrm{H}} \left(\widehat{\boldsymbol{h}}_{nk}^{p\mathrm{H}} \boldsymbol{g}_{nl}^p\right)\right)\right), \\
&= \sum_{l=1}^{L}\sum_{m=1}^{M} \xi \dot{a}^4 Q_p \beta_{ml}^p \beta_{mk}^p.
\end{aligned} \tag{C.32}$$

Futhermore,

$$\begin{aligned}
\mathbb{V}\text{ar}\,(\text{term}⑥) &= \sum_{k'\neq k}^{K} \dot{a}^4 P_u^p \mathbb{E}\left|\sum_{m=1}^{M} \widehat{\boldsymbol{h}}_{mk}^{p\,\mathrm{H}} \boldsymbol{h}_{mk'}^p\right|^2, \\
&= \sum_{k'\neq k}^{K} P_u^p \dot{a}^4 \left(\sum_{m=1}^{M} \mathbb{E}\left|\widehat{\boldsymbol{h}}_{mk}^{p\,\mathrm{H}} \boldsymbol{h}_{mk'}^p\right|^2 + \sum_{m=1}^{M}\sum_{n\neq m}^{M} \mathbb{E}\left(\left(\widehat{\boldsymbol{h}}_{mk}^{p\mathrm{H}} \boldsymbol{h}_{mk'}^p\right)^{\mathrm{H}} \left(\widehat{\boldsymbol{h}}_{nk}^{p\mathrm{H}} \boldsymbol{h}_{nk'}^p\right)\right)\right),
\end{aligned}$$

$$= \sum_{k' \neq k}^{K} \sum_{m=1}^{M} P_u^p \dot{a}^4 \mathbb{E}\left(\boldsymbol{h}_{mk'}^{p\,\mathrm{H}} \mathbb{E}\left(\widehat{\boldsymbol{h}}_{mk}^{p} \widehat{\boldsymbol{h}}_{mk}^{p\,\mathrm{H}} \right) \boldsymbol{h}_{mk'}^{p} \right),$$

$$= \sum_{k' \neq k}^{K} \sum_{m=1}^{M} P_u^p \dot{a}^4 Q_p \, \beta_{mk'}^p \beta_{mk}^p. \tag{C.33}$$

The variance of term⑦ represents the strength of error arising due to quantization of CSI and received signal and is given by

$$\begin{aligned}
\mathbb{V}\mathrm{ar}\,(\text{term⑦}) &= \mathbb{E}\left| \sum_{m=1}^{M} \left(\dot{a} \boldsymbol{e}_{mk}^{\widehat{h}^p\,\mathrm{H}} \boldsymbol{y}_m + \dot{a} \widehat{\boldsymbol{h}}_{mk}^{p\,\mathrm{H}} \boldsymbol{e}_m^{\widehat{y}} + \boldsymbol{e}_{mk}^{\widehat{h}^p\,\mathrm{H}} \boldsymbol{e}_m^{\widehat{y}} \right) \right|^2, \\
&= \mathbb{E}\left| \sum_{m=1}^{M} \dot{a} \boldsymbol{e}_{mk}^{\widehat{h}^p\,\mathrm{H}} \boldsymbol{y}_m \right|^2 + \mathbb{E}\left| \sum_{m=1}^{M} \dot{a} \widehat{\boldsymbol{h}}_{mk}^{p\,\mathrm{H}} \boldsymbol{e}_m^{\widehat{y}} \right|^2 + \mathbb{E}\left| \sum_{m=1}^{M} \boldsymbol{e}_{mk}^{\widehat{h}^p\,\mathrm{H}} \boldsymbol{e}_m^{\widehat{y}} \right|^2, \\
&= \sum_{m=1}^{M} \left(\mathbb{E}\left| \dot{a} \boldsymbol{e}_{mk}^{\widehat{h}^p\,\mathrm{H}} \boldsymbol{y}_m \right|^2 + \mathbb{E}\left| \dot{a} \widehat{\boldsymbol{h}}_{mk}^{p\,\mathrm{H}} \boldsymbol{e}_m^{\widehat{y}} \right|^2 + \mathbb{E}\left| \boldsymbol{e}_{mk}^{\widehat{h}^p\,\mathrm{H}} \boldsymbol{e}_m^{\widehat{y}} \right|^2 \right), \\
&= \sum_{m=1}^{M} \left(\dot{a}^2 \mathbb{E}\left(\boldsymbol{y}_m^{\mathrm{H}} \mathbb{E}\left(\boldsymbol{e}_{mk}^{\widehat{h}^p} \boldsymbol{e}_{mk}^{\widehat{h}^p\,\mathrm{H}} \right) \boldsymbol{y}_m \right) + \dot{a}^2 \mathbb{E}\left(\boldsymbol{e}_m^{\widehat{y}\,\mathrm{H}} \mathbb{E}\left(\widehat{\boldsymbol{h}}_{mk}^{p} \widehat{\boldsymbol{h}}_{mk}^{p\,\mathrm{H}} \right) \boldsymbol{e}_m^{\widehat{y}} \right) + \mathbb{E}\left(\boldsymbol{e}_m^{\widehat{y}\,\mathrm{H}} \mathbb{E}\left(\boldsymbol{e}_{mk}^{\widehat{h}^p} \boldsymbol{e}_{mk}^{\widehat{h}^p\,\mathrm{H}} \right) \boldsymbol{e}_m^{\widehat{y}} \right) \right), \\
&\approx \left(2\dot{a}^2 \sigma_{\dot{e}}^2 + \sigma_{\dot{e}}^4 \right) \sum_{m=1}^{M} \left(\sum_{k'=1}^{K} P_u^p Q_p \, \beta_{mk'}^p \, \beta_{mk}^p + \sum_{l=1}^{L} \xi Q_p \, \beta_{ml}^p \beta_{mk}^p + Q_p \, \beta_{mk}^p \sigma_w^2 \right).
\end{aligned} \tag{C.34}$$

C.7 Proof of Theorem 4.3

To simplify (4.36), we compute the variance of every term in (4.35). Now

$$\begin{aligned}
\mathbb{V}\mathrm{ar}\,(\text{term①}) &= \left| \sum_{n=1}^{N} \dot{a}^2 s_s \mathbb{E}\left(\sqrt{\widehat{P}_{uq}^s} \| \widehat{\boldsymbol{h}}_{nl}^s \|^2 \right) \right|^2 \mathbb{E}|s_l|^2, \\
&= \left(\sum_{n=1}^{N} \dot{a}^2 s_s \lambda Q_s \, \beta_{nl}^s \right)^2.
\end{aligned} \tag{C.35}$$

Since $\widetilde{\boldsymbol{h}}_{nl}^s$ and $\widehat{\boldsymbol{h}}_{nl}^s$ are uncorrelated RVs

$$\begin{aligned}
\mathbb{V}\mathrm{ar}\,(\text{term②}) &= \mathbb{E}\left| \sum_{n=1}^{N} \dot{a}^2 \sqrt{(1 - s_s{}^2) \widehat{P}_{uq}^s} \widehat{\boldsymbol{h}}_{nl}^{s\mathrm{H}} \widetilde{\boldsymbol{h}}_{nl}^s \right|^2, \\
&= \sum_{n=1}^{N} \dot{a}^4 \left(1 - s_s{}^2 \right) \mathbb{E}(\widehat{P}_{uq}^s) \mathbb{E}\left| \widehat{\boldsymbol{h}}_{nl}^{s\mathrm{H}} \widetilde{\boldsymbol{h}}_{nl}^s \right|^2, \\
&= \sum_{n=1}^{N} \dot{a}^4 \left(1 - s_s{}^2 \right) \xi Q_s \, (\beta_{nl}^s)^2.
\end{aligned} \tag{C.36}$$

The term③ variance is given by

$$\begin{aligned}
\mathbb{V}\text{ar}\,(\text{term}③) &= \mathbb{E}\left|\sum_{n=1}^{N} \dot{a}^2 s_s \left(\sqrt{\widehat{P}^s_{uq}}\|\widehat{\boldsymbol{h}}^s_{nl}\|^2 - \mathbb{E}\left(\sqrt{\widehat{P}^s_{uq}}\|\widehat{\boldsymbol{h}}^s_{nl}\|^2 \right)\right)\right|^2, \\
&= \sum_{n=1}^{N} \mathbb{E}\left[\dot{a}^4 s_s^2 \left(\sqrt{\widehat{P}^s_{uq}}\|\widehat{\boldsymbol{h}}^s_{nl}\|^2 - \mathbb{E}\left(\sqrt{\widehat{P}^s_{uq}} \right)\mathbb{E}\|\widehat{\boldsymbol{h}}^s_{nl}\|^2 \right)^2 \right], \\
&\approx \sum_{n=1}^{N} \dot{a}^4 {s_s}^2 \left[\mathbb{E}(\widehat{P}^s_{uq})\mathbb{E}\|\widehat{\boldsymbol{h}}^s_{nl}\|^4 - \left(\mathbb{E}\left(\sqrt{\widehat{P}^s_{uq}} \right)\mathbb{E}\|\widehat{\boldsymbol{h}}^s_{nl}\|^2 \right)^2 \right], \\
&= \sum_{n=1}^{N} \dot{a}^4 {s_s}^2 \left[\xi\left(Q_s + Q_s^2\right)(\beta^s_{nl})^2 - \lambda^2 \left(Q_s \beta^s_{nl}\right)^2 \right]. \qquad \text{(C.37)}
\end{aligned}$$

The term④ variance is

$$\begin{aligned}
\mathbb{V}\text{ar}\,(\text{term}④) &= \mathbb{E}\left|\sum_{n=1}^{N} \dot{a}^2\, \widehat{\boldsymbol{h}}^{s\mathrm{H}}_{nl}\boldsymbol{n}_n\right|^2 = \sum_{n=1}^{N} \dot{a}^4 \mathbb{E}\left(\boldsymbol{n}_n^{\mathrm{H}} \mathbb{E}\left(\widehat{\boldsymbol{h}}^s_{nl}\widehat{\boldsymbol{h}}^{s\mathrm{H}}_{nl} \right)\boldsymbol{n}_n \right), \\
&= \sum_{n=1}^{N} Q_s \dot{a}^4 \beta^s_{nl}\sigma_w^2. \qquad \text{(C.38)}
\end{aligned}$$

The term⑤ variance computation uses the fact that $\boldsymbol{h}^s_{nl'}$ and $\widehat{\boldsymbol{h}}^s_{nl}$ are independent of each other and also that $\mathbb{E}\,(s_l s_{l'}) = 0$, for $l \neq l'$. Thus,

$$\begin{aligned}
\mathbb{V}\text{ar}\,(\text{term}⑤) &= \sum_{l'\neq l}^{L} \mathbb{E}\left|\sum_{n=1}^{N} \dot{a}^2 \sqrt{\widehat{P}^s_{uq}}\, \widehat{\boldsymbol{h}}^{s\mathrm{H}}_{nl}\boldsymbol{h}^s_{nl'}\right|^2, \\
&\approx \sum_{l'\neq l}^{L} \mathbb{E}\left(\widehat{P}^s_{uq}\right)\dot{a}^4 \mathbb{E}\left|\widehat{\boldsymbol{h}}^{s\mathrm{H}}_{nl}\boldsymbol{h}^s_{nl'}\right|^2, \\
&= \sum_{l'\neq l}^{L}\sum_{n=1}^{N} \mathbb{E}\left(\widehat{P}^s_{uq}\right)\dot{a}^4 \mathbb{E}\left(\boldsymbol{h}^{s\mathrm{H}}_{nl'} \mathbb{E}\left(\widehat{\boldsymbol{h}}^s_{nl}\widehat{\boldsymbol{h}}^{s\mathrm{H}}_{nl} \right)\boldsymbol{h}^s_{nl'} \right), \\
&= \sum_{l'\neq l}^{L}\sum_{n=1}^{N} \xi \dot{a}^4 Q_s\, \beta^s_{nl'}\beta^s_{nl}. \qquad \text{(C.39)}
\end{aligned}$$

Furthermore,

$$\begin{aligned}
\mathbb{V}\text{ar}\,(\text{term}⑥) &= \sum_{k=1}^{K} \mathbb{E}\left|\sum_{n=1}^{N} \sqrt{P^p_u}\, \widehat{\boldsymbol{h}}^{s\mathrm{H}}_{nl}\boldsymbol{g}^s_{nk}\right|^2, \\
&= \sum_{k=1}^{K}\sum_{n=1}^{N} P^p_u \mathbb{E}\left(\boldsymbol{g}^{s\mathrm{H}}_{nk}\, \mathbb{E}\left(\widehat{\boldsymbol{h}}^s_{nl}\widehat{\boldsymbol{h}}^{s\mathrm{H}}_{nl} \right)\boldsymbol{g}^s_{nk} \right),
\end{aligned}$$

$$= \sum_{k=1}^{K} \sum_{n=1}^{N} P_u^p Q_s \beta_{nl}^s \beta_{nk}^s. \tag{C.40}$$

And the variance of term⑦ is given by

$$\begin{aligned}
\mathbb{V}\text{ar}\,(\text{term⑦}) &= \mathbb{E}\left| \sum_{n=1}^{N} \left(\dot{a} \boldsymbol{e}_{nl}^{\widehat{h}^s \mathrm{H}} \boldsymbol{y}_n + \dot{a} \widehat{\boldsymbol{h}}_{nl}^{s\mathrm{H}} \boldsymbol{e}_n^{\widehat{y}} + \boldsymbol{e}_{nl}^{\widehat{h}^s \mathrm{H}} \boldsymbol{e}_n^{\widehat{y}} \right) \right|^2, \\
&= \mathbb{E}\left| \sum_{m=1}^{M} \dot{a} \boldsymbol{e}_{nl}^{\widehat{h}^s \mathrm{H}} \boldsymbol{y}_n \right|^2 + \mathbb{E}\left| \sum_{n=1}^{N} \dot{a} \widehat{\boldsymbol{h}}_{nl}^{s\mathrm{H}} \boldsymbol{e}_n^{\widehat{y}} \right|^2 + \mathbb{E}\left| \sum_{n=1}^{N} \boldsymbol{e}_{nl}^{\widehat{h}^s \mathrm{H}} \boldsymbol{e}_n^{\widehat{y}} \right|^2, \\
&= \sum_{n=1}^{N} \left(\mathbb{E}\left| \dot{a} \boldsymbol{e}_{nl}^{\widehat{h}^s \mathrm{H}} \boldsymbol{y}_n \right|^2 + \mathbb{E}\left| \dot{a} \widehat{\boldsymbol{h}}_{nl}^{s\mathrm{H}} \boldsymbol{e}_n^{\widehat{y}} \right|^2 + \mathbb{E}\left| \boldsymbol{e}_{nl}^{\widehat{h}^s \mathrm{H}} \boldsymbol{e}_n^{\widehat{y}} \right|^2 \right), \\
&\approx \left(2\dot{a}^2 \sigma_{\dot{e}}^2 + \sigma_{\dot{e}}^4 \right) \sum_{n=1}^{N} \left(\sum_{l'=1}^{L} \xi Q_s \beta_{nl'}^s \beta_{nl}^s + \sum_{k=1}^{K} P_u^p Q_s \beta_{nl}^s \beta_{nk}^s + Q_p \beta_{nl}^s \sigma_w^2 \right).
\end{aligned} \tag{C.41}$$

Bibliography

[1] "*Cisco Annual Internet Report (2018–2023) White Paper*," Ericsson, Stockholm, Sweden, Mar. 2020.

[2] FCC, "Amendment of the Commission's Rules with Regard to Commercial Operations in the 3550-3650 MHz band," *FCC-15-47*, 2015.

[3] ——, "Amendment of the Commission's Rules with Regard to Commercial Operations in the 3.7-24 GHz band," *FCC-18-147*, 2018.

[4] R. Sarvendranath and N. B. Mehta, "Exploiting power adaptation with transmit antenna selection for interference-outage constrained underlay spectrum sharing," *IEEE Trans. Commun.*, vol. 68, no. 1, pp. 480–492, Jan. 2020.

[5] FCC, "Unlicensed use of the 6 GHz band; expanding flexible use in mid-band spectrum between 3.7 and 24 GHz," *FCC-20-51*, 2020.

[6] A. Goldsmith, S. A. Jafar, I. Maric, and S. Srinivasa, "Breaking spectrum gridlock with cognitive radios: An information theoretic perspective," *Proc. IEEE*, vol. 97, no. 5, pp. 894–914, May 2009.

[7] D. L. Galappaththige and G. A. A. Baduge, "Exploiting underlay spectrum sharing in cell-free massive MIMO systems," *IEEE Trans. Commun.*, vol. 69, no. 11, pp. 7470–7488, Nov. 2021.

[8] N. N. Krishnan, R. Kumbhkar, N. B. Mandayam, I. Seskar, and S. Kompella, "Coexistence of radar and communication systems in CBRS bands through downlink power control," in *Proc. IEEE Military Commun. Conf.*, Oct. 2017, pp. 713–718.

[9] E. G. Larsson, F. Tufvesson, O. Edfors, and T. L. Marzetta, "Massive MIMO for next generation wireless systems," *IEEE Commun. Mag.*, vol. 52, no. 2, pp. 186–195, Feb. 2014.

[10] E. Björnson, E. G. Larsson, and T. L. Marzetta, "Massive MIMO: ten myths and one critical question," *IEEE Commun. Mag.*, vol. 54, no. 2, pp. 114–123, Feb. 2016.

[11] G. Geraci, A. G.-Rodriguez, D. L.-Perez, A. Bonfante, G. Giordano, and H. Claussen, "Operating massive MIMO in unlicensed bands for enhanced coexistence and spatial reuse," *IEEE J. Sel. Areas Commun.*, vol. 35, no. 6, pp. 1282–1293, Jun. 2017.

[12] E. Björnson and L. Sanguinetti, "Cell-free versus cellular massive MIMO: what processing is needed for cell-free to win?" in *Proc. SPAWC*, 2019, pp. 1–5.

[13] M. Giordani, M. Polese, M. Mezzavilla, S. Rangan, and M. Zorzi, "Toward 6G networks: Use cases and technologies," *IEEE Commun. Mag.*, vol. 58, no. 3, pp. 55–61, Mar. 2020.

[14] H. Q. Ngo, A. Ashikhmin, H. Yang, E. G. Larsson, and T. L. Marzetta, "Cell-free massive MIMO versus small cells," *IEEE Trans. Wireless Commun.*, vol. 16, no. 3, pp. 1834–1850, Jan. 2017.

[15] S. Elhoushy, M. Ibrahim, and W. Hamouda, "Cell-free massive MIMO: A survey," *IEEE Commun. Surveys Tuts.*, vol. 24, no. 1, pp. 492–523, Oct. 2022.

[16] E. V. Pothan and S. Kashyap, "Cell-free massive MIMO enabled wireless communication with UAVs in underlay spectrum access networks," *IEEE Trans. Commun.*, vol. 71, no. 12, pp. 7363–7377, Aug. 2023.

[17] Ö. Demir, E. Björnson, and L. Sanguinetti, *Foundations of User-Centric Cell-Free Massive MIMO*. Boston, MA, USA: Now Publishers, 2021.

[18] R. Sarvendranath and N. B. Mehta, "Transmit antenna selection for interference-outage constrained underlay CR," *IEEE Trans. Commun.*, vol. 66, no. 9, pp. 3772–3783, Sep. 2018.

[19] S. Kashyap and N. B. Mehta, "SEP-optimal transmit power policy for peak power and interference outage probability constrained underlay cognitive radios," *IEEE Trans. Wireless Commun.*, vol. 12, no. 12, pp. 6371–6381, Dec. 2013.

[20] P. Das, N. B. Mehta, and P. N. Arya, "Cognitive relay selection with incomplete channel state information of interference links," in *Proc. IEEE Int. Conf. Commun.*, May 2017, pp. 1–6.

[21] M. Vu, N. Devroye, and V. Tarokh, "On the primary exclusive region of cognitive networks," *IEEE Trans. Wireless Commun.*, vol. 8, no. 7, pp. 3380–3385, Jul. 2009.

[22] D. P. Bertsekas and J. N. Tsitsiklis, *Introduction to Probability*, 2nd ed. Athena Scientific, 2008.

[23] " Study on Enhanced LTE Support for Aerial Vehicles," 3rd Generation Partnership Project (3GPP), Technical Specification (TS) 36.777, May 2017.

[24] D. L. Galappaththige and G. Amarasuriya, "Cell-free massive MIMO with underlay spectrum-sharing," in *Proc. IEEE Int. Conf. Commun.*, May 2019, pp. 1–7.

[25] Z. H. Shaik, R. Sarvendranath, and E. G. Larsson, "Energy-efficient power allocation for an underlay spectrum sharing radioweaves network," in *Proc. IEEE Int. Conf. Commun.*, May 2022, pp. 799–804.

[26] A. A. Khuwaja, Y. Chen, N. Zhao, M.-S. Alouini, and P. Dobbins, "A survey of channel modeling for UAV communications," *IEEE Commun. Surveys Tuts.*, vol. 20, no. 4, pp. 2804–2821, Jul. 2018.

[27] B. Li, Z. Fei, and Y. Zhang, "UAV communications for 5G and beyond: Recent advances and future trends," *IEEE. Internet Things J.*, vol. 6, no. 2, pp. 2241–2263, Apr. 2019.

[28] Q. Wu, J. Xu, Y. Zeng, D. W. K. Ng, N. Al-Dhahir, R. Schober, and A. L. Swindlehurst, "A comprehensive overview on 5G-and-beyond networks with UAVs: From communications to sensing and intelligence," *IEEE J. Sel. Areas Commun.*, vol. 39, no. 10, pp. 2912–2945, Oct. 2021.

[29] M. Bashar, K. Cumanan, A. G. Burr, H. Q. Ngo, M. Debbah, and P. Xiao, "Max–min rate of cell-free massive MIMO uplink with optimal uniform quantization," *IEEE Trans. Commun.*, vol. 67, no. 10, pp. 6796–6815, Jul. 2019.

[30] S. Chaudhari and D. Cabric, "Downlink transceiver beamforming and admission control for massive MIMO cognitive radio networks," in *Proc. Asilomar Conf. on Signals, Syst., and Comput.*, Nov. 2015, pp. 1257–1261.

[31] L. Wang, H. Q. Ngo, M. Elkashlan, T. Q. Duong, and K.-K. Wong, "Massive MIMO in spectrum sharing networks: Achievable rate and power efficiency," *IEEE Syst. J.*, vol. 11, no. 1, pp. 20–31, Mar. 2017.

[32] H. Al-Hraishawi and G. A. A. Baduge, "Wireless energy harvesting in cognitive massive MIMO systems with underlay spectrum sharing," *IEEE Commun. Lett.*, vol. 6, no. 1, pp. 134–137, Feb. 2017.

[33] M. Cui, B. J. Hu, X. Li, H. Chen, S. Hu, and Y. Wang, "Energy-efficient power control algorithms in massive MIMO cognitive radio networks," *IEEE Access*, vol. 5, pp. 1164–1177, Jan. 2017.

[34] G. Amarasuriya and Y. Li, "Cognitive massive MIMO relay networks," in *Proc. IEEE Wireless Commun. Netw. Conf. (WCNC)*, Mar. 2017, pp. 1–6.

[35] M. Cui, B.-J. Hu, J. Tang, and Y. Wang, "Energy-efficient joint power allocation in uplink massive MIMO cognitive radio networks with imperfect CSI," *IEEE Access*, vol. 5, pp. 27 611–27 621, Nov. 2017.

[36] S. Kusaladharma and C. Tellambura, "Massive MIMO based underlay networks with power control," in *Proc. IEEE Int. Conf. Commun.*, May 2016, pp. 1–6.

[37] A. G.-Rodriguez and C. Masouros, "Exploiting the tolerance of massive MIMO to incomplete CSI for low-complexity transmission," in *Proc. IEEE Glob. Commun. Conf.*, Dec. 2015, pp. 1–6.

[38] S. Silva, M. Ardakani, and C. Tellambura, "Relay selection for cognitive massive MIMO two-way relay networks," in *Proc. IEEE Wireless Commun. Netw. Conf. (WCNC)*, Mar. 2017, pp. 1–6.

[39] R. Gupta, S. Kashyap, and E. V. Pothan, "Interference violation probability constrained underlay cognitive massive MIMO network under imperfect channel knowledge," in *Proc. IEEE Nat. Conf. Commun.*, Feb. 2019, pp. 1–6.

[40] Y. Li, D. Kudathanthirige, and G. A. A. Baduge, "Massive MIMO relay networks with underlay spectrum sharing," *IEEE Trans. Cognitive Commun. Netw.*, vol. 4, no. 4, pp. 677–691, Dec. 2018.

[41] H. Al-Hraishawi, G. A. Aruma Baduge, H. Q. Ngo, and E. G. Larsson, "Multi-cell massive MIMO uplink with underlay spectrum sharing," *IEEE Trans. Cognitive Commun. Netw.*, vol. 5, no. 1, pp. 119–137, Mar. 2019.

[42] S. Kusaladharma and C. Tellambura, "Secondary user interference characterization for spatially random underlay networks with massive MIMO and power control," *IEEE Trans. Veh. Technol.*, vol. 66, no. 9, pp. 7897–7912, Sep. 2017.

[43] K. Hosseini, W. Yu, and R. S. Adve, "Large-scale MIMO versus network MIMO for multicell interference mitigation," *IEEE J. Sel. Topics Signal Process.*, vol. 8, no. 5, pp. 930–941, May 2014.

[44] S. Chaudhari and D. Cabric, "QoS aware power allocation and user selection in massive MIMO underlay cognitive radio networks," *IEEE Trans. Cognitive Commun. Netw.*, vol. 4, no. 2, pp. 220–231, Jun. 2018.

[45] Z. Shi, X. Xie, and H. Lu, "Deep reinforcement learning based intelligent user selection in massive MIMO underlay cognitive radios," *IEEE Access*, vol. 7, pp. 110 884–110 894, Jul. 2019.

[46] W. Hao, O. Muta, H. Gacanin, and H. Furukawa, "Power allocation for massive MIMO cognitive radio networks with pilot sharing under SINR requirements of primary users," *IEEE Trans. Veh. Technol.*, vol. 67, no. 2, pp. 1174–1186, Feb. 2018.

[47] H. Zhang, J. Feng, Z. Shi, S. Ma, and G. Yang, "Rate maximization of wireless powered cognitive massive MIMO systems," *IEEE. Internet Things J.*, vol. 8, no. 7, pp. 5632–5644, Apr. 2021.

[48] H. Q. Ngo, E. G. Larsson, and T. L. Marzetta, "Energy and spectral efficiency of very large multiuser MIMO systems," *IEEE Trans. Commun.*, vol. 61, no. 4, pp. 1436–1449, Feb. 2013.

[49] B. Nosrat-Makouei, J. G. Andrews, and R. W. Heath, "MIMO interference alignment over correlated channels with imperfect CSI," *IEEE Trans. Signal Process.*, vol. 59, no. 6, pp. 2783–2794, Jun. 2011.

[50] C. Wang, E. K. Au, R. D. Murch, W. H. Mow, R. S. Cheng, and V. Lau, "On the performance of the MIMO zero-forcing receiver in the presence of channel estimation error," *IEEE Trans. Wireless Commun.*, vol. 6, no. 3, pp. 805–810, Mar. 2007.

[51] L. Musavian, M. R. Nakhai, M. Dohler, and A. H. Aghvami, "Effect of channel uncertainty on the mutual information of MIMO fading channels," *IEEE Trans. Veh. Technol.*, vol. 56, no. 5, pp. 2798–2806, Sep. 2007.

[52] G. Caire, N. Jindal, M. Kobayashi, and N. Ravindran, "Multiuser MIMO achievable rates with downlink training and channel state feedback," *IEEE Trans. Inf. Theory*, vol. 56, no. 6, pp. 2845–2866, Jun. 2010.

[53] I. S. Gradshteyn and I. M. Ryzhik, *Tables of Integrals, Series and Products*. Academic Press, 2000.

[54] M. Simon and M.-S. Alouini, *Digital Communication over Fading Channels*, 2nd ed. Wiley-Interscience, 2005.

[55] T. L. Marzetta, E. G. Larsson, H. Yang, and H. Q. Ngo, *Fundamentals of Massive MIMO*. Cambridge, U.K.:Cambridge Univ. Press, 2016.

[56] A. Papoulis and S. Pillai, *Probability, Random Variables, and Stochastic Processes*, ser. McGraw-Hill electrical and electronic engineering series. McGraw-Hill, 2002.

[57] E. Björnson, D. Hammarwall, and B. Ottersten, "Exploiting quantized channel norm feedback through conditional statistics in arbitrarily correlated MIMO systems," *IEEE Trans. Signal Process.*, vol. 57, no. 10, pp. 4027–4041, Jun. 2009.

[58] E. Björnson, E. Jorswieck, and B. Ottersten, "Impact of spatial correlation and precoding design in OSTBC MIMO systems," *IEEE Trans. Wireless Commun.*, vol. 9, no. 11, pp. 3578–3589, Oct. 2010.

[59] L. Zhang, G. Zhao, W. Zhou, L. Li, G. Wu, Y. Liang, and S. Li, "Primary channel gain estimation for spectrum sharing in cognitive radio networks," *IEEE Trans. Commun.*, vol. 65, no. 10, pp. 4152–4162, 2017.

[60] E. Björnson, J. Hoydis, and L. Sanguinetti, *Massive MIMO Networks: Spectral, Energy, and Hardware Efficiency*. Boston, MA, USA: Now Publishers, 2017, vol. 11.

[61] X. Lin, V. Yajnanarayana, S. D. Muruganathan, S. Gao, H. Asplund, H.-L. Maattanen, M. Bergstrom, S. Euler, and Y.-P. E. Wang, "The sky is not the limit: LTE for unmanned aerial vehicles," *IEEE Commun. Mag.*, vol. 56, no. 4, pp. 204–210, Apr. 2018.

[62] C. D'Andrea, A. Garcia-Rodriguez, G. Geraci, L. G. Giordano, and S. Buzzi, "Analysis of UAV communications in cell-free massive MIMO systems," *IEEE. Open J. Commun. Soc.*, vol. 1, pp. 133–147, Jan. 2020.

[63] "*Drones and networks: Ensuring safe and secure operations*," Ericsson, Stockholm, Sweden, Nov. 2018.

[64] S. Silva, M. Ardakani, and C. Tellambura, "Interference suppression and energy efficiency improvement with massive MIMO and relay selection in cognitive two-way relay networks," vol. 4, no. 2, pp. 326–339, Jan. 2020.

[65] F. Rezaei, A. R. Heidarpour, C. Tellambura, and A. Tadaion, "Underlaid spectrum sharing for cell-free massive MIMO-NOMA," *IEEE Commun. Lett.*, vol. 24, no. 4, pp. 907–911, Jan. 2020.

[66] E. V. Pothan and S. Kashyap, "Massive MIMO based underlay spectrum access under incomplete and/or imperfect channel state information," *IEEE Trans. Cognitive Commun. Netw.*, vol. 8, no. 3, pp. 1482–1496, Sep. 2022.

[67] Y. Li and G. A. Aruma Baduge, "Underlay spectrum-sharing massive MIMO NOMA," *IEEE Commun. Lett.*, vol. 23, no. 1, pp. 116–119, Jan. 2019.

[68] S. M. Kay, *Fundamentals of Statistical Signal Processing: Estimation Theory*, 1st ed. Prentice Hall Signal Processing Series, 1993, vol. 1.

[69] W. Wang, G. Yu, and A. Huang, "Cognitive radio enhanced interference coordination for femtocell networks," *IEEE Commun. Mag.*, vol. 51, no. 6, pp. 37–43, Jun. 2013.

[70] F. A. Khan, C. Masouros, and T. Ratnarajah, "Interference-driven linear precoding in multiuser MISO downlink cognitive radio network," *IEEE Trans. Veh. Technol.*, vol. 61, no. 6, pp. 2531–2543, May 2012.

[71] J.-H. Noh and S.-J. Oh, "Beamforming in a multi-user cognitive radio system with partial channel state information," *IEEE Trans. Wireless Commun.*, vol. 12, no. 2, pp. 616–625, Jan. 2013.

[72] M. Abramowitz and I. A. Stegun, *Handbook of Mathematical Functions with Formulas, Graphs, and Mathematical Tables*, 9th ed. Dover, 1972.

[73] M. Ataeeshojai, R. C. Elliott, W. A. Krzymien, C. Tellambura, and I. Maljevic, "Symbiotic backscatter communication underlying a cell-free massive MIMO system," *IEEE. Internet Things J.*, vol. 10, no. 19, pp. 16 758–16 777, Apr. 2023.

[74] C. D.Andrea and E. G. Larsson, "Improving cell-free massive MIMO by local per-bit soft detection," *IEEE Commun. Lett.*, vol. 25, no. 7, pp. 2400–2404, Jul. 2021.

[75] X. Yu, Q. Li, M. Xie, and H. Shi, "Performance of uplink multicell multiuser massive SM-MIMO systems with imperfect CSI and pilot contamination," *IEEE Syst. J.*, vol. 15, no. 3, pp. 3573–3584, Jul. 2021.

[76] H. Song, T. Goldstein, X. You, C. Zhang, O. Tirkkonen, and C. Studer, "Joint channel estimation and data detection in cell-free massive MU-MIMO systems," *IEEE Trans. Wireless Commun.*, vol. 21, no. 6, pp. 4068–4084, Jun. 2022.

[77] J. Craig, "A new, simple and exact result for calculating the probability of error for two-dimensional signal constellations," in *Proc. IEEE Military Commun. Conf.*, vol. 2, Nov. 1991, pp. 571–575.

[78] A. J. Goldsmith, *Wireless Communications*, 2nd ed. Cambridge Univ. Press, 2005.

[79] A. Kumar, V. Tentu, D. N. Amudala, and R. Budhiraja, "WSEE optimization of cell-free mMIMO uplink using deep deterministic policy gradient," *IEEE Commun. Lett.*, vol. 27, no. 1, pp. 219–223, Jan. 2023.

[80] M. Bashar, K. Cumanan, A. G. Burr, H. Q. Ngo, E. G. Larsson, and P. Xiao, "Energy efficiency of the cell-free massive MIMO uplink with optimal uniform quantization," *IEEE Trans. Green Commun. Netw.*, vol. 3, no. 4, pp. 971–987, Dec. 2019.

[81] M. Bashar, A. Akbari, K. Cumanan, H. Q. Ngo, A. G. Burr, P. Xiao, M. Debbah, and J. Kittler, "Exploiting deep learning in limited-fronthaul cell-free massive MIMO uplink," *IEEE J. Sel. Areas Commun.*, vol. 38, no. 8, pp. 1678–1697, Aug. 2020.

[82] H. Masoumi and M. J. Emadi, "Performance analysis of cell-free massive MIMO system with limited fronthaul capacity and hardware impairments," *IEEE Trans. Wireless Commun.*, vol. 19, no. 2, pp. 1038–1053, Feb. 2020.

[83] M. Bashar, P. Xiao, R. Tafazolli, K. Cumanan, A. G. Burr, and E. Björnson, "Limited-fronthaul cell-free massive MIMO with local MMSE receiver under rician fading and phase shifts," *IEEE Commun. Lett.*, vol. 10, no. 9, pp. 1934–1938, Sep. 2021.

[84] S. Datta, D. N. Amudala, E. Sharma, R. Budhiraja, and S. S. Panwar, "Full-duplex cell-free massive MIMO systems: Analysis and decentralized optimization," *IEEE. Open J. Commun. Soc.*, vol. 3, pp. 31–50, Dec. 2022.

[85] M. Bashar, H. Q. Ngo, K. Cumanan, A. G. Burr, P. Xiao, E. Björnson, and E. G. Larsson, "Uplink spectral and energy efficiency of cell-free massive MIMO with optimal uniform quantization," *IEEE Trans. Commun.*, vol. 69, no. 1, pp. 223–245, Jan. 2021.

[86] P. Zillmann, "Relationship between two distortion measures for memoryless nonlinear systems," *IEEE Signal Process. Lett.*, vol. 17, no. 11, pp. 917–920, Nov. 2010.

[87] E. Björnson and L. Sanguinetti, "Scalable cell-free massive MIMO systems," *IEEE Trans. Commun.*, vol. 68, no. 7, pp. 4247–4261, Jul. 2020.

[88] B. Widrow, "A study of rough amplitude quantization by means of nyquist sampling theory," *IRE Trans. Circuit Theory.*, vol. 3, no. 4, pp. 266–276, Dec. 1956.

[89] T. L. Marzetta, E. G. Larsson, H. Yang, and H. Q. Ngo, *Fundamentals of Massive MIMO*, Cambridge University Press, 2016.

[90] Z. Wang, J. Zhang, E. Björnson, and B. Ai, "Uplink performance of cell-free massive MIMO over spatially correlated rician fading channels," *IEEE Commun. Lett.*, vol. 25, no. 4, pp. 1348–1352, 2021.

[91] N. T. Nguyen, V.-D. Nguyen, H. V. Nguyen, H. Q. Ngo, S. Chatzinotas, and M. Juntti, "Spectral efficiency analysis of hybrid relay-reflecting intelligent surface-assisted cell-free massive MIMO systems," *IEEE Trans. Wireless Commun.*, vol. 22, no. 5, pp. 3397–3416, May 2023.

[92] C. Kumar, S. Kashyap, R. Sarvendranath, and S. K. Sharma, "On the feasibility of wireless energy transfer based on low complexity antenna selection and passive IRS beamforming," *IEEE Trans. Commun.*, vol. 70, no. 8, pp. 5663–5678, 2022.

[93] P. Das, S. Kashyap, R. Sarvendranath, and A. Mishra, "Binary power control and passive beamforming for RIS-assisted spectrum sharing network," in *Proc. IEEE Glob. Commun. Conf.*, 2023, pp. 1621–1626.

[94] T. Izawa, "Two or multi-dimensional gamma-type distribution and its application to rainfall data," *Papers in Meteorology and Geophysics*, vol. 15, no. 3-4, pp. 167–200, Mar. 1965.

[95] D. P. Bertsekas and J. N. Tsitsiklis, *Introduction to Probability*, 2nd ed. Athena Scientific, 2008.

[96] M. H. Protter and C. B. Morrey, *Intermediate Calculus*, 2nd ed. Springer Science and Business Media, 2012.

[97] A. Papoulis, *Probability, Random Variables and Stochastic Processes*, 3rd ed. McGraw Hill, 1991.

[98] M. Simon, *Probability Distributions Involving Gaussian Random Variables: A Handbook for Engineers, Scientists and Mathematicians*. Springer-Verlag, New York, Inc., 2006.

[99] M. Fréchet, "Généralisation du théoreme des probabilités totales," *Fundamenta mathematicae*, vol. 1, no. 25, pp. 379–387, 1935.

[100] Ö. Özdogan, E. Björnson, and J. Zhang, "Performance of cell-free massive MIMO with Rician fading and phase shifts," *IEEE Trans. Wireless Commun.*, vol. 18, no. 11, pp. 5299–5315, Aug. 2019.